Doctoral Dissertation

Study on the development of rhodium-catalyzed selective hydroformylation of vinylheteroarenes using formaldehyde

（ロジウム触媒によるホルムアルデヒドを用いたビニルヘテロアレーン類の選択的ヒドロホルミル化反応の開発に関する研究）

June 2019

Synthetic Organic Chemistry Laboratory

Division of Materials Science

Nara Institute of Science and Technology

Jian Pan

Table of Contents

List of Abbreviations

acac	acetylacetonate
Ar	aryl
BINAP	2,2’-bis(diphenylphosphino)-1,1’-binaphthyl
BIPHEP	2,2’-bis(diphenylphospino)-1,1’-biphenyl
BIPHEPHOS	2,2'-Bis[(1,1'-biphenyl-2,2'-diyl)phosphite]-3,3'-di-tert butyl-5,5'-dimethoxy-1,1'-biphenyl
BISBI	2,2’-bis(diphenylphosphinomethyl)-1,1’-biphenyl
Bn	Benzyl
Boc	*tert*-Butyloxycarbonyl
Bu	Butyl
*t*BuXantphos	9,9-dimethyl-4,5-bis(di-tert-butylphosphino)xanthene
cod	1,5-cyclooctadiene
conv.	conversion
Cy	cyclohexyl
DFT	density functional theory
DIFLUORPHOS	[4-(5-diphenylphosphanyl-2,2-difluoro-1,3-benzodioxol-4-yl)-2,2-difluoro-1,3-benzodioxol-5-yl]-diphenylphosphane
DME	1,2-dimethoxyethane
DMF	*N*,*N*-dimethylformamide
dppb	1,4-bis(diphenylphosphino)butane
dppe	1,2-bis(diphenylphosphino)ethane
dppp	1,3-bis(diphenylphosphino)propane

ee	enantiomeric excess
EI	electron impact ionization
eq. or equiv.	equivalent
IR	infrared absorption spectrometry
Me	Methyl
Nixantphos	4,6-bis(diphenylphosphino)-10*H*-phenoxazine
NMP	*N*-methylpyrrolidone
NMR	nuclear magnetic resonance
Ph	phenyl
Ph-bpe	1,2-bis(2,5-diphenylphospholano)ethane
R_f	retention factor
SYNPHOS	[5-(6-diphenylphosphanyl-2,3-dihydro-1,4-benzodioxin-5-yl)-2,3-dihydro-1,4-benzodioxin-6-yl]-diphenylphosphane
THF	tetrahydrofuran
Triphos	1,1,1-tris(diphenylphosphinomethyl)ethane
TLC	thin layer chromatography
Ts	*p*-toluenesulfonyl
Tol	*p*-methylphenyl
Xantphos	4,5-bis(diphenylphosphino)-9,9-dimethylxanthene
Xyl	3,5-dimethylphenyl

Chapter 1 Introduction

1.1 General Introduction to Hydroformylation

Hydroformylation, also known as *oxo synthesis* or *oxo process*, is a highly atom-economic reaction in which an alkene is converted into an aldehyde by the addition of *syngas*, a mixture of carbon monoxide (CO) and hydrogen (H_2), in the presence of a transition-metal complex (Scheme 1.1). Unless ethylene is used as a substrate, this reaction leads to a mixture of isomeric products: *linear*-aldehydes and *branched*-aldehydes. Therefore, the regioselectivity is an important issue as well as the stereoselectivity of a branched aldehyde.

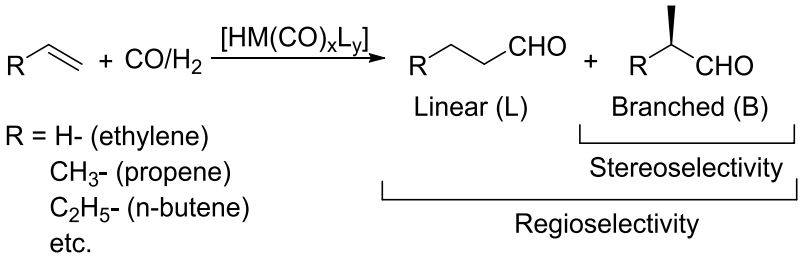

Scheme 1.1 Hydroformylation

The reaction was first discovered in 1938 by Otto Roelen during the course of his studies on the oxygenated side products of cobalt-catalyzed Fischer–Tropsch reactions in Oberhausen, Germany.[1] It is a homogeneous reaction, catalyzed by carbonyl-forming transition metal complexes, which gives linear and branched aldehydes (with the exception of ethylene). Accidentally, Otto Roelen discovered the reaction, — in which ethylene reacted with CO and H_2 in the presence of a catalyst consisting of cobalt, thorium, and magnesium oxide — produces not only alkanes but also diethyl ketone and propionaldehyde, so-called oxo products. Therefore,

he named this reaction to the oxo process, which is still used today, especially by industrial companies.

After the end of the Second World War, the great potential of the new process was immediately discovered. Up to now, more than 10 million metric tons of aliphatic aldehydes of different chain lengths have been produced annually in the whole world using this reaction.[2] For decades, a lot of patents and academic publications were published in this field, indicating that the hydroformylation is still an important research focus in industrial and academic research.[3,4]

These resulting aldehydes are very important functional groups in organic synthesis, and are usually used as intermediates of more complex molecules, such as alcohols by hydrogenation, acids by oxidation, or amines by reductive amination (Scheme 1.2).[4h] Through these transformations, highly functionalized compounds with extended and branched carbon chains were obtained.

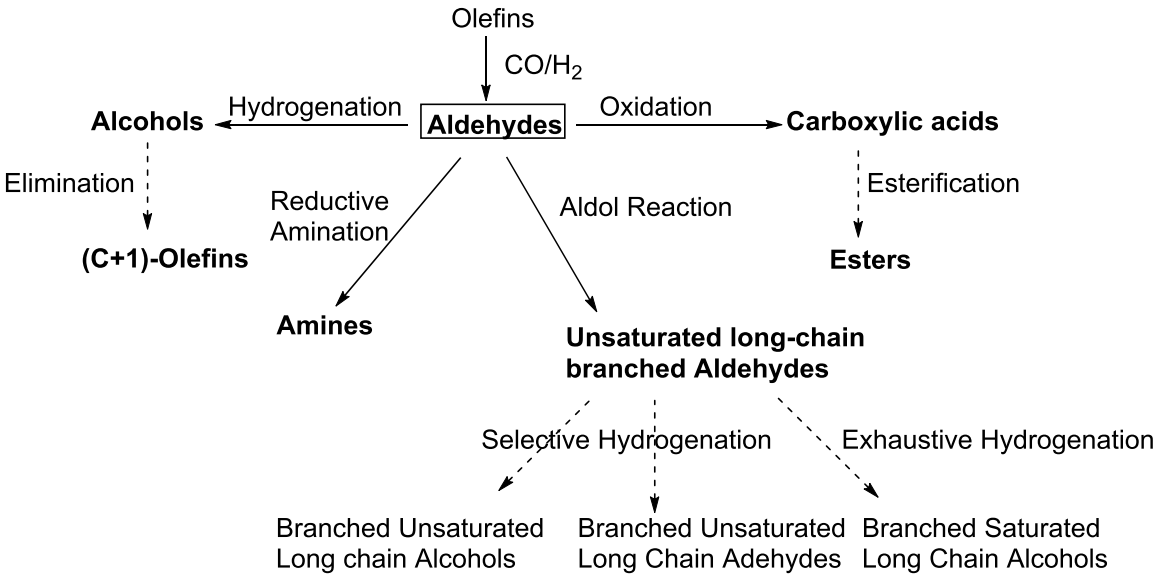

Scheme 1.2 Transformation from aldehydes

Moreover, in most cases, aldehydes are not final products in a general synthesis, and various one-pot and domino reactions offer more valuable products following the combination of hydroformylation with other reactions without isolation of the formed aldehydes, such as hydrogenation, aminomethylation, acetalization, C–C coupling reactions, etc (Scheme 1.3).[3b] These domino reactions or multicomponent reactions represent a trend of organic synthesis of the most useful homogeneously catalyzed processes in a step or one-pot economic manner. Particularly, tandem protocols have recently attracted great attention because of their outstanding applications in the synthesis of decorated molecules.[3b,5] Especially, the application of synthesis of some natural products using domino hydroformylation reaction were detailed in the framework of a book edited by Taddei and Mann,[3b,6] occasionally accompanied by experimental protocols.

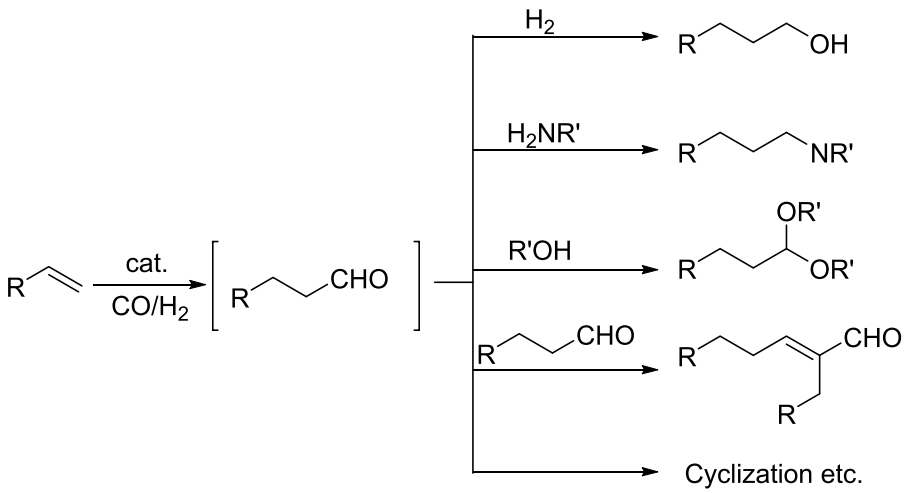

Scheme 1.3 Domino hydroformylation without isolation of the aldehydes

1.2 Transition Metals in Hydroformylation

A typical catalysts model for the hydroformylation of olefins is homogeneous hydride complexes of the type $[HM(CO)_xL_y]$, where M = transition metal and L = CO or an organic ligand. The process without ligands is called an unmodified or sometimes "naked" catalyst, while the process involving the use of ligands to attain specific demands such as high regio-, chemo-, and enantio-selectivities is called a "modified" catalyst. In early (mainly patent) literature, besides Co and Rh, Ni, Ir, and other metals of the VIII group, also Cr, Mo, W, Cu, Mn, and even Ca, Mg, and Zn were suggested or claimed for hydroformylation.[3b,3c,7] However, some of these metals do not exhibit any activity. Now, Ru, Ir, Pd, Pt, and Fe catalysts are also applied in hydroformylation.[8] Nevertheless, so far, only Rh and Co have usually been used metals for hydroformylations in industrial processes.[4h] Rhodium is by far the most active metal, allowing for reactions to run under mild pressures of CO/H_2 (20-80 bar) at temperatures below 140 °C, while cobalt-based catalysts usually require higher pressures (200-350 bar) and

temperatures up to 190 °C to touch acceptable activities.[3d] Currently, with unmodified metal carbonyl complexes, a generally accepted series of the activities are as follows:[9]

Rh >> Co > Ir > Ru > Os ~ Tc > Pt > Pd > Mn > Fe > Ni >> Re

Historically, the early generation of hydroformylation catalysts was usually based on cobalt carbonyl without phosphine ligands.[10] However, because of the low activity of cobalt, the reaction conditions were too harsh. Very soon, mechanistic studies showed that the active species is the homogeneous complex, $HCo(CO)_4$, which was stable only under CO/H_2 pressure.[3d] In the 1950s, Shell Co. Ltd. developed a phosphine modified catalyst system for the synthesis of detergent alcohols, which is still in use today.[11] To date, due to the remarkable stability of Co-catalysts toward poisons, Co-based hydroformylation processes are still important reactions for petrochemical giants like Shell, Exxon, CdF, Chimie, Nissan, and BASF chemical companies.

Additionally, there is some drawback in chemo- and regio-selectivity using the cobalt-based processes. For example, because of the high hydrogenation activity of Co catalysts, a large amount of undesired product, alkane, is produced. Other disadvantages of Co-catalyzed systems are the harsh reaction conditions, which require high investment costs. In 1965, J. A. Osborn, G. Wilkinson, and J. F. Young reported $[RhCl(PPh_3)_3]$-catalyzed hydroformylation under mild conditions with superior chemo- and regio-selectivity.[12] Subsequently, to date, the rhodium-catalyzed system has attracted more and more attention and significant progress in chemo- and

regio-selectivity has been made.[3] Other investigations showed the activity of Rh catalysts can be up to 1000 times more than that of Co complexes. A significant advantage of using Rh catalysts is that reactions can be conducted under reduced syngas pressure and low reaction temperature.[3d] Currently, rhodium is the best metal of choice for the hydroformylation of short-chain olefins.

As mentioned above, only one metal catalyst was used in the previous work. However, there is also a trend of the combination of two or more different metal catalysts, called bimetallic catalysts. Early investigations on the stoichiometric reaction of Co–acyl complexes in the absence of CO or at low CO pressure showed the evidence that the second cobalt complex, $HCo(CO)_4$, can promote the hydrogenolysis process (Scheme 1.4).[13]

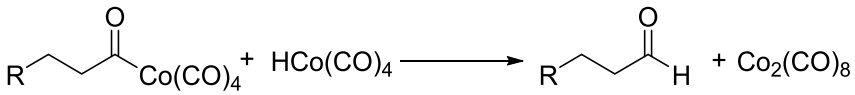

Scheme 1.4 The hydrogenolysis by the second catalyst

This discovery led to the use of combinations of different metals (e.g., Co/Rh, Co/Pt, Co/Fe, Co/Mo, Rh/Fe, Rh/Mn, Rh/Re, Rh/W, Rh/Mo) with the aim of creating new efficient catalyst system.[14] Indeed, the cooperative or successive interaction of two or more different metal centers with the substrate molecules can lead to enhanced catalytic activities and selectivities and, in some cases, to new reactions which cannot be achieved by using monometallic systems.[15,16] Especially, in 2003, Marc Garland and co-workers provided more evidence through spectroscopic measurements and density functional theory (DFT) calculations.[17] In this

work, the addition of manganese carbonyl hydride $Mn_2(CO)_{10}$/$HMn(CO)_5$ to rhodium precursor $Rh_4(CO)_{12}$ in the hydroformylation of 3,3-dimethylbut-1-ene led to a significant increase in catalytic activity, giving the aldehyde, 4,4-dimethylpentanal, in more than 95% selectivity (Scheme 1.5). Detailed in situ spectroscopic information indicated that this increase in the rate of product formation is due to the existence of bimetallic catalytic binuclear elimination. Later, more explanations supported previous observations.[18] The reductive elimination of the aldehyde from the Rh–acyl intermediate in a second catalytic cycle proceeded simultaneously.

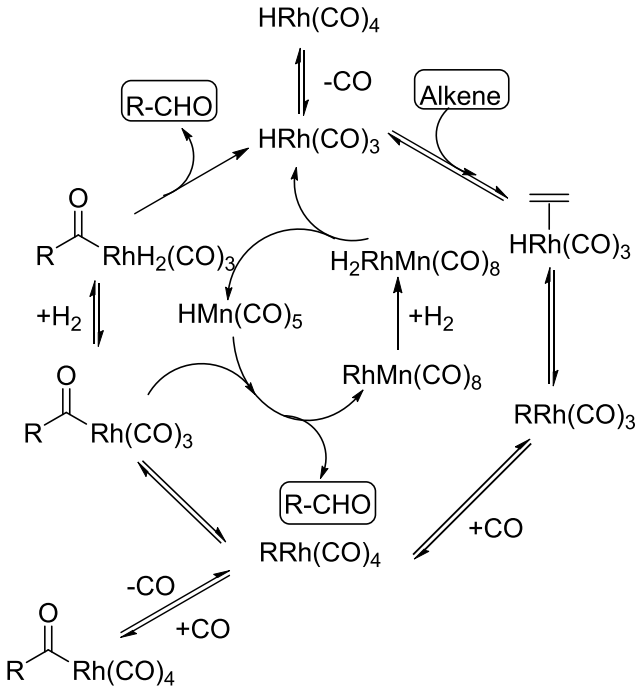

Scheme 1.5 Proposed mechanism by bimetallic catalysis

1.3 Ligands in Hydroformylation

Ligands play an important role in the modification of intermediate metal complexes in hydroformylation and have a dramatic influence on the reactivity as well as chemo-, regio-, and stereo-selectivity. The structure and concentration of ligands are key factors for transformation.

Although the first investigation in the framework of Rh-catalyzed hydroformylation by Otto Roelen was based on "ligand-free" systems, Wilkison reported in 1965 that phosphine-modified rhodium complexes [$RhCl(Ph_3P)_3$] displayed higher activity and selectivity on hydroformylation.[12] Since then, the design and modification of monodentate ligands has attracted attention, influencing the catalyst activity and selectivity.[3a,19] Notably, the first phosphoramidites were successfully applied to hydroformylation by Van Leeuwen in 1996.[20] One year later, N-Heterocyclic carbenes were also introduced to hydroformylation by Herrmann (Scheme 1.6).[21]

The other big breakthrough of ligands is the discovery of bidentate P-ligands (Scheme 1.6). The rigidity of the spacer between the two phosphorus atoms greatly affects their coordination ability. The bulkiness of the coordinated ligand should be described using the Tolman angle (θ) for monodentate ligands and using the natural bite angle (β) for bidentate ligands.[3] Depending on its bulkiness and rigidity, a ligand can coordinate the metal in an equatorial-equatorial (ee) or equatorial-axial (ea) coordination mode. In addition, electronic effects of ligands also determine the regio- and enantio-selective character. In this dissertation, I mainly describe this kind of ligand.

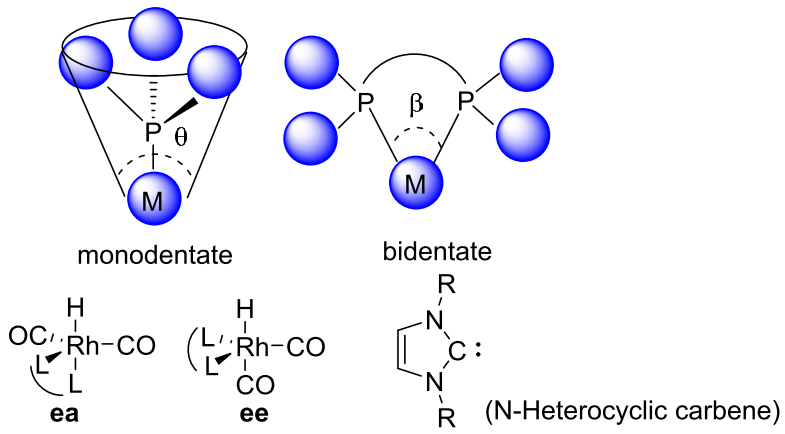

Scheme 1.6 Monodentate, bidentate, carbene ligand model and ee or ea coordination modes of bidentate ligands (L–L) in the $[HRh(CO)_2(L–L)]$ complexes

A very few multidentate ligands, such as 1,1,1-tris(diphenylphosphinomethyl)ethane (Triphos), have also been investigated in hydroformylation (Scheme 1.7).[22] Tetradentate phosphite ligands derived from pentaerythritol for rhodium-catalyzed hydroformylation were claimed by Mitsubishi Kasei Co. Ltd.[23] Recently, Zhang's group[24] have discovered new ligand motifs, such as tetraphosphoroamidite **I**,[24c] tetraphosphines **II**[24d] and hybrid phosphine-phosphoramidite **III** [24e] (Scheme 1.7).

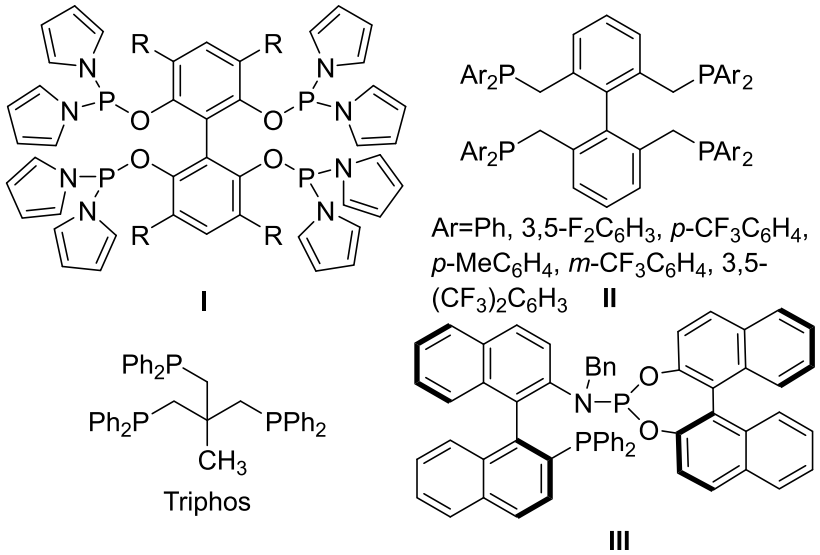

Scheme 1.7 Multidentate ligands

1.3 General Rh-Catalyzed Hydroformylation Mechanism

In Scheme 1.8, the well-accepted mechanism of the Rh-catalyzed hydroformylation mechanism proposed by Heck is described for bidentate ligands.[25] It is consistent with Wilkinson's so-called dissociative mechanism.[12, 26] This mechanism is also supported by the observation and structural characterization of the resting state of the catalyst by in situ spectroscopic techniques (HR-IR, HP-NMR).[3a, 3e, 27]

In general, for bidentate ligands, the mechanism cycle starts from the $[RhH(L\text{-}L)(CO)_2]$ species **IV**, containing the ligand coordinated in equatorial positions (denoted eq–eq throughout the Scheme 1.8) or in an apical-equatorial position (denoted eq–ax).

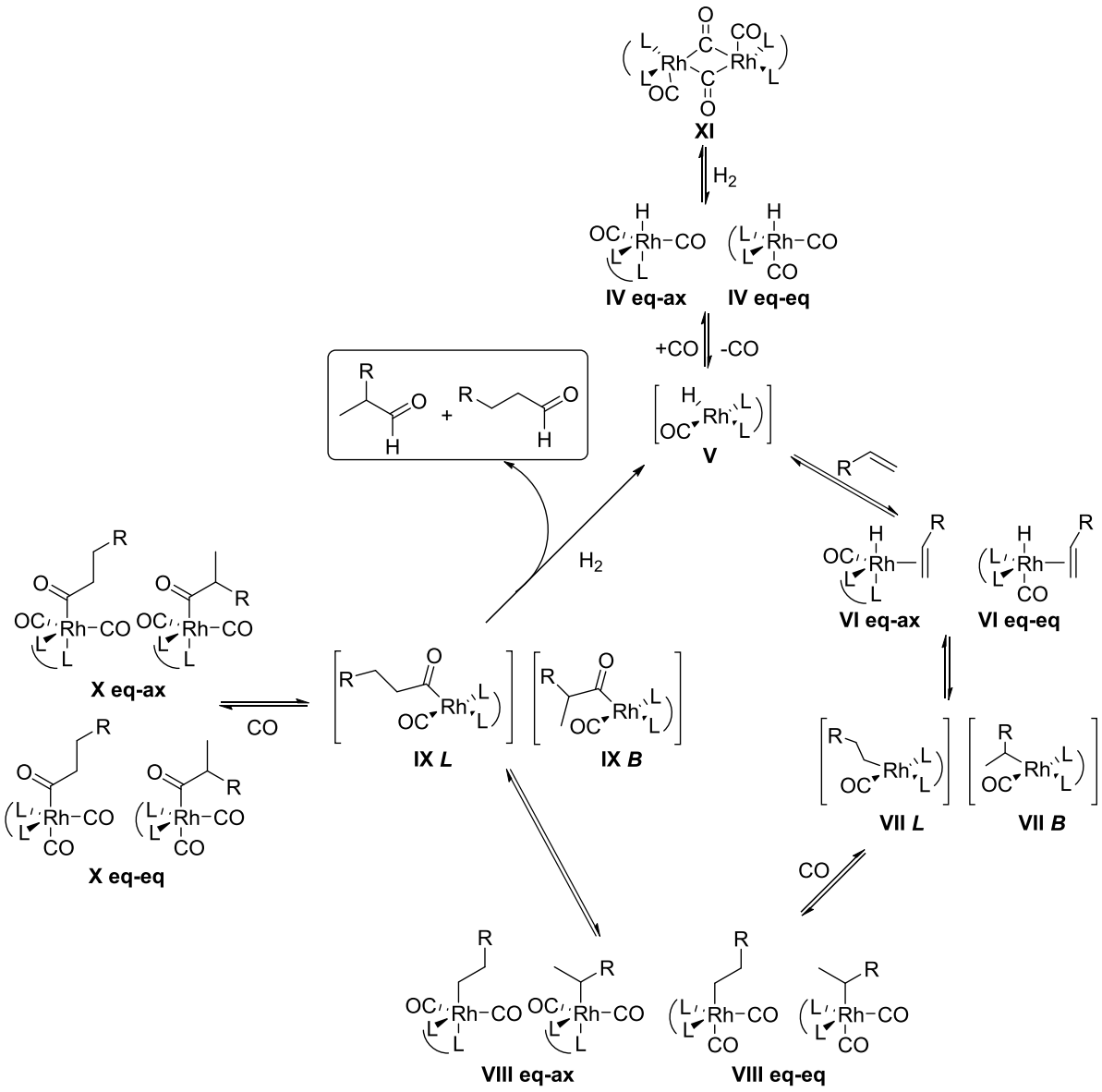

Scheme 1.8 Mechanism of the Rh-catalyzed hydroformylation in the presence of bidentate ligand (L–L)

Dissociation of equatorial CO from the [RhH(L-L)$(CO)_2$] species **IV** leads to the formation of the square-planar intermediate **V**. Subsequently, the intermediate **V** associates with an alkene to give complexes **VI**, where the ligand can again be coordinated in two isomeric forms eq–ax and eq–eq, while a hydride and an alkene coordinate from an axial and equatorial directions, respectively, having a hydride in an apical position and alkene coordinated in the equatorial plane. On the basis of experimental results and theoretical calculations, it has been proposed

that the regioselectivity of aldehydes is determined by the coordination of the alkene to the square-planar intermediate **V** to give the pentacoordinate intermediates **VI**.[28] This step is also crucial in determining the enantioselectivity since the enantioface discrimination occurs between **V** and **VII**, and particularly from **V** to **VII**. The CO dissociation from **IV** was shown to be much faster than the overall hydroformylation process, indicating that the rate of the reaction is dominated by the reaction of **V** with either CO or the alkene to form **IV** or **VI**, respectively.[29] It has not been established experimentally whether alkene complexation is reversible or not; although in Scheme 1.8, all steps are described as reversible except the final hydrogenolysis. Experiments using deuterated substrates suggest that alkene coordination and insertion into the Rh–H bond can be reversible, certainly when the pressures are low. Complexes **VI** undergo migratory insertion to give the square-planar alkyl complex **VII**. This species can undergo *β*-hydride elimination, thus leading to isomerization, or can react with CO to form the trigonal bipyramidal (TBP) complexes **VIII**. Thus, under low pressure of CO more isomerization may be expected. At low temperatures (< 70°C) and sufficiently high pressure of CO (>10 bar) the insertion reaction is usually irreversible and thus the regioselectivity and the enantioselectivity in the hydroformylation of alkenes is determined at this point. Complexes **VIII** undergo second migratory insertion to form the acyl complex **IX**, which can react with CO to give the saturated acyl intermediates **X** or with H_2 to give the aldehyde product and the unsaturated intermediate **V**. The reaction with H_2 involves presumably oxidative addition and

reductive elimination, but for rhodium, no trivalent intermediates have been observed.[30] At low hydrogen pressures and high rhodium concentrations, the formation of dirhodium dormant species such as **XI** becomes significant. [31]

Recently, the full catalytic cycle for mono- and bis-ligated monophosphine Rh complexes has been investigated using DFT calculations.[32]

1.4 Syngas and Alternative Syngas Sources

Synthesis gas (syngas), the mixture of CO and H_2 required as a reagent for hydroformylation, can be derived from almost every carbon source, such as natural gas, naphtha, or coal (Scheme 1.9). In addition, biomass and plastic waste also come into the focus.[33]

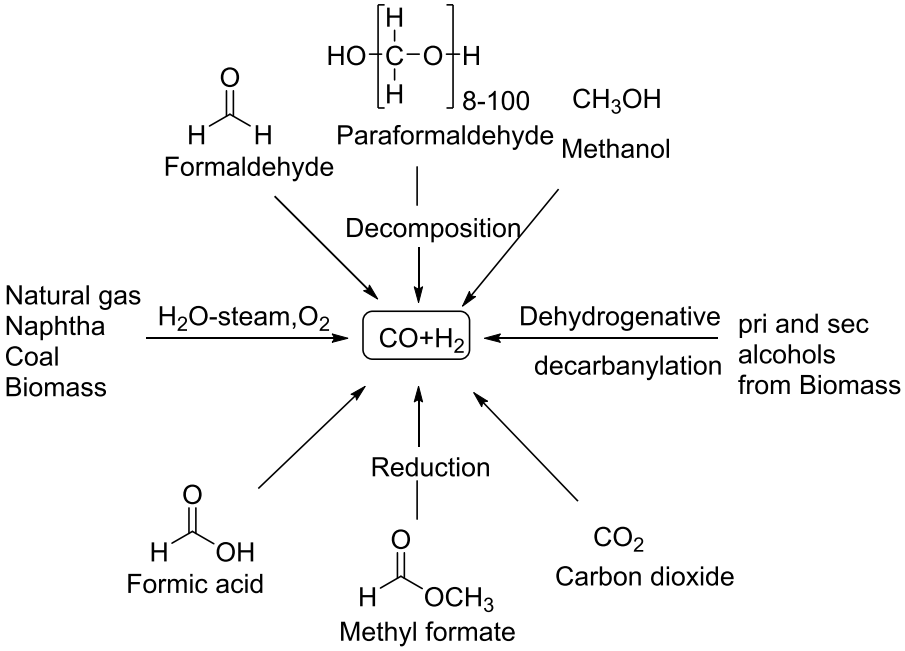

Scheme 1.9 Sources for syngas used in hydroformylation

In 2004, my group provided the first review of carbonylation reactions with CO surrogates, which included hydrocarbonylation (hydroesterification, hydroamination, and hydrocarboxylation) of alkenes and alkynes, hydroformylation of alkenes, alkoxy-, amino-, and

hydroxy-carbonylation of aromatic and alkenyl halides, and the Pauson–Khand type reaction.[34] Since then, much more efforts have been made in search of new CO surrogates for carbonylation reaction from the viewpoint of green organic chemistry.[35] In 2014, Beller's group also provided an update.[36] In the same year, Konishi and Manabe reported formic acid derivatives such as phenyl formate and N-formylsaccharin as practical carbon monoxide surrogates for metal-catalyzed carbonylation reactions.[37] Skrydstrup and co-workers summarized the development and application of two-chamber reactors and carbon monoxide precursors for safe carbonylation reactions.[38] Very recently, Jian Cao and co-works reviewed transition-metal-catalyzed transfer carbonylation with HCOOH or HCHO as non-gaseous C1 source.[39] These reviews indicate using syngas surrogate is a trend in green chemistry.

In this dissertation, the development of hydroformylation using formaldehyde or paraformaldehyde as syngas surrogate is described as primary coverage.

a) Syngas Generation from Formaldehyde or Paraformaldehyde

Commercial solution of formaldehyde in water is a saturated water solution of about 40 vol% or 37 mass% formaldehyde, which are called *formol* or *formalin*. Paraformaldehyde is the solid polymerization product (mp ≈ 120 °C) of formaldehyde with an average degree of polymerization of 8–100 units. It depolymerizes to formaldehyde upon heating. In the hydroformylation with formaldehyde, formaldehyde decomposes to CO and H_2 in the presence of some transition catalysts such as rhodium, iridium, ruthenium, or cobalt.[40]

In 1982, Okano and Kiji were the first to use paraformaldehyde in the hydroformylation of alkenes in the presence of an Rh(hydrogencarbonate)phosphine catalyst without additional ligands (Scheme 1.10).[41] This catalytic system led to aldehydes as major products. The TON was up to 384 and conversion was 59.3%. Small amounts of C_7-alcohols, C_7-carboxylates, and hexane were also formed in the above turnover number.

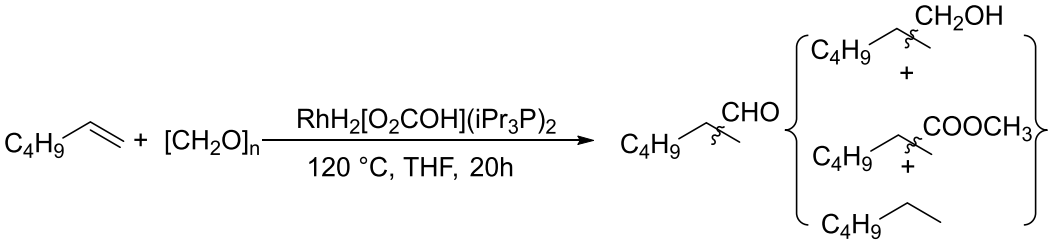

Scheme 1.10 Hydroformylation of olefins with paraformaldehyde

Under these conditions, $RhCl(PPh_3)_3$ or $Ru(CO)_3(PPh_3)$ was virtually inactive. Raising temperature (from 120 °C to 150 °C) resulted in a decrease in the yield of aldehydes and in an increase in the formation of alcohols and esters.

In 1999, Seok and co-workers examined the hydroformylation of allyl alcohol with paraformaldehyde in the presence of $HRh(CO)(PPh_3)_3$ and triphenylphosphine (Scheme 1.11).[42] Especially, the selectivity to isomeric product from allyl alcohol was extremely high with *L/B*-ratio of 21. The additions of syngas and excess phosphine inhibited the formation of linear product.

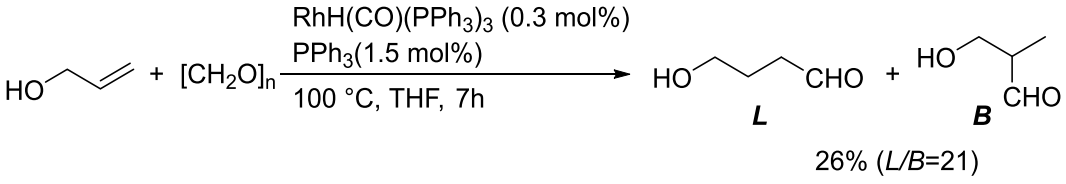

Scheme 1.11 Hydroformylation of allyl alcohol with paraformaldehyde

In 2005, Rosales and co-workers reported that hydroformylation with paraformaldehyde enabled the reaction to be performed under atmospheric pressure of inert gas in conventional glassware, not requiring high-pressure equipment and avoiding the use of CO.[43] Three years later, they discovered that the reaction rate with complexes of the type $[Rh(diphos)_2]^+$ decreased from dppe to dppp with the enlargement of the carbon chain in a series of bidentate diphenylphosphines (Scheme 1.12)[44] These results were explained by both electronic and steric effects of ligands, whereas for the hydroformylation reaction under syngas conditions, the increasing in the activity was explained by the bite angle of the corresponding diphosphine.

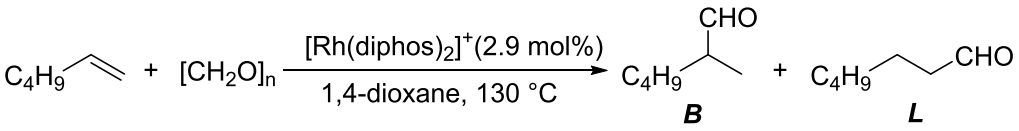

diphos = dppe	*L/B* = 1.7/1	bite angle 85°	initial rate(10^5 Ms^{-1}): 4.70
dppp	2.1/1	bite angle 91°	1.65
dppb	2.2/1	bite angle 98°	1.15

syngas

diphos = dppe	*L/B* = 2.9/1	bite angle 85°	initial rate(10^5 Ms^{-1}): 0.94
dppp	3.1/1	bite angle 91°	4.43
dppb	3.7/1	bite angle 98°	6.23

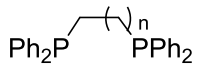

n = 1: dppe
2: dppp
3: dppb

Scheme 1.12 Hydroformylation of 1-hexene by dppe, dppp, dppb

In 2010, my group showed that a combination of two Rh catalysts [Rh(BINAP), Rh(xantphos)] can be beneficial: the former causes the decomposition of formaldehyde,

whereas the latter attains the hydroformylation of olefins in the presence of formaldehyde (formalin) or paraformaldehyde (Scheme 1.13a).[45] Under this catalytic system, aldehydes were obtained with a conversion of 98% and a ratio of *L/B* = 97/3. The use of paraformaldehyde required a longer reaction time than the reaction with formalin. BIPHEP and Nixantphos as ligands gave better results (Scheme 1.13b).

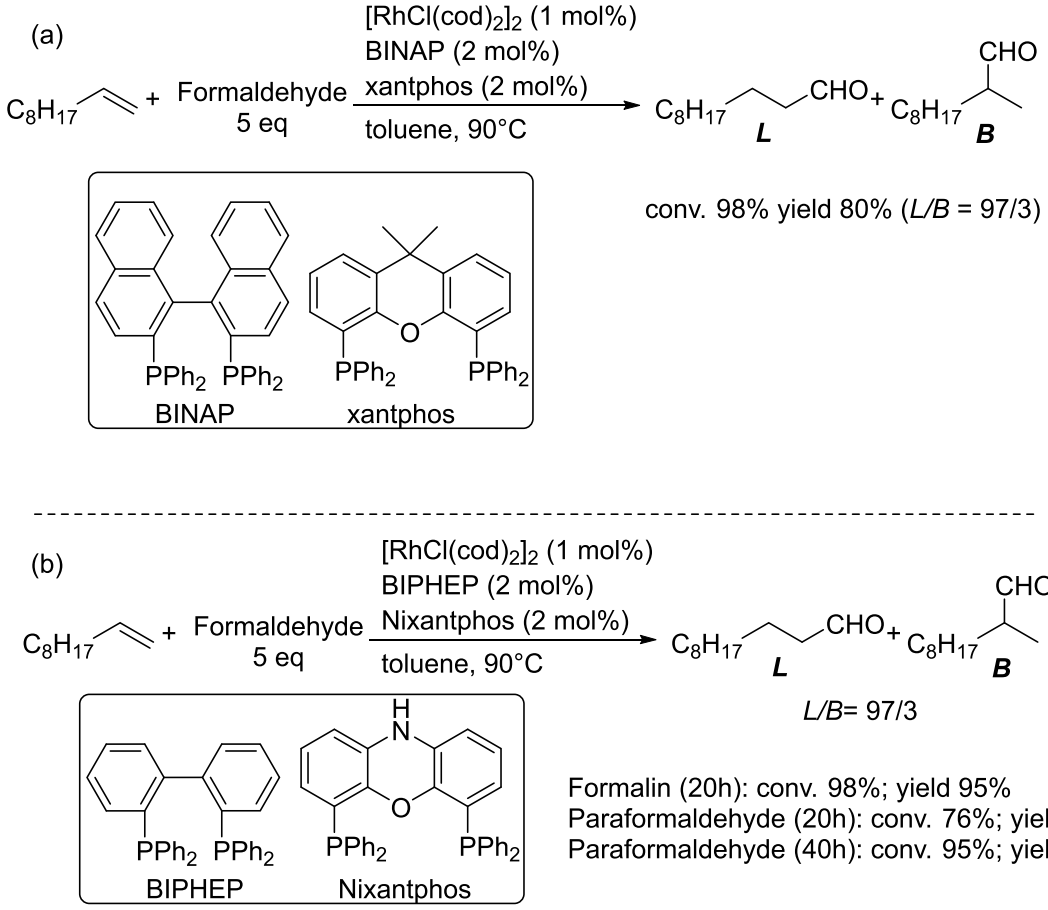

Scheme 1.13 Hydroformylation of 1-decene with formalin or paraformaldehyde

In 2011, Taddei's group applied this catalytic system to the hydroformylation of complex substrates, designed for domino processes by microwave heating (Scheme 1.14).[46] This method was also applied to hydroformylation-cyclization tandem reactions, as exemplarily illustrated with a final *N*,*O*-acetalization step (Scheme 1.15).

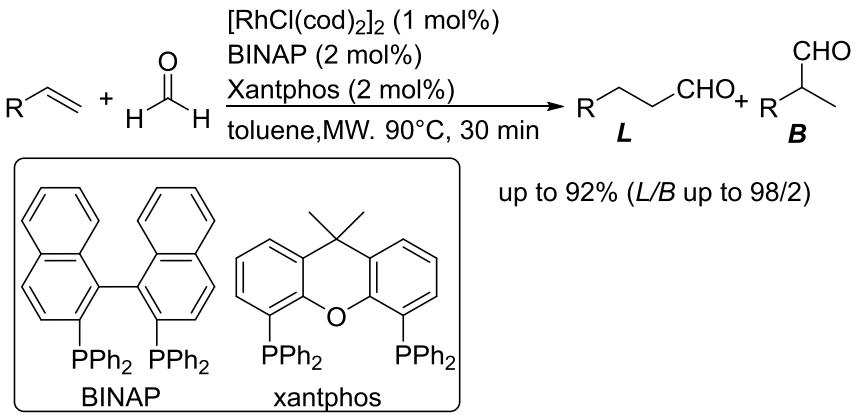

Scheme 1.14 Hydroformylation by microwave heating

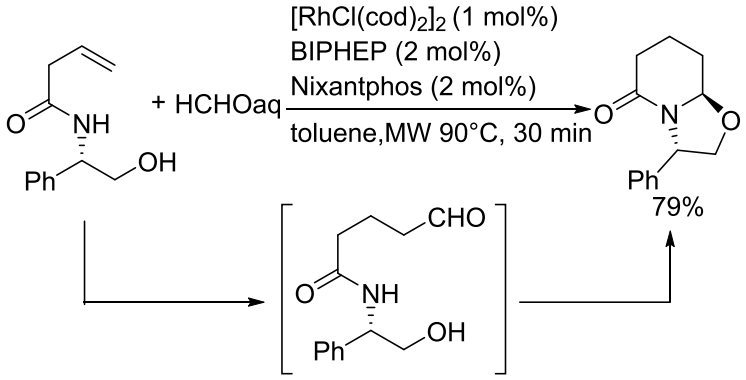

Scheme 1.15 Tandem hydroformylation–acetalization with formalin and a rhodium catalyst with two different diphosphine ligands

In 2013, Börner and coworkers discovered that the addition of external hydrogen gas is beneficial in hydroformylation with formaldehyde by running the reaction with formalin at 5-10 atm hydrogen pressure.[47] In this case, turnover numbers and regioselectivity were improved (Table 1.1).

Table 1.1 Rh catalyzed hydroformylation of 1-octene with formaldehyde/H_2[a]

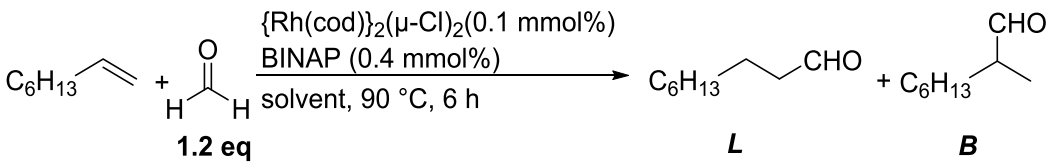

Solvent	pH_2(bar)	Conv.	Yield	*L*/*B*	Isomerization	Octane
Toluene	-	34%	30%	1.8	4%	-
Toluene	10	79%	69%	3.9	5%	5%

THF	-	27%	23%	1.9	4%	-
THF	10	59%	56%	2.4	2%	1%

[a]conditions:1-octene = 1*M*; 1.2 eq. formaldehyde, $[RhCl(cod)]_2$/BINAP/1-octene = 1/4/1000, 90 °C, solvent, 6h.

In the same year, Ren and Wulff established syngas-free hydroformylation to synthesize natural piperidines, such as (-)-coniine (Scheme 1.16).[48] The key intermediate was a chiral tetrahydropyridine. The chiral allylamines were synthesized by amino allylation of butanal with unsaturated diarylamines, then subsequently protection by Boc group. Rhodium-catalyzed hydroformylation with both BIPHEP and Nixantphos gave the chiral dihydropyridine. As a formyl group source, paraformaldehyde showed higher yields than formalin. The piperidine alkaloid was obtained following hydrogenation and removal of the protective group. The *syn* and *anti*-1,3-aminoalcohols (+)-allosedridine and (+)-sedridine were obtained with similar methods.

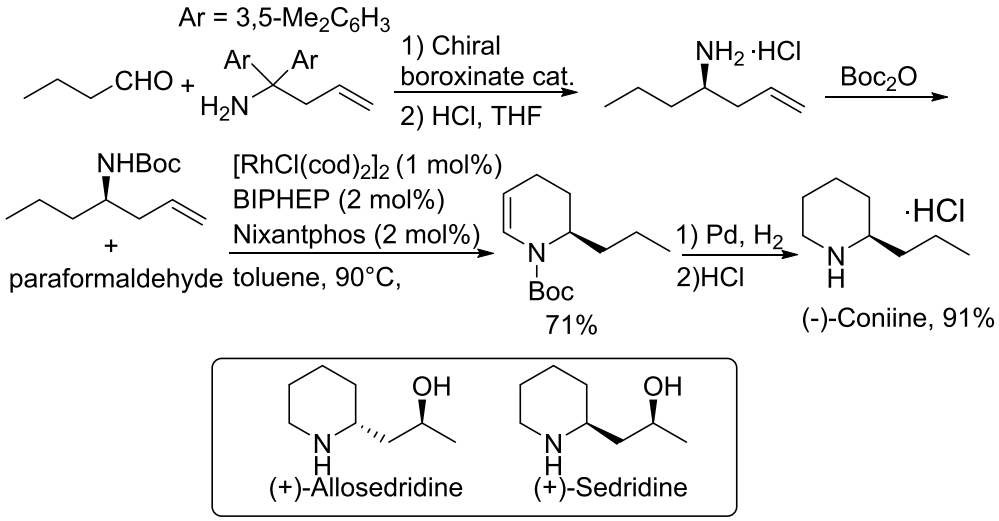

Scheme 1.16 Synthesis of natural piperidines by hydroformylation with paraformaldehyde

In 2015, formaldehyde and paraformaldehyde were employed in asymmetric

hydroformylation by my group (Scheme 1.17).[49] The regioselectivity (*B/L* = up to 96/4) and enantioselectivity (up to 95% ee) can be attributed to the use of chiral Ph-bpe as a ligand. Both the decarbonylative degradation of formaldehyde to a CO moiety and hydrogen and the subsequent hydroformylation of vinylarenes are catalyzed by the singly-loaded catalyst, Rh(I)/chiral Ph-bpe. In the labeling experiment, the employment of ^{13}C-formaldehyde showed the evidence that the carbonyl moiety releasing occurs in the coordination sphere of rhodium.

In the same year, Clarke and co-workers demonstrated that hydroformylation with paraformaldehyde is also suitable for quite poorly reactive substrates, such as 1,2-difunctionalized alkenes (Scheme 1.18).[50] It was a rapid asymmetric transfer hydroformylation (5~40 min).

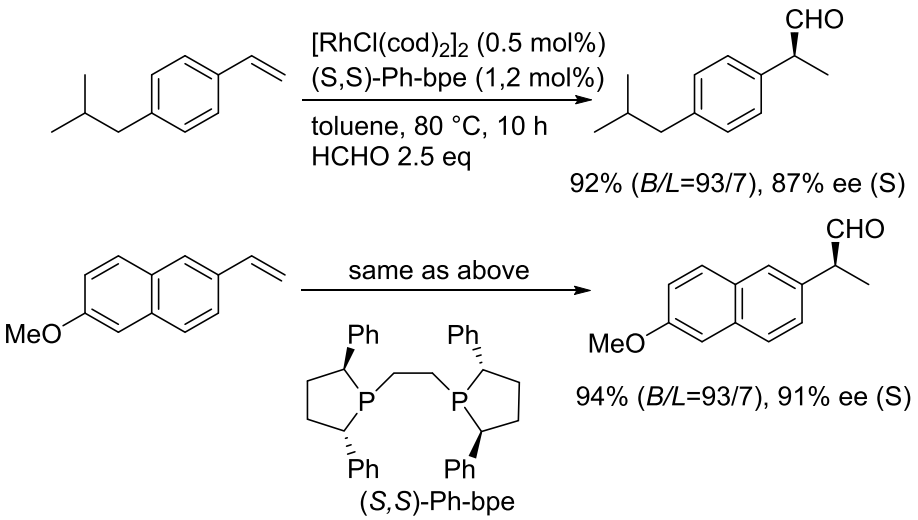

Scheme 1.17 Asymmtric hydroformylation of vinylarenes with formalin

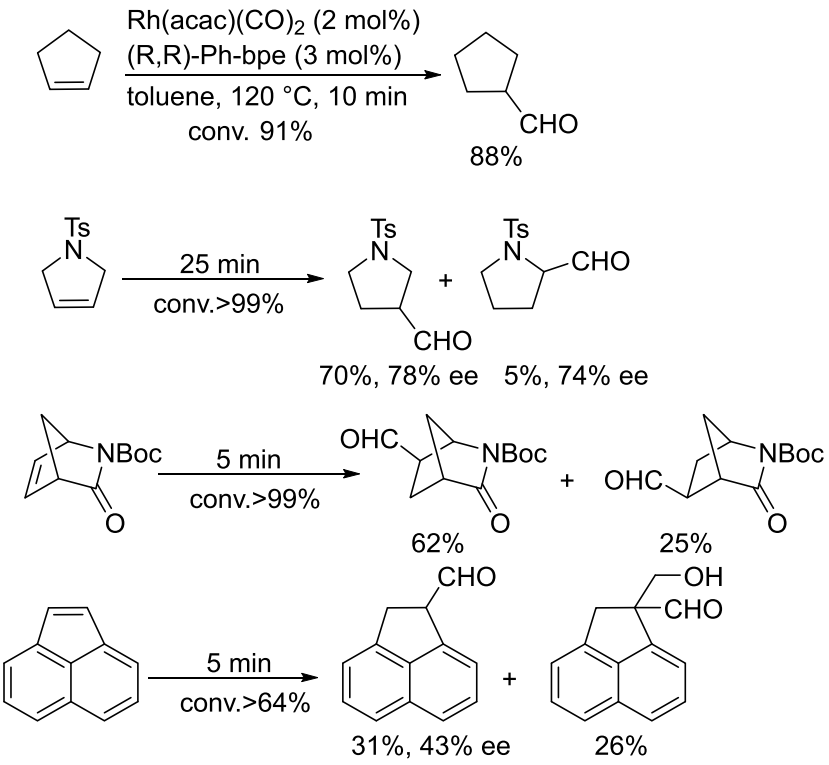

Scheme 1.18 Hydroformylation of disubstituted alkenes with paraformaldehyde

b) Syngas Generation from CO_2

In 1994, Tominaga and Sasaki discovered that ruthenium catalysts such as $Ru_3(CO)_{12}$ were able to reduce CO_2 to CO in the presence of bis(triphenylphosphine)iminium chloride, [PPN]Cl (Scheme 1.19).[51] This reaction was usually at a high temperature (160 °C). This process was called reversed water gas shift (RWGS) reaction.

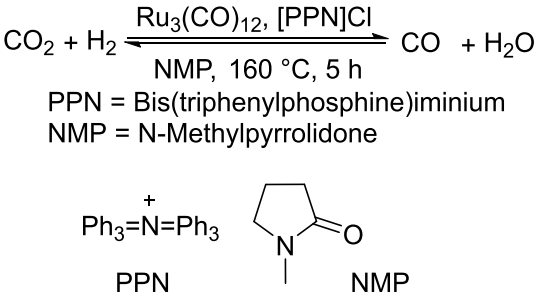

Scheme 1.19 Generation of CO by the Ru-catalyzed

In 2000, they reported the first ruthenium-catalyzed hydroformylation-reduction of alkenes with carbon dioxide (Scheme 1.20).[52a] Cyclohexylmethanol was obtained in 88% yield in the

presence of LiCl and [$Ru_4H_4(CO)_{12}$] at 140 °C using CO_2/H_2, meanwhile, a small amount of cyclohexanecarbaldehyde was also obtained.

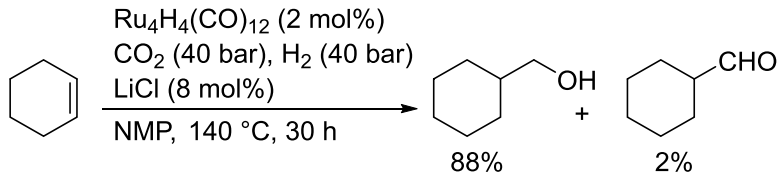

Scheme 1.20 Ruthenium-catalyzed hydroformylation-reduction of cyclohexene with carbon dioxide

Recently, Beller's group reported a ruthenium-catalyzed tandem hydroformylation-hydrogenation reaction (Scheme 1.21).[52b] This was the first example of phosphite ligands applied in hydroformylation and reverse water-gas shift (RWGS) processes using carbon dioxide.

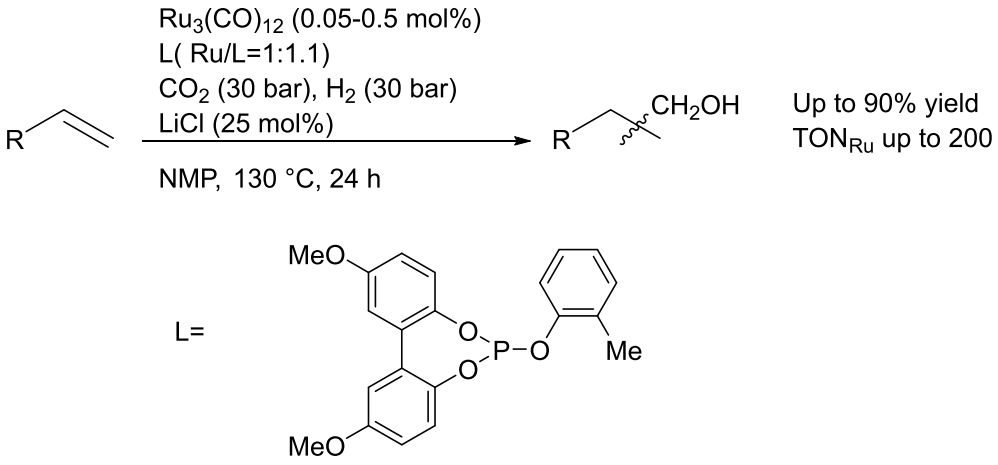

Scheme 1.21 Ruthenium catalyzed tandem hydroformylation-hydrogenation reaction

c) Syngas Generation from Methanol

At >200 °C, decomposition of methanol produces CO and H_2 over a plate-type palladium catalyst (Scheme 1.22).[53] However, the use of methanol as a carbonyl source is quite underdeveloped.

Scheme 1.22 Methanol decarbonylation

In 1986, Keim and co-workers first reported the use of methanol as a CO and H_2 source in ruthenium-catalyzed hydroesterification reactions (Scheme 1.23).[54]

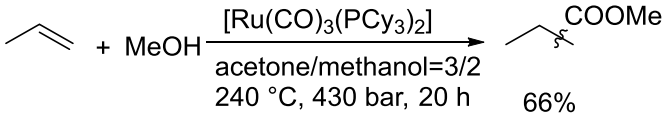

Scheme 1.23 First example using methanol as the CO and H_2 source in alkene hydroesterification reactions

d) Formic Acid or Methyl Formate as Source for Hydrogen

In 1979, Shriver and co-workers reported decomposition of formic acid produces CO and H_2 in the presence of Rhodium catalysts, such as $Rh(C_6H_4PPh_2)(PPh_3)_2$ (Scheme 1.24).[55]

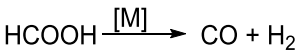

Scheme 1.24 Decomposition of formic acid

In 1994, Alper and Somasunderam found that alkenes reacted with carbon monoxide and formic acid in the presence of 5% Rh on carbon and 1,3-bis (diphenylphosphino) propane (dppp) in 1,2-dimethoxyethane (DME), giving the aldehydes (Scheme 1.25).[56] This system gave a variety of aldehydes in good yields, with excellent selectivity toward the branched chain products in most cases.

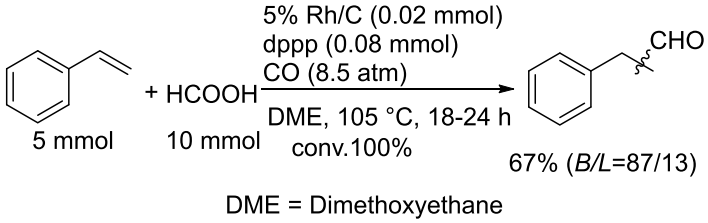

Scheme 1.25 Hydroformylation using formic acid as hydrogen source

As an alternative, the decomposition of methyl formate forms methanol and CO in the

presence of ruthenium catalysts in the first step.[57] In water, the water gas equilibrium is established, then CO reacts with H_2O to produce H_2 and CO_2, finally, H_2 and CO are formed in equal amounts (Scheme 1.26).

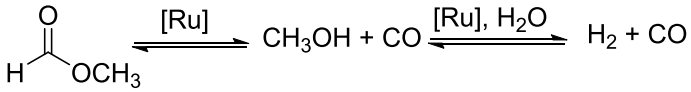

Scheme 1.26 Ru-catalyzed conversion of methyl formate into methanol and syngas

Jenner and co-workers showed that hydroformylation of cyclohexene gave aldehydes, which were immediately reduced to the corresponding alcohol, in the presence of $Ru_3(CO)_{12}$, tricyclohexylphosphine, methyl formate, and water (Scheme 1.27).[58]

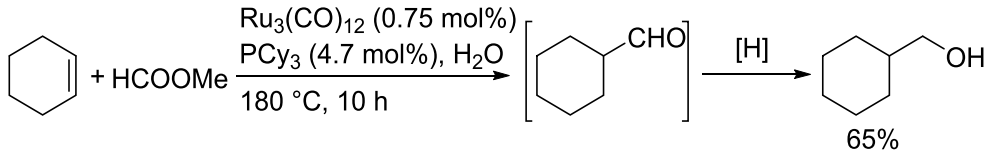

Scheme 1.27 Ru catalyzed hydroformylation-hydrogenation of cyclohexene with methyl formate

1.5 Substrates for Hydroformylation

In the preparation of bulk chemicals, substrates are usually non-functionalized olefins of different chain lengths. In general, the activity of terminal C=C bonds is higher than internal C=C bonds. The rate of the hydroformylation decreases with increasing steric hindrance of the substrate in the order:[59]

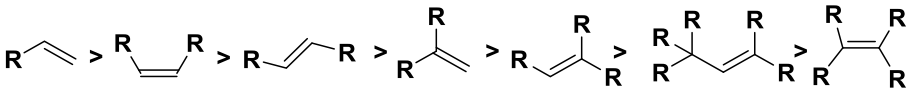

Except for terminal olefins, branched olefins always require more severe conditions or alternatively a more active catalyst. In principle, the hydroformylation of trifold substituted sp^2-configured C-atoms is unfavorable, resulting in difficulty of formation of formyl groups at

quaternary centers (Keulemans' rule).[59] However, some exceptions have been found.[60]

To date, most of substrates employed in studies on rhodium-catalyzed hydroformylation have been monosubstituted alkenes, such as vinyl arenes, allyl cyanide, and vinyl acetate. With these substrates, a major challenge is to achieve high regioselectivity and high enantioselectivity. Alkenes have to be classified according to the number and nature of their substituents (Scheme 1.28).[61] The regioselectivity issue usually occurs only for terminal and 1,2-disubstituted alkenes **XII** and **XV**. Alkyl-substituted terminal alkenes **XII** slightly favor for the linear product **XIV**. Electron-withdrawing terminal alkenes **XII** always favor for the branched product **XIII**. Both 1,1-disubstituted **XVIII** and trisubstituted **XXI** alkenes generally give only one regioisomer (**XIX** and **XXII**, respectively) based on Keuleman's rule.[59]

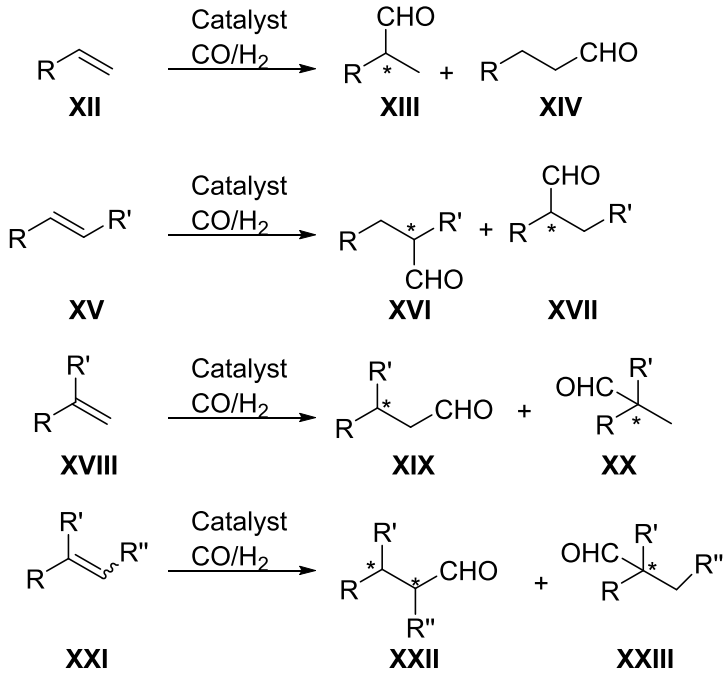

Scheme 1.28 Regioselective trends on hydroformylation of different alkenes

In 1999, Paciello and Röper developed a simplified kinetic model to allow the determination

of relative rate constants for linear and branched aldehyde formation from terminal olefins using data analysis of complex product mixtures.[62]

In 2015, Jörke and co-workers calculated thermodynamic properties and the resulting equilibrium composition of 1-decene in the presence of Rh(BIPHEPHOS) catalyst at a temperature interval between 95 °C and 115 °C in DMF or toluene, where plausible decene isomers were considered in the calculation.[63]

1.6 Research Purpose

In industry, hydrogen of syngas can be produced in a huge amount from steam reforming from methane or other hydrocarbons or partial oxidation of heavy oil. In comparison to H_2, the cost of CO is significant for small companies, especially when CO/H_2 ratios of greater than one are required.[64] Another concern is the purity of the gas, because the purity affects the stability of the hydroformylation catalysts, and conversion and selectivity of aldehydes. In addition, due to the high toxicity of CO, transportation usually uses special equipments. So, these reasons lead to the high price of CO.

Therefore, it is essential to develop a green, safe, easy-to-handle and efficient approach for hydroformylation. In-house solutions based on cheap and less toxic alternatives of syngas or CO, such as formaldehyde and its polymer paraformaldehyde, CO_2, methanol, or formic acid and its methyl ester are attracting more and more attention.[34, 36]

Previous studies on hydroformylation have focused on discovering a highly active rhodium

catalyst system and developing a new phosphine ligand for highly stereoselective reaction and a novel solvent system for efficient catalyst recycling. Another recent progress in this chemistry is the development of a protocol using formaldehyde as a substitute for synthesis gas, from a viewpoint of convenience and safety of the procedure. The procedure without the use of syngas promises to be an accessible alternative to the conventional transformation, because we can avoid using toxic carbon monoxide and explosive hydrogen. Several works on the use of formaldehyde in the hydroformylation, instead of syngas, have been reported (see section 1.4). These finding, indeed, have provided an operationally convenient hydroformylation procedure, however, they have not yet reached a synthetically useful level of the chemical yield and selectivity. My research group also have developed enantioselective hydroformylation reaction of styrenes[45] and linear-selective reaction of 1-alkenes[49] using formaldehyde as a syngas substitute. However, there are still some challenges in the development of the hydroformylation reaction using formaldehyde: the use of substrates containing heteroarenes. In addition, while most investigations have focused on the development of hydroformylation of styrene and its derivatives, vinylheteroarenes as substrates have received less attention. As Scheme 1.29 shown, the heterocyclic compounds are an important framework of drugs and bioactive molecules. The hydroformylation of heteroarenes will offer a convenient and easy method to produce these drugs and bioactive molecules.

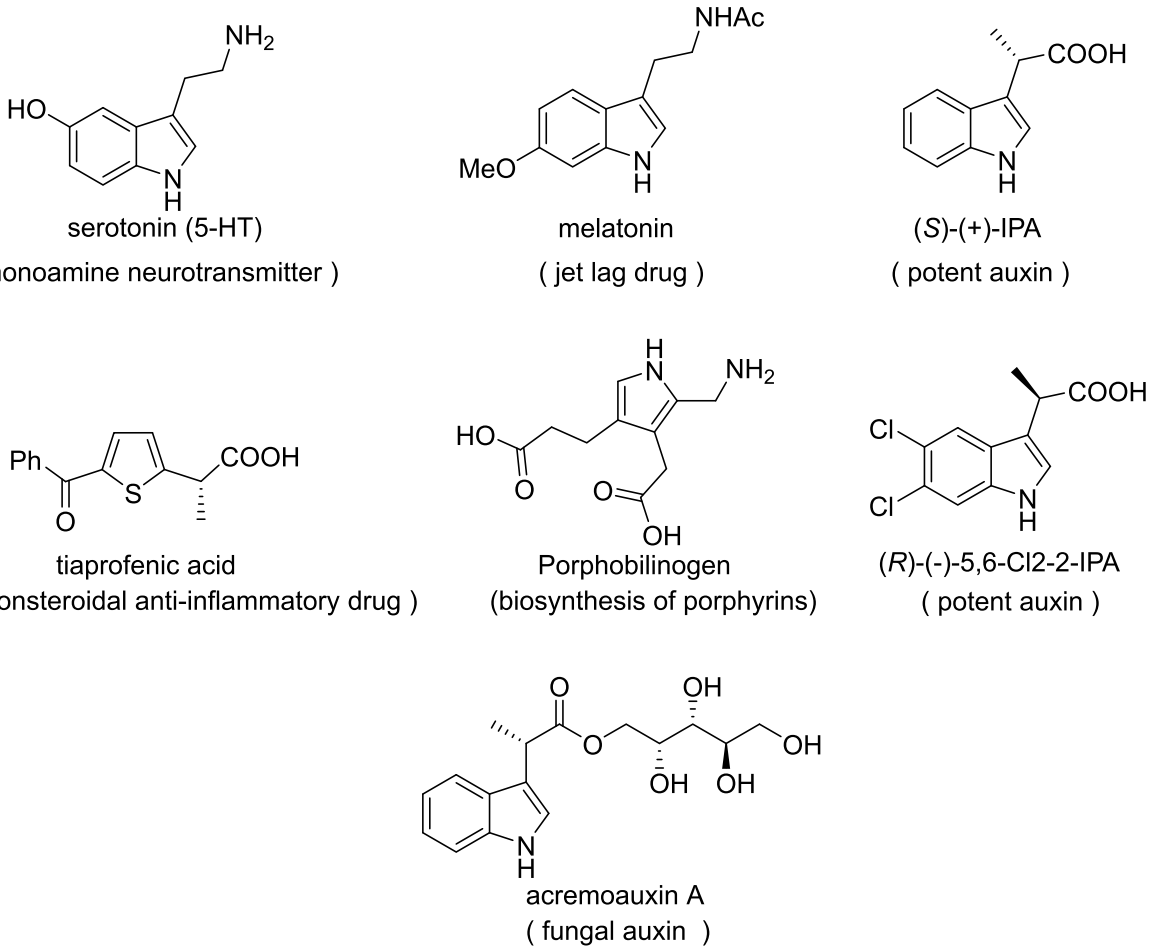

Scheme 1.29 Application of heterocyclic compounds

In this dissertation, rhodium-catalyzed selective hydroformylation of vinylheteroarenes using formaldehyde as a syngas substitute was explored. Because heterocyclic compounds are very important intermediates of some drugs and bioactive molecules, as mentioned above, the investigation on hydroformylation of heteroarenes is an important research target. This dissertation consists of four chapters. In chapter 1, the general introduction is described. In chapter 2, I investigated the linear-selective hydroformylation of vinylheteroarenes using formaldehyde. In chapter 3, I then developed the branched-selective hydroformylation of vinylheteroarenes using formaldehyde. In chapter 4, I summarize the results of my research and take an outlook using formalin.

1.7 References

1. (a) Roelen, O. (Chemische Verwertungsgesselschaft Oberhausen), DE849548, **1938/52**; US2327066 **1943**; (b) Cornils, B., Herrmann, W. A., & Rasch, M. *Angew. Chem. Int. Ed.* **1944**, *33*, 2144-2163.

2. Naqvi, S. *Oxo Alcohols. Process Economics Program Report 21E.* **2010**.

3. (a) Van Leeuwen, P. W. & Carmen, C. eds. *Rhodium-catalyzed hydroformylation*. Vol. 22. Springer Science & Business Media, **2002**; (b) Taddei, M. & André, M. eds. *Hydroformylation for organic synthesis*. Springer, **2013**; (c) Börner, A. & Robert, F. eds. *Hydroformylation: fundamentals, processes, and applications in organic synthesis*. John Wiley & Sons, **2016**; (d) Cornils, B. eds. *Applied Homogeneous Catalysis with Organometallic Compounds: A Comprehensive Handbook in Four Volumes*. Vol. 4. John Wiley & Sons, **2017**; (e) Claver, C. eds. *Rhodium Catalysis*. Springer, **2018**.

4. For review, see: (a) Beller, M., Cornils, B., Frohning, C. D., & Kohlpaintner, C. W. *J. Mol. Catal. A–Chem*. **1995**, *104*, 17-85; (b) Agbossou, F., Carpentier, J. F., & Mortreux, A. *Chem. Rev.* **1995**, *95*, 2485-2506; (c) Breit, B., & Seiche, W. *Synthesis*, **2001**, 1-36. (d) Breit, B. *Acc. Chem. Res.* **2003**, *36*, 264-275; (d) Diéguez, M., Pàmies, O., & Claver, C. *Tetrahedron: Asymmetry* **2004**, *15*, 2113-2122; (e) Nozaki, K. *Chem. Rec.* **2005**, *5*, 376-384; (f) Klosin, J. & Landis, C. R. *Acc. Chem. Res.* **2007**, *40*, 1251-1259; (g) Gual, A., Godard, C., Castillón, S., & Claver, C. *Tetrahedron: Asymmetry* **2010**, *21*, 1135-1146; (h)

Franke, R., Selent, D., & Börner, A. *Chem. Rev.* **2012**, *112*, 5675-5732; (i) Chen, C., Dong, X. Q., & Zhang, X., *Chem. Rec.* **2016**, *16*, 2674-2686; (j) Brezny, A. C. & Landis, C. R. *Acc. Chem. Res.*, **2018**, *51*, 2344-2354; (k) Phanopoulos, A. & Nozaki, K. *ACS Catal.* **2018**, *8*, 5799-5809.

5. (a) Tietze, L. F. & Uwe B. *Angew. Chem. Int. Ed.* **1993**, *32*, 131-163; (b) Tietze, L. F. *Chem. Rev.* **1996**, *96,* 115-136; (c) Eilbracht, P., Bärfacker, L., Buss, C., Hollmann, C., Kitsos-Rzychon, B. E., Kranemann, C. L., & Schmidt, A. *Chem. Rev.* **1999**, *99*, 3329-3366; (d) Pellissier, H. *Chem. Rev.* **2012**, *113*, 442-524; (e) Bolm, C. & Beller M. eds. *Transition metals for organic synthesis*. Wiley-VCH: Weinheim, **2004**; (f) Beller, M. eds. *Catalytic carbonylation reactions*. Vol. 18. Springer, **2006**.

6. (a) Petricci, E. & Cini, E. *Top. Curr. Chem.* **2013**, *342*, 117-188; (b) Settambolo, A. *Top. Curr. Chem.* **2013**, *342*, 151-186; (c) Bates, R. & Kasinathan, S. *Top. Curr. Chem.* **2013**, *342*, 187-224.

7. Falbe, J., Bredereck, H., Hafner, K., & Müller, E. *Synthesen mit Kohlenmonoxyd*. Springer, **1967**, p21.

8. (a) Hebrard, F. & Kalck, P. *Chem. Rev.* **2009**, *109*, 4272-4282; (b) Pospech, J., Fleischer, I., Franke, R., Buchholz, S., & Beller, M. *Angew. Chem. Int. Ed.* **2013**, *52*, 2852-2872.

9. Pruchnik, F. P. eds. *Organometallic chemistry of the transition elements*. Springer Science & Business Media, **2013**.

10. Frohning, C. D. & Kohlpaintner, C. W. *Applied Homogeneous Catalysis with Organometallic Compounds*, eds. By Comils B. & Herrmann, W. A., Wiley-VCH: Weinheim, **1996**.

11. Lutz, E. F. *J. Chem. Educ.* **1986**, *63*, 202-203.

12. (a) Osborn, J. A., Wilkinson, G., & Young, J. F. *J. Chem. Soc. Chem. Commun.* **1965**, 131-132; (b) Evans, D., Osborn, J. A., & Wilkinson, G. *J. Chem. Soc. A* **1968**, 3133-3142.

13. Rupilius, W. & Orchin, M. *J. Org. Chem.* **1972**, *37*, 936-939.

14. Klähn, M. & Garland, M. V. *ACS Catal.* **2015**, *5*, 2301-2316.

15. Cotton, F. A., Chisholm, M. H., Expanding, D., Housecroft, C. E., Welch, A. J., Cardin, D. J., & Moïse, C. eds. *Metal clusters in chemistry*, Wiley-VHC: Weinheim, **1999**, p616.

16. Wilkinson, G., Stone, F. G. A., & Abel, E. W. eds. *Comprehensive organometallic chemistry*. Pergamon, **1982**, p763.

17. Li, C., Widjaja, E., & Garland, M. *J. Am. Chem. Soc.* **2013**, *125*, 5540-5548.

18. (a) Li, C., Chen, L., & Garland, M. *Adv. Synth. Catal.* **2008**, *350*, 679-690; (b) Li, C., Cheng, S., Tjahjono, M., Schreyer, M., & Garland, M. *J. Am. Chem. Soc.* **2010**, *132*, 4589-4599.

19. Kamer, P. C. & Van Leeuwen, P. W. eds. *Phosphorus (III) ligands in homogeneous catalysis: design and synthesis*, John Wiley & Sons, **2012**.

20. Van Rooy, A., Burgers, D., Kamer, P. C., & Van Leeuwen, P. W. *Recl. Trav. Chim. Pays–Bas*, **1996**, *115*, 492-498.

21. Herrmann, W. A. & Koecher, C. *Angew. Chem. Int. Ed.* **1997**, *36*, 2162-2187.

22. Rosales, M., Chacón, G., González, A., Pacheco, I., Baricelli, P. J., & Melean, L. G. *J. Mol. Catal. A: Chem.* **2008**, *287*, 110-114, and references cited therein.

23. Keiichi, S., Kawaragi, Y., Takai, M., & Ookoshi, T. (to Mitsubishi Kasei) EP Pat. 518241, **1992**; *Chem. Abstr.* **1993**, *118*, 191183.

24. (a) Yan, Y., Zhang, X., & Zhang, X. *J. Am. Chem. Soc.* **2006**, *128*, 16058-16061; (b) Yu, S., Chie, Y. M., Guan, Z. H., & Zhang, X. *Org. Lett.* **2008**, *10*, 3469-3472; (c) Yu, S., Chie, Y. M., Guan, Z. H., Zou, Y., Li, W., & Zhang, X. *Org. Lett.* **2008**, *11*, 241-244; (d) Yu, S., Zhang, X., Yan, Y., Cai, C., Dai, L., & Zhang, X. *Chem. –Eur. J.* **2010**, *16*, 4938-4943; (e) Wei, B., Chen, C., You, C., Lv, H., & Zhang, X. *Org. Chem. Fron.* **2017**, *4*, 288-291.

25. Heck, R. F. *Acc. Chem. Res.***1969**, *2*, 10-16.

26. Evans D., Yagupsky G., & Wilkinson G. *J. Chem. Soc. A* **1968**, 2660-2665.

27. Kamer, P. C., Van Rooy, A., Schoemaker, G. C., & Van Leeuwen, P. W. *Coord. Chem. Rev.* **2004**, *248*, 2409-2424.

28. Van der Veen, L. A., Boele, M. D., Bregman, F. R., Kamer, P. C., Van Leeuwen, P. W., Goubitz, K., & Bo, C. *J. Am. Chem. Soc.* **1998**, *120*, 11616-11626.

29. Van der Veen, L. A., Keeven, P. H., Schoemaker, G. C., Reek, J. N., Kamer, P. C., Van Leeuwen, P. W., & Spek, A. L. *Organometallics* **2000**, *19*, 872-883.

30. Deutsch P. P. & Eisenberg R. *Organometallics* **1990**, *9*, 709-718.

31. Castellanos-Páez, A., Castillón, S., Claver, C., Van Leeuwen, P. W., & de Lange, W. G. *Organometallics* **1998**, *17*, 2543-2552.

32. Jacobs, I., de Bruin, B., & Reek, J. N. *ChemCatChem*. **2015**, *7*, 1708-1718.

33. Rostrup-Nielsen, J. & Christiansen, L. J. eds. *Concepts in syngas manufacture*, Vol. 10, World Scientific, **2011**.

34. Morimoto, T. & Kakiuchi, K. *Angew. Chem. Int. Ed.* **2004**, *43*, 5580-5588.

35. Odell, L. R., Russo, F., & Larhed, M. *Synlett* **2012**, *23*, 685-698.

36. Wu, L., Liu, Q., Jackstell, R., & Beller, M. *Angew. Chem. Int. Ed.* **2014**, *53*, 6310-6320.

37. Konishi, H., & Manabe, K. *Synlett* **2014**, *25*, 1971-1986.

38. Friis, S. D., Lindhardt, A. T., & Skrydstrup, T. *Acc. Chem. Res.* **2016**, *49*, 594-605.

39. Cao, J., Zheng, Z. J., Xu, Z., & Xu, L. W. *Coordin. Chem. Rev.* **2017**, *36*, 43-53.

40. (a) Beck, C. M., Rathmill, S. E., Park, Y. J., Chen, J., Crabtree, R. H., Liable-Sands, L. M., & Rheingold, A. L. *Organometallics* **1999**, *18*, 5311-5317; (b) Lenges, C. P. & Brookhart, M. *Angew. Chem. Int. Ed.* **1999**, *8*, 3533-3537; (c) Kreis, M., Palmelund, A., Bunch, L., & Madsen, R. *Adv. Synth. Catal.* **2006**, *348*, 2148-2154.

41. Okano, T., Kobayashi, T., Konishi, H., & Kiji, J. *Tetrahedron Lett*. **1982**, *23*, 4967-4968.

42. Ahn, H. S., Han, S. H., Uhm, S. J., Seok, W. K., Lee, H. N., & Korneeva, G. A. *J. Mol. Catal. A: Chem.* **1999**, *144*, 295-306.

43. Rosales, M., González, A., González, B., Moratinos, C., Pérez, H., Urdaneta, J., &

Sánchez-Delgado, R. A. *J. Organomet. Chem.* **2005**, *690*, 3095-3098.

44. Rosales, M., Arrieta, F., Baricelli, P., González, Á., González, B., Guerrero, Y., & Urdaneta, J. *Catal. Lett.* **2008**, *126*, 367-370.

45. Makado, G., Morimoto, T., Sugimoto, Y., Tsutsumi, K., Kagawa, N., & Kakiuchi, K. *Adv. Synth. Catal.* **2010**, *352*, 299–304.

46. Cini, E., Airiau, E., Girard, N., Mann, A., Salvadori, J., & Taddei, M. *Synlett* **2011**, 199-202.

47. Uhlemann, M., Doerfelt, S., & Börner, A. *Tetrahedron Lett.* **2013**, *54*, 2209-2211.

48. Ren, H. & Wulff, W. D. *Org. Lett.* **2013**, *15*, 242-245.

49. Morimoto, T., Fuji, T., Miyoshi, K., Makado, G., Tanimoto, H., Nishiyama, Y., & Kakiuchi, K. *Org. Biomol. Chem.* **2015**, *13*, 4632-4636;

50. Fuentes, J. A., Pittaway, R., & Clarke, M. L. *Chem. –Eur. J.* **2015**, *21*, 10645-10649.

51. Sasaki, Y., Hagihara, K., Watanabe, T., & Saito, M. *Chem. Lett.* **1994**, 1391-1394.

52. (a)Tominaga, K. I. & Sasaki, Y. *Catal. Commun.* **2000**, *1*, 1-3; (b) Liu, Q., Wu, L., Fleischer, I., Selent, D., Franke, R., Jackstell, R., & Beller, M. *Chem. –Eur. J.* **2014**, *20*, 6888-6894.

53. Shiizaki, S., Nagashima, I., Matsumura, Y., & Haruta, M. *Catal. Lett.* **1998**, *56*, 227-230.

54. Behr, A., Kanne, U., & Keim, W. *J. Mol. Catal.* **1986**, *35*, 19-28.

55. Strauss, S. H., Whitmire, K. H., & Shriver, D. F. *J. Organomet. Chem.* **1979**, *174*, C59-C62.

56. Somasunderam, A. & Alper, H. *J. Mol. Catal.* **1994**, *92*, 35-40.

57. (a) Lee, J. S., Kim, J.C., & Kim, Y. G. *Appl. Catal.* **1990**, *57*, 1-30.

58. (a) Jenner, G., Nahmed, E. M., & Libs-Konrath, S. *J. Mol. Catal.* **1991**, *64*, 337-347; (b) Jenner, G. *Tetrahedron Lett.* **1991**, *32*, 505-508.

59. Van Rooy, A., de Bruijn, J. N., Roobeek, K. F., Kamer, P. C., & Van Leeuwen, P. W. *J. Organomet. Chem.* **1996**, *507*, 69-73.

60. (a) Lee, C. W. & Alper, H. *J. Org.Chem.* **1995**, *60*, 499-503; (b) Clarke, M. L. & Roff, G. J. *Chem. –Eur. J.* **2016**, 12, 7978-7986; (c) Clarke, M. & Roff, G. J. *Green Chem.* **2007**, *9*, 792-796; (d) Sun, X., Frimpong, K., & Tan, K. L. *J. Am. Chem. Soc.* **2010**, *132*, 11841-11843.

61. (a) Breit, B. eds. *Aldehydes: synthesis by hydroformylation of alkenes.* In *Science of synthesis*. Vol. 25, Thieme: Stuttgart, **2007**, 277-317; (b) Van Leeuwen, P. W. eds. *Homogeneous catalysis: understanding the art*. Springer Science & Business Media, **2004**.

62. Paciello, R., Siggel, L., Kneuper, H. J., Walker, N., & Röper, M. *J. Mol. Catal. A: Chem.* **1999**, *143*, 85-97.

63. Jörke, A., Seidel-Morgenstern, A., & Hamel, C. *Chem. Eng. J.* **2015**, *260*, 513-523.

64. Cornils, B., Herrmann, W. A., & Rasch, M. *Angew. Chem. Int. Ed.* **1994**, *33*, 2144 -2163.

Chapter 2 Linear-selective Hydroformylation of Vinylheteroarenes

2.1 Introduction to Linear-selective Hydroformylation

In contrast to branched-selective hydroformylation, steric effects play an import role in the rate and selectivity of the linear-selective hydroformylation reaction.[1] Since the discovery of PPh_3 as a metal-stabilizing ligand in the hydroformylation, new phosphorus ligands have been developed with specific properties in terms of regioselectivity. In the early mechanistic study of hydroformylation using PPh_3 as a ligand,[2] the key role of intermediate species **V** (see section 1.3, L = PPh_3) containing two triphenylphosphines for obtaining a high selectivity to linear products has been recognized. For monodentate ligands, Tolman's cone-angle θ (Scheme 1.6) and the electronic parameter χ,[3] which is a measure for the overall effect of electron donating and withdrawing properties of the phosphorus ligand, have a significant influence on the activity and the selectivity of the resulting catalyst system.[4] For bidentate ligands, which provide two coordination centers to the transition metal, so-called bite angle β (Scheme 1.6) determines the selectivity of the formed aldehydes.

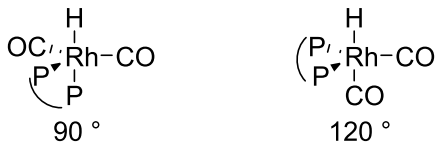

Scheme 2.1 Two configurations of a bidentate phosphorous ligand with rhodium

Van Leeuwen concluded that the equatorial/equatorial configuration (Scheme 1.6), in

particular, imposes high linearity of the formed aldehydes.[5] Thus, the best selectivities to the linear aldehyde species should be obtained when the bite angle has a value of about 120°. The configuration of the ligand in equatorial/axial positions (bite angle 90°) leads to lower linearity of the formed aldehydes (Scheme 2.1). In 2017, they reported an updated data[6] where the linear/branched (*L/B*) ratio increased from 2.6 with DPPE (β_n = 87°) to 99 with NAPHOS (β_n = 123°). An even higher linearity preference (*L/B* = 123) was observed for the BISBI derivative with CF_3 substitution on the aryl rings at phosphorus (Scheme 2.2).

According to these facts, various ligands have been specially designed for introduction of the formyl group at the terminal position of olefin. The wider the natural bite angle the higher the steric hindrance. Therefore, bulky P-ligands have especially attracted much attention as sterically encumbered ligands give rise to reduced accessibility of the metal atom, thereby promoting the formation of linear aldehydes. Bidentate P-ligands are of particular interest. Most linear-selective hydroformylations were achieved based on Biphephos and Xantphos ligands (Scheme 2.3).[1c]

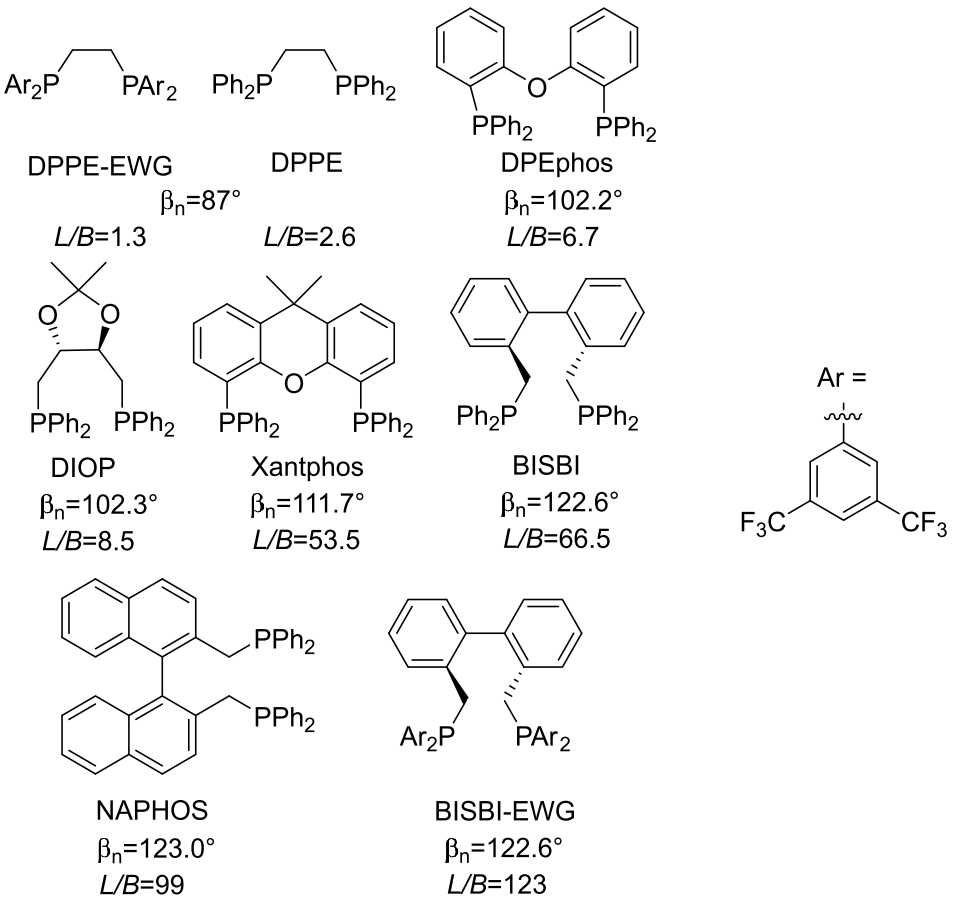

Scheme 2.2 Bite angle effect in the *L/B* ratio using different bisphosphine ligands in the Rh-catalyzed hydroformylation of 1-alkenes

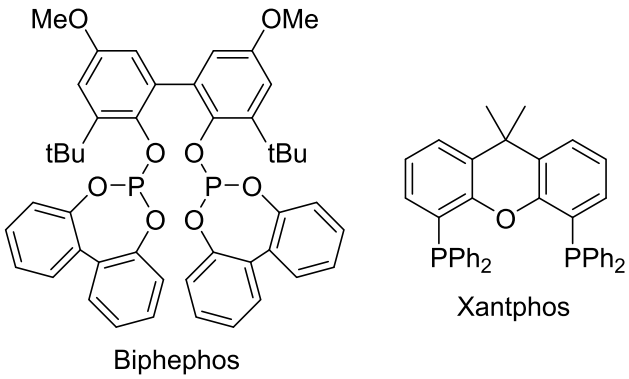

Scheme 2.3 Biphephos and Xantphos

In 1981, Hughes and Unruh were the first to report on diphosphines, unlike the common dppe and dppp, which led to higher *L/B* ratios (5-8) under standard conditions (Scheme 2.4).[7]

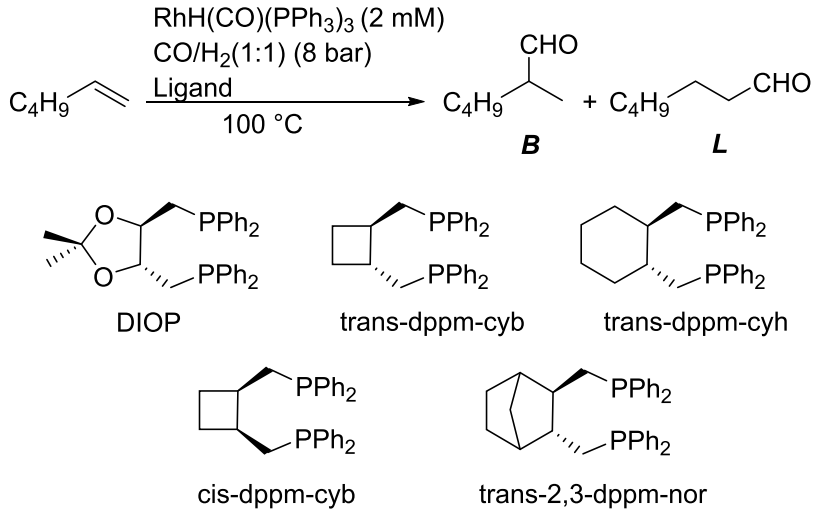

Scheme 2.4 Diphosphine ligands used by Unruh

Up to now, a few examples concerning hydroformylation of styrene toward the linear product exist in the literature.

In 2008, Sémeril and co-workers showed *L/B* ratios of up to 4.5 in the Rh-catalyzed hydroformylation of styrene with calixarene-based diphosphites (Scheme 2.5).[8]

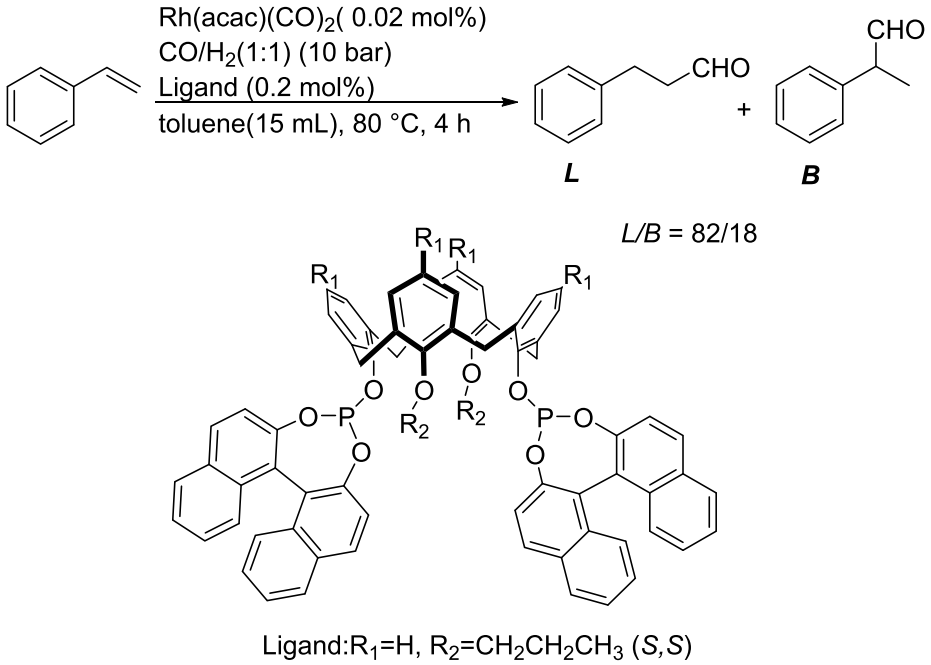

Scheme 2.5 Hydroformylation of styrene with calixarene-based diphosphites

A surprisingly high regioselectivity (*L/B* = up to 22) in hydroformylation of styrene using Rh complex with tetraphosphorus ligand was reported by Zhang'group in 2009 (Scheme 2.6).[9]

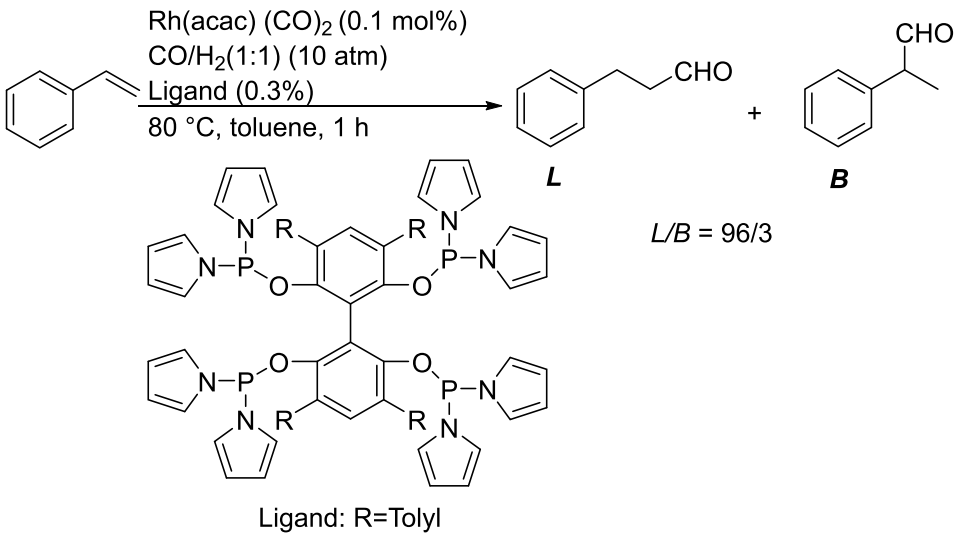

Scheme 2.6 A highly linear-selective hydroformylation of styrene

Recently, my group reported on the highly linear-selective hydroformylation of 1-alkenes using formaldehyde as a syngas substitute.[10] The high regioselectivity (*L/B* = up to 98/2) and efficiency (up to 95%) can be attributed to the simultaneous use of two types of phosphanes as ligands. Two rhodium species associated with each phosphane separately catalyzed the decarbonylative decomposition of formaldehyde to a CO moiety and hydrogen, and the hydroformylation of 1-alkenes.

In this chapter, based on this work, I explored to extend the scope of substrates from vinylarenes to vinylheteroarenes using formalin. Up to now, a few examples, as above mentioned, were reported. However, no linear-selective hydroformylation of vinylheteroarenes using formaldehyde was reported. Hence, it is very meaningful to study.

2.2 Results and Discussion

2.2.1 Optimization of reaction

I first examined the effect of ratio BIPHEP/Nixantphos in the Rh-catalyzed hydroformylation

of styrene, which was selected as a reaction model, with formalin under the modified conditions of the previous report of my group: styrene (1 mmol), formalin (37%; 0.37 mL, 5 mmol), $[RhCl(cod)]_2$ (0.005 mmol), ligands (0.012 mmol), toluene (3 mL), 90 °C, 20 h (Table 2.1).

Table 2.1 Optimization of ratio of BIPHEP/Nixantphos

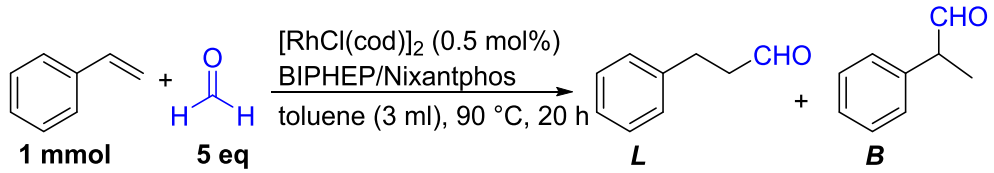

Entry	BIPHEP	Nixantphos	Conv.[a]	Yield[a]	Ratio(*L*/*B*)[a]
1	0.6 mol%	0.6 mol%	93%	93%	68/32
2	0.4 mol%	0.8 mol%	52%	51%	75/25
3	0.3 mol%	0.9 mol%	47%	49%	76/24
4	0.24 mol%	0.96 mol%	43%	35%	77/23
5	0.8 mol%	0.4 mol%	89 %	87 %	64/36
6	0.9 mol%	0.3 mol%	95%	95%	60/40
7	1.2 mol%	-	49%	48%	25/75
8	-	1.2 mol%	35%	1%	100/0

[a]Determined by GC using dodecane as an internal standard.

Under the reported conditions, styrene reacted with formalin to give the corresponding aldehydes in 93% yield with *L*/*B* = 68/32 (Table 2.1, Entry 1). Next, different ratios of BIPHEP/Nixantphos were investigated under these conditions. With increasing the ratio of Nixantphos/BIPHEP from 1/1 to 4/1, the reaction gave the improved the *L*/*B* ratio from 68/32 to 77/23 (Table 2.1, Entries 1-4). However, there was a huge drop in the conversion (from 93% to 43%) and yield (from 93% to 35%). In contrast, with increasing the ratio of

BIPHEP/Nixantphos from 1/1 to 3/1, the reaction gave the slightly decreased the *L/B* ratio from 68/32 to 60/40 (Table 2.1, Entries 1, 5 and 6). The conversion and yield also slightly decreased (Table 2.1, Entry 5). Interestingly, when BIPHEP/Nixantphos ratio = 3/1 was used, the conversion and yield showed a slight rise (Table 2.1, Entry 6). When only BIPHEP was used as ligand, the aldehydes (*L/B* = 25/75) were obtained (Table 2.1, Entry 7) with moderate conversion and yield. Compared to BIPHEP, Nixantphos as single ligand resulted in only linear aldehyde in very low yield (Table 2.1, Entry 8). In the previous work,[10] it showed that BIPHEP was responsible for decarbonylation, meanwhile, Nixantphos was responsible for hydroformylation. In the carbonylation process, under the excessive Nixantphos conditions, the rate of formation of Rh(CO)(BIPHEP) species is so slow that the carbonyl moiety is not enough for the formation of RhH(CO)(Nixantphos) species to produce linear aldehyde in hydroformylation process. It results in low conversion and yield. On the other hand, under the excessive BIPHEP conditions, it promotes both the decarbonylation and hydroformylation process. Because BIPHEP is usually used for branched-selective hydroformylation, therefore, the usage of BIPHEP would form a small amount of RhH(CO)(BIPHEP) species in the hydroformylation process to lead to a small amount of branched aldehyde. The *L/B* ratio could be influenced by it. The detail is described in section 2.3.

As a result, the BIPHEP/Nixantphos = 1/1 is the best choice for linear-selective hydroformylation.

Taking the temperature into consideration, the effect of temperature was examined (Table 2.2) under the following conditions: styrene (1 mmol), formalin (37%; 0.37 mL, 5 mmol), $[RhCl(cod)]_2$ (0.005 mol), BIPHEP (0.006 mol), Nixantphos (0.006 mol), toluene (3 mL), 80-120 °C, 20 h.

Table 2.2 Optimization of temperature

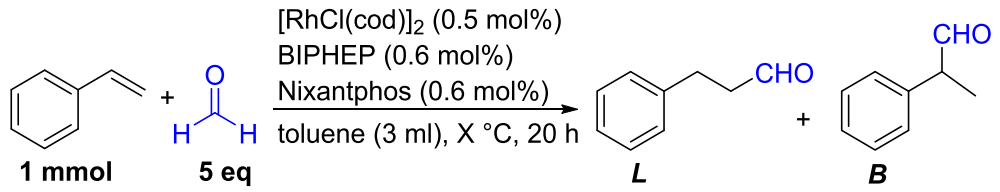

Entry	Temperature	Conv.[a]	Yield[a]	Ratio(*L*/*B*)[a]
1	80 °C	56%	50%	70/30
2	90 °C	93%	95%	68/32
3	100 °C	89%	86%	68/32
4	120 °C	90%	86%	71/29
5[b]	90 °C	52%	52%	73/27
6[b]	100 °C	58%	58%	75/25

[a]Determined by GC using dodecane as an internal standard.

[b]BIPHEP 0.4 mol%, Nixantphos 0.8 mol%

With the increasing temperature, ranging from 80 °C to 120 °C, the temperature had almost no effect on the *L/B* ratio although the *L/B* ratio increased slightly from 73/27 to 71/29 (Table 2.2, Entries 1-4). In particular, between 90 °C and 100 °C, the *L/B* ratios were kept the same. However, when BIPHEP/Nixantphos = 1/2 was used, the *L/B* ratio increased from 73/27 to 75/25 at 100 °C (Table 2.2, Entries 5 and 6). It indicates the higher ratio of Nixantphos/BIPHEP

contributes to forming linear aldehyde at 100 °C.

As mentioned in Section 2.1, the wide bite angle and large steric hindrance are beneficial to the formation of linear aldehyde. Hence, the wide bite angle ligands and bulk ligands were investigated (Table 2.3) at 100 °C.

Table 2.3 Optimization of ligands

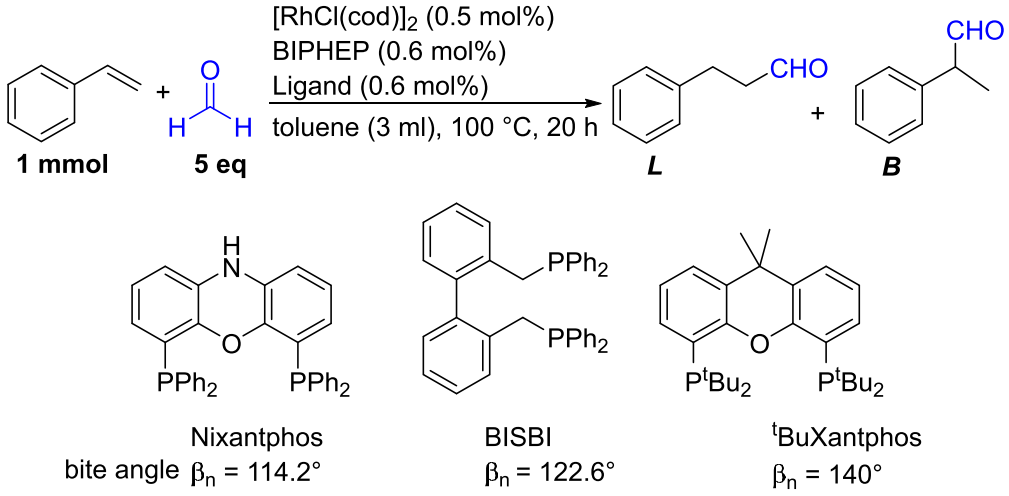

Entry	Ligand	β_n	Conv.[a]	Yield[a]	Ratio(*L*/*B*)[a]
1	Nixantphos	114.2°	89%	86%	68/32
2	BISBI	122.6°	36%	23%	48/52
3	^{t}BuXantphos	140°	19%	8%	38/62

[a]Determined by GC using dodecane as an internal standard.

I had attempted to increase the bite angle or steric hindrance to improve the *L*/*B* ratio, therefore the BISBI and ^{t}BuXantphos were served as ligands. To my disappointment, the BISBI and ^{t}BuXantphos ligand gave the lower *L*/*B* ratio with dramatic decreased conversion and yield (Table 2.3, Entries 1-3). Ligands with too large bite angle could not participate in hydroformylation process due to steric hindrance. In these cases, only BIPHEP is involved in

two processes. Hence, Nixantphos is a better ligand.

Next, the amount of formaldehyde was also investigated in the presence of BIPHEP and Nixantphos (1/1) (Table 2.4).

Table 2.4 Optimization of the amount of formalin

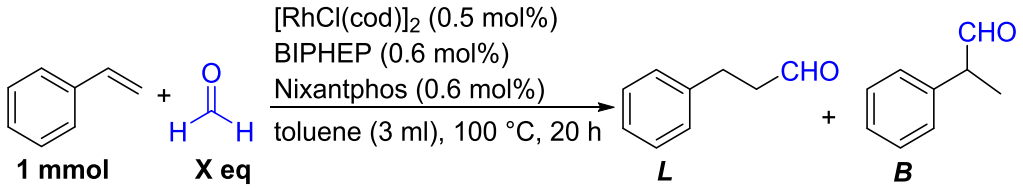

Entry	Formalin	Conv.[a]	Yield[a]	Ratio(*L*/*B*)[a]
1	2 eq.	78%	82%	70/30
2	5 eq.	89%	86%	68/32
3	10 eq.	83%	89%	67/33

[a]Determined by GC using dodecane as an internal standard.

I had attempted to reaction with less amount of formalin. When the amount of formalin was decreased from 5.0 eq. to 2.0 eq. to that of styrene, although the *L/B* ratio increased from 68/32 to 70/30, lower conversion and yield were obtained (Table 2.4, Entry 2). The more equivalent of formalin gave decreased slightly *L/B* ratio (Table 2.4, Entry 3). Hence, the 5.0 eq. to that of the starting material compound was best.

The concentration is also an important factor in the reaction. The influence of concentration was investigated (Table 2.5).

Table 2.5 Optimization of concentration

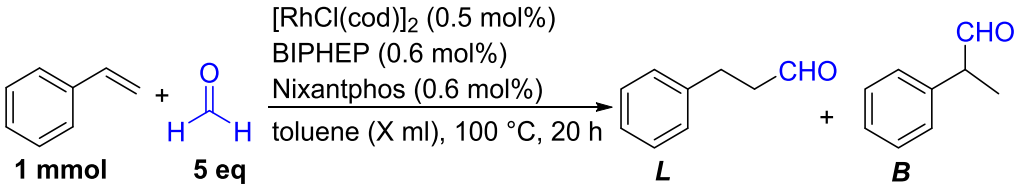

Entry	Toluene	Conv.[a]	Yield[a]	Ratio(*L*/*B*)[a]
1	1 ml	>99%	90%	73/27
2	3 ml	89%	86%	68/32
3	5 ml	78%	73%	68/32

[a]Determined by GC using dodecane as an internal standard.

When the reaction was carried out in 1 ml toluene, the conversion was almost 100%. However, the yield of aldehydes was low due to the formation of a small amount of hydrogenated styrene. Compared with the reaction in 3 ml toluene, the reaction in 5 ml toluene gave the low conversion and yield with constant *L*/*B* ratio.

Considering the low conversion and yield using BIPHEP/Nixantphos = 1/1, the effect of the ratio of BIPHEP and Nixantphos was examined (Table 2.6) in presence of 1.0 mol% $[RhCl(cod)]_2$.

Table 2.6 Optimization of the ratio of BIPHEP/Nixantphos in the presence of 1 mol% $[RhCl(cod)]_2$

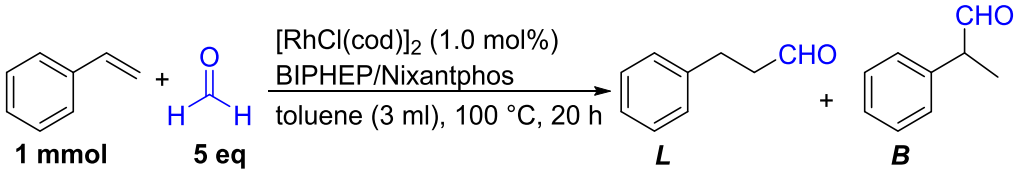

Entry	BIPHEP	Nixantphos	Conv.[a]	Yield[a]	Ratio(*L*/*B*)[a]
1	1.2 mol%	1.2 mol%	>99%	98%	54/46

2	0.8 mol%	1.6 mol%	>99%	98%	59/41
3	0.6 mol%	1.8 mol%	>99%	97%	71/29
4	0.48 mol%	1.92 mol%	87%	82%	75/25

[a]Determined by GC using dodecane as an internal standard.

As I expected, the conversion and yield had a significant increase from 86% to 98% (Table 2.6, Entry 1), whereas a lower *L/B* ratio was observed. Then the various BIPHEP/Nixantphos ratios were studied. With increasing Nixantphos/BIPHEP ratio (1/1 to 3/1), the *L/B* ratio increased accordingly. Meanwhile, the conversion and yield were at high level (Table 2.6, Entries 2 and 3). When BIPHEP/Nixantphos = 1/3 was used, the best *L/B* ratio was achieved (Table 2.6, Entry 4). However, excessive Nixantphos (more than Nixantphos/BIPHEP = 3/1) gave the inhibited reaction (Table 2.6, Entry 4).

2.2.2 Hydroformylation of 2-vinylbenzothiophene

Based on the above results, I next investigated the hydroformylation of vinylheteroarenes. At first, 2-vinylbenzothiophene was used as the substrate, and the best ratio of BIPHEP/Nixantphos (1/3) was also obtained (Table 2.7). The linear and branched aldehydes were obtained with *L/B* = 93/7 in 58% yield. The simultaneous use of (*R*)-BINAP and Xantphos in the same ratio gave similar linear selectivity. However, the yield was somewhat lower (Table 2.7, Entry 5).

Table 2.7 Optimization of the ratio of BIPHEP/Nixantphos using 2-vinylbenzothiophene [a]

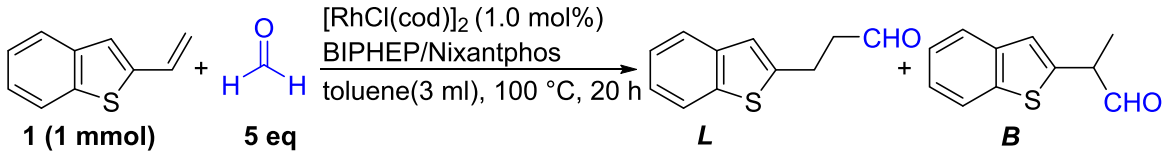

1 (1 mmol) 5 eq *L* *B*

Entry	BIPHEP	Nixantphos	Yield[b]	Ratio(*L*/*B*)[b]
1	1.2 mol%	1.2 mol%	57%	65/35
2	0.8 mol%	1.6 mol%	58%	85/15
3	0.6 mol%	1.8 mol%	58%	93/7
4	0.48 mol%	1.92 mol%	57%	83/17
	(*R*)-BINAP	**Xantphos**		
5	0.6 mol%	1.8 mol%	49%	94/6

[a]Conditions: **1** (1 mmol), formalin (37%; 0.37 mL,5 mmol), [RhCl(cod)]2 (0.01 mmol), ligands (0.024 mmol), toluene (3 mL), 100 °C, 20 h.

[b]Yields of isolated product are the sum of L and B, ratios (*L*/*B*) were determined by ^{1}H NMR of the crude reaction mixture.

As the results were described, the standard conditions were the following conditions: substrate (1 mmol), formalin (37 wt% aqueous solution, 0.19 mL, 5 mmol), $[RhCl(cod)]_2$ (0.01 mol), BIPHEP (0.006 mmol), Nixantphos (0.018 mmol) in toluene (3 mL) at 100 °C for 20 h.

2.2.3 Substrate scope

With the standard conditions in hand, then the scope of hydroformylation of vinylheteroarenes was explored (Scheme 2.8).

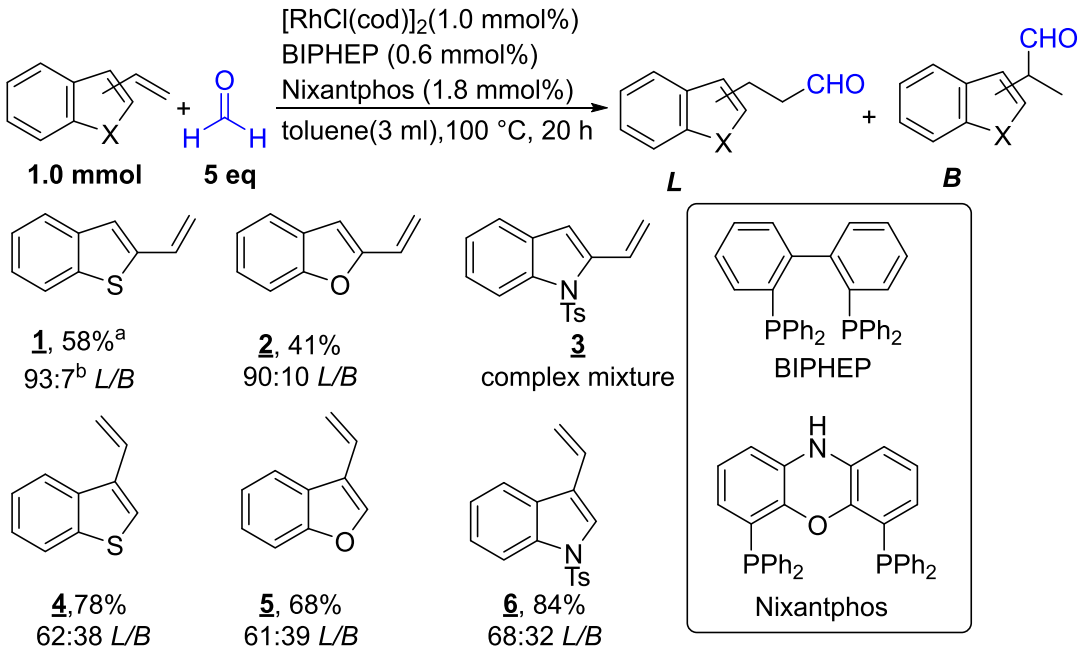

Reactions were performed on a 1 mmol scale at 100 °C in 3 ml toluene with substrate/Rh =100:1, BIPHEP: Rh = 0.6 : 1, Nixantphos : Rh = 1.8 : 1, 5 eq formaldehyde (37 wt% aqueous solution), and a reaction time of 20 hours.[a] Isolated yield, [b]Determined by ^{1}H NMR analysis of crude reaction mixtures.

Scheme 2.8 Scope of linear-selective hydroformylation

As shown in Scheme 2.8, the substrates containing the heteroatom (O, S, NTs) were performed in the hydroformylation using formaldehyde, affording the corresponding linear and branched aldehydes. When vinyl substituted benzothiophene (**1** and **4**) and benzofuran (**2** and **5**) were used as substrates, the reaction for the vinyl group at the 2-position proceeded very smoothly. The 2-vinyl substrates (**1** and **2**) gave the linear aldehydes with very high *L/B* ratio (up to 93/7) in moderate yield. In fact, due to the loss of separation, the actual yield should be higher. On the contrary, the 3-vinyl substrates (**4** and **5**) gave the moderate *L/B* ratio in higher yields. The yields depend on the stability of the products. It was noteworthy that the reaction afforded the aldehydes (branched and linear) in 84% yield with 68/32 selectivity when 3-vinyl

indole **6** was used as the substrate. However, because of instability of 2-vinyl indole, this reaction gave a complex mixture. The selectivity of 3-vinyl substituted substrates was similar to that of styrene. The high yield was obtained when 3-vinylindole was applied to this reaction. It also showed that the products (linear and branched) of 3-vinylindole were more stable than other substrates under the experimental conditions. The reason for different ratio between 2- and 3-vinyl substrates was described in the following section.

2.3 Mechanistic Speculation

In the previous work of my group,[10] ^{31}P NMR experiments implied that two rhodium species, RhCl(CO)(*R*)-BINAP) and $RhH(CO)_2$(Xantphos), participate in the reaction. These two rhodium species, RhCl(CO)((*R*)-BINAP) and $RhH(CO)_2$(Xantphos), would be directly involved in the linear-selective hydroformylation catalysis using formaldehyde in the presence of both BINAP and Xantphos. Similar results were observed in my case (Figure 1). (*R*)-BINAP and Xantphos instead of BIPHEP and Nixantphos, respectively, were used for more easily understanding ^{31}P NMR analysis.

A mixture of $[RhCl(cod)]_2$, (*R*)-BINAP, and Xantphos (in a molar of 1/0.6/1.8) in toluene-d_8 at room temperature showed two NMR signals at δ = 49.5 ppm (d, $J_{P\text{-}Rh}$ = 195.4 Hz) and 2.4 ppm (d, $J_{P\text{-}Rh}$ = 90.7 Hz). These two signals were assigned to $[RhCl((R)\text{-BINAP})]_2$[11] and RhCl(cod)(xantphos),[10] respectively. When the mixture was treated with a large excess (100 eq.) of formaldehyde (formalin), new signals appeared at δ = 45.7 ppm (dd, $J_{p\text{-}p}$ = 44.1 Hz, $J_{P\text{-}}$

$_{Rh}$ = 115.6 Hz), 25.3 ppm (dd, $J_{p\text{-}p}$ = 44.1 Hz, $J_{P\text{-}Rh}$ = 129.2 Hz) as a pair, and 20.7 ppm (d, $J_{P\text{-}Rh}$ = 133.2 Hz), which are assigned to RhCl(CO)((*R*)-BINAP)[10b] and $RhH(CO)_2$(xantphos),[12] respectively. It is noteworthy that no simultaneous coordination of these phosphines to one rhodium center was observed during these reactions. It therefore appears that RhCl(CO)((*R*)-BINAP) and $RhH(CO)_2$(xantphos) are both involved in the present *linear*-selective hydroformylation using formaldehyde. The simultaneous use of BIPHEP and Nixantphos also has a similar role in the catalysis.

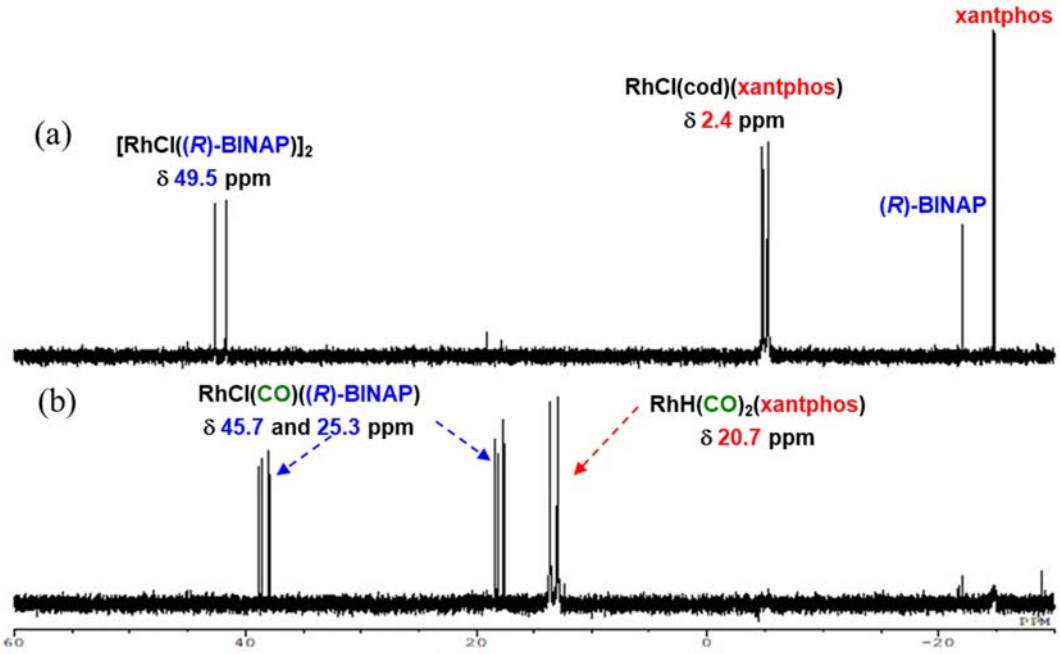

Figure 1. ^{31}P NMR spectra of (a) a mixture of $[RhCl(cod)]_2$, (*R*)-BINAP, and xantphos (molar ratio 1:0.6:1.8) in toluene-d_8 solution and (b) treatment of the mixture with large excess of formaldehyde.

Based on the above result, an acceptable catalytic cycle is as follows. There are two processes involved in the reaction: the decarbonylation of formaldehyde and the subsequent hydroformylation of the vinylheteroarene derivative. The decarbonylation of formaldehyde begins with the oxidative addition of the aldehydic C-H bond of formaldehyde to a rhodium(I)

complex (**A**), followed by the migratory extrusion of the carbonyl group on the rhodium(III) center (**C**)and the subsequent reductive elimination of hydrogen to generate a carbonyl moiety and H_2 (Scheme 2.9a). On the other hand, the vinylheteroarene derivative is hydrorhodated by the Rh(I)-H species (**E**) (Scheme 2.10), which is generated *in situ* from the reaction of a Rh(I)-Cl and H_2, to give the vinylheteroarene coordinated Rh(I) species (**F**), followed by alkene insertion to produce the heteroarylalkyl-Rh(I) complex (**G**). The aldehydes are produced when the formed carbonyl is inserted into the Rh(I)-C bond of **G**, followed by the hydrogenolysis of the acyl complex (**H**) by the formed H_2, accompanied by the regeneration of the Rh-H species (**E**) (Scheme 2.9b). Rh-BINAP and Rh-Xantphos, which were observed in the above ^{31}P NMR experiments, are responsible for the former decarbonylation process of formaldehyde and the latter hydroformylation process, respectively.[10] A similar role-sharing (decarbonylation and hydroformylation) would also function well under catalytic conditions in the presence of BIPHEP and Nixantphos.

(a) Decarbonylation

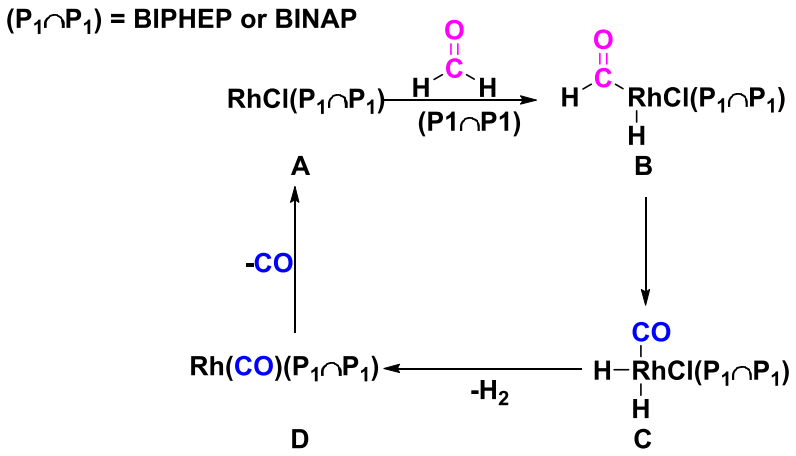

(b) Hydroformylation

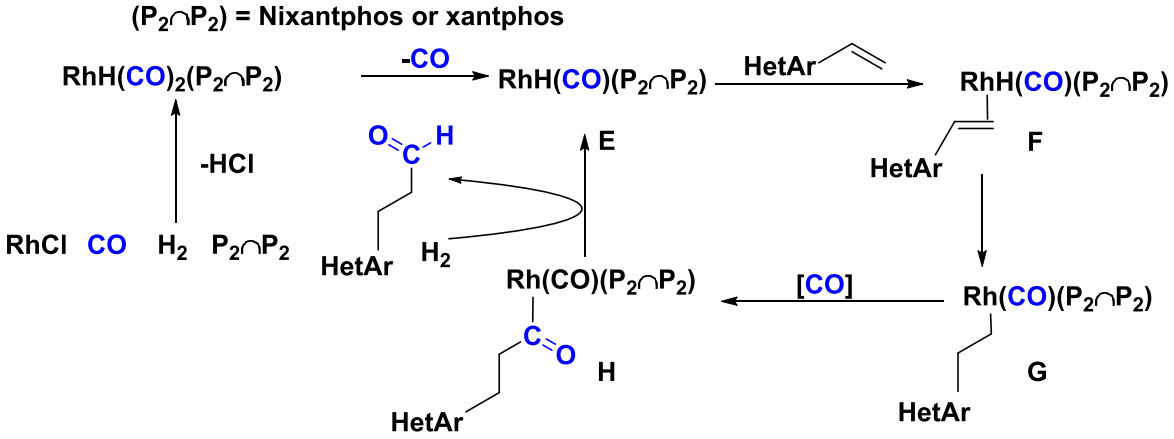

Scheme 2.9 Proposed reaction mechanism for linear selectivity

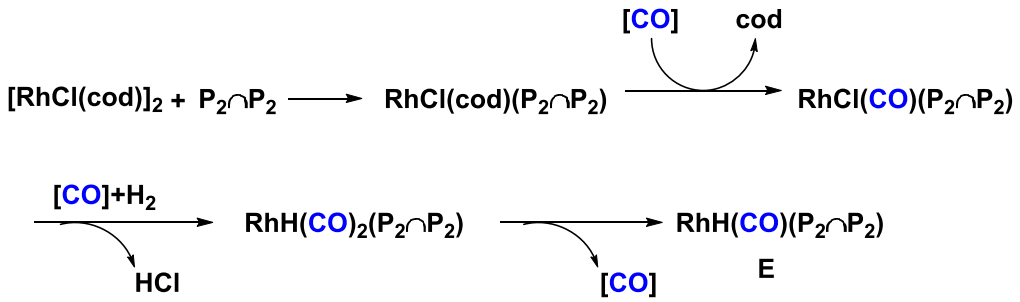

Scheme 2.10 Generation of Rh(I)-H species

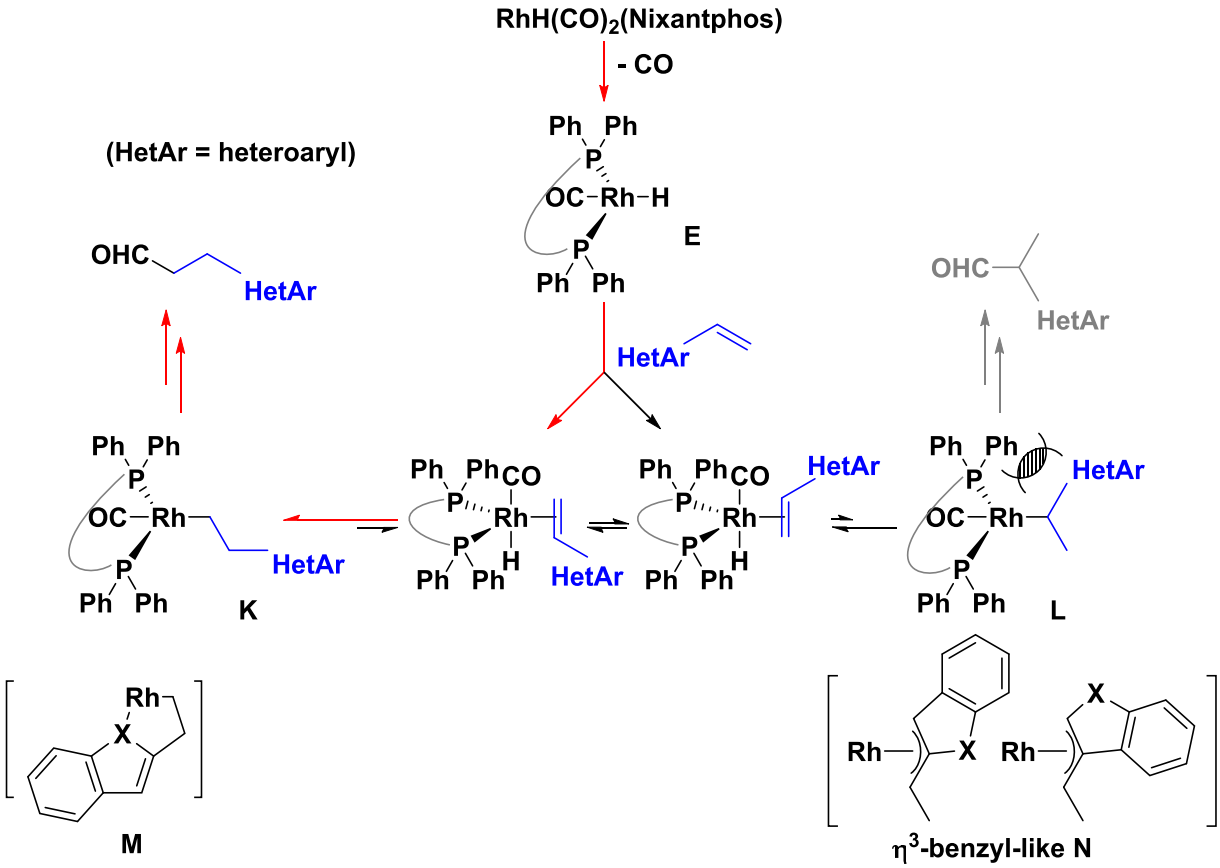

Scheme 2.11 Origin of linear-selectivity

In 2001, Rh-diphosphine catalyzed hydroformylation has been studied by Van Leeuwen's group using an integrated molecular orbital/molecular mechanics method, IMOMM.[13] In this work, they have proved that correlation between bite angles of phosphine lingands and regioselectivity takes place at the point where the regioselectivity is determined: the transition states for alkene insertion. The origin of selectivity of my hydroformylation of vinylheteroarenes can be rationalized as shown in Scheme 2.11. First, the *in situ*-generated Rh-H species adds to a vinylheteroarene to give two types of alkyl-rhodium intermediates (**K**) and (**L**). Complex (**K**) gives rise to the linear aldehyde via the insertion of a carbonyl followed by hydrogenolysis, while (**L**) gives the branched aldehyde. It is likely that the addition manner of

Rh-H that gives rise to the intermediate (**L**) takes place predominantly due to the contribution of η^3-benzyl-like form in (**N**).[8,9,14] On the other hand, steric repulsion between the Ph group on the phosphorous atom of the (Ni)xantphos and the heteroaryl group (*Het*Ar) prevents the formation of intermediate (**L**). In the present catalysis, the steric effects conferred by (Ni)xantphos are superior to the contribution of η^3-benzyl-like intermediate, resulting in predominant formation of the intermediate (**K**), leading to *linear* aldehyde in all of the reactions. In addition, in reactions of 2-vinylheteroarenes, when the heteroatom is at position amenable for ligation to the rhodium center, cyclometalation would be promoted, giving rise to the formation of a stable five-membered metallacycle (**M**). Therefore, it is reasonable to consider that reactions of 2-vinylheteroarenes show a higher regioselectivity (*linear*-selectivity) than the corresponding reaction of 3-vinylheteroarenes.

2.4 Conclusion

In chapter 2, I have developed an approach for highly linear-selective hydroformylation of vinylheteroarenes using formaldehyde. In this work, the high regioselectivity (up to *L*/*B* = 93/7) can be attributed to the simultaneous use of two types of phosphines (BIPHEP and Nixantphos) as ligands to $[RhCl(cod)]_2$ as a catalyst. Rh/BIPHEP complex is responsible for decarbonylation process, while Rh/Nixantphos complex catalyzes the hydroformylation process to yield linear aldehydes with high linear selectivity. Although not all substrates gave the high linear-selectivity, it is also a good green and operational method to synthesize linear aldehydes and its

derivatives. Under such catalytic conditions, reactions of vinylheteroarenes having a vinyl group at the 2-position in the heterocycles produced more *linear*-selectively with formaldehyde than those at the 3-position. In addition, the origin of linear-selectivity was also described.

2.5 References

1. (a) Van Leeuwen, P. W. & Carmen, C. eds. *Rhodium-catalyzed hydroformylation*. Vol. 22. Springer Science & Business Media, **2002**; (b) Taddei, M. & André, M. eds. *Hydroformylation for organic synthesis*. Springer Berlin Heidelberg, **2013**; (c) Börner, A. & Robert, F. eds. *Hydroformylation: fundamentals, processes, and applications in organic synthesis*. John Wiley & Sons, **2016**; (d) Cornils, B. eds. *Applied Homogeneous Catalysis with Organometallic Compounds: A Comprehensive Handbook in Four Volumes*. Vol. 4. John Wiley & Sons, **2017**; (e) Claver, C. eds. *Rhodium Catalysis*. Springer, **2018**.
2. (a) Evans, D., Osborn, J. A., & Wilkinson, G. *J. Chem. Soc. A* **1968**, 3133-3142; (b) Evans D., Yagupsky G., Wilkinson G. *J. Chem. Soc. A* **1968**, 2660-2665; (c) Brown, C. K. & Wilkinson, G. *J. Chem. SOC. A* **1970**, 2753-2764.
3. Bartik, T., Himmler, T., Schulte, H. G., & Seevogel, K. *J. Oganomet. Chem.* **1984**, *272*, 29-41.
4. (a) Tolman, C., Seidel, W. C., & Gosser, L. W. *J. Am. Chem. Soc.* **1974**, *96*, 53-60; (b) Tolman, C. A. *Chem. Rev.* **1977**, *77*, 313-348.
5. (a) Wiese, K. D. & Obst, D. eds. *Hydroformylation. In Catalytic Carbonylation Reactions*. Springer, **2006**, p1-33; (b) Van der Veen, L. A., Kamer, P. C., & Van Leeuwen, P. W. *Cattech*, **2002**, *6*, 116-120; (c) Dieleman, C. B., Kamer, P. C., Reek, J. N., & Van Leeuwen, P. W. *Helv. Chim. Acta*, **2001**, *84*, 3269-3280; (d) Van Leeuwen, P. W., Kamer, P.

C., Van der Veen, L. A., & Reek, J. N. *Chinese J. Chem.* **2001**, *19*, 1-8.

6. Jiao, Y., Torne, M. S., Gracia, J., Niemantsverdriet, J. H., & Van Leeuwen, P. W. *Catal. Sci. Technol.* **2017**, *7*, 1404-1414.
7. Hughes, O. R. & Unruh, J. D. *J. Mol. Catal.* **1981**, *12,* 71-83.
8. Sémeril, D., Matt, D., & Toupet, L. *Chem.–Eur. J.* **2008**, *14*, 7144-7155.
9. Yu, S., Chie, Y. M., Guan, Z. H., Zou, Y., Li, W., & Zhang, X. *Org. Lett.* **2009**, *11*, 241-244.
10. Makado, G., Morimoto, T., Sugimoto, Y., Tsutsumi, K., Kagawa, N., & Kakiuchi, K. *Adv. Synth. Catal.* **2010**, *352*, 299-304.
11. (a) Hayashi, T., Takahashi, M., Takaya, Y., & Ogasawara, M. *J. Am. Chem. Soc.* **2002**, *124*, 5052-5058; (b) Bunten, K. A., Farrar, D. H., Poë, A. J., & Lough, A. *Organometallics* **2002**, *21*, 3344-3350.
12. Kranenburg, M., Van der Burgt, Y. E., Kamer, P. C., Van Leeuwen, P. W., Goubitz, K., & Fraanje, J. *Organometallics* **1995**, *14*, 3081-3089.
13. Carbó, J. J., Maseras, F., Bo, C., & Van Leeuwen, P. W. *J. Am. Chem. Soc.* **2001**, *123*, 7630-7637.
14. (a) Goudriaan, P. E., Kuil, M., Jiang, X. B., Van Leeuwen, P. W., & Reek, J. N. *Dalton Trans.* **2009**, 1801-1805; (b) Boymans, E., Janssen, M., Müller, C., Lutz, M., & Vogt, D. *Dalton Tran.* **2013**, *42*, 137-142; (c) Pignolet, L. M. eds. *Homogeneous catalysis with metal phosphine complexes*. Springer Science & Business Media, **2013**.

Chapter 3 Branched-selective Hydroformylation of Vinylheteroarenes

3.1 Introduction to Branched-selective Hydroformylation

Branched-selective and especially asymmetric hydroformylation are a very potential catalytic reaction that produces chiral aldehydes from inexpensive feedstock (alkenes, syngas) in a single step under mid-reaction conditions. However, several technical challenges should be overcome. The big challenge is to control simultaneously the regio- and enantio-selectivity. Besides, low reaction rates at low temperature and limited substrate scope should also be paid attention.

Highly enantioselective hydroformylation was achieved by chiral metal complexes with a few catalytic systems. The metals in asymmetric hydroformylation are generally Pt(II) and Rh(I).

In 1991, Consiglio and co-workers reported the first highly asymmetric hydroformylation of styrene with up to 86% ee, based on Pt-Sn systems (Scheme 3.1).[1] The Pt-diphosphite/$SnCl_2$ systems also show a little bite low enantioselectivity. When bisphosphite (Scheme 3.2c) is employed, ee values increase up to 91%.[2] The use of rhodium-based catalysts stops the tendency to hydrogenate the substrates.[3]

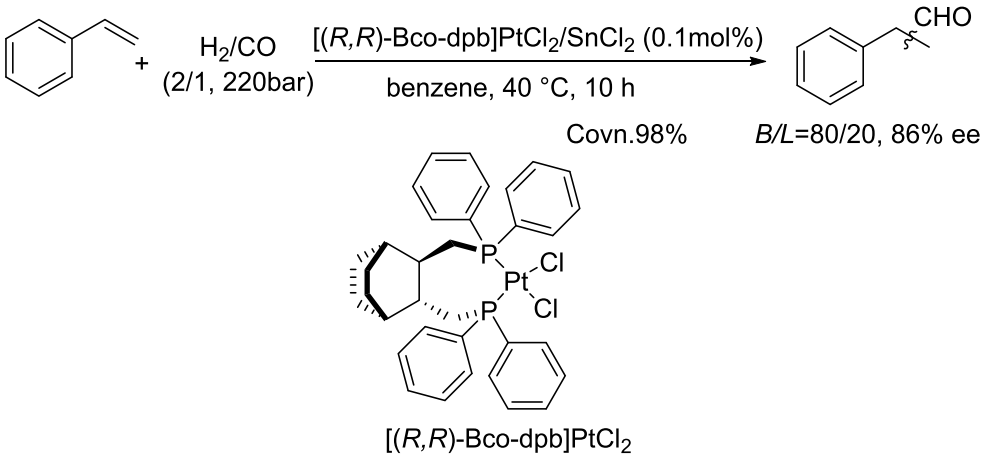

Scheme 3.1 First highly asymmetric hydroformylation of styene

A big breakout of asymmetric hydroformylation is the usage of bulky diphosphites derived from homochiral (2*R*,4*R*)-pentane-2,4-diol, UC-PP***** (Scheme 3.2a) to give chiral aldehydes with up to 90% ee by Babin and Whiteker at Union Carbide Co. Ltd.[4] The bisphosphite ligand (2*R*,4*R*)-chiraphite (R_1=Me, R_2=MeO, UC-PP*****) was the first effective ligand in Rh-catalyzed hydroformylation for the synthesis of anti-inflammatory 2-aryl-propionic acid drugs, such as (*S*)-naproxen.[5] A phosphine-phosphite ligand of C1 symmetry [(*R,S*)-BINAPHOS], discovered by Takaya, has shown 96% ee as well as total conversions and high regioselectivities.[6]

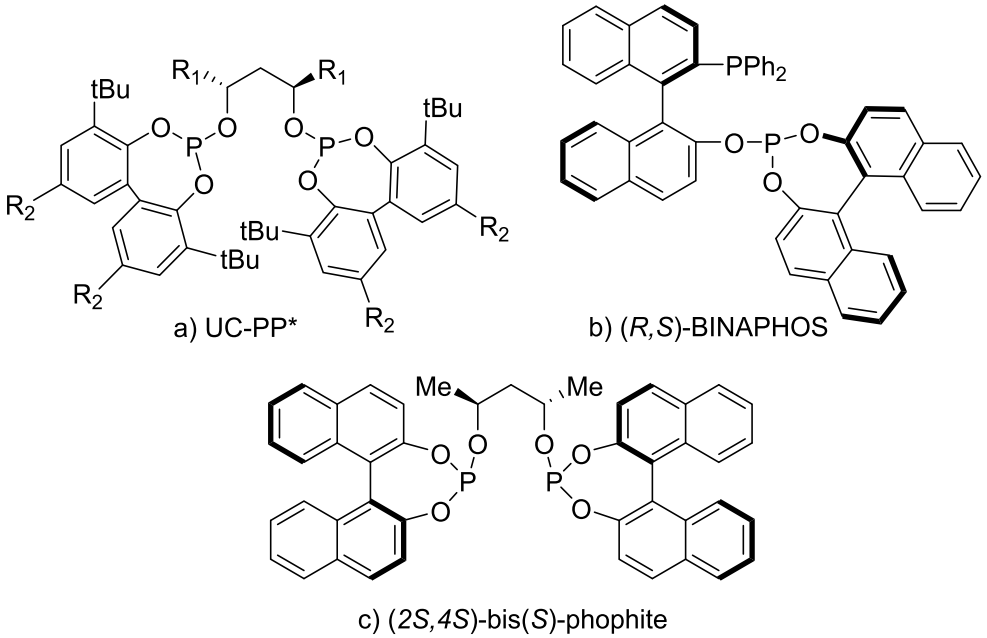

Scheme 3.2 Chiral diphosphites and phosphine-phosphite ligands

Since the discovery of chiraphite, many chiral ligands have been synthesized to apply to extend the scope of substrates. In numerous studies, the α-heteroarenes as substrates have less attention.[7]

In 2007, Nozaki and co-workers[7a] applied a slightly modified (*R,S*)-BINAPHOS [Rh(I)-(*R,S*)-MeO-BINAPHOS] to hydroformylation-oxidation reaction using vinylheteroarenes (vinylfurans and vinylthiophenes) as substrates (Scheme 3.3). The protocol was used for the synthesis of (*S*)-tiaprofenic acid and its derivatives, one of the most popular nonsteroidal anti-inflammatory drugs.

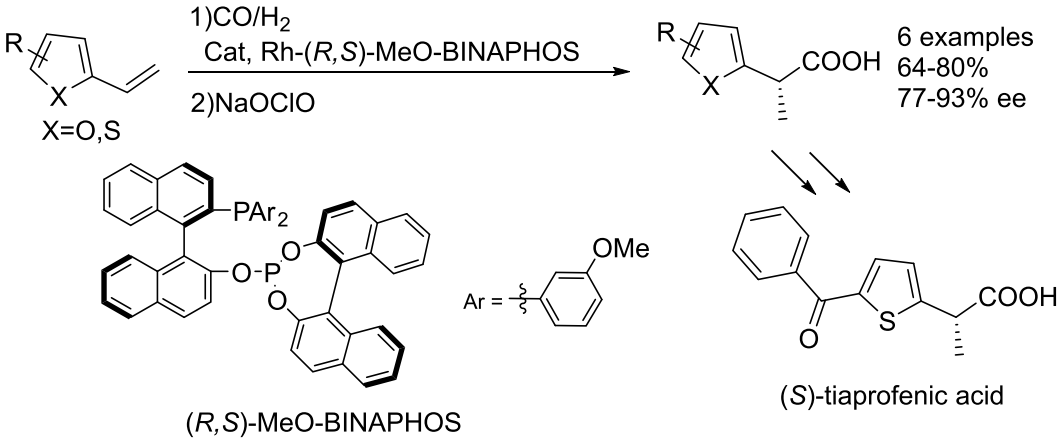

Scheme 3.3 Asymmetric hydroformylation of heteroarenes using syngas

In 2017, Zhang's group[7b] provided a new hybrid phosphine-phosphoramidite ligand to give chiral heteroaryl aldehydes in good yields with high regio- and enantioselectivities (up to 96% ee) using vinylheteroarenes (Scheme 3.4).

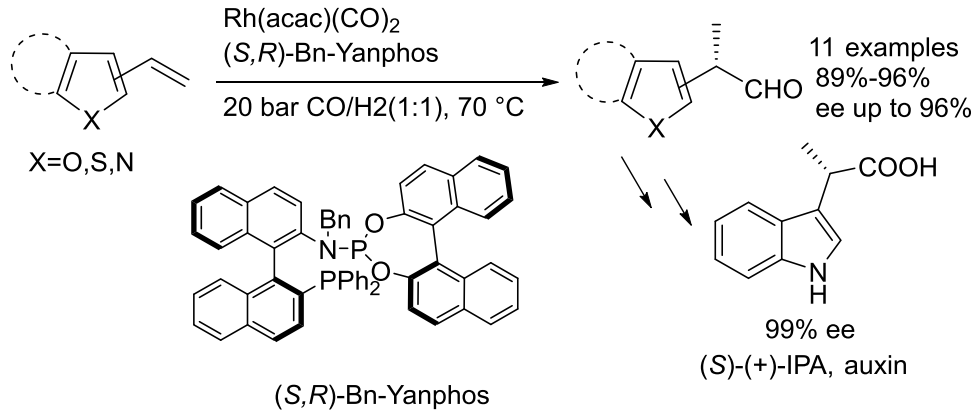

Scheme 3.4 Asymmetric hydroformylation of heteroarenes using new ligand

Recently, my group reported on an accessible protocol for the asymmetric hydroformylation of vinylarenes using formaldehyde as a substitute for syngas.[8] The regioselectivity (*B/L* = up to 96/4) and enantioselectivity (up to 95% ee) can be attributed to the single use of chiral Ph-bpe as a ligand.

In this chapter, based on this work, I explored to extend the scope of substrates from vinyl arenes to vinylheteroarenes using formalin. To the best of my knowledge, the rhodium-

catalyzed hydroformylation of vinylheteroarenes using formaldehyde has not been reported.

3.2 Results and Discussion

3.2.1 Optimization of reaction

I first examined the Rh-catalyzed hydroformylation of 2-vinylbenzothiophene (**1**) with formalin under the modified conditions of the previous report of my group: **1** (1 mmol), formalin (37 wt% aqueous solution, 0.19 mL, 2.5 mmol), $[RhCl(cod)]_2$ (0.005 mol), (*R,R*)-Ph-bpe (0.012 mol) in toluene (4 mL) at 80 °C for 10 h. However, this catalytic system can not work under the previously reported conditions (Table 3.1, Entry 1). I supposed that, due to the low activity of 2-vinyl benzothiophene than styrene, the temperature may be a key factor. Hence, high temperature (100 °C) was investigated (Table 3.1, Entry 2). As I expected, the branched aldehyde was obtained in 59% isolated yield with *B/L* = 95/5 ratio (determined by ^{1}H NMR).

According to the previous work,[9] temperature strongly influences the regioselectivity in the hydroformylation of vinyl substrates. It showed that, in the case of styrene, a strong increase of linear aldehyde in hydroformylation of styrene with increasing temperature was observed (*B*/*L* = 98/2 at 20 °C to 64/36 at 130 °C). For this reason, I also supposed the ratio of rhodium to ligand or amount of rhodium and ligand may result in an improvement of regioselectivity. Next, I conducted the reaction with Rh/ligands=1/4 and 5 eq. formalin (Table 3.1, Entries 3 and 4). When the ratio of Rhodium to (*R,R*)-Ph-bpe = 1/4 was employed, the conversion was 96%, whereas the yield was only 79% with low ee value (21%).

Table 3.1 Hydroformylation using (*R,R*)-Ph-bpe

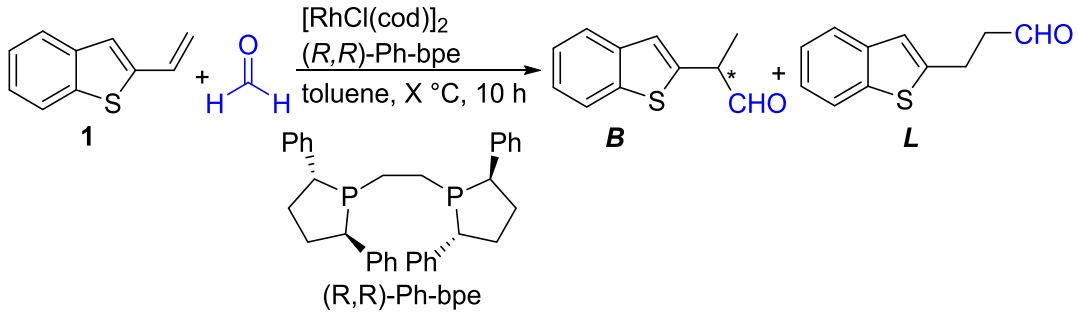

Entry	[Rh]/Ligand	Temp.	Conv.	Yield	ratio(*B*/*L*)	ee
1[a]	1/2.4	80 °C		n.d.		
2[a]	1/2.4	100 °C	-	59% (*B*)	95/5	-
3[b]	1/4	80 °C		n.d.		
4[b]	1/4	80 °C	96%	79%	93/6	21%

[a]conditions: **1** (1 mmol), formalin (37 wt% aqueous solution, 0.19 mL, 2.5 mmol), $[RhCl(cod)]_2$ (0.005 mmol), (*R,R*)-Ph-bpe (0.012 mmol) in toluene (4 mL) for 10 h. Yield was isolated yield. Ratio (*B/L*) was determined by ^1H NMR.

[b]conditions: **1** (0.5 mmol), formalin (37 wt% aqueous solution, 0.19 mL, 2.5 mmol), $[RhCl(cod)]_2$ (0.005 mmol), (*R,R*)-Ph-bpe (0.02 mmol) in toluene (4 mL) for 10 h. ee was determined by HPLC after conversion to alcohol.

n.d.: not detected

Next, various bidentate phosphine ligands for developing the regioselectivity and enantioselectivity were investigated, such as BINAP, SEGPHOS, DIFLUROPHOS, and so on (Table 3.2 and Scheme 3.5). The reactions were carried out under the followed conditions: **1** (0.5 mmol), formalin (37 wt% aqueous solution, 0.19 mL, 2.5 mmol), $[RhCl(cod)]_2$ (0.005 mmol), ligand (0.02 mmol) in toluene (4 mL) at 80 °C for 20 h.

Table 3.2 Optimization of Ligands

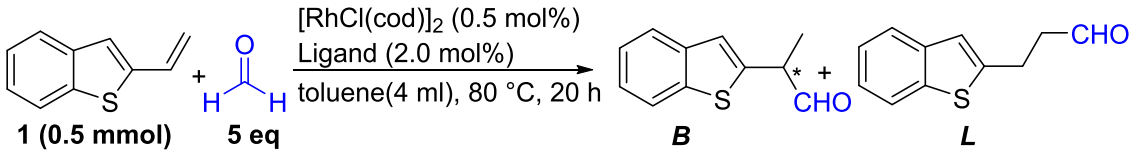

Entry	ligand	Conv.[a]	Yield[a]	Ratio(*B*/*L*)[a]	ee[b]
1	(*R*)-XylBINAP	89%	89% (84%)	83/17	21% (*S*)
2	(*R*)-H_8-BINAP	88%	86% (81%)	85/15	33% (*S*)
3	(*R*)-SEGPHOS	53%	56% (50%)	91/9	37% (*S*)
4[c]	(*R*)-SEGPHOS	82%	82%	92/8	37% (*S*)
5	(*R*)-DIFLUORPHOS	85%	87%(81%)	89/11	43% (*S*)
6[c]	(*R*)-DIFLUORPHOS	95%	97%	89/11	43% (*S*)
7	(*R*)-SYNPHOS	65%	59% (54%)	90/10	27% (*S*)
8	(*S*)-TolBINAP	74%	73% (71%)	90/10	29% (R)
9	(*S*)-BINAP	83%	79% (78%)	89/11	28% (R)
10	(*S,S*)-BDPP	96%	93% (89%)	61/39	43% (*S*)
11	(*S*)-MeO-BIPHEP	46%	43%(39%)	88/12	28% (R)

[a]Determined by GC using n-pentadecane as an internal standard. Yield of isolated product in parentheses after reduced to an alcohol.

[b]Determined by HPLC after conversion to alcohol.

[c]Reaction time: 40 h.

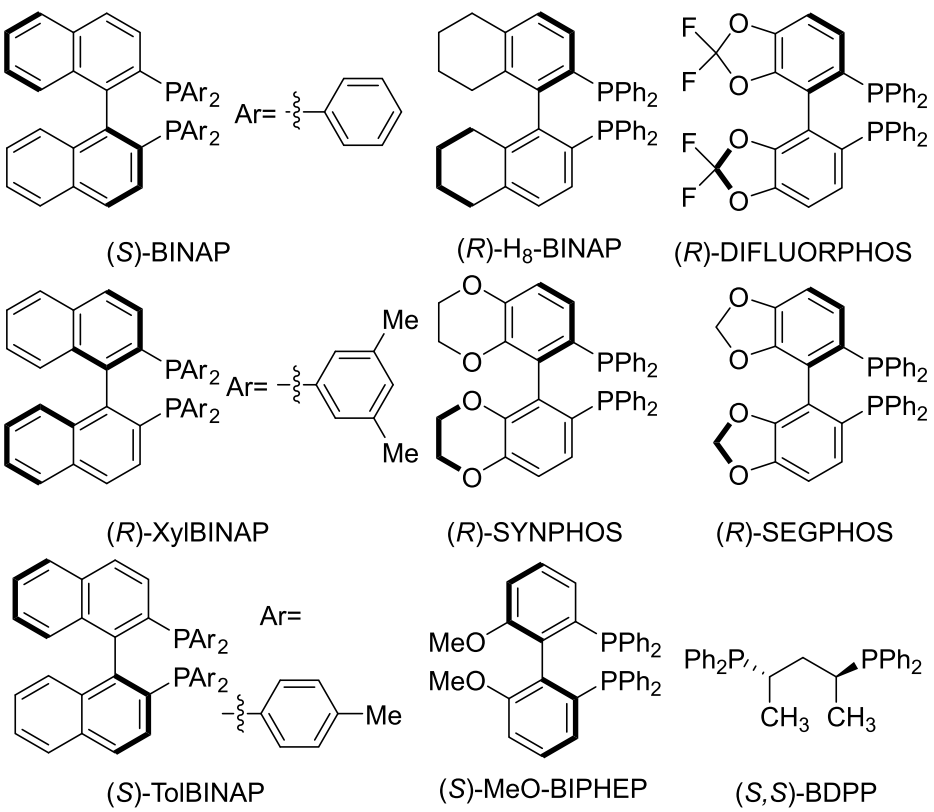

Scheme 3.5 Ligands structure

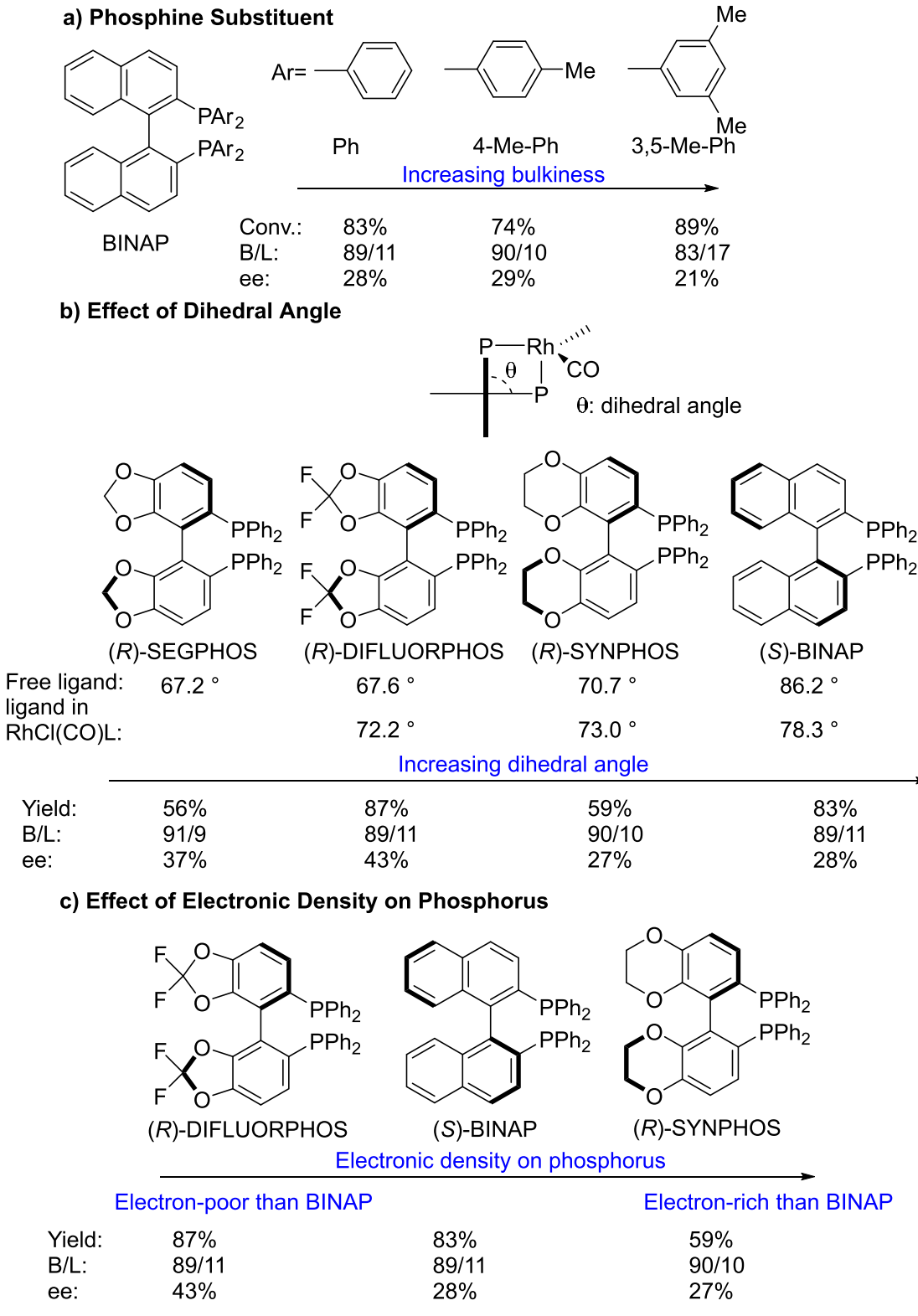

Scheme 3.6 Effect of ligands in Hydroformylation[10]

Screening of ligands in the hydroformylation of **1** revealed very high regioselectivity in all cases except (*S,S*)-BDPP (Table 3.2, Entry 10). In all other instances, the formation of the

branched aldehyde was highly preferred. Examination of various BINAP derivatives revealed that phosphine substitution influenced regio- and enantio-selectivity (Scheme 3.6a). The BINAP ligand afforded the aldehydes (Branched and Linear) in 79% yield with high selectivity (*B*/*L* = 89/11) and low enantioselectivity (28% ee) (Table 3.2, Entry 9). Increasing the steric bulkiness (Scheme 3.6a) of the phosphine substituents gave slightly improved conversion (Table 3.2, Entries 1 and 9). However, increasing the steric bulkiness of the phosphine substituents resulted in decreased regio- and enantio-selectivity. Although the 4-Me-phenyl group substituted ligand (TolBINAP) afforded the higher regio- (*B*/*L* = 90/10) and enantio-selectivity (29% ee) (Table 3.2, Entry 8), there was also a trend that increasing the steric bulk of ligands could improve the regio- and enantio-selectivity. In TolBINAP case, as the methyl group is a weak electron-donor, the electronic effect is stronger than steric factor.

Dihedral angles of biaryl ligands can be tuned by changing the backbone of the ligand, and this angle is to impact the efficiency in enantioselective hydroformylation (Scheme 3.6b).[11] Effects of dihedral angles of ligands on reactivities were investigated. Ligands with larger dihedral angles gave the improved the yield (Scheme 3.6b). SYNPOHS afforded the aldehydes in 59% yield, whereas BINAP afforded the aldehydes in 83% yield. A similar steric effect is also demonstrated in the cases of SEGPHOS and BINAP (Table 3.2, Entries 4 and 9). In DIFLUORPHOS case, although the dihedral angle of ligand increased, the reaction led to higher enantioselectivity and yield (Table 3.2, Entry 5 and Scheme 3.6c). The main reason

should be electronic effect. As the fluorine atom is not located at the resonance position, it works as a strong electron-withdrawing group. As a result, the effect of electronic is stronger than that of the dihedral angle.

Electronic effects are also an important factor to determine the regio- and enantio-selective hydroformylation (Scheme 3.6c). Comparison of SYNPHOS and DIFLUORPHOS indicated that electron-rich ligand inhibited the catalytic activity and enantioselectivity. SYNPOHS afforded the aldehydes in 59% yield with 27% ee (Table 3.2, Entry 7), whereas DIFLUORPHOS afforded the aldehydes in 85% yield with 43% ee (Table 3.2, Entry 5). Nevertheless, the electron-withdrawing groups on the backbone (DIFLUORPHOS) have slightly decreased the selectivity from 90/10 to 89/11. A similar electronic effect is also demonstrated in the cases of SEGPHOS and DIFLUORPHOS (Table 3.2, Entries 5 and 7). The trend of inhibited activity and enantioselectivity by electron-rich ligands cannot be generalized to a wider scope as the electron-richer methyl ligand TolBINAP. In TolBINAP ligand case, it has slightly higher enantioselectivity than BINAP (Table 3.2, Entries 8 and 9). But there are same possibilities to effect on these selectivities. Electronic factor has more effect than dihedral angle.

As stated above, on some level, electron-poor ligands can promote the regio- and enantio-selective hydroformylation. And in some ways, increasing the dihedral angles can increase the catalytic activity. In addition, increasing the steric bulkiness of ligands can develop the regio-

and enantio-selectivity in some cases. However, in a word, the relationship between enantioselectivity and steric or electronic effect is not clear. Within the ligands for rhodium-catalyzed hydroformylation in this dissertation, it shows that electronic control is more important than the dihedral angle. This result is similar to van Leeuwen's results.[12]

After the various bidentate phosphine ligands were examined, the SEGPHOS and DIFLUORPHOS gave the best result in yield and enantioselectivity. However, the reaction time was up to 40 h under the standard conditions. Hence, I hypothesized the concentration of reaction mixture is the limiting conditions. Next, the influence of concentration was investigated (Table 3.3). From viewpoints of ready availability, regioselectivity, and enantioselectivity, SEGPHOS was selected as the most suitable ligand for this reaction.

Table 3.3 Optimization of concentration

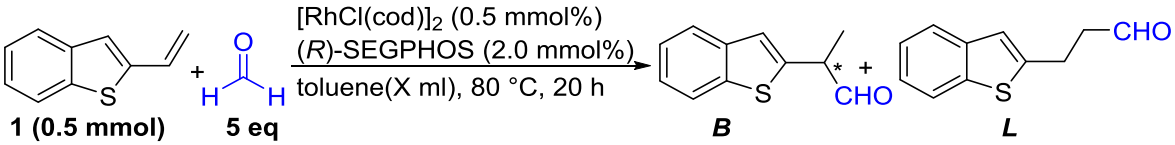

Entry	Toluene	Conv.[a]	Yield[a]	Ratio(B/L)[a]	ee[b]
1	4 ml	53%	56% (50%)	91/9	37% (*S*)
2	2 ml	82%	80% (76%)	91/9	38% (*S*)
3	1 ml	92%	92% (89%)	90/10	36% (*S*)

[a]Determined by GC using n-pentadecane as an internal standard. Yield of isolated product in parentheses.

[b]Determined by HPLC after conversion to alcohol.

The concentration of reaction mixture had a remarkable effect on the reaction activity. The

conversion dramatically improved from 53% to 82% when the amount of solvent was decreased from 4 ml to 2 ml (Table 3.3, Entries 1 and 2). Then, when the reaction was carried out in 1 ml toluene, the conversion can be up to 92% with slightly decreased enantioselectivity (Table 3.3, Entry 3). This phenomenon encouraged me to study the effect of temperature and the amount of formalin.

Table 3.4 Optimization of the amount of formalin

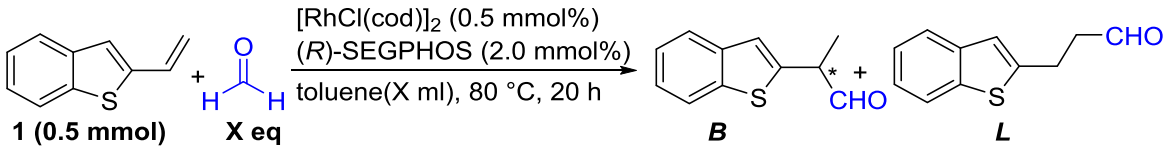

Entry	Toluene	Formalin	Conv.[a]	Yield[a]	Ratio(B/L)[a]	ee[b]
1	4 ml	5.0 eq.	53%	56% (50%)	91/9	37% (*S*)
2	4 ml	2.5 eq.	46%	44% (41%)	90/10	38% (S)
3	1 ml	5.0 eq.	92%	92% (89%)	90/10	36% (*S*)
4	1 ml	2.5 eq.	72%	69% (67%)	90/10	38% (*S*)

[a]Determined by GC using n-pentadecane as an internal standard. The yield of isolated product in parentheses.

[b]Determined by HPLC after conversion to alcohol.

I had attempted to reaction with less amount of formalin. Unluckily, when the amount of formalin was decreased from 5.0 eq. to 2.5 eq. to that of the starting material compound **1**, low yields were obtained (Table 3.4, Entries 1 and 2, Entries 3 and 4). When the amount of formalin was from 5.0 eq. to 2.5 eq. to that of the starting material compound **1** in 4 ml toluene, the yield was slight decrease from 56% to 44% (Table 3.4, Entries 1 and 2), whereas when the reaction

was carried out in 1 ml toluene, the yield was a notable decrease from 92% to 69% (Table 3.4, 3 and 4). Noteworthy, when 2.5 eq. formalin was used, the ee values increased slightly both in 4 ml and in 1 ml toluene (Table 3.4, 1 and 2, 3 and 4). When the reaction was carried out in 4 ml, the 2.5 eq. formalin resulted in slightly decreased branched-selectivity. Comparison to the reaction in 4 ml toluene, there was no influence in branched-selectivity when the reaction was in 1 ml toluene.

These results indicate the amount of formalin has great influence in rhodium-catalyzed hydroformylation when the reaction mixture is in high concentration.

As it is known, the temperature is also an important limiting factor in organic synthesis. I also had attempted the reaction was carried out at high temperature (Table 3.5)

Table 3.5 Optimization of temperature

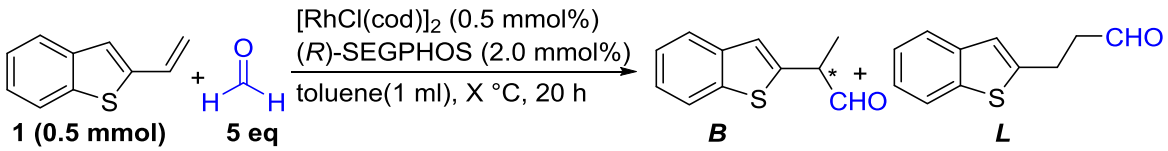

Entry	Temperature	Conv.[a]	Yield[a]	Ratio(B/L)[a]	ee[b]
1	80 ℃	92%	92% (89%)	90/10	36% (*S*)
2[c]	100 ℃	>99%	99% (93%)	86/14	31% (*S*)

[a]Determined by GC using n-pentadecane as an internal standard. Yield of isolated product in parentheses.

[b]Determined by HPLC after conversion to alcohol.

[c]Reaction time:10 h.

The temperature experiment was carried out under the standard conditions: **1** (0.5 mmol), formalin (37 wt% aqueous solution, 0.19 mL, 2.5 mmol), $[RhCl(cod)]_2$ (0.005 mmol), (*R*)-

SEGPHOS (0.02 mol) in toluene (1 mL) at 100 °C for 10 h (Table 3.5, Entry 2). The reaction was almost completed in a short time (10 h). At 100 °C, the yield was 99% with the almost full conversion. In contrast, the regio- and enantio-selectivity were decreased. The ratio of *B*/*L* was decreased from 90/10 to 86/14, meanwhile, the ee value was decreased from 36% to 31%. This result indicates high-temperature results in the formation of more branched aldehyde with low enantioselectivity as described at the beginning of this section.[9]

As the results were as described, the standard conditions were as follows: substrate (0.5 mmol), formalin (37 wt% aqueous solution, 0.19 mL, 2.5 mmol), $[RhCl(cod)]_2$ (0.005 mmol), (*R*)-SEGPHOS (0.02 mmol) in toluene (1 mL) at 80 °C for 20 h.

The hydroformylation using syngas under standard conditions was also investigated (Scheme 3.7).

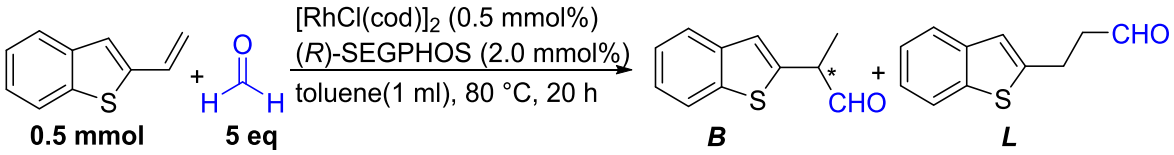

(a) formalin Conv. 92% 92% Yield (B/L=90/10)
(b) syngas(CO/H_2=50/50) not detected
(c) syngas($N_2/CO/H_2$=90/10/10) not detected
(d) syngas(CO/H_2=50/50)(100 °C) only hydrogenated product was detected (chiral Ph-bpe as ligand)

Scheme 3.7 Branched hydroformylation using syngas

I conducted the reaction under standard conditions using syngas (CO/H_2 = 50/50). Contrary to my expectation, this catalytic system did not work in the presence of a syngas atmosphere (1 atm) (Scheme 3.7b). In consideration of the effect of syngas pressure, I tried the reaction in the syngas containing N_2 (totally 1 atm), the same result was obtained (Scheme 3.7c). At a high

temperature of 100 °C, only hydrogenated product was observed when Ph-bpe served as a ligand. At present, the reason for this difference in reactivity is unclear. A higher syngas pressure should be introduced to this catalytic system. In such a case, the special reactor would be required under high pressure. This also indicates that the formalin showed a higher activity than syngas under mild conditions.

2.2.2 Substrate scope

With the standard reactions in hand, then the scope of hydroformylation of vinylheteroarenes was explored (Scheme 3.8).

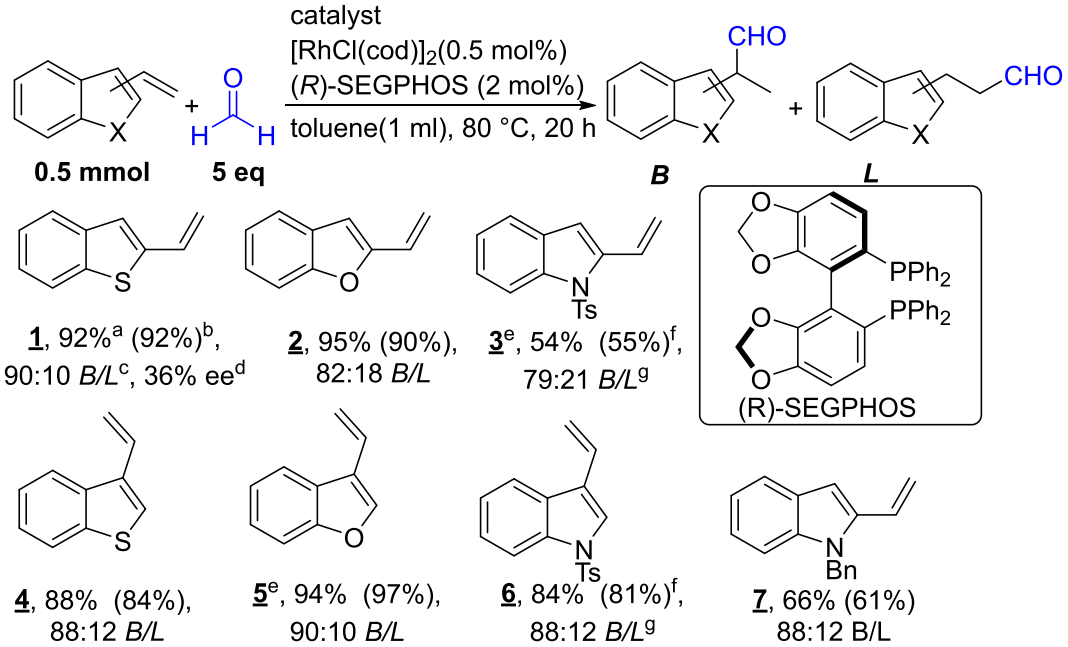

Reactions were performed on a 0.5 mmol scale at 80 °C in 1 ml toluene with substrate/Rh =100:1, R-SEGPHOS: Rh = 4 : 1, 5 eq formaldehyde (37 wt% aqueous solution), and a reaction time of 20 hours. [a]Conversion, [b]Chemical yield, [c]Determined by GC analysis. [d]The hydroformylation products of vinyl heteroarenes were reduced to alcohols and then the enantiomeric excesses were determined by HPLC analysis using a chiral stationary phase. [e]Reaction time of 40 hours. [f]Isolated yield based on alcohols. [g]Determined by ^{1}H NMR analysis of crude reaction mixtures.

Scheme 3.8 Scope of branched-selective hydroformylation

As shown in Scheme 3.8, almost the substrates containing the heteroatom (O, S, N) were well performed in the hydroformylation using formaldehyde, affording the corresponding chiral aldehydes with good yields and moderate enantioselectivities. When vinyl substituted benzothiophene (**1** and **4**) and benzofuran (**2** and **5**) were used as substrates, the reaction proceeded very smoothly (except for 3-vinylbenzofuran **5** for 40 h reaction time). Wherever the position of the vinyl group, this reaction gave high yields and selectivities. It was worth mentioning that the reaction afforded the better aldehydes (branched and linear) in 84% yield with 88/12 selectivity when 3-vinylindole **6** was used as the substrate. When S atom was introduced to the substrate, both 2- and 3-vinylbenzothiophene (**1** and **4**) afforded the corresponding aldehydes in similar yields and selectivities. In contrast, when O atom was introduced to the substrate, only 2-vinylbenzofuran gave the corresponding aldehydes in high yield and selectivity (Scheme 3.8, compound **2** and Table 3.6, Entry 1). In the case of 3-vinylbenzofuran, increasing the reaction time to 40 h, the improved yield (from 64% to 97%) was observed with slightly increased selectivity (Table 3.6, Entries 1 and 2). In addition, when the vinyl group was at 2-position, the slightly decreased ratio of *B/L* was obtained (Scheme 3.8, compound **2** and **5**).

Table 3.6 Hydroformylation of 3-vinylbenzofuran

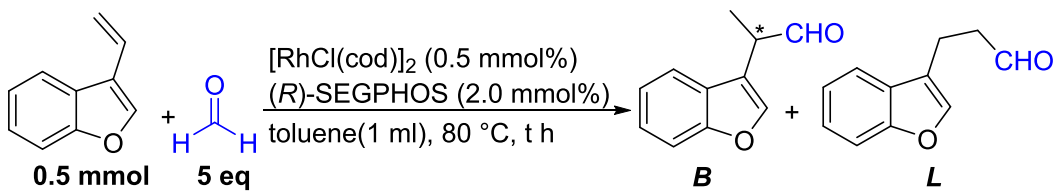

Entry	Time	Formalin	Conv.[a]	Yield[a]	Ratio(B/L)[a]
1	20 h	5 eq.	67%	64% (61%)	88/12
2	40 h	5 eq.	99%	97% (95%)	90/10

[a]Determined by GC using tridecane as an internal standard. Yield of isolated product in parentheses.

Because the rhodium easily reacted with N atom to form some complex, when N atom was introduced to the substrate, no desired product was obtained when no protecting vinylindole was used. However, vinylindole protected by Ts group could afford the aldehydes in 81% isolated yield when 3-vinylindole **6** was used as the substrate. In contrast, using the same protecting group, 2-vinylindole **3** afforded the aldehydes in lower yield (55%) and selectivity (*B/L* = 79/21). It should be caused by instability of 2-vinylindole, which is easy polymerization. Hence, the benzyl protecting group was also employed to the 2-vinylindole. Under the standard conditions, the benzyl protecting 2-vinylindole gave similar results (Scheme 3.8, compound **7**). However, the selectivity increased. When substrate **7** was performed in a long time (40 h), the yield and the ratio of *B/L* was a significant decrease (Table 3.7, Entry 2). In this case, longer reaction time resulted in decomposition of aldehydes (especially branched aldehyde). These results indicate that, when vinylindole was as the substrate, the reaction activity depends on the position of the vinyl group and stability of substrates. Hence, 3-position could afford the high selectivity, whereas, 2-position resulted in low selectivity.

Table 3.7 Hydroformylation of 2-Bn-vinylindole

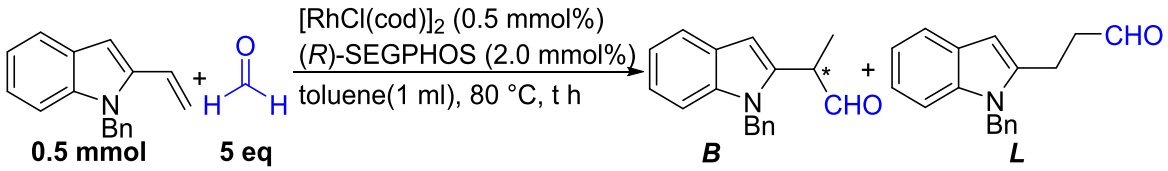

Entry	Time	Formalin	Conv.[a]	Yield[a]	Ratio(B/L)[a]
1	20 h	5 eq.	66%	61% (63%)	88/12
2	40 h	5 eq.	98%	43%	77/23

[a]Determined by GC using heneicosane as an internal standard. Yield of isolated product in parentheses.

In a word, vinylheteroarenes containing S, O atom can afford the high rigio- and enantio-selectivity, whereas only 3-vinylheteroarenes containing N afforded the better yield.

3.3 Mechanistic Speculation

In the previous work of my group,[8] in ^{13}C-labeled experiments (Scheme 3.9) under 1 atm of ^{12}CO, the result showed that only 29% of the ^{13}C was introduced into the CHO group. That suggested that the pathway for the present hydroformylation reaction involves the incorporation of a carbonyl unit in the form of a CO ligand; thus, the carbonyl group of formaldehyde is transformed to a CO ligand, which can be easily exchanged with external CO on the rhodium center. It also means that rhodiumhydride species, which is essential for the hydroformylation, is also generated as well as a carbonyl moiety. In this case, the same principle also goes for (*R*)-SEGPHOS ligand.

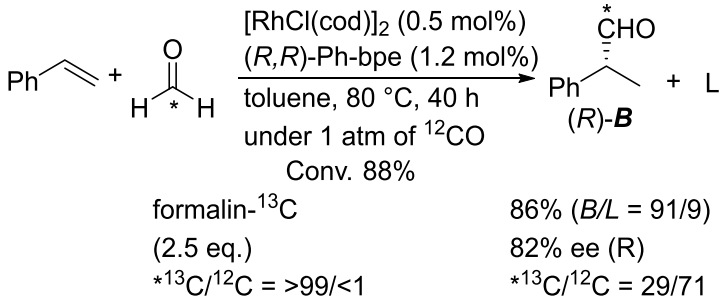

Scheme 3.9 ^{13}C-labeled experiment

A possible reaction pathway is as follows (Scheme 3.10). The reaction starts with decarbonylation of formaldehyde to form carbonyl moiety and two hydrogen moieties (Scheme 3.10, cycle above). In this cycle, the oxidative addition of formaldehyde to the metal center of the complex (**A'**) gives the complex (**B'**). With the migratory extrusion of the carbonyl moiety of complex (**C'**), complex (**D'**) is subsequently formed involving the H_2 released. Complex (**A'**) is regenerated by the release of CO from complex (**D'**). This cycle is decarbonylation process. Next, the coordination of the vinylheteroarene (**1**) with rhodium(I)-hydride species (**E'**), which is generated from (i) (**A'**), [CO] and H_2, (ii) (**D'**) and H_2, and/or (**C'**), forms the π-complex (**F'**). Subsequent insertion of the **CO** into the metal–aryl bond of (**G'**) leads to the corresponding acyl species (**H'**). Finally, insertion of a H_2 forms the desired product and regenerates the catalyst (**E'**). As a consequence, the branched aldehydes are obtained.

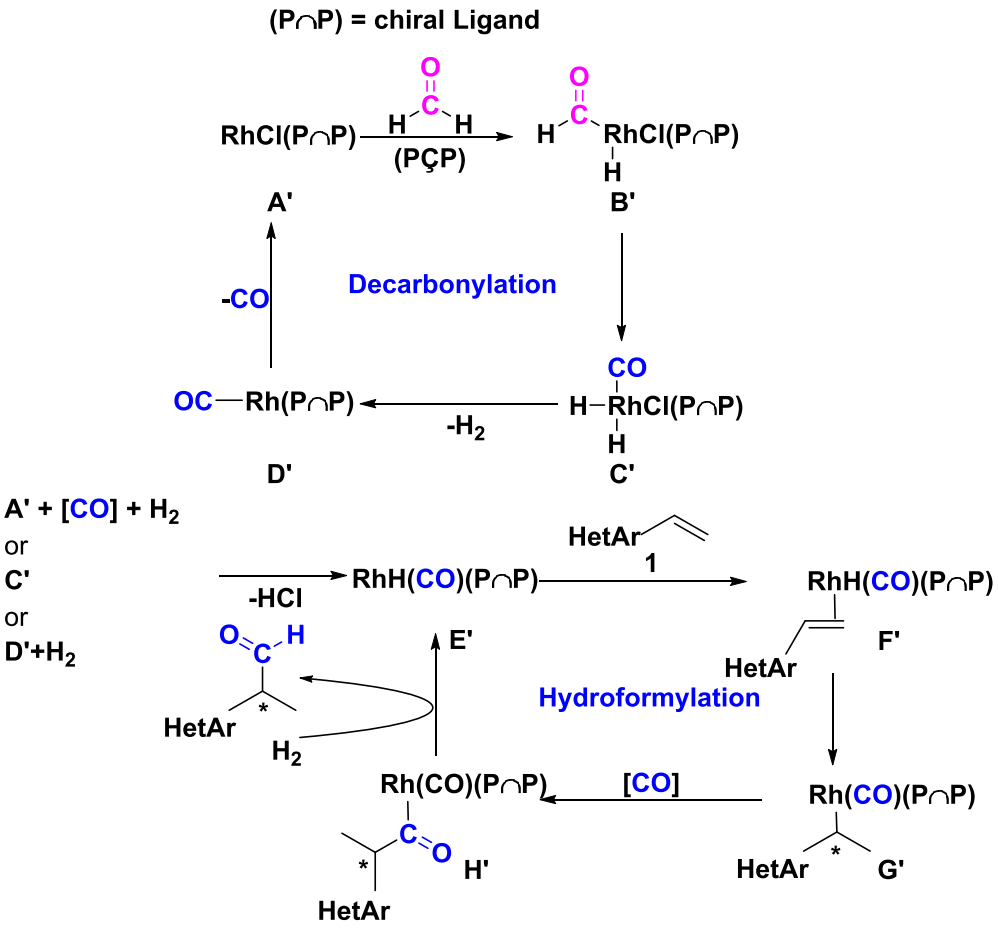

Scheme 3.10 Proposed reaction mechanism for branched-selectivity

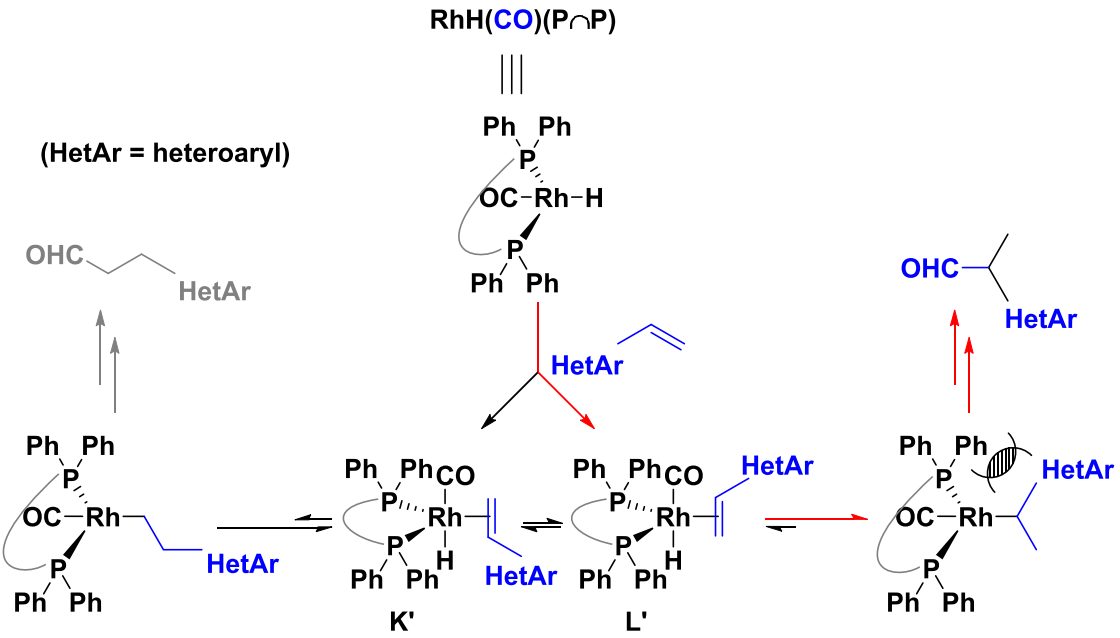

Scheme 3.11 Origin of branched selectivity

As section 2.3 mentioned, Rh-diphosphine catalyzed hydroformylation has been studied by Van Leeuwen.[12] Addition of Rh-H species to vinylheteroarene leads to two types of pentacoordinated rhodium intermediates (**K**) and (**L**). The left intermediate yields the linear aldehyde, and the right one the branched aldehyde (Scheme 3.11). As the previous work described,[13] when the bite angle of ligand is around 90°, branched aldehydes are easily formed predominantly. In our case, it was easily speculated that branched aldehydes were produced in the presence of SEGPHOS ligand.

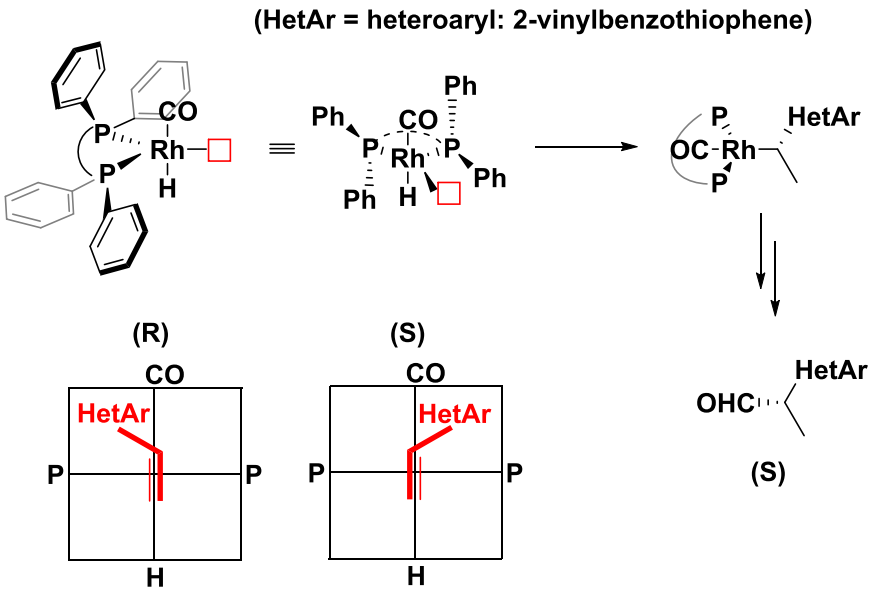

Scheme 3.12 Enantioface discrimination

As mentioned in section 1.3, pentacoordinated rhodium intermediate is a key intermediate in determining the enantioselectivity, particularly the step of addition of Rh-H species to vinylheteroarene. The key intermediate, rhodium, (*R*)-SEGPHOS, carbonyl, and hydride ligands, was shown in Scheme 3.12. Vinylheteroarenes coordinate to the rhodium center at this site in two manners, as shown in these simplified quadrant diagrams. In the left coordination manner, the hetAr group of vinylheteroarene is located in the left zone to give (*R*)-enantiomer. On the other hand, in the right coordination manner, HetAr group of vinylheteroarene is located in the right zone to give (*S*)-enantiomer. However, these two manners show no obvious preference, resulting in somewhat low ee values.

3.4 Conclusion

In chapter 3, I have developed an approach for asymmetric hydroformylation of vinylheteroarenes using formaldehyde. The reaction of 2-vinyl benzothiophene with

formaldehyde (37 wt% aqueous solution) in the presence of a catalytic amount of $[RhCl(cod)]_2$ (1.0 mol%) and (*R*)-SEGPHOS (4.0 mol%) in toluene gave a mixture of branched and linear hydroformylated products in a ratio of up to 90/10 (*B*/*L*) with a moderate enantioselectivity (36% ee). Various substrates containing a heteroatom (O, S, and N) were also successfully applied to this method. Although the moderate ee values were obtained, it is also a potential method to produce chiral aldehydes. In addition, the origin of enantioselectivity was also described.

3.5 References

1. Consiglio, G., Nefkens, S. C., & Borer, A. *Organometallics* **1991**, *10,* 2046-2051.

2. Cserépi-Szücs, S. & Bakos, J. *Chem. Commun.* **1997**, 635-636.

3. (a) Agbossou, F., Carpentier, J. F., & Mortreux. *Chem. Rev.* **1995**, *95*, 2485-2506; (b) Gladiali, S., Bayón, J. C., & Claver, C. *Tetrahedron: Asymmetry* **1995**, *6*, 1453-1474.

4. Babin, J. E. & Whiteker, G. T. Pat. WO 93103830, **1992**.

5. Whiteker G. T., Briggs J. R., Babin J. E., & Barner B. A. In: Morrell D. G. eds. *Catalysis of organic reactions*, Vol 89. Marcel Dekker, Inc., New York, **2003**, p359–367

6. (a) Sakai, N., Mano, S., Nozaki, K., & Takaya, H. *J. Am. Chem.Soc.* **1993**, *115,* 7033-7034; (b) Nozaki K., Sakai, N., Nanno, T., Higashijima, T., Mano, S., Horiuchi, T., & Takaya, H. *J. Am. Chem. Soc.* **1997**, *119,* 4413-4423.

7. (a) Tanaka, R., Nakano, K., & Nozaki, K. *J. Org. Chem.* **2007**, *72*, 8671-8676; (b) Wei, B., Chen, C., You, C., Lv, H., & Zhang, X. *Org. Chem. Front.* **2017**, *4*, 288-291.

8. Morimoto, T., Fuji, T., Miyoshi, K., Makado, G., Tanimoto, H., Nishiyama, Y., & Kakiuchi, K. *Org. Biomol. Chem.* **2015**, *13*, 4632-4636;

9. Lazzaroni, R., Raffaelli, R., Settambolo, R., Bertozzi, S., & Vitulli, G. *J. Mol. Cat.* **1989**, *50,* 1-9.

10. (a) Kim, D. E., Choi, C., Kim, I. S., Jeulin, S., Ratovelomanana-Vidal, V., Genêt, J. P., & Jeong, N. *Adv. Synth. Catal.* **2007**, *349*, 1999-2006; (b) Jeulin, S., de Paule, S. D.,

Ratovelomanana-Vidal, V., Genêt, J. P., Champion, N., & Dellis, P. *P. Natl. Acad. Sci. USA*, **2004**, *101*, 5799-5804.

11. Van Leeuwen, P. W. & Carmen C. eds. *Rhodium-catalyzed hydroformylation*. Vol. 22. Springer Science & Business Media, **2002**.

12. Carbó, J. J., Maseras, F., Bo, C., & Van Leeuwen, P. W. *J. Am. Chem. Soc.* **2001**, *123*, 7630-7637.

13. Jiao, Y., Torne, M. S., Gracia, J., Niemantsverdriet, J. H., & Van Leeuwen, P. W. *Catal. Sci. Technol.* **2017**, *7*, 1404-1414.

Chapter 4 Summary and Outlook

The hydroformylation of olefins is a highly atom-economic reaction in which an alkene is converted into an aldehyde by the addition of syngas, a mixture of carbon monoxide (CO) and hydrogen (H_2), in the presence of a transition-metal complex. The resulting aldehydes are great important intermediates in the chemical industry, pharmaceuticals, cosmetics, and agrochemicals. In general, chemists carry out this hydroformylation in the syngas atmosphere at high temperature and high syngas pressure conditions using special experimental equipment. Nowadays, chemical researchers pay more attention to green, safe, easy-to-handle, and efficient approach. From a viewpoint of convenience and safety for user, the hydroformylation without the direct use of toxic CO and explosive H_2 have attracted more and more attention. My group also follows with this interest and have developed some safe and convenient methods using formaldehyde as a carbonyl source, which is commercially available as paraformaldehyde and formalin. However, there are still some challenges in high region-, stereo-, and enantio-selectivity to produce linear aldehydes and chiral aldehydes using vinylheteroarenes as substrates.

In this dissertation, I have developed two methods for Rh(I)-catalyzed selective hydroformylation of vinylheteroarenes using formaldehyde as the substitute for syngas: (i) a highly linear-selective hydroformylation of vinylheteroarenes, and (ii) a branched- and enantio-selective hydroformylation of vinylheteroarenes. In chapter 2, an approach for highly linear-

selective hydroformylation of vinylheteroarenes using formaldehyde was developed. The high regioselectivity (*L/B* = up to 93/7) can be attributed to the simultaneous use of two types of phosphines (BIPHEP and Nixantphos) as ligands. Furthermore, the 2-vinyl substrates gave higher *L/B* ratio than 3-vinyl substrates. It means the selectivity was affected by the position of the vinyl group, which is caused by stable five-membered metallacycle intermediate. In chapter 3, an approach for asymmetric hydroformylation of vinylheteroarenes using formaldehyde was developed. (*R*)-SEGPHOS as single ligand gave the best result, leading to corresponding aldehydes with good regioselectivity (*B/L*= up to 90/10) and moderate enantioselectivity (around 36% ee), catalyzed by $[RhCl(cod)]_2$. It was found that electronic control is more important than the dihedral angle by ligand screening.

The success of using formaldehyde in the hydroformylation reaction offers a safe, convenient access to hydroformylate olefin to yield the linear or branched aldehydes without using toxic and flammable syngas, and contributes to the development of carbonyl reaction using formaldehyde as CO surrogate. This research also indicates formaldehyde is a huge potential CO surrogate.

Chapter 5 Experimental Section and Supporting Information

5.1 Experimental Section

General information

Nuclear magnetic resonance spectra were recorded on a JEOL JNM-ECP500 spectrometer. Chemical shifts of ^{1}H NMR spectra are given in ppm using the solvent signal as the internal standard ($CDCl_3$, 7.26 ppm; DMSO-d_6, 2.50 ppm). Data are reported as follows: multiplicity (s = singlet, d = doublet, t = triplet, q = quartet, and m = multiplet), coupling constant in Hz, and integration. ^{13}C NMR chemical shifts are given in ppm using the solvent signal ($CDCl_3$, 77.0 ppm; DMSO-d_6, 39.5 ppm) as the internal standard. Infrared spectra (IR) were collected on a JASCO FT/IR-4200 spectrometer; absorption peaks are reported in reciprocal centimeters (cm^{-1}) with the following relative intensities: s (strong), m (medium), or w (weak). The products were analyzed by gas chromatography (SHIMADZU GC-2025) with INERTCAP 1 column Φ ×0.25 mm. Mass spectra were obtained with ionization voltages of 70 eV by SHIMADZU GCMS PARVUM 2. High-performance liquid chromatography was conducted using an ultraviolet detector (HITACHI L-7420). Column chromatography was performed using a SiO_2 (MERCK Silica gel 60).

Materials.

All commercial reagents were used as supplied or purified by standard techniques when necessary. $[RhCl(cod)]_2$[1], vinylhetroareans **1**,[2] **2**,[2] **3**,[3] **4**,[4] **6**,[5] and **7**[6] were prepared using a

previously reported method. Formalin, (-)-1,2-bis((*2R*,*5R*)-diphenylphospholano)ethane ((*R,R*)-Ph-bpe), (2*S*,4*S*)-2,4-bis(diphenylphosphino)pentane ((*S*,*S*)-BDPP), (*R*)-(+)-2,2'-Bis(diphenylphosphino)-5,5',6,6',7,7',8,8'-octahydro-1,1'-binaphthyl ((*R*)-H_8-BINAP), (*S*)-(-)-2,2'-Bis(diphenylphosphino)-6,6'-dimethoxy-1,1'-biphenyl, ((*S*)-MeO-BIPHEP) were purchased from Aldrich Chemical Co. *R*-(+)-6,6'-Bis(diphenylphosphino)-2,2',3,3'-tetrahydro-5,5'-bi-1,4-benzodioxin, ((*R*)-SYNPHOS), (*R*)-(+)-2,2'-Bis[di(3,5-xylyl)phosphino]-1,1'-binaphthyl, ((*R*)-XylBINAP), *R*-(-)-5,5'-Bis(diphenylphosphino)-2,2,2',2'-tetrafluoro-4,4'-bi-1,3-benzodioxole ((*R*)-DIFLUORPHOS), (*S*)-(-)-2,2'-Bis(di-p-tolylphosphino)-1,1'-binaphthyl ((*S*)-TolBINAP) were purchased from Strem Chemicals Inc. (*S*)-(-)-2,2'-Bis(diphenylphosphino)-1,1'-binaphthyl ((*S*)-(-)-BINAP) was purchased from Tokyo Chemical Industry Co. (*R*)-(+)-5,5'-Bis(diphenylphosphino)-4,4'-bi-1,3-benzodioxole ((*R*)-(+)-SEGPHOS) was purchased from Strem Chemicals Inc. or Tokyo Chemical Industry Co. 4,6-Bis(diphenylphosphino)phenoxazine (Nixantphos) was purchased from Aldrich Chemical Co. or Tokyo Chemical Industry Co. Toluene (dehydrated) was purchased from Kanto Chemical Co.

Typical procedure for the preparation of vinylhetroarenes 1, 2, 3, 4, 6 by Wittig olefination

To a suspension of methyltriphenyl phosphonium bromide (1.2 equiv.) in dry THF (2 mL per mmol) was added n-BuLi (1.6 M in hexane, 1.2 equiv.) dropwise at –78 °C. The resulting solution was then allowed to warm up to 0 °C over a period of 1 h. Then it was cooled to –30 °C and treated with a mixture of corresponding aldehyde (1.00 equiv.) with stirring at room

temperature until the starting material had disappeared as evidenced by TLC. The reaction mixture was quenched by adding H_2O (10 mL per mmol), the phases were separated, the aqueous phase was extracted with Et_2O, and the combined organic layers were dried over $MgSO_4$ and concentrated under reduced pressure. The product was obtained by column chromatography.

Preparation of 3-vinylbenzofuran

To a stirred solution of 3-bromobenzofuran (197.03mg, 1 mmol) and potassium vinyltrifluoroborate (267.90 mg, 2 mmol) in EtOH (10 ml) was added TEA (0.42 mL, 3 mmol) and the resulting mixture was degassed with nitrogen for 30 minutes. $PdCl_2(dppf)Cl_2•CH_2Cl_2$ (40.80 mg, 0.05 mmol) was then added and the resulting mixture was sealed and heated at 85 °C for 12 h. The reaction mixture was cooled to ambient temperature, filtered through a pad of cellite and washed with EtOAc (10×3 mL) and the filtrate was evaporated under reduced pressure. The residue was purified by column chromatography (hexane) to afford the product as colorless oil (64%).

Typical procedure for branched-hydroformylation of vinylheteroarenes using formalin

A 10 mL J-young tube containing a stirring bar was charged with $[RhCl(cod)]_2$ (2.47 mg, 0.005 mmol), ligand (0.02 mmol), substrate (0.5 mmol), formalin (37%, 0.19 mL, 2.5 mmol), and toluene (1 mL) under nitrogen. The mixture was degassed and purged with nitrogen (three freeze-pump-thaw cycles). The J-young tube containing the mixture was placed in 80°C oil bath

and stirred for 20 h. Then internal standard (25 mg) was added for GC analysis. The conversion of vinylarene, the chemical yields of produced aldehydes, and the regioselectivity of the aldehydes (*B/L* ratio) were determined by GC. After the GC analysis, methanol (2 mL) and $NaBH_4$ (37.8 mg, 2 mmol) were added to the mixture at 0 °C, and the resulting mixture was stirred at the same temperature for 2 h. Then the solvent was removed under reduced pressure. The product was obtained by column chromatography. The enantiomeric excess (ee%) of the branched alcohols was determined by HPLC using a chiral column stationary phase.

Typical procedure for linear-hydroformylation of vinylheteroarenes using formalin

A 10 mL J-young tube containing a stirring bar was charged with $[RhCl(cod)]_2$ (4.93 mg, 0.01 mmol), Nixantphos (9.93 mg, 0.018 mmol), BIPHEP (3.14 mg, 0.006 mmol), substrate (1.0 mmol), formalin (37%, 0.37 mL, 5.0 mmol), and toluene (3 mL) under nitrogen. The mixture was degassed and purged with nitrogen (three freeze-pump-thaw cycles). The J-young tube containing the mixture was placed in 100°C oil bath and stirred for 20 h. After the reaction was completed, the solvent was removed under reduced pressure. The product was obtained by column chromatography.

Measurement of ee% of branched aldehydes.

Enantiomeric excess (ee%) of branched aldehydes was determined by HPLC equipped with a chiral column stationary phase, after conversion to the corresponding alcohols.

Determination of absolute configuration.

The absolute configurations were assigned from specific optical rotation data for the purified corresponding *branched*-alcohols.

Spectral data of starting material, branched and linear aldehydes (alcohols).

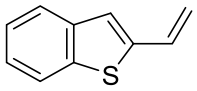

1

2-Vinylbenzo[b]thiophene.[2] White solid; R_f 0.88 (hexane/AcOEt = 1/1); ^{1}H NMR (500 MHz, $CDCl_3$) δ 5.31 (1H, d, *J* = 10.9 Hz), 5.66 (1H, d, *J* = 17.2 Hz), 6.92 (1H, dd, *J* = 17.2, 8.6 Hz), 7.17 (1H, s), 7.28-7.33 (2H, m), 7.68-7.70 (1H, m), 7.75-7.77 (1H, m); ^{13}C NMR ($CDCl_3$, 125 MHz) δ 115.92, 115.94, 122.2, 123.1, 124.4, 124.8, 130.6, 138.8, 140.0, 143.1; MS (GC-MS): *m/z* (%) = 160 ($[M]^+$, 100), 128 (15), 116 (18), 115 (53).

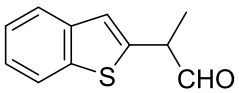

1*B*

2-(Benzo[b]thiophen-2-yl)propanal. Colorless oil; R_f 0.67 (hexane/AcOEt = 1/1); ^{1}H NMR (500 MHz, $CDCl_3$) δ 1.59 (3H, d, *J* = 6.9 Hz), 3.93-3.95 (1H, m), 7.17 (1H, s), 7.32-7.36 (2H, m), 7.74 (1H, d, *J* = 3.4 Hz), 7.81 (1H, d, *J* = 4.6 Hz), 9.73 (1H, d, *J* = 1.1 Hz); ^{13}C NMR ($CDCl_3$, 125 MHz) δ 15.0, 45.5, 122.2, 122.3, 123.3, 124.3, 124.5, 139.5, 139.8, 141.0, 196.6; IR (neat) 3056 w, 2976 w, 2931 w, 1727 s, 1666 w, 1457 m, 1435 m, 1067 w, 830 w, 746 s, 726 m; MS (GC-MS): *m/z* (%) = 190 ($[M]^+$, 34), 161 (100), 128 (62), 115 (21); Exact mass (EI) calcd for $C_{11}H_{10}OS$ 190.0452, found 190.0430.

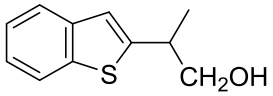

1*BB*

2-(Benzo[b]thiophen-2-yl)propan-1-ol.[7] White solid; R_f 0.60 (hexane/AcOEt = 1/1); ^{1}H NMR (500 MHz, $CDCl_3$) δ 1.42 (3H, d, *J* = 6.9 Hz), 1.55 (1H, d, *J* = 3.4 Hz), 3.31-3.34 (1H, m), 3.75-3.83 (2H, m), 7.14 (1H, s), 7.29 (1H, td, *J* = 7.6, 1.3 Hz), 7.34 (1H, td, *J* = 7.4, 1.1 Hz), 7.71 (1H, d, *J* = 7.4 Hz), 7.80 (1H, d, *J* = 8.0 Hz); ^{13}C NMR ($CDCl_3$, 125 MHz) δ 16.2, 38.9, 68.5, 120.7, 122.3, 123.0, 123.8, 124.2, 137.0, 139.8, 146.2; IR (KBr) 3220 m, 2926 m, 2870 m, 1457 m, 1435 m, 1378 w, 1044 m, 832 w, 744 m, 726 m; MS (GC-MS): *m/z* (%) = 192 ([M]$^+$, 26), 161 (100), 128 (43), 115 (16); Exact mass (EI) calcd for $C_{11}H_{12}OS$ 192.0609, found 190.0610.

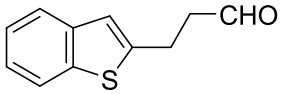

1*L*

3-(Benzo[b]thiophen-2-yl)propanal. Colorless oil; R_f 0.56 (hexane/AcOEt = 1/1); ^{1}H NMR (500 MHz, $CDCl_3$) δ 2.94 (2H, t, *J* = 7.4 Hz), 3.26 (2H, t, *J* = 7.4 Hz), 7.05 (1H, s), 7.27-7.34 (2H, m), 7.68 (1H, d, *J* = 8.0 Hz), 7.77 (1H, d, *J* = 8.0 Hz), 9.87 (1H, s); ^{13}C NMR ($CDCl_3$, 125 MHz) δ 23.2, 44.7, 121.3, 122.1, 122.9, 123.8, 124.2, 139.3, 140.0, 143.8, 200.6; IR (neat) 3126 w, 3056 w, 2920 w, 2823 w, 2722 w, 1722 s, 1435 m, 820 w, 746 m, 726 m, 528 w, 512 m; MS (GC-MS): *m/z* (%) = 190 ([M]$^+$, 51), 161 (26), 148 (41), 147 (100), 134 (51), 128 (22), 115 (21); Exact mass (EI) calcd for $C_{11}H_{10}OS$ 190.0452, found 190.0430.

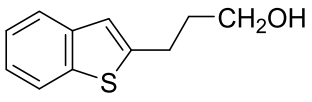

1*LL*

3-(Benzo[b]thiophen-2-yl)propan-1-ol. White solid; R_f 0.30 (hexane/AcOEt = 1/1); ^{1}H NMR (500 MHz, $CDCl_3$) δ 1.33 (1H, t, *J* = 5.4 Hz), 1.99-2.05 (2H, m), 3.01-3.04 (2H, m), 3.75 (2H, q, *J* = 5.9 Hz), 7.04 (1H, s), 7.25 (1H, td, *J* = 7.2, 1.4 Hz), 7.31 (1H, td, *J* = 7.4, 1.1 Hz), 7.67 (1H, d, *J* = 7.4 Hz), 7.77 (1H, d, *J* = 8.0 Hz); ^{13}C NMR ($CDCl_3$, 125 MHz) δ 27.0, 33.8, 61.8, 120.8, 122.1, 122.7, 123.5 124.1, 139.3, 140.1, 145.6; IR (KBr) 3285 m, 2927 m, 2858 m, 1435 m, 1055 m, 1030 s, 835 m, 745 s, 725 s, 570 w; MS (GC-MS): m/z (%) = 192 ([M]$^+$, 38), 173 (17), 148 (72), 147 (100), 128 (16), 115 (17); Exact mass (EI) calcd for $C_{11}H_{12}OS$ 192.0609, found 190.0609.

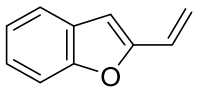

2

2-Vinylbenzofuran.[2] Colorless oil; R_f 0.69 (hexane/AcOEt = 2/1); ^{1}H NMR (500 MHz, $CDCl_3$) 5.39 (1H, dd, *J* = 11.5, 1.1 Hz), 5.96 (1H, dd, *J* = 17.2, 1.1 Hz), 6.60-6.67 (2H, m), 7.20 (1H, t, *J* = 7.4 Hz), 7.27-7.28 (1H, m), 7.45 (1H, d, *J* = 9.2 Hz), 7.53 (1H, d, *J* = 7.4 Hz); ^{13}C NMR ($CDCl_3$, 125 MHz) δ 104.7, 111.0, 115.7, 121.0, 122.8, 124.6, 125.2, 126.8, 154.7, 154.8; MS (GC-MS): *m/z* (%) = 144 ([M]$^+$, 100), 115 (78), 63 (13).

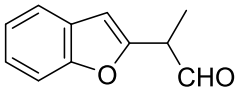

2*B*

2-(Benzofuran-2-yl)propanal. Colorless oil; R_f 0.59 (hexane/AcOEt = 3/1); ^{1}H NMR (500 MHz,

$CDCl_3$) δ 1.55 (3H, d, *J* = 6.9 Hz), 3.84-3.87 (1H, m), 6.61 (1H, s), 7.22-7.24 (1H, m), 7.26-7.30 (1H, m), 7.46 (1H, d, *J* = 8.0 Hz), 7.55 (1H, d, *J* = 6.9 Hz), 9.79 (1H, d, *J* = 1.1 Hz); ^{13}C NMR ($CDCl_3$, 125 MHz) δ 12.1, 47.0, 104.2, 111.3, 120.8, 122.9, 124.2, 128.2, 128.3, 154.5 155.1; IR (neat) 2917 w, 2830 w, 2727 w, 1718 s, 1676 m, 1627 m, 1603 m, 1455 s, 1252 m, 1105 m, 946 w, 798 w, 749 s; MS (GC-MS): *m/z* (%) = 174 ($[M]^+$, 41), 145 (21), 132 (19), 131 (100), 118 (46), 115 (19), 77 (22); Exact mass (EI) calcd for $C_{11}H_{10}O_2$ 174.0681, found 174.0670.

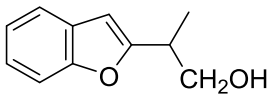

2BB

2-(Benzofuran-2-yl)propan-1-ol. Colorless oil; R_f 0.36 (hexane/AcOEt = 2/1); ^1H NMR (500 MHz, $CDCl_3$) δ 1.38 (3H, d, *J* = 6.9 Hz), 1.63 (1H, t, *J* = 6.6 Hz), 3.17-3.20 (1H, m), 3.81-3.89 (2H, m), 6.50 (1H, s), 7.18-7.25 (2H, m), 7.44 (1H, dd, *J* = 7.7, 1.4 Hz), 7.51 (1H, dd, *J* = 7.4, 1.7 Hz); ^{13}C NMR ($CDCl_3$, 125 MHz) δ 15.1, 36.6, 66.3, 102.4, 110.9, 120.5, 122.6, 123.5, 128.5, 160.5; IR (neat) 3336 m, 2966 m, 2928 m, 2877 m, 1584 w, 1455 s, 1254 m, 1170 w, 1026 m, 939 w, 802 w, 750 m, 512 m; MS (GC-MS): *m/z* (%) = 176 ($[M]^+$, 40), 145 (100), 117 (20), 115 (33); Exact mass (EI) calcd for $C_{11}H_{12}O_2$ 176.0837, found 176.0838.

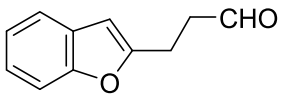

2L

3-(Benzofuran-2-yl)propanal.[8] Colorless oil; R_f 0.48 (hexane/AcOEt = 3/1); ^{1}H NMR (500 MHz, $CDCl_3$) δ 2.91-2.94 (2H, m), 3.13 (2H, t, *J* = 7.2 Hz), 6.43 (1H, d, *J* = 1.1 Hz), 7.19-7.23 (2H, m), 7.41 (1H, d, *J* = 7.4 Hz), 7.49 (1H, dd, *J* = 7.2, 1.4 Hz), 9.87 (1H, t, *J* = 1.1 Hz); ^{13}C NMR ($CDCl_3$, 125 MHz) δ 21.1, 41.6, 102.7, 110.8, 120.4, 122.6, 123.5, 126.6, 156.9, 200.6; IR (neat) 2900 w, 2831 w, 2730 w, 1721 s, 1603 w, 1455 s, 1252 m, 1166 w, 944 w, 797 w, 750 s; MS (GC-MS): *m/z* (%) = 174 ([M]$^+$, 43), 145 (21), 131 (100), 118 (51), 115 (21),77 (24); Exact mass (EI) calcd for $C_{11}H_{10}O_2$ 174.0681, found 174.0670.

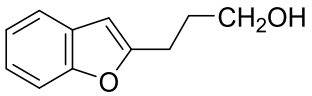

2*LL*

3-(Benzofuran-2-yl)propan-1-ol.[9] Colorless oil; R_f 0.25 (hexane/AcOEt = 2/1); ^{1}H NMR (500 MHz, $CDCl_3$) δ 1.41 (1H, s), 1.99-2.05 (2H, m), 2.89 (2H, t, *J* = 7.4 Hz), 3.75 (2H, t, *J* = 6.3 Hz), 6.42 (1H, t, *J* = 1.1 Hz), 7.16-7.23 (2H, m), 7.41 (1H, dd, *J* = 8.0, 1.1 Hz), 7.48 (1H, dd, *J* = 6.3, 1.1 Hz); ^{13}C NMR ($CDCl_3$, 125 MHz) δ 24.8, 30.6, 61.9, 102.2, 110.7, 120.2, 122.5, 123.2, 128.8, 154.6, 158.7; IR (neat) 3351 m, 2942 m, 2879 m, 1602 w, 1455 s, 1251 m, 1168 m, 1054 m, 945 m, 798 m, 750 s; MS (GC-MS): m/z (%) = 176 ([M]$^+$, 40), 158 (22), 157 (25), 132 (33), 131 (100),77 (23); Exact mass (EI) calcd for $C_{11}H_{12}O_2$ 176.0837, found 176.0842.

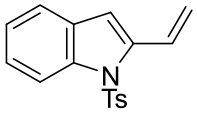

3

1-Tosyl-2-vinyl-1H-indole.[3] Colorless syrup; R_f 0.69 (hexane/AcOEt = 3/1); ^{1}H NMR (500 MHz, DMSO-d_6) δ 2.29 (3H, s), 7.04 (1H, s), 7.25-7.28 (2H, m), 7.33-7.34 (3H, m), 7.52 (1H, d, J = 7.4 Hz), 7.64 (2H, d, J = 8.6 Hz), 8.08 (1H, d, J = 7.4 Hz); ^{13}C NMR (DMSO-d_6 125 MHz) δ 21.0, 109.0, 114.6, 118.9, 121.1, 124.2, 125.0, 126.2, 126.7, 129.5, 130.2, 134.3, 136.4, 139.1, 145.5; MS (GC-MS): *m/z* (%) = 297 ([M]$^+$, 42), 233 (36), 232 (33), 218 (30), 142 (100), 116 (28), 115 (91), 91 (76), 89 (29), 65 (27).

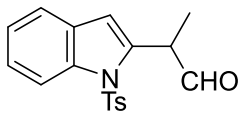

3*B*

2-(1-Tosyl-1H-indol-2-yl)propanal. Colorless oil; R_f 0.47 (hexane/AcOEt = 3/1); ^{1}H NMR (500 MHz, $CDCl_3$) δ 1.50 (3H, d, J = 7.4 Hz), 2.34 (3H, s), 4.55-4.56 (1H, m), 6.53 (1H, s), 7.21-7.24 (3H, m), 7.31 (1H, td, J = 1.3 Hz), 7.47 (1H, d, J = 7.4 Hz), 7.62 (2H, d, J = 8.6 Hz), 8.12 (1H, d, J = 8.0 Hz), 9.76 (1H, s); ^{13}C NMR ($CDCl_3$, 125 MHz) δ 14.4, 21.7, 45.6, 110.8, 115.0, 120.9, 123.9, 124.9, 126.4, 129.4, 130.1, 135.0, 135.9, 137.3, 145.2, 198.9; IR (neat) 2985 w, 2937 w, 2827 w, 1728 m, 1596 w, 1450 m, 1366 m, 1273 s, 1150 m, 1090 m, 812 w, 749 w, 676 w, 573 m, 543 m; MS (GC-MS): *m/z* (%) = 327 ([M]$^+$, 21), 299 (28), 298 (41), 234 (22), 155 (31), 144 (61), 143 (100), 142 (48), 117 (24), 115 (38), 91 (78), 65 (25); Exact mass (EI) calcd for $C_{18}H_{17}NO_3S$ 327.0929, found 327.0927.

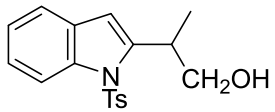

3*BB*

2-(1-Tosyl-1H-indol-2-yl)propan-1-ol. Colorless oil; R_f 0.21 (hexane/AcOEt = 2/1); ^{1}H NMR (500 MHz, $CDCl_3$) δ 1.35 (3H, d, *J* = 6.9 Hz), 1.55 (1H, d, *J* = 6.9 Hz), 2.33 (3H, s), 3.74-3.78 (1H, m), 3.83-3.89 (2H, m), 6.52 (1H, s), 7.17-7.19 (3H, m), 7.29-7.27 (1H, m), 7.43 (1H, d, *J* = 7.4), 7.58 (2H, d, *J* = 8.6 Hz), 8.19 (1H, d, *J* = 8.6 Hz); ^{13}C NMR ($CDCl_3$, 125 MHz) δ 17.5, 21.6, 35.5, 67.7, 108.8, 111.7, 115.3, 120.3, 123.71, 123.74, 124.3, 126.1, 126.2, 126.4, 129.7, 130.1, 135.8, 144.1; IR (neat) 3412 s, 2962 w, 2877 w, 1645 m, 1451 m, 1366 m, 1173 s, 1090 m, 1039 w, 910 w, 962 m, 812 w, 748 m, 656 m, 579 s, 547 m, 511 m; MS (GC-MS): *m/z* (%) = 329 ($[M]^+$, 29), 299 (42), 298 (39), 155 (27), 144 (81), 143 (100), 142 (41), 117 (26), 115 (30), 91 (58); Exact mass (EI) calcd for $C_{18}H_{19}O_3NS$ 329.1086, found 329.1085.

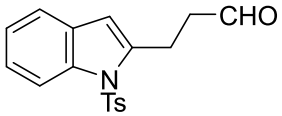

3*L*

3-(1-Tosyl-1H-indol-2-yl)propanal.[10] White solid; R_f 0.31 (hexane/AcOEt = 3/1); ^{1}H NMR (500 MHz, $CDCl_3$) δ 2.33 (3H, s), 2.97 (2H, td, *J* = 7.2, 1.1 Hz), 3.34 (2H, t, *J* = 6.9 Hz), 6.39 (1H,s), 7.18-7.23 (3H, m), 7.26-7.29 (1H, m), 7.40 (1H, d, *J* = 8.0 Hz), 7.63 (2H, d, *J* = 8.6 Hz), 8.16 (1H, d, *J* = 9.2 Hz), 9.83 (1H, d, *J* = 1.1 Hz); ^{13}C NMR ($CDCl_3$, 125MHz) δ 21.6, 21.9, 43.4, 110.0, 114.8, 120.3, 123.7, 124.3, 126.2, 129.5, 129.9, 135.7, 137.2, 139.8, 144.9, 200.9; IR

(neat) 2922 w, 2828 w, 2726 w, 1723 m, 1596 w, 1452 m, 1366 m, 1173 s, 1147 m, 1091 m, 1051 w, 812 w, 749 w , 683 w, 573 m, 543m; MS (GC-MS): *m/z* (%) = 327 ([M]$^+$, 29), 172 (67), 156 (48), 155 (21), 144 (96), 143 (59), 130 (43), 117 (64), 115 (25), 91 (100), 89 (24), 65 (34), 55 (90); Exact mass (EI) calcd for $C_{18}H_{17}NO_3S$ 327.0929, found 327.0928.

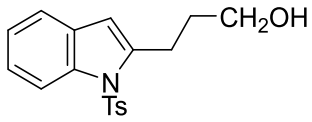

3*LL*

3-(1-Tosyl-1H-indol-2-yl)propan-1-ol.[10] Yellowish oil; R_f 0.11 (hexane/AcOEt = 2/1); ^{1}H NMR (500 MHz, $CDCl_3$) δ 1.49 (1H, s), 2.02-2.05 (2H, m), 2.33 (3H, s), 3.11 (2H, t, *J* = 7.2 Hz), 3.76 (2H, m), 6.42 (1H, s), 7.17-7.28 (4H, m), 7.41 (1H, d, *J* = 8.0 Hz), 7.62 (2H, d, *J* = 8.6 Hz), 8.16 (1H, d, *J* = 9.2 Hz); ^{13}C NMR ($CDCl_3$, 125 MHz) δ 21.5, 25.4, 32.3, 62.0, 109.3, 114.9, 120.1, 123.6, 124.0, 126.2, 129.7, 129.8, 135.9, 137.2, 141.5, 144.7; IR (neat) 3574 m, 3339 m, 2949 w, 2877 w, 1646 m, 1596 m, 1452 m, 1365 m, 1173 s, 1146 m, 1091 m, 1049 m, 812 m, 748 m, 666 m, 579 s, 543 m; MS (GC-MS): *m/z* (%) = 329 ([M]$^+$, 16), 221 (25), 174 (27), 143 (18), 130 (100), 91 (39); Exact mass (EI) calcd for $C_{18}H_{19}NO_3S$ 329.1086, found 329.1076.

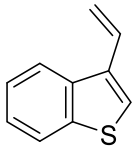

4

3-Vinylbenzo[b]thiophene.[4] Yellowish oil; R_f 0.82 (hexane/AcOEt = 2/1); ^{1}H NMR (500 MHz, $CDCl_3$) δ 5.39 (1H, dd, *J* = 11.2, 1.4 Hz), 5.82 (1H, dd, *J* = 17.2, 1.1 Hz), 6.96-7.02 (1H, m),

7.36-7.39 (1H, m), 7.40-7.44 (1H, m), 7.48 (1H, s), 7.87 (1H, d, *J* = 8.0 Hz), 7.93 (1H, d, *J* = 7.4 Hz); ^{13}C NMR ($CDCl_3$, 125 MHz) δ 115.6, 121.9, 122.2, 122.9, 124.2, 124.4, 129.2, 134.5, 140.4; MS (GC-MS): *m/z* (%) = 160 ($[M]^+$, 100), 159 (21), 116 (32), 115 (90).

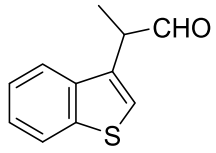

4B

2-(Benzo[b]thiophen-3-yl)propanal.[11] Colorless oil; R_f 0.38 (hexane/CH_2Cl_2= 1/1); ^{1}H NMR (500 MHz, $CDCl_3$) δ 1.58 (3H, d, *J* = 6.9 Hz), 4.04-4.07 (1H, m), 7.27 (1H, s), 7.38-7.44 (2H, m), 7.76 (1H, dd, *J* = 6.6, 2.0 Hz), 7.90 (1H, dd, *J* = 6.6, 2.0 Hz), 9.67 (1H, d, *J* = 1.7 Hz); ^{13}C NMR ($CDCl_3$, 125 MHz) δ 13.6, 46.7, 121.5, 123.1, 123.7, 124.4, 124.8, 132.2, 136.0, 140.6, 200.0; IR (neat) 3067 w, 2977 w, 2935 w, 1718 s, 1542 w, 1457 w, 1427 m, 1053 w, 846 w, 761 s, 732 s; MS (GC-MS): *m/z* (%) = 190 ($[M]^+$, 33), 161 (100), 128 (63), 115 (24); Exact mass (EI) calcd for $C_{11}H_{10}OS$ 190.0452, found 190.0430.

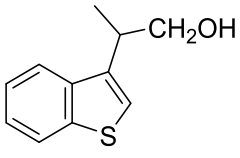

4BB

2-(Benzo[b]thiophen-3-yl)propan-1-ol. Colorless oil; R_f 0.41 (hexane/AcOEt = 2/1); ^{1}H NMR (500 MHz, $CDCl_3$) δ 1.43 (3H, d, *J* = 6.9 Hz), 3.44-3.47 (1H, m), 3.78-3.83 (1H, m), 3.87-3.92

(1H, m), 7.21 (1H, s), 7.36-7.40 (2H, m), 7.82 (1H, dd, J = 7.4, 1.1 Hz), 7.88 (1H, dd, J = 7.4, 1.1 Hz); ^{13}C NMR ($CDCl_3$, 125 MHz) δ 17.1, 35.8, 67.4, 121.2, 121.7, 123.0, 124.4, 138.4, 138.5, 140.6; IR (neat) 3347 m, 2963 m, 2930 m, 2874 m, 1456 m, 1427 m, 1381 w, 1314 w, 1252 w, 1031 m, 840 w, 762 s, 733 s; MS (GC-MS): *m/z* (%) = 192 ([M]$^+$, 27), 162 (12), 161 (100), 128 (45), 115 (18); Exact mass (EI) calcd for $C_{11}H_{12}OS$ 192.0609, found 192.0606.

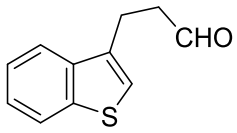

4*L*

3-(Benzo[b]thiophen-3-yl)propanal. Colorless oil; R_f 0.24 (hexane/CH_2Cl_2= 1/1); ^{1}H NMR (500 MHz, $CDCl_3$) δ 2.91-2.94 (2H, m), 3.18-3.21 (2H, m), 7.12 (1H, s), 7.35-7.43 (2H, m), 7.74 (1H, dd, J = 7.4, 1.1 Hz), 7.87 (1H, dd, J = 7.7, 1.4 Hz), 9.88 (1H, d, J = 1.1 Hz); ^{13}C NMR ($CDCl_3$, 125 MHz) δ 20.8, 43.0, 121.4, 121.6, 123.0, 124.0, 124.4, 134.6, 136.5, 140.4, 201.4; IR (neat) 3056 w, 2904 w, 2820 w, 2722 w, 1719 s, 1434 m, 993 w, 821 w, 744 m, 725 m, 568 w, 512 m; MS (GC-MS): *m/z* (%) = 190 ([M]$^+$, 51), 161 (26), 148 (40), 147 (100), 134 (49), 128 (21), 115 (21); Exact mass (EI) calcd for $C_{11}H_{10}OS$ 190.0452, found 190.0430.

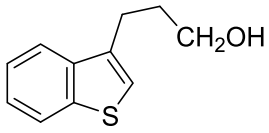

4*LL*

3-(Benzo[b]thiophen-3-yl)propan-1-ol.[12] Colorless oil; R_f 0.29 (hexane/AcOEt = 2/1); ^{1}H NMR

(500 MHz, $CDCl_3$) δ 1.40 (1H, s), 2.02-2.04 (2H, m), 2.96 (2H, t, *J* = 7.2 Hz), 3.76 (2H, t, *J* = 6.0 Hz), 7.12 (1H, s), 7.35-7.39 (2H, m), 7.77 (1H, d, *J* = 7.4 Hz), 7.87 (1H, d, *J* = 7.4 Hz); ^{13}C NMR ($CDCl_3$, 125 MHz) δ 24.7, 32.0, 62.3, 121.2, 121.6, 122.9, 123.8, 124.2, 136.1, 138.9, 140.4; IR (neat) 3309 m, 3055 w, 2935 m, 2870 m, 1426 m, 1055 m, 914 w, 849 w, 760 s, 731 s; MS (GC-MS): *m/z* (%) = 192 ($[M]^+$, 32), 148 (83), 147 (100), 115 (18); Exact mass (EI) calcd for $C_{11}H_{12}OS$ 192.0609, found 192.0614.

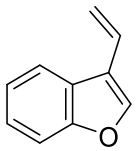

5

3-Vinylbenzofuran.[4] Colorless oil; R_f 0.93 (hexane/AcOEt = 4/1); ^1H NMR (500 MHz, $CDCl_3$) δ 5.36 (1H, d, *J* = 11.5 Hz), 5.85 (1H, d, *J* = 17.8 Hz), 6.79 (1H, dd, *J* = 17.8, 11.5 Hz), 7.30-7.33 (2H, m), 7.50 (1H, d, *J* = 8.0 Hz), 7.66 (1H, s), 7.83 (1H, d, *J* = 7.4 Hz); ^{13}C NMR ($CDCl_3$, 125 MHz) δ 111.7, 115.0, 119.6, 120.8, 123.0, 125.8, 126.5, 143.5, 155.8; MS (GC-MS): *m/z* (%) = 144 ($[M]^+$, 97), 116 (18), 115 (100), 89 (14), 63 (14).

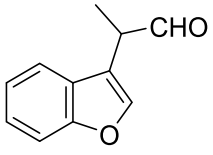

5B

2-(Benzofuran-3-yl)propanal. Colorless oil; R_f 0.57 (hexane/AcOEt = 4/1); ^1H NMR (500 MHz,

$CDCl_3$) δ 1.56 (3H, d, *J* = 5.4 Hz), 3.83 (1H, q, *J* = 6.9 Hz), 7.27 (1H, t, *J* = 8.0 Hz), 7.33 (1H, t, *J* = 7.7 Hz), 7.52 (2H, t, *J* = 6.9 Hz), 7.56 (1H, s), 9.72 (1H, d, *J* = 1.7 Hz); ^{13}C NMR ($CDCl_3$, 125 MHz) δ 13.3, 43.2, 111.8, 117.2, 119.7, 122.8, 124.8, 126.8, 142.2, 155.5, 200.1; IR (neat) 2981 w, 2808 w, 2714 w, 1725 s, 1453 m, 1185 w, 1104 m, 856 w, 745 s, 519 m; MS (GC-MS): *m/z* (%) = 174 ($[M]^+$, 31), 145 (100), 117 (37), 115 (56), 91 (17); Exact mass (EI) calcd for $C_{11}H_{10}O_2$ 174.0681, found 174.0665.

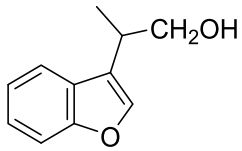

5*BB*

2-(Benzofuran-3-yl)propan-1-ol. Colorless oil; R_f 0.30 (hexane/AcOEt = 4/1); ^1H NMR (500 MHz, $CDCl_3$) δ 1.41 (3H, d, *J* = 6.9 Hz), 3.19-3.21 (1H, m), 3.79-3.90 (2H, m), 7.24 (1H, t, *J* = 8.0 Hz), 7.31 (1H, td, *J* = 7.6, 1.3 Hz), 7.49 (2H, t, *J* = 4.0 Hz), 7.62 (1H, d, *J* = 7.4 Hz); ^{13}C NMR ($CDCl_3$, 125 MHz) δ 16.5, 32.9, 67.1, 111.7, 120.0, 122.2, 122.4, 124.4, 127.2, 141.4, 155.6; IR (neat) 3353 m, 2946 m, 2934 m, 2876 m, 1452 s, 1185 m, 1093 m, 1037 m, 1007 m, 857 m, 744 s; MS (GC-MS): *m/z* (%) = 176 ($[M]^+$, 27), 145 (100), 117 (25), 115 (33); Exact mass (EI) calcd for $C_{11}H_{10}O_2$ 176.0837, found 176.0834.

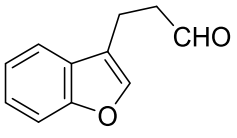

5*L*

3-(Benzofuran-3-yl)propanal.[13] Colorless oil; R_f 0.43 (hexane/AcOEt = 4/1); ^{1}H NMR (500 MHz, $CDCl_3$) δ 2.91-2.94 (2H, m), 3.18-3.21 (2H, m), 7.12 (1H, s), 7.35-7.43 (2H, m), 7.74 (1H, dd, *J* = 7.4, 1.1 Hz), 7.87 (1H, dd, *J* = 7.7, 1.4 Hz), 9.88 (1H, d, *J* = 1.1 Hz); ^{13}C NMR ($CDCl_3$, 125 MHz) δ 16.1, 43.0, 111.6, 118.7, 119.3, 122.4 124.4, 127.6, 141.4, 155.3, 201.3; IR (neat) 2920 w, 2825 w, 2727 w, 1722 s, 1453 s, 1388 w, 1280 w, 1186 m, 1092 m, 1009 w, 857 m, 745 s; MS (GC-MS): *m/z* (%) = 174 ([M]$^+$, 27), 132 (41), 131 (100), 118 (26), 115 (29), 103 (21), 77 (28); Exact mass (EI) calcd for $C_{11}H_{10}O_2$ 174.0681, found 174.0665.

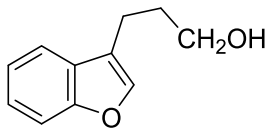

5*LL*

3-(Benzofuran-3-yl)propan-1-ol.[13] Colorless oil; R_f 0.23 (hexane/AcOEt = 4/1); ^{1}H NMR (500 MHz, $CDCl_3$) δ 1.34 (1H, s), 1.96-2.02 (2H, m), 2.79 (2H, td, *J* = 7.4, 1.0 Hz), 3.74 (2H, t, *J* = 6.6 Hz), 7.24 (1H, td, *J* = 7.4, 1.1 Hz), 7.29 (1H, td, *J* = 7.7, 1.5 Hz), 7.44 (1H, s), 7.47 (1H, d, *J* = 8.0 Hz), 7.57 (1H, d, *J* = 8.0 Hz); ^{13}C NMR ($CDCl_3$, 125 MHz) δ 19.8, 31.8, 62.2, 111.5, 119.6, 119.8, 122.2, 124.1, 128.1, 141.1, 155.3; IR (neat) 3378 s, 2925 m, 2850 m, 1636 w, 1451 m, 1182 w, 1089 m, 1056 m, 860 w, 742 s, 520 m, 504 m; MS (GC-MS): *m/z* (%) = 176 ([M]$^+$, 22), 132 (76), 131 (100), 115 (17), 103 (18), 77 (20); Exact mass (EI) calcd for $C_{11}H_{12}O_2$ 176.0837, found 174.0830.

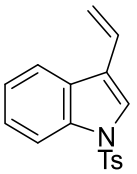

6

1-Tosyl-3-vinyl-1H-indole.[5] White solid; R_f 0.77 (hexane/AcOEt = 1/1); ^{1}H NMR (500 MHz, $CDCl_3$) δ 2.34 (3H, s), 5.35 (1H, dd, *J* = 11.5, 1.1 Hz), 5.80 (1H, dd, *J* = 17.8, 1.1 Hz), 6.77 (1H, dd, *J* = 17.8, 12.0 Hz), 7.22 (2H, d, *J* = 8.0 Hz), 7.28 (1H, td, *J* = 8.0, 1.1 Hz), 7.34 (1H, td, *J* = 7.9, 1.3 Hz), 7.61 (1H, s), 7.75-7.77 (3H, m), 7.99 (1H, d, *J* = 8.0 Hz); ^{13}C NMR ($CDCl_3$, 125 MHz) δ 21.6, 113.7, 115.3, 120.4, 120.9, 123.5, 124.1, 124.9, 126.8, 127.5, 129.0, 129.9, 135.0, 135.4, 145.0; MS (GC-MS): *m/z* (%) = 297 ([M]$^+$, 23), 142 (100), 115 (97), 91 (37), 89 (18), 65 (24).

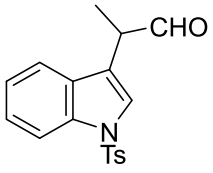

6*B*

2-(1-Tosyl-1H-indol-3-yl)propanal.[14] Colorless oil; R_f 0.66 (hexane/AcOEt = 1/1); ^{1}H NMR (500 MHz, $CDCl_3$) δ 1.52 (3H, d, *J* = 7.4 Hz), 2.35 (3H, s), 3.81 (1H, q, *J* = 6.9 Hz), 7.25 (3H, t, *J* = 7.4 Hz), 7.35 (1H, t, *J* = 7.7 Hz), 7.47 (2H, d, *J* = 8.6 Hz), 7.78 (2H, d, *J* = 8.0 Hz), 7.99 (1H, d, *J* = 8.6 Hz), 9.61 (1H, d, *J* = 1.7 Hz); ^{13}C NMR ($CDCl_3$, 125MHz) δ 13.4, 21.6, 44.1, 113.8, 118.9, 119.5, 123.4, 123.7, 125.2, 126.8, 129.7, 130.0, 135.0, 135.2, 145.1, 199.9; IR (neat) 1728 m, 1600 w, 1447 m, 1369 m, 1290 w, 1173 s, 1129 m, 1088 m, 964 w, 814 w, 747

m, 668 m, 575 m, 538, m, 512 m; MS (GC-MS): *m/z* (%) = 327 ([M]$^+$, 12), 299 (15), 298 (75), 207 (13), 155 (56), 144 (13), 143 (17), 115 (26), 91 (100), 65 (20); Exact mass (EI) calcd for $C_{18}H_{17}NO_3S$ 327.0929, found 327.0922.

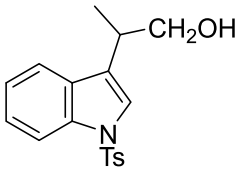

6*BB*

2-(1-Tosyl-1H-indol-3-yl)propan-1-ol. White solid; R_f 0.45 (hexane/AcOEt = 1/1); ^{1}H NMR (500 MHz, $CDCl_3$) δ 1.37 (3H, d, *J* = 6.9 Hz), 2.34 (3H, s), 3.18-3.21 (1H, m), 3.71-3.83 (2H, m), 7.21-7.25 (3H, m), 7.32 (2H, t, *J* = 7.4 Hz), 7.40 (1H, s), 7.54 (1H, d, *J* = 8.0 Hz), 7.76 (2H, d, *J* = 8.6 Hz), 7.98 (1H, d, *J* = 8.0 Hz); ^{13}C NMR ($CDCl_3$, 125MHz) δ 16.7, 21.6, 33.5, 67.2, 113.8, 119.7, 122.7, 123.0, 124.8, 126.8, 129.9, 130.3, 135.1, 135.3, 144.9; IR (KBr) 3561 w, 3345 w, 2967 w, 2877 w, 1596 w, 1448 m, 1366 m, 1284 w, 1173 s, 1133 m, 1091 m, 1022 m, 962 m, 814 w, 747 m, 667 m, 586 m, 539 m; MS (GC-MS): *m/z* (%) = 329 ([M]$^+$, 20), 298 (99), 155 (70), 144 (25), 143 (23), 115 (23), 91 (100); Exact mass (EI) calcd for $C_{18}H_{19}NO_3S$ 329.1086, found 329.1087.

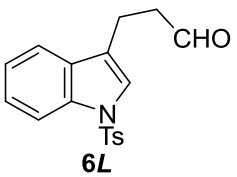

6*L*

3-(1-Tosyl-1H-indol-3-yl)propanal.[15] White solid; R_f 0.54 (hexane/AcOEt = 1/1); ^{1}H NMR (500

MHz, $CDCl_3$) δ, 2.35 (3H, s), 2.87 (2H, t, *J* = 7.2 Hz), 3.02 (2H, t, *J* = 7.2 Hz), 7.23-7.25 (3H, m), 7.34 (2H, t, *J* = 6.9 Hz), 7.48 (1H, d, *J* = 7.4 Hz), 7.75 (2H, d, *J* = 8.0 Hz), 7.99 (1H, d, *J* = 8.0 Hz), 9.85 (1H, s); ^{13}C NMR ($CDCl_3$, 125 MHz) δ 17.3, 21.5, 42.8, 113.8, 119.2, 121.3, 122.9, 123.1, 124.8, 126.7, 129.8, 130.5, 135.1, 135.2, 144.8, 201.1; IR (KBr) 2919 w, 2842 w, 1715 m, 1451 m, 1371 m, 1171 m, 1173 m, 1133 m, 979 w, 754 m, 667 m, 570 w , 537 w; MS (GC-MS): *m/z* (%) = 327 ($[M]^+$, 34), 271 (61), 155 (64), 144 (39), 143 (31), 115 (31), 91 (100), 65 (36), 55 (53); Exact mass (EI) calcd for $C_{18}H_{17}NO_3S$ 327.0929, found 327.0935.

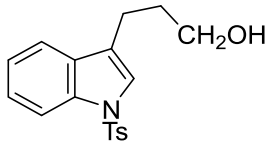

6*LL*

3-(1-Tosyl-1H-indol-3-yl)propan-1-ol.[16] Colorless oil; R_f 0.35 (hexane/AcOEt = 1/1); ^1H NMR (500 MHz, $CDCl_3$) δ 1.41 (1H, s), 1.92-1.97 (2H, m), 2.32 (3H, s), 2.76 (2H, t, *J* = 7.7 Hz), 3.70 (2H, t, *J* = 6.3 Hz), 7.20-7.23 (3H, m), 7.31 (1H, t, *J* = 7.7 Hz), 7.34 (1H, s), 7.49 (1H, d, *J* = 8.0 Hz), 7.74 (2H, d, *J* = 8.0 Hz), 7.98 (1H, d, *J* = 8.0 Hz); ^{13}C NMR ($CDCl_3$, 125 MHz) δ 21.0, 21.5, 31.7, 62.1, 113.7, 119.4, 122.7, 123.0, 124.6, 126.7, 129.8, 131.0, 135.2, 135.3, 144.7; IR (neat) 3559 w, 3367 w, 2919 w, 2866 w, 1596 w, 1447 m, 1363 m, 1276 w, 1172 s, 1120 m, 973 w, 813 w, 746 m, 670 s, 599 m, 573 m, 537 m; MS (GC-MS): *m/z* (%) = 329 ($[M]^+$, 32), 285 (40), 156 (68), 155 (47), 130 (100), 129 (34), 128 (28), 91 (75), 65 (25); Exact mass (EI) calcd for $C_{18}H_{19}NO_3S$ 329.1086, found 329.1087.

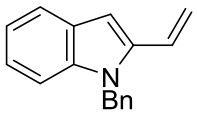

7

1-Benzyl-2-vinyl-1H-indole.[6] White solid; R_f 0.59 (hexane/AcOEt = 4/1); ^{1}H NMR (ACETONE-d_6, 500 MHz) δ 5.29 (1H, dd, J = 10.9, 1.1 Hz), 5.53 (2H, s), 5.87 (1H, dd, J = 17.8, 1.1 Hz), 6.83 (1H, s), 6.85-6.91 (1H, m), 7.02-7.06 (3H, m), 7.10 (1H, t, J = 7.4 Hz), 7.22 (1H, t, J = 7.2 Hz), 7.28 (2H, t, J = 7.4 Hz) 7.38 (1H, d, J = 8.6 Hz), 7.56 (1H, d, J = 7.4 Hz); ^{13}C NMR (ACETONE-d_6, 125 MHz) δ 46.8, 99.9, 110.7, 116.6, 120.7, 121.2, 122.6, 126.9, 127.0, 128.0, 128.9, 129.4, 138.6, 139.0, 139.4; MS (GC-MS): *m/z* (%) = 233 ([M]$^+$, 56), 232 (31), 218 (26), 217 (15), 91 (100), 65 (19).

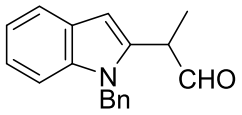

7B

2-(1-Benzyl-1H-indol-2-yl)propanal. Colorless oil; R_f 0.44 (hexane/AcOEt = 4/1); ^{1}H NMR (500 MHz, $CDCl_3$) δ 1.49 (3H, d, J = 6.9 Hz), 3.72-3.76 (1H, m), 5.41 (2H, s), 6.51 (1H, s), 6.95 (2H, d, J = 6.9 Hz), 7.17 (1H, t, J = 6.9 Hz), 7.21 (1H, t, J = 11.2 Hz), 7.26-7.31 (4H, m), 7.67 (1H, d, J = 7.4 Hz), 9.49 (1H, d, J = 2.3 Hz); ^{13}C NMR ($CDCl_3$, 125 MHz) δ 13.9, 44.8, 46.5, 101.4, 109.6, 120.0, 120.5, 122.1, 125.7, 127.5, 127.7, 128.9, 136.1, 137.3, 137.7, 198.7; IR (neat) 3056 w, 3030 w, 2981 w, 2935 w, 2812 w, 1721 s, 1453 s, 1347 m, 1315 m, 1167 w, 786 w, 750 m, 730 s, 969 m, 816 m; MS (GC-MS): *m/z* (%) = 263 ([M]$^+$, 34), 235 (15), 234

(75), 117 (21), 91 (100), 16 (16); Exact mass (EI) calcd for $C_{18}H_{17}NO$ 263.1310, found 263.1304.

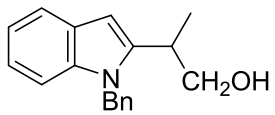

7BB

2-(1-Benzyl-1H-indol-2-yl)propan-1-ol. Colorless oil; R_f 0.44 (hexane/AcOEt = 2/1); ^{1}H NMR (500 MHz, $CDCl_3$) δ 1.26 (3H, d, J = 6.9 Hz), 1.54 (1H, d, J = 6.3 Hz), 3.11-3.18 (1H, m), 3.66-3.77 (2H, m), 5.39-5.44 (2H, m), 6.44 (1H, s), 6.95 (2H, d, J = 7.4 Hz), 7.10-7.15 (2H, m), 7.21-7.29 (4H, m), 7.61 (1H, d, J = 6.9 Hz); ^{13}C NMR ($CDCl_3$, 125MHz) δ 17.6, 34.0, 46.4, 67.3, 98.4, 109.6, 119.8, 120.1, 121.3, 125.7, 127.3, 127.9, 128.8, 137.1, 137.8, 142.8; IR (neat) 3376 w, 3056 w, 2030 w, 2966 w, 2931 w, 2875 w, 1462 m, 1453 m, 1354 w, 1313 m, 1027 m, 780 w, 749 m, 729 m, 695 w; MS (GC-MS): *m/z* (%) = 265 ($[M]^+$, 47), 235 (17), 234 (89), 117 (22), 91 (100); Exact mass (EI) calcd for $C_{18}H_{19}NO$ 265.1467, found 265.1459.

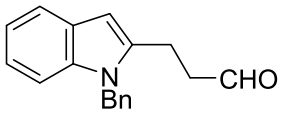

7L

3-(1-Benzyl-1H-indol-2-yl)propanal. Yellowish oil; R_f 0.25 (hexane/AcOEt = 4/1); ^{1}H NMR (500 MHz, $CDCl_3$) δ 2.78 (4H, s), 4.43 (2H, d, J = 5.7 Hz), 5.06 (1H, s), 6.52 (1H, d, J = 8.0 Hz), 6.60 (1H, t, J = 7.4 Hz), 7.11 (1H, t, J = 11.7 Hz), 7.24-7.29 (2H, m), 7.33-7.37 (4H, m),

9.82 (1H, s); ^{13}C NMR ($CDCl_3$, 125MHz) δ 12.9, 42.8, 47.6, 78.1, 93.6, 107.6, 109.7, 116.3, 127.0, 127.1, 128.6, 129.5, 131.9, 139.2, 148.8, 200.4; IR (neat) 3392 w, 3024 w, 2900 w, 2835 w, 1722 m, 1599 m, 1574 m, 1508 s, 1456 m, 1324 m, 745 m, 525 w, 511 m; MS (GC-MS): *m/z* (%) = 263 ([M]$^+$, 49), 218 (21), 206 (47), 186 (32), 144 (29), 130 (24), 91 (100), 65 (24); Exact mass (EI) calcd for $C_{18}H_{17}NO$ 263.1310, found 263.1310.

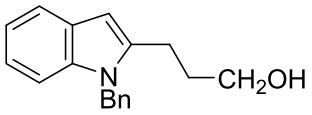

7LL

3-(1-Benzyl-1H-indol-2-yl)propan-1-ol. Colorless oil; R_f 0.22 (hexane/AcOEt = 2/1); ^{1}H NMR (500 MHz, $CDCl_3$) δ 1.34 (1H, s), 1.86-1.81 (2H, m), 2.59 (2H, t, *J* = 6.9 Hz), 3.76 (2H, s), 4.41 (2H, s), 5.04 (1H, s), 6.55 (1H, d, *J* = 8.0 Hz), 6.62 (1H, t, *J* = 7.2 Hz), 7.12 (1H, t, *J* = 7.2 Hz), 7.27-7.30 (2H, m), 7.34-7.39(4H, m); ^{13}C NMR ($CDCl_3$, 125 MHz) δ 16.3, 31.3, 47.7, 61.7, 77.6, 95.2, 108.1, 109.6, 116.4, 127.1, 127.2, 128.6, 129.2, 131.9, 139.1, 148.6; IR (neat) 3398 m, 3029 w, 2928 m, 2873 m, 1600 m, 1575 m, 1511 s, 1454 m, 1324 m, 1281 m, 1061 m, 746 m, 698 m, 512 w; MS (GC-MS): *m/z* (%) = 265 ([M]$^+$, 59), 206 (56), 188 (54), 144 (26), 130 (22), 91 (100). Exact mass (EI) calcd for $C_{18}H_{19}NO$ 265.1467, found 265.1462.

References

1. Giordano, G., Crabtree, R. H., Heintz, R. M., Forster, D., & Morris, D. E. *Inorg. Synth.,* **1979**, *19*, 218-220.
2. Falk, A., Cavalieri, A., Nichol, G. S., Vogt, D., & Schmalz, H. G. *Adv. Synth. Catal.* **2015**, *357*, 3317-3320.
3. Wang, Y. F. & Chiba, S. *J. Am. Chem. Soc.* **2009**, *131*, 12570-12572.
4. Retich, C. & Bräse, S. *Eur. J. Org. Chem.* **2018**, 60-77.
5. Cowell, J., Abualnaja, M., Morton, S., Linder, R., Buckingham, F., Waddell, P. G., & Hall, M. J. *RSC Adv.* **2015**, *5*, 16125-16152.
6. Cao, Y. J., Cheng, H. G., Lu, L. Q., Zhang, J. J., Cheng, Y., Chen, J. R., & Xiao, W. J. *Adv. Synth. Catal.* **2011**, *353*, 617-623.
7. Wei, B., Chen, C., You, C., Lv, H., & Zhang, X. *Org. Chem. Front.* **2017**, *4*, 288-291.
8. Masutani, K., Minowa, T., Hagiwara, Y., & Mukaiyama, T. *Chem. Soc. Jpn.* **2006**, *79*, 1106-1117.
9. (a) Zhou, L., Shi, Y., Xiao, Q., Liu, Y., Ye, F., Zhang, Y., & Wang, J. *Org. Lett.* **2011**, *13*, 968-971; (b) Zhou, R., Wang, W., Jiang, Z. J., Wang, K., Zheng, X. L., Fu, H. Y. & Li, R. X. *Chem. Commun.* **2014**, *50*, 6023-6026; (c) Bruneau, A., Gustafson, K. P., Yuan, N., Tai, C. W., Persson, I., Zou, X., & Bäckvall, J. E. *Chem.–Eur. J.* **2017**, *23*, 12886-12891.
10. (a) Hiroya, K., Itoh, S., & Sakamoto, T. *J. Org. Chem.* **2004**, *69*, 1126-1136; (b) Namba,

K., Yamamoto, H., Sasaki, I., Mori, K., Imagawa, H., & Nishizawa, M. *Org. Lett.* **2008**, *10*, 1767-1770.

11. Tanaka, R., Nakano, K., & Nozaki, K. *J. Org. Chem.* **2007**, *72*, 8671-8676.
12. (a) Martins, A., Alberico, D., & Lautens, M. *Org. Lett.* **2006**, *8*, 4827-4829; (b) Martins, A., & Lautens, M. *J. Org. Chem.* **2008**, *73*, 8705-8710.
13. Jui, N. T., Lee, E. C., & MacMillan, D. W. *J. Am. Chem. Soc.* **2010**, *132*, 10015-10017.
14. Fridén-Saxin, M., Pemberton, N., da Silva Andersson, K., Dyrager, C., Friberg, A., Grøtli, M., & Luthman, K. *J. Org. Chem.* **2009**, *74*, 2755-2759.
15. Fridén-Saxin, M., Pemberton, N., da Silva Andersson, K., Dyrager, C., Friberg, A., Grøtli, M., & Luthman, K. *J. Org. Chem.* **2009**, *74*, 2755-2759.
16. Ryzhakov, D., Jarret, M., Guillot, R., Kouklovsky, C., & Vincent, G. *Org. Lett.* **2017**, *19*, 6336-6339.

5.2 Supporting Information

5.2.1 HPLC Charts

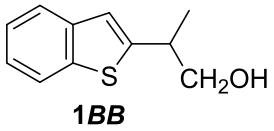

1*BB*

The ee valune was determined on an AD-H column (n-hexane/2-propanol = 98/2, flow = 1.0 mL/min, detection at 254 nm), with enantiomers eluting at 27.0 (*R*) and 30.0 (*S*) min. $[\alpha]_D^{22}$ -9.3° (c 1.1, $CHCl_3$) for 36%ee (*S*) (Table 3.3, Entry 3); lit. $[\alpha]_D^{25}$ +21.8° (c 1.0, $CHCl_3$) for 100%ee (*R*).[1]

racemate

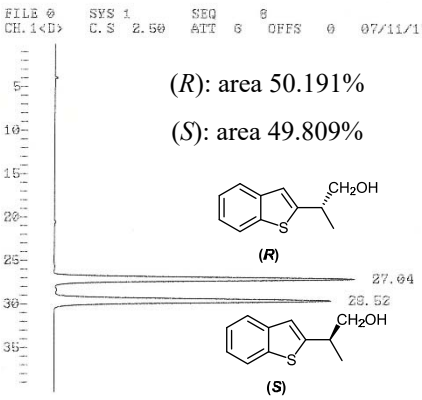


```
FILE @    SYS 1       SEQ     @
CH.1<D>   C.S  2.50   ATT  6   OFFS   @   07/11/17  17:30

                D-7500 INTEGRATOR REPORT

ANALYZED: 07/11/17  17:30                REPORTED: 07/11/17  18:10
SYSTEM  : 1
METHOD  :                    OPERATOR:
CHANNEL : 1 <DIGITAL>        SEQ     :      6

FILE    : @                  MODULE T-PROG :          DETECTOR= 1
CALC-METHOD: AR/HI%  <AREA>  COMPONENT TBL :   @

  NO.      RT        AREA       CONC  BC
    1   27.04     1083758     50.191  BB
    2   29.52     1075518     49.809  BB
TOTAL
                  2159276    100.000
PEAK REJ :       20000
```

Table 3.1 entry 4

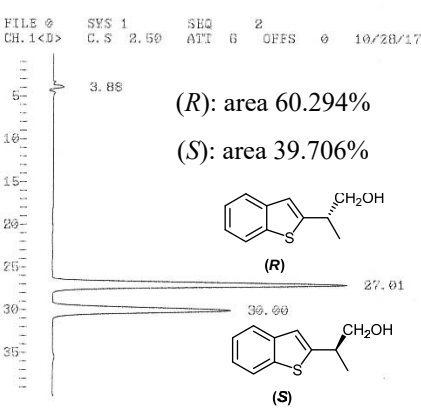


```
FILE @    SYS 1       SEQ     2
CH.1<D>   C.S  2.50   ATT  6   OFFS   @   10/28/17  17:39

                D-7500 INTEGRATOR REPORT

ANALYZED: 10/28/17  17:39                REPORTED: 10/28/17  18:22
SYSTEM  : 1
METHOD  :                    OPERATOR:
CHANNEL : 1 <DIGITAL>        SEQ     :      2

FILE    : @                  MODULE T-PROG :          DETECTOR= 1
CALC-METHOD: AR/HI%  <AREA>  COMPONENT TBL :   @

  NO.      RT        AREA       CONC  BC
    2   27.01     1394931     60.294  BB
    3   30.00      918615     39.706  BB
TOTAL
                  2313546    100.000
PEAK REJ :       35000
```

Table 3.2 entry 1

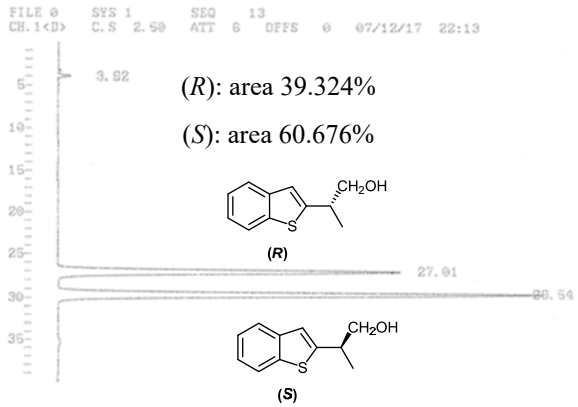

(*R*): area 39.324%

(*S*): area 60.676%

D-7500 INTEGRATOR REPORT

ANALYZED: 07/12/17 22:13 REPORTED: 07/12/17 22:53
SYSTEM : 1
METHOD : OPERATOR:
CHANNEL : 1 <DIGITAL> SEQ : 13

FILE : 0 MODULE T-PROG : DETECTOR= 1
CALC-METHOD: AR/HI% <AREA> COMPONENT TBL : 0

NO.	RT	AREA	CONC	BC
2	27.01	1284039	39.324	BB
3	28.54	1982616	60.676	BB
TOTAL		3267655	100.000	

PEAK REJ : 20000

Table 3.2 entry 2

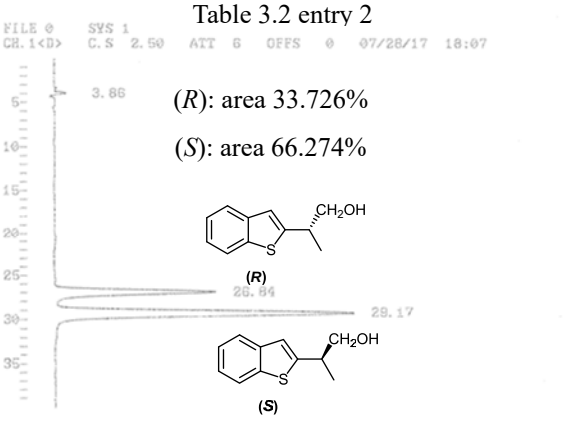

(*R*): area 33.726%

(*S*): area 66.274%

D-7500 INTEGRATOR REPORT

ANALYZED: 07/28/17 18:07 REPORTED: 07/28/17 18:58
SYSTEM : 1
METHOD : OPERATOR:
CHANNEL : 1 <DIGITAL> SEQ : 6

FILE : 0 MODULE T-PROG : DETECTOR= 1
CALC-METHOD: AR/HI% <AREA> COMPONENT TBL : 0

NO.	RT	AREA	CONC	BC
2	26.84	735602	33.726	BB
3	29.17	1445511	66.274	BB
TOTAL		2181113	100.000	

PEAK REJ : 30000

Table 3.2 entry 3

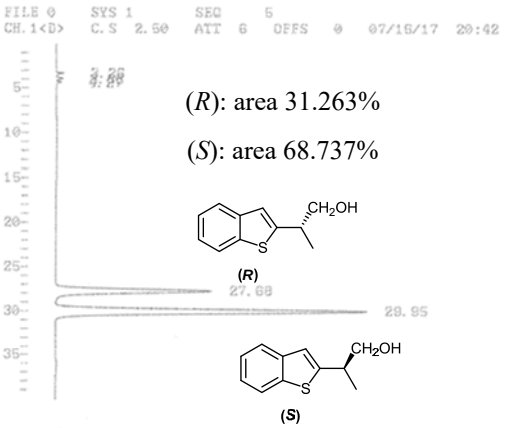

(*R*): area 31.263%

(*S*): area 68.737%

D-7500 INTEGRATOR REPORT

ANALYZED: 07/16/17 20:42 REPORTED: 07/16/17 21:22
SYSTEM : 1
METHOD : OPERATOR:
CHANNEL : 1 <DIGITAL> SEQ : 5

FILE : 0 MODULE T-PROG : DETECTOR= 1
CALC-METHOD: AR/HI% <AREA> COMPONENT TBL : 0

NO.	RT	AREA	CONC	BC
4	27.68	562013	31.263	BB
5	29.95	1235685	68.737	BB
TOTAL		1797698	100.000	

PEAK REJ : 20000

Table 3.2 entry 4

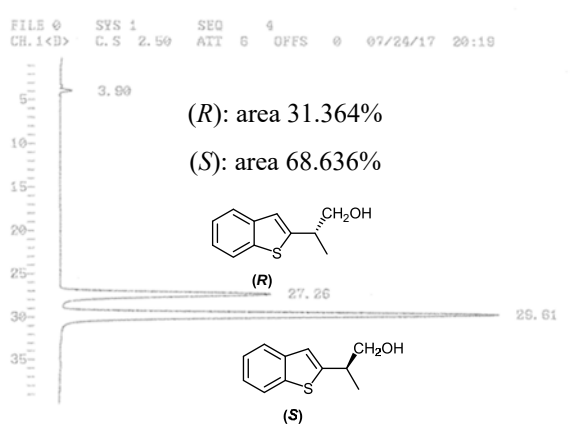

(*R*): area 31.364%

(*S*): area 68.636%

D-7500 INTEGRATOR REPORT

ANALYZED: 07/24/17 20:19 REPORTED: 07/24/17 21:02
SYSTEM : 1
METHOD : OPERATOR:
CHANNEL : 1 <DIGITAL> SEQ : 4

FILE : 0 MODULE T-PROG : DETECTOR= 1
CALC-METHOD: AR/HI% <AREA> COMPONENT TBL : 0

NO.	RT	AREA	CONC	BC
2	27.26	994719	31.364	BB
3	29.61	2176816	68.636	BB
TOTAL		3171535	100.000	

PEAK REJ : 27000

Table 3.2 entry 5

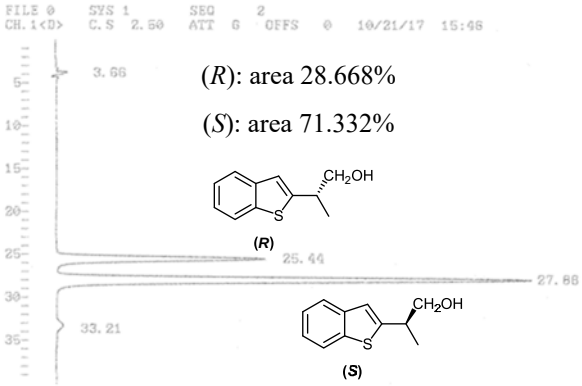

(*R*): area 28.668%

(*S*): area 71.332%

D-7500 INTEGRATOR REPORT

ANALYZED: 10/21/17 15:46 REPORTED: 10/21/17 16:34
SYSTEM : 1
METHOD : OPERATOR:
CHANNEL : 1 <DIGITAL> SEQ : 2

FILE : 0 MODULE T-PROG : DETECTOR= 1
CALC-METHOD: AR/HI% <AREA> COMPONENT TBL : 0

NO.	RT	AREA	CONC	BC
2	25.44	918023	28.668	BB
3	27.88	2284204	71.332	BB
TOTAL		3202227	100.000	

PEAK REJ : 35000

Table 3.2 entry 6

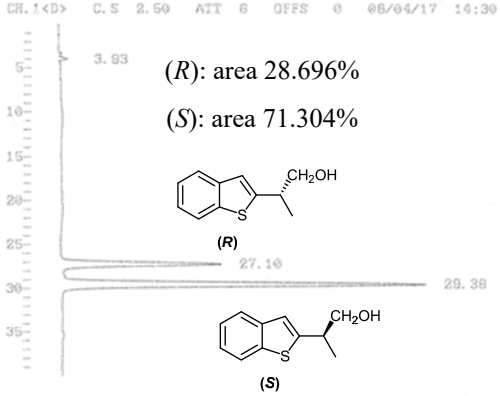

(*R*): area 28.696%

(*S*): area 71.304%

D-7500 INTEGRATOR REPORT

ANALYZED: 08/04/17 14:30 REPORTED: 08/04/17 15:10
SYSTEM : 1
METHOD : OPERATOR:
CHANNEL : 1 <DIGITAL> SEQ : 3

FILE : 0 MODULE T-PROG : DETECTOR= 1
CALC-METHOD: AR/HI% <AREA> COMPONENT TBL : 0

NO.	RT	AREA	CONC	BC
2	27.10	564310	28.696	BB
3	29.39	1402210	71.304	BB
TOTAL		1966520	100.000	

PEAK REJ : 20000

Table 3.2 entry 7

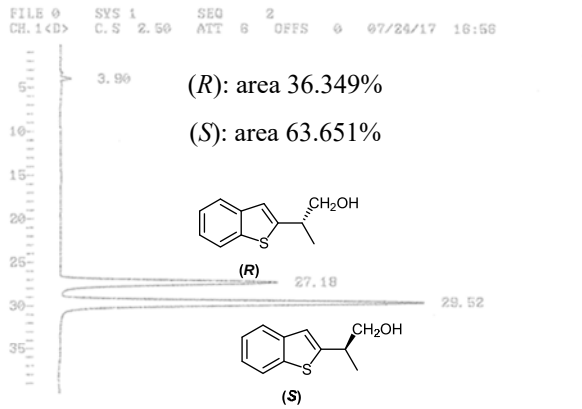

(*R*): area 36.349%

(*S*): area 63.651%

D-7500 INTEGRATOR REPORT

ANALYZED: 07/24/17 16:56 REPORTED: 07/24/17 17:47
SYSTEM : 1
METHOD : OPERATOR:
CHANNEL : 1 <DIGITAL> SEQ : 2

FILE : 0 MODULE T-PROG : DETECTOR= 1
CALC-METHOD: AR/HI% <AREA> COMPONENT TBL : 0

NO.	RT	AREA	CONC	BC
2	27.18	1009435	36.349	BB
3	29.52	1767612	63.651	BB
TOTAL		2777047	100.000	

PEAK REJ : 23000

Table 3.2 entry 8

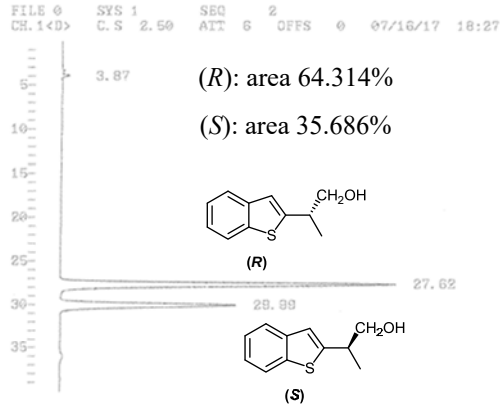

(*R*): area 64.314%

(*S*): area 35.686%

D-7500 INTEGRATOR REPORT

ANALYZED: 07/16/17 18:27 REPORTED: 07/16/17 19:07
SYSTEM : 1
METHOD : OPERATOR:
CHANNEL : 1 <DIGITAL> SEQ : 2

FILE : 0 MODULE T-PROG : DETECTOR= 1
CALC-METHOD: AR/HI% <AREA> COMPONENT TBL : 0

NO.	RT	AREA	CONC	BC
2	27.62	1237983	64.314	BB
3	29.99	686928	35.686	BB
TOTAL		1924911	100.000	

PEAK REJ : 20000

Table 3.2 entry 9

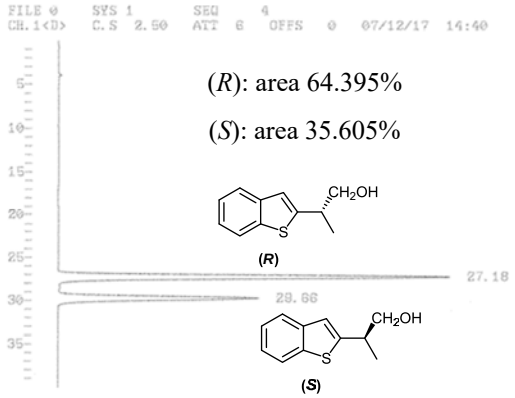

(*R*): area 64.395%

(*S*): area 35.605%

D-7500 INTEGRATOR REPORT

ANALYZED: 07/12/17 14:40 REPORTED: 07/12/17 15:20
SYSTEM : 1
METHOD : OPERATOR:
CHANNEL : 1 <DIGITAL> SEQ : 4

FILE : 0 MODULE T-PROG : DETECTOR= 1
CALC-METHOD: AR/HI% <AREA> COMPONENT TBL : 0

NO.	RT	AREA	CONC	BC
1	27.18	1436548	64.395	BB
2	29.66	794291	35.605	BB
TOTAL		2230839	100.000	

PEAK REJ : 20000

Table 3.2 entry 10

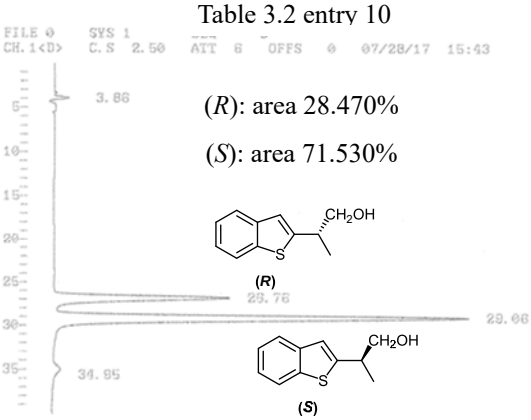

(*R*): area 28.470%

(*S*): area 71.530%

D-7500 INTEGRATOR REPORT

ANALYZED: 07/28/17 15:43 REPORTED: 07/28/17 16:23
SYSTEM : 1
METHOD : OPERATOR:
CHANNEL : 1 <DIGITAL> SEQ : 3

FILE : 0 MODULE T-PROG : DETECTOR= 1
CALC-METHOD: AR/HI% <AREA> COMPONENT TBL : 0

NO.	RT	AREA	CONC	BC
2	29.76	804185	28.470	BB
3	29.06	2020519	71.530	BB
TOTAL		2824704	100.000	

PEAK REJ : 40000

Table 3.2 entry 11

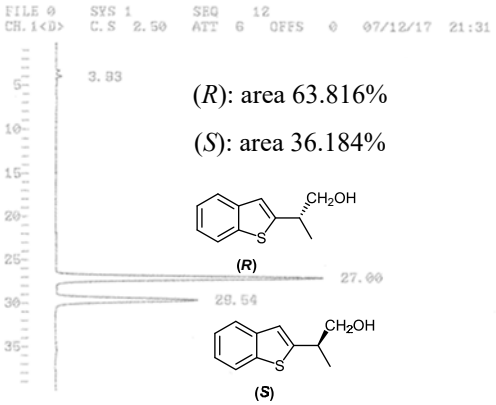

(*R*): area 63.816%

(*S*): area 36.184%

D-7500 INTEGRATOR REPORT

ANALYZED: 07/12/17 21:31 REPORTED: 07/12/17 22:12
SYSTEM : 1
METHOD : OPERATOR:
CHANNEL : 1 <DIGITAL> SEQ : 12

FILE : 0 MODULE T-PROG : DETECTOR= 1
CALC-METHOD: AR/HI% <AREA> COMPONENT TBL : 0

NO.	RT	AREA	CONC	BC
2	27.00	962327	63.816	BB
3	29.54	545650	36.184	BB
TOTAL		1507977	100.000	

PEAK REJ : 20000

Table 3.3 entry 2

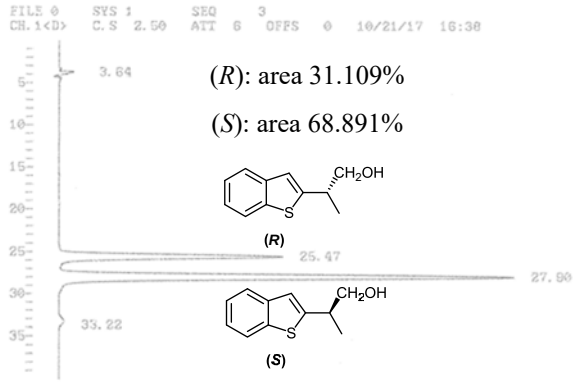

(*R*): area 31.109%

(*S*): area 68.891%

D-7500 INTEGRATOR REPORT

ANALYZED: 10/21/17 16:38 REPORTED: 10/21/17 17:22
SYSTEM : 1
METHOD : OPERATOR:
CHANNEL : 1 <DIGITAL> SEQ : 3

FILE : 0 MODULE T-PROG : DETECTOR= 1
CALC-METHOD: AR/HI% <AREA> COMPONENT TBL : 0

NO.	RT	AREA	CONC	BC
2	25.47	1004770	31.109	BB
3	27.90	2225019	68.891	BB
TOTAL		3229789	100.000	

PEAK REJ : 41000

Table 3.3 entry 3

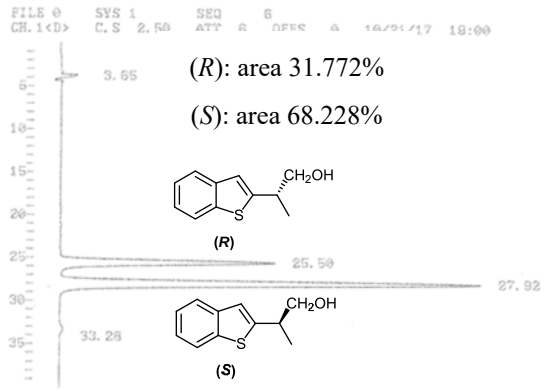

(*R*): area 31.772%

(*S*): area 68.228%

D-7500 INTEGRATOR REPORT

ANALYZED: 10/21/17 18:00 REPORTED: 10/21/17 18:44
SYSTEM : 1
METHOD : OPERATOR:
CHANNEL : 1 <DIGITAL> SEQ : 6

FILE : 0 MODULE T-PROG : DETECTOR= 1
CALC-METHOD: AR/HI% <AREA> COMPONENT TBL : 0

NO.	RT	AREA	CONC	BC
2	25.50	945036	31.772	BB
3	27.92	2029367	68.228	BB
TOTAL		2974403	100.000	

PEAK REJ : 50000

Table 3.4 entry 2

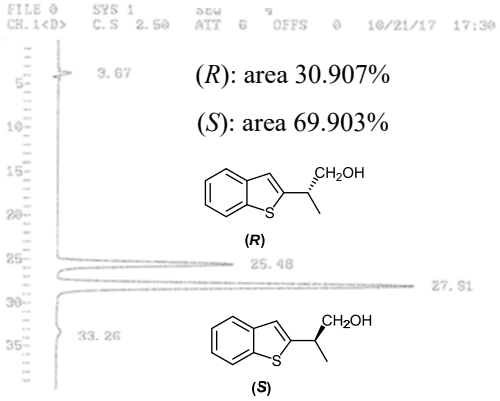

(*R*): area 30.907%

(*S*): area 69.903%

D-7500 INTEGRATOR REPORT

ANALYZED: 10/21/17 17:30 REPORTED: 10/21/17 18:10
SYSTEM : 1
METHOD : OPERATOR:
CHANNEL : 1 <DIGITAL> SEQ : 4

FILE : 0 MODULE T-PROG : DETECTOR= 1
CALC-METHOD: AR/HI% <AREA> COMPONENT TBL : 0

NO.	RT	AREA	CONC	BC
2	25.48	756216	30.907	BB
3	27.91	1690519	69.093	BB
TOTAL		2446735	100.000	

PEAK REJ : 41000

Table 3.4 entry 4

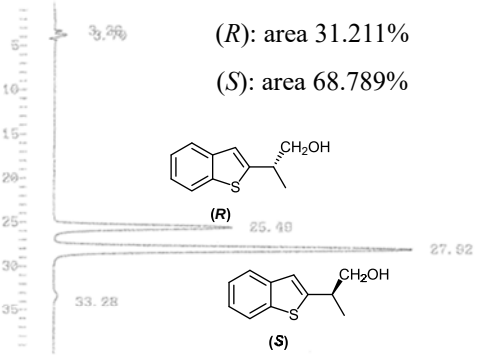

(*R*): area 31.211%

(*S*): area 68.789%

D-7500 INTEGRATOR REPORT

ANALYZED: 10/21/17 16:13 REPORTED: 10/21/17 16:53
SYSTEM : 1
METHOD : OPERATOR:
CHANNEL : 1 <DIGITAL> SEQ : 5

FILE : 0 MODULE T-PROG : DETECTOR= 1
CALC-METHOD: AR/HI% <AREA> COMPONENT TBL : 0

NO.	RT	AREA	CONC	BC
3	25.48	771284	31.211	BB
4	27.92	1699874	68.789	BB
TOTAL		2471138	100.000	

PEAK REJ : 41000

Table 3.5 entry 2

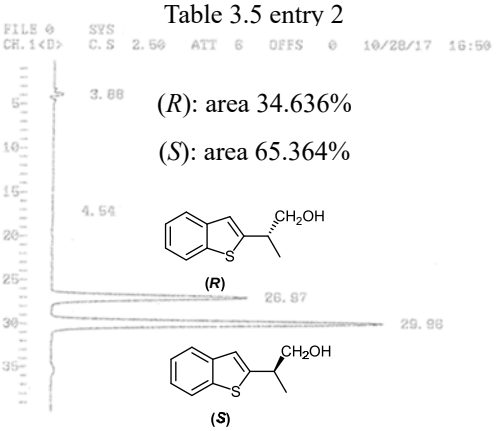

(*R*): area 34.636%

(*S*): area 65.364%

D-7500 INTEGRATOR REPORT

ANALYZED: 10/28/17 16:50 REPORTED: 10/28/17 17:31
SYSTEM : 1
METHOD : OPERATOR:
CHANNEL : 1 <DIGITAL> SEQ : 1

FILE : 0 MODULE T-PROG : DETECTOR= 1
CALC-METHOD: AR/HI% <AREA> COMPONENT TBL : 0

NO.	RT	AREA	CONC	BC
3	26.87	891502	34.636	BB
4	29.96	1682413	65.364	BB
TOTAL		2573915	100.000	

PEAK REJ : 30000

Reference

1. Sjoeberg, *Arkiv foer Kemi*, **1958**, *12*, 565-570.

5.2.2 NMR Charts

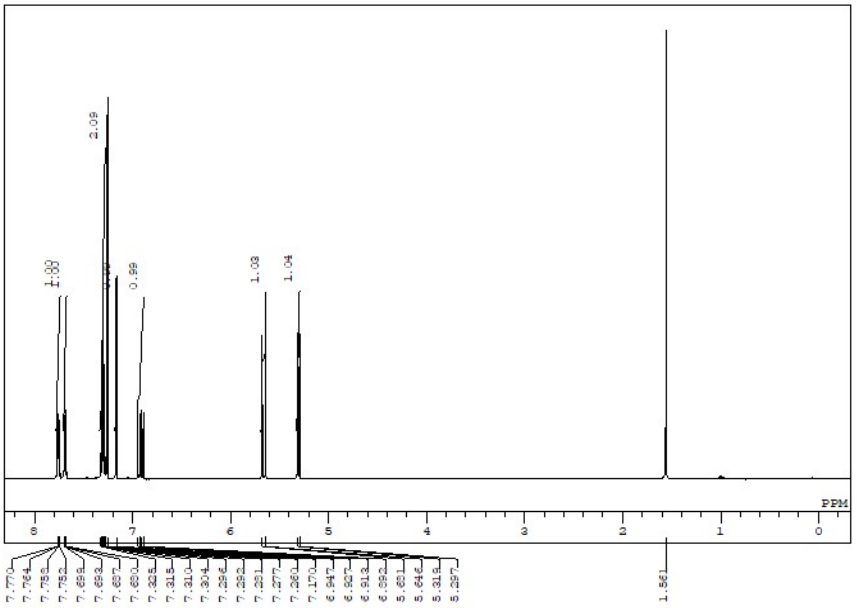


```
DFILE  20160503-pure_proton-1-1.als
COMNT  single_pulse
DATIM  2016-05-06 16:13:48
OBNUC  1H
EXMOD  proton.jxp
OBFRQ        500.16 MHz
OBSET          2.41 KHz
OBFIN          6.01 Hz
POINT         13107
FREQU       7507.51 Hz
SCANS             8
ACQTM         1.7459 sec
PD            5.0000 sec
PW1             6.22 usec
IRNUC  1H
CTEMP          17.2 c
SLVNT  CDCL3
EXREF          7.26 ppm
BF             0.10 Hz
RGAIN            48
```

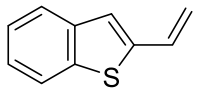

1

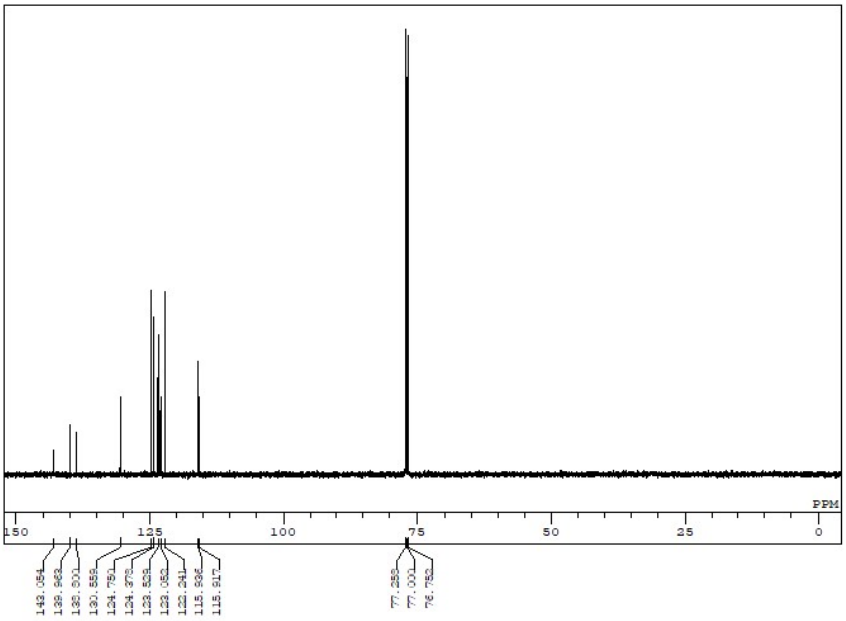


```
DFILE  20160503-pure-c_carbon-1-1.als
COMNT  single pulse decoupled gated NC
DATIM  2016-05-06 16:41:59
OBNUC  13C
EXMOD  carbon.jxp
OBFRQ        125.77 MHz
OBSET          7.87 KHz
OBFIN          4.21 Hz
POINT         26214
FREQU      31446.54 Hz
SCANS          1024
ACQTM         0.8336 sec
PD            2.0000 sec
PW1             3.12 usec
IRNUC  1H
CTEMP          17.9 c
SLVNT  CDCL3
EXREF         77.00 ppm
BF             0.10 Hz
RGAIN            60
```

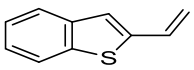

1

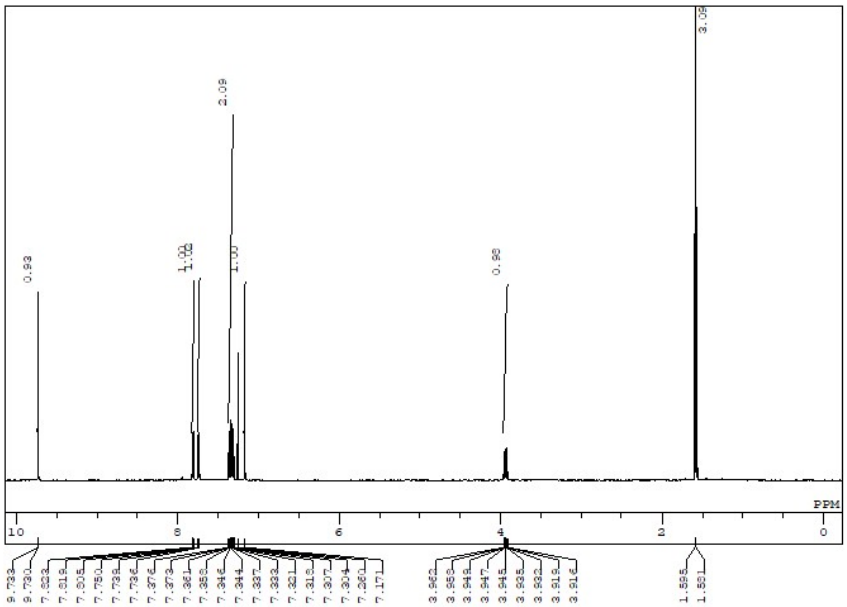


```
DFILE  2-S-B-aldehyde_proton-1-1.als
COMNT  single_pulse
DATIM  2017-11-15 21:40:39
OBNUC  1H
EXMOD  proton.jxp
OBFRQ        500.16 MHz
OBSET          2.41 KHz
OBFIN          6.01 Hz
POINT         13107
FREQU       7507.51 Hz
SCANS             8
ACQTM         1.7459 sec
PD            5.0000 sec
PW1             6.85 usec
IRNUC  1H
CTEMP          17.7 c
SLVNT  CDCL3
EXREF          7.26 ppm
BF             0.10 Hz
RGAIN            42
```

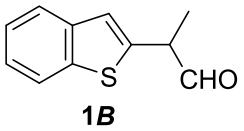

1*B*

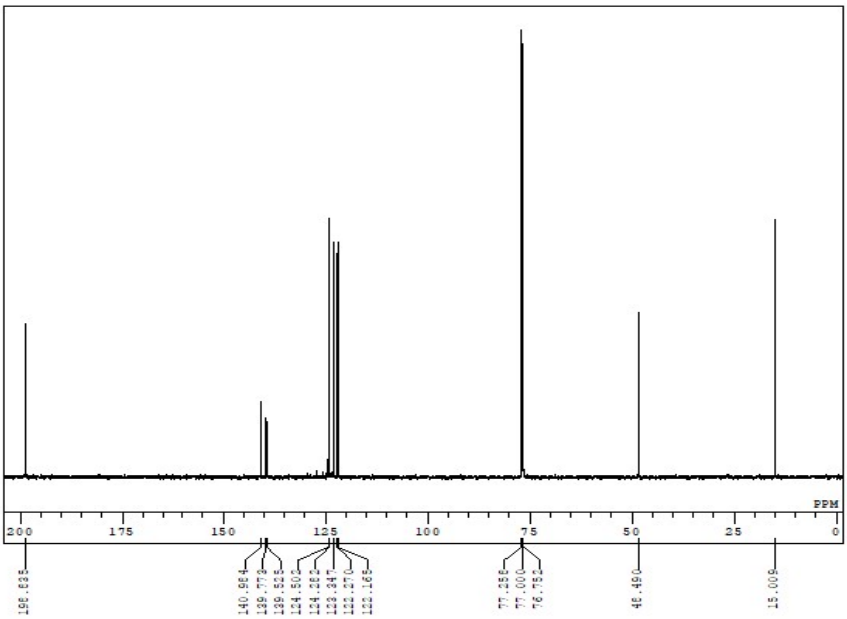


```
DFILE  2-S-B-aldehyde_carbon-1-1.als
COMNT  single pulse decoupled gated NC
DATIM  2017-11-15 22:28:42
OBNUC  13C
EXMOD  carbon.jxp
OBFRQ        125.77 MHz
OBSET          7.87 KHz
OBFIN          4.21 Hz
POINT         26214
FREQU      31446.54 Hz
SCANS          1024
ACQTM         0.8336 sec
PD            2.0000 sec
PW1             3.12 usec
IRNUC  1H
CTEMP          18.5 c
SLVNT  CDCL3
EXREF         77.00 ppm
BF             1.20 Hz
RGAIN            60
```

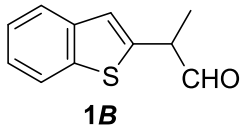

1*B*

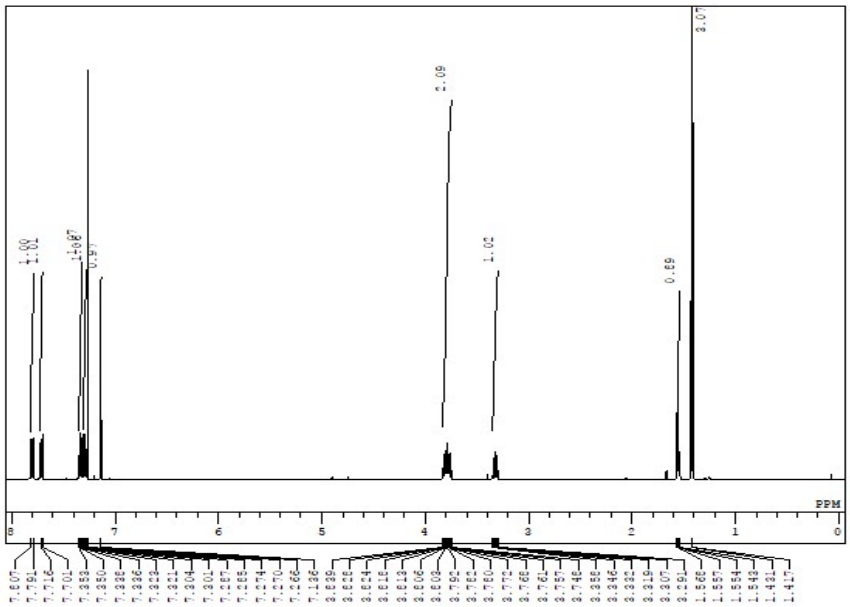


```
DFILE  2-S-B-alcohol_proton-1-1.als
COMNT  single_pulse
DATIM  2017-11-11 17:55:45
OBNUC  1H
EXMOD  proton.jxp
OBFRQ        500.16 MHz
OBSET          2.41 KHz
OBFIN          6.01 Hz
POINT         16384
FREQU       9384.38 Hz
SCANS             8
ACQTM        1.7459 sec
PD           5.0000 sec
PW1            6.85 usec
IRNUC  1H
CTEMP         16.0 c
SLVNT  CDCL3
EXREF         7.26 ppm
BF            0.10 Hz
RGAIN           46
```

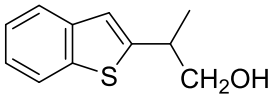

1*BB*

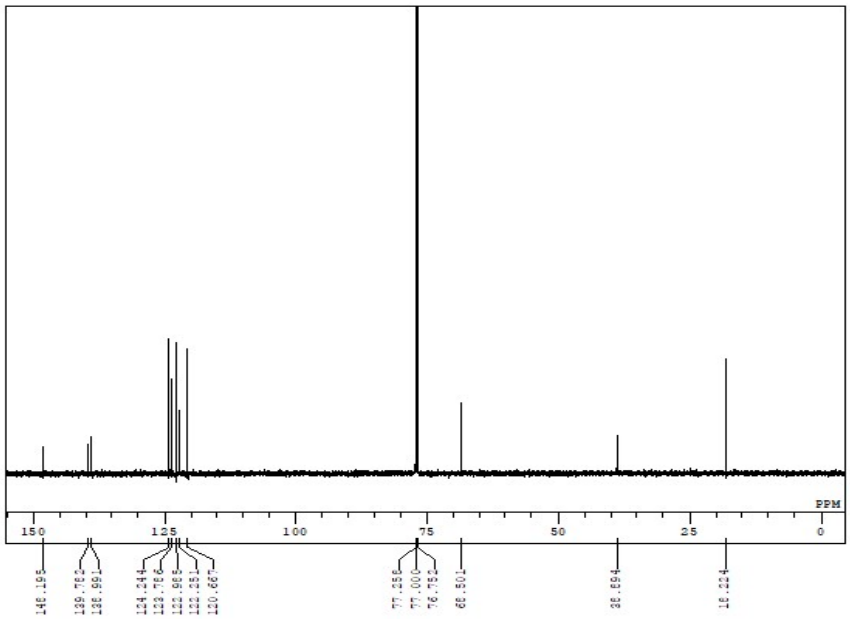


```
DFILE  2-S-B-alcohol_carbon-1-1.als
COMNT  single pulse decoupled gated NC
DATIM  2017-11-11 18:06:43
OBNUC  13C
EXMOD  carbon.jxp
OBFRQ        125.77 MHz
OBSET          7.87 KHz
OBFIN          4.21 Hz
POINT         26214
FREQU      31446.54 Hz
SCANS          1024
ACQTM        0.8336 sec
PD           2.0000 sec
PW1            3.12 usec
IRNUC  1H
CTEMP         16.3 c
SLVNT  CDCL3
EXREF        77.00 ppm
BF            0.10 Hz
RGAIN           60
```

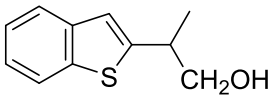

1*BB*

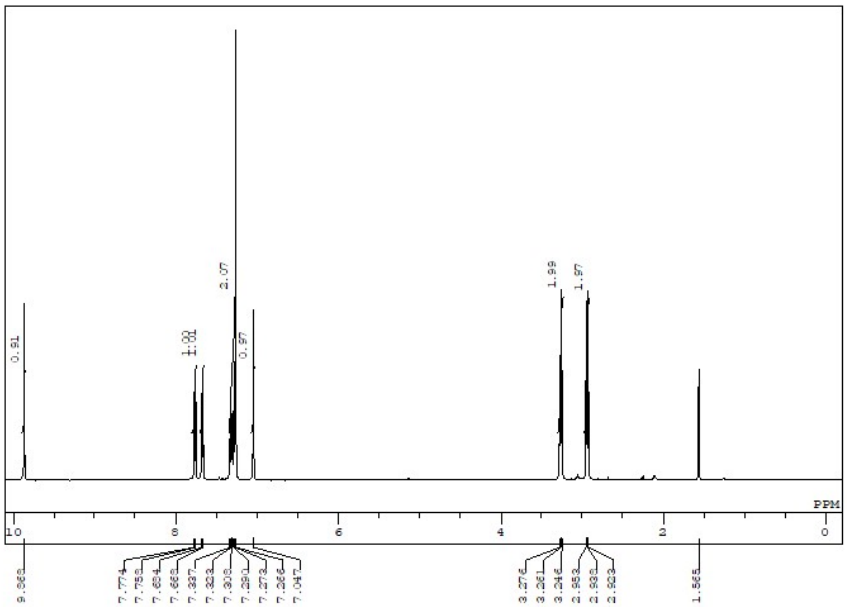


```
DFILE  2-S-L-aldehyde_proton-1-1.als
COMNT  single_pulse
DATIM  2017-11-30 17:56:06
OBNUC  1H
EXMOD  proton.jxp
OBFRQ        500.16 MHz
OBSET          2.41 KHz
OBFIN          6.01 Hz
POINT         13107
FREQU       7507.51 Hz
SCANS             8
ACQTM        1.7459 sec
PD           5.0000 sec
PW1            6.85 usec
IRNUC  1H
CTEMP          15.2 c
SLVNT  CDCL3
EXREF          7.26 ppm
BF             1.20 Hz
RGAIN            46
```

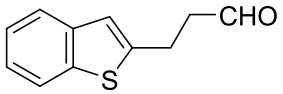

1*L*

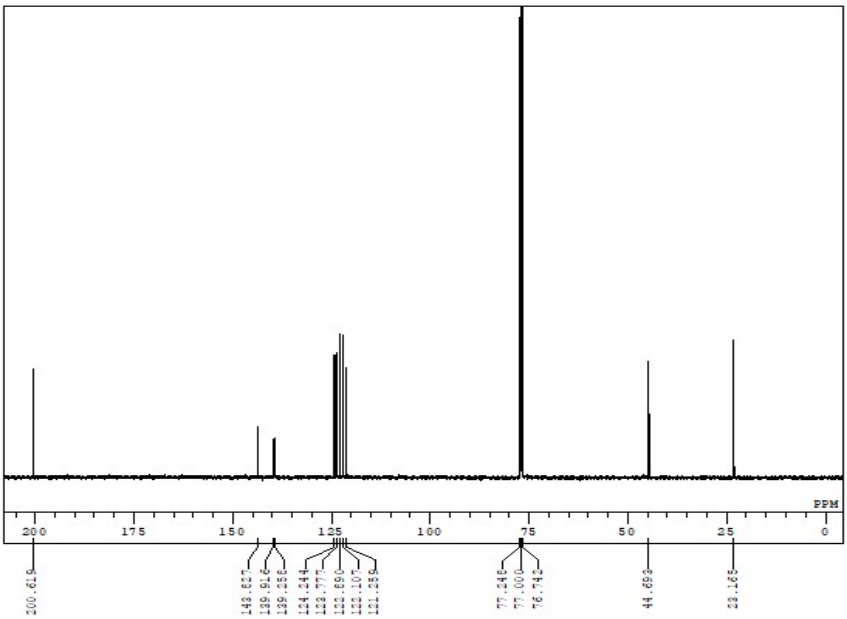


```
DFILE  2-S-L-aldehyde_carbon-1-1.als
COMNT  single pulse decoupled gated NC
DATIM  2017-11-30 20:26:24
OBNUC  13C
EXMOD  carbon.jxp
OBFRQ        125.77 MHz
OBSET          7.87 KHz
OBFIN          4.21 Hz
POINT         26214
FREQU      31446.54 Hz
SCANS          1024
ACQTM        0.8336 sec
PD           2.0000 sec
PW1            3.12 usec
IRNUC  1H
CTEMP          15.6 c
SLVNT  CDCL3
EXREF         77.00 ppm
BF             1.20 Hz
RGAIN            60
```

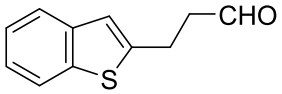

1*L*

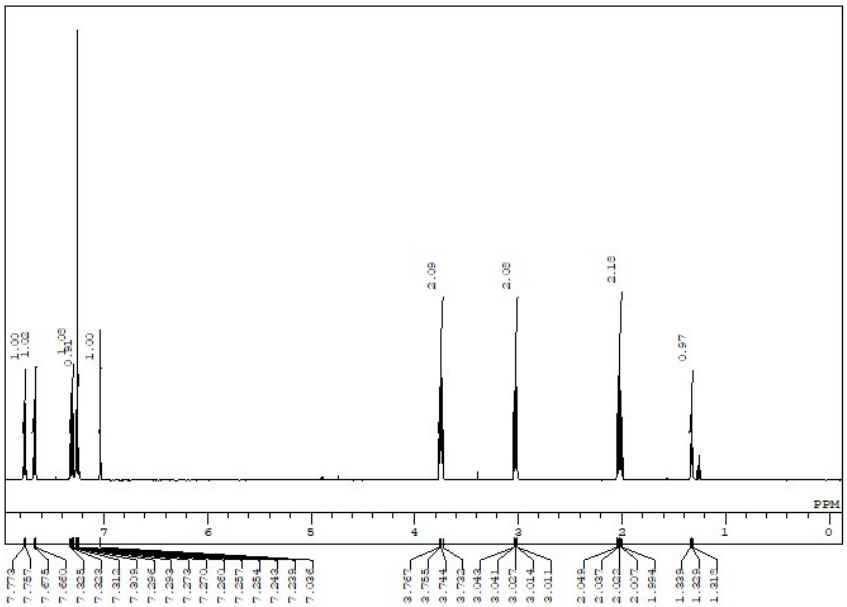


```
DFILE  2-S-L-alcohol_proton-1-1.als
COMNT  single_pulse
DATIM  2017-11-22 16:57:39
OBNUC  1H
EXMOD  proton.jxp
OBFRQ        500.16 MHz
OBSET          2.41 KHz
OBFIN          6.01 Hz
POINT         13107
FREQU       7507.51 Hz
SCANS             8
ACQTM         1.7459 sec
PD            5.0000 sec
PW1             6.85 usec
IRNUC  1H
CTEMP          17.8 c
SLVNT  CDCL3
EXREF          7.26 ppm
BF             0.10 Hz
RGAIN            44
```

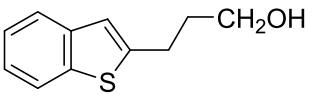

1*LL*

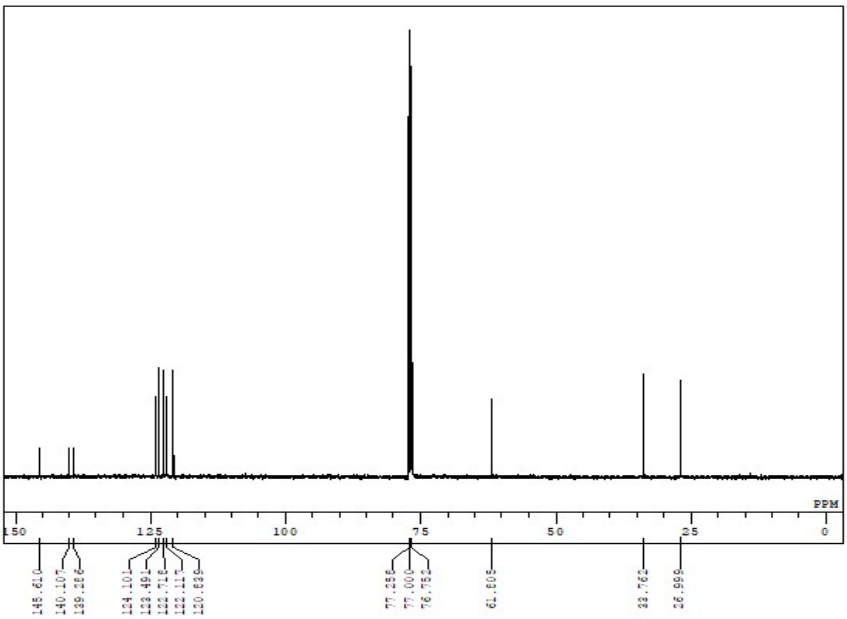


```
DFILE  2-S-L-alcohol_carbon-1-1.als
COMNT  single pulse decoupled gated NC
DATIM  2017-11-22 20:36:20
OBNUC  13C
EXMOD  carbon.jxp
OBFRQ        125.77 MHz
OBSET          7.87 KHz
OBFIN          4.21 Hz
POINT         26214
FREQU      31446.54 Hz
SCANS          1024
ACQTM         0.8336 sec
PD            2.0000 sec
PW1             3.12 usec
IRNUC  1H
CTEMP          17.9 c
SLVNT  CDCL3
EXREF         77.00 ppm
BF             1.20 Hz
RGAIN            60
```

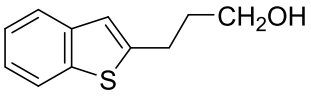

1*LL*

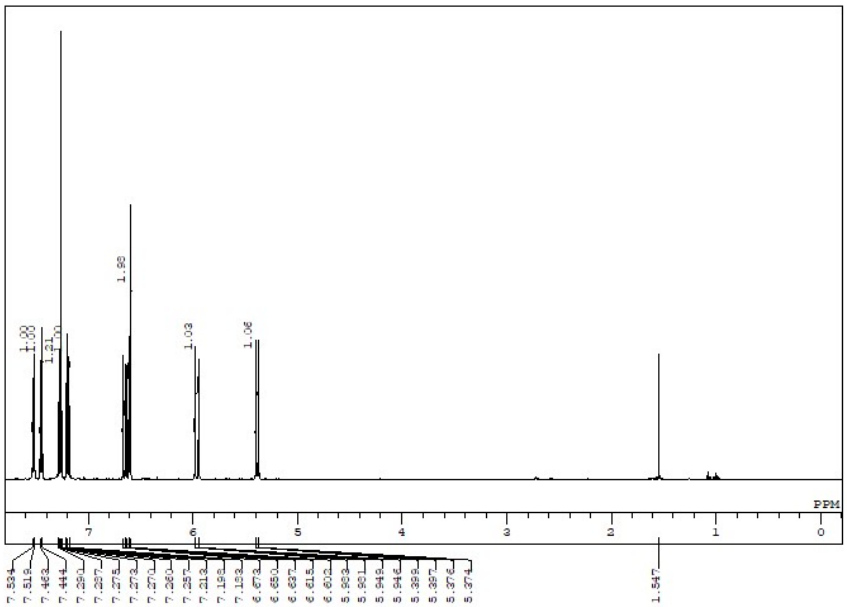


```
DFILE  2-O-olefin_proton-1-1.als
COMNT  single_pulse
DATIM  2017-11-13 14:45:58
OBNUC  1H
EXMOD  proton.jxp
OBFRQ        500.16 MHz
OBSET          2.41 KHz
OBFIN          6.01 Hz
POINT         13107
FREQU       7507.51 Hz
SCANS             8
ACQTM        1.7459 sec
PD           5.0000 sec
PW1            6.85 usec
IRNUC  1H
CTEMP         17.7 c
SLVNT  CDCL3
EXREF         7.26 ppm
BF            0.10 Hz
RGAIN           44
```

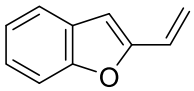

2

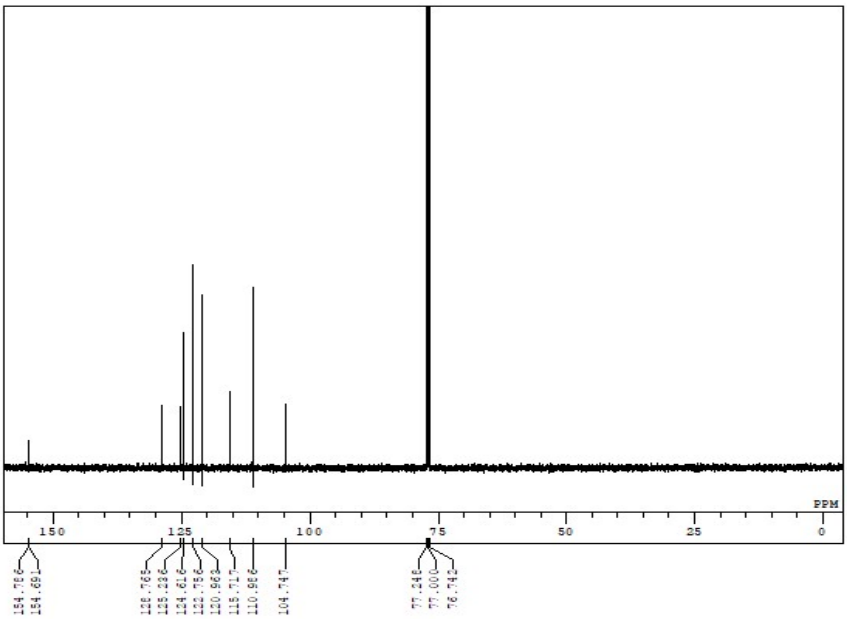


```
DFILE  2-O-olefin_carbon-1-1.als
COMNT  single pulse decoupled gated NC
DATIM  2017-11-13 16:19:16
OBNUC  13C
EXMOD  carbon.jxp
OBFRQ        125.77 MHz
OBSET          7.87 KHz
OBFIN          4.21 Hz
POINT         26214
FREQU      31446.54 Hz
SCANS          1024
ACQTM        0.8336 sec
PD           2.0000 sec
PW1            3.12 usec
IRNUC  1H
CTEMP         17.1 c
SLVNT  CDCL3
EXREF        77.00 ppm
BF            0.10 Hz
RGAIN           60
```

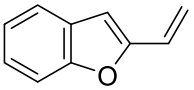

2

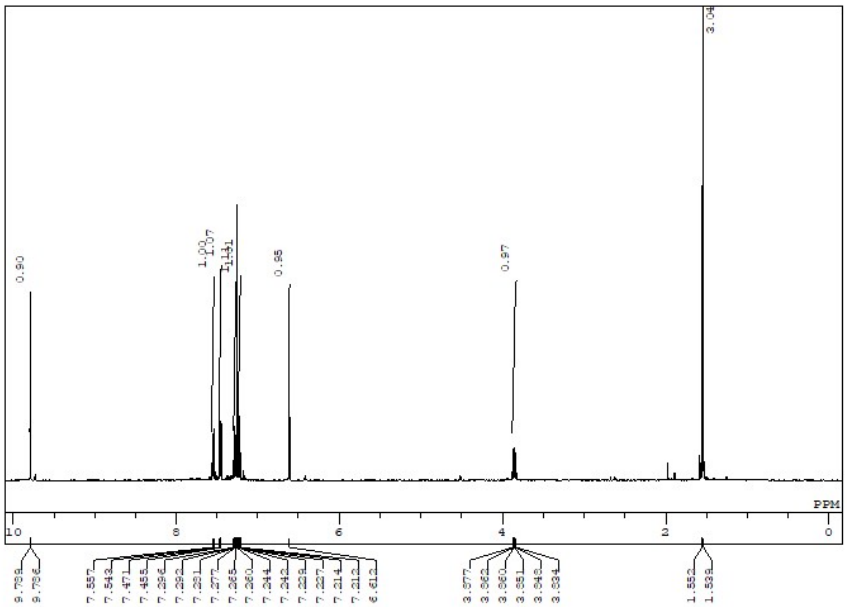


```
DFILE  2-O-B-aldehyde_proton-1-1.als
COMNT  single_pulse
DATIM  2017-11-13 20:52:54
OBNUC  1H
EXMOD  proton.jxp
OBFRQ        500.16 MHz
OBSET          2.41 KHz
OBFIN          6.01 Hz
POINT         13107
FREQU       7507.51 Hz
SCANS            8
ACQTM        1.7459 sec
PD           5.0000 sec
PW1            6.85 usec
IRNUC  1H
CTEMP         17.0 c
SLVNT  CDCL3
EXREF         7.26 ppm
BF            0.10 Hz
RGAIN           44
```

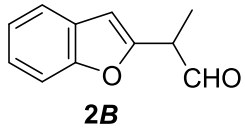

2B

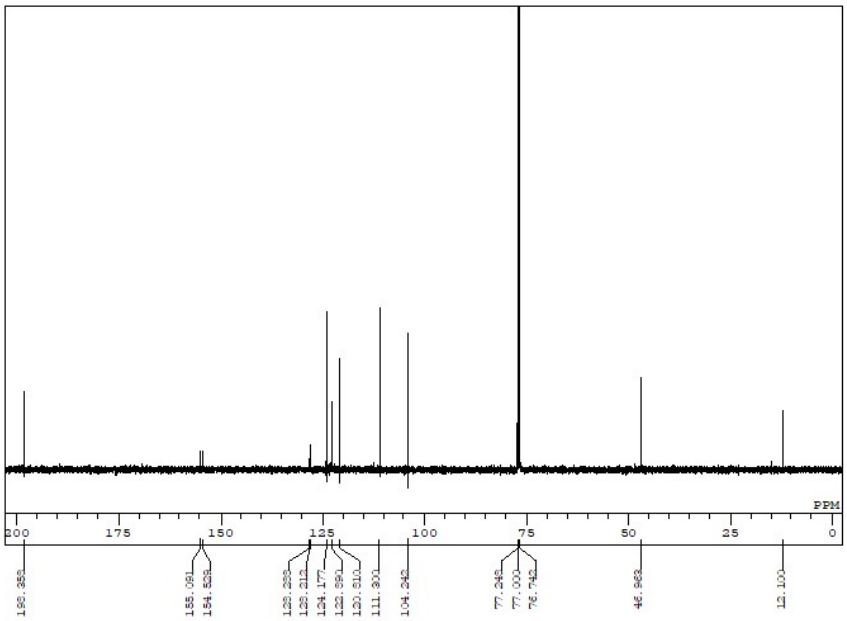


```
DFILE  2-O-B-aldehyde_carbon-1-1.als
COMNT  single pulse decoupled gated NC
DATIM  2017-11-14 22:17:23
OBNUC  13C
EXMOD  carbon.jxp
OBFRQ        125.77 MHz
OBSET          7.87 KHz
OBFIN          4.21 Hz
POINT         26214
FREQU      31446.54 Hz
SCANS          1024
ACQTM        0.8336 sec
PD           2.0000 sec
PW1            3.12 usec
IRNUC  1H
CTEMP         19.7 c
SLVNT  CDCL3
EXREF        77.00 ppm
BF            0.10 Hz
RGAIN           60
```

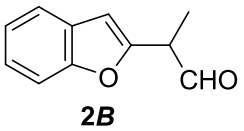

2B

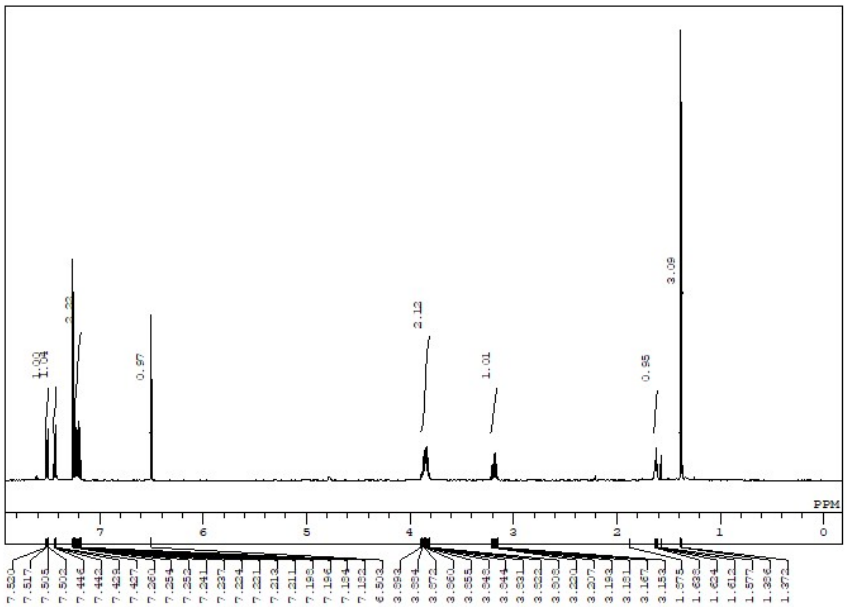


```
DFILE  2-O-B-rac alcohol_proton-1-1.al
COMNT  single_pulse
DATIM  2017-11-11 15:05:19
OBNUC  1H
EXMOD  proton.jxp
OBFRQ        500.16 MHz
OBSET          2.41 KHz
OBFIN          6.01 Hz
POINT         13107
FREQU       7507.51 Hz
SCANS             8
ACQTM         1.7459 sec
PD            5.0000 sec
PW1             6.85 usec
IRNUC  1H
CTEMP          16.5 c
SLVNT  CDCL3
EXREF          7.26 ppm
BF             0.10 Hz
RGAIN            42
```

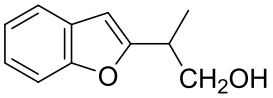

2*BB*

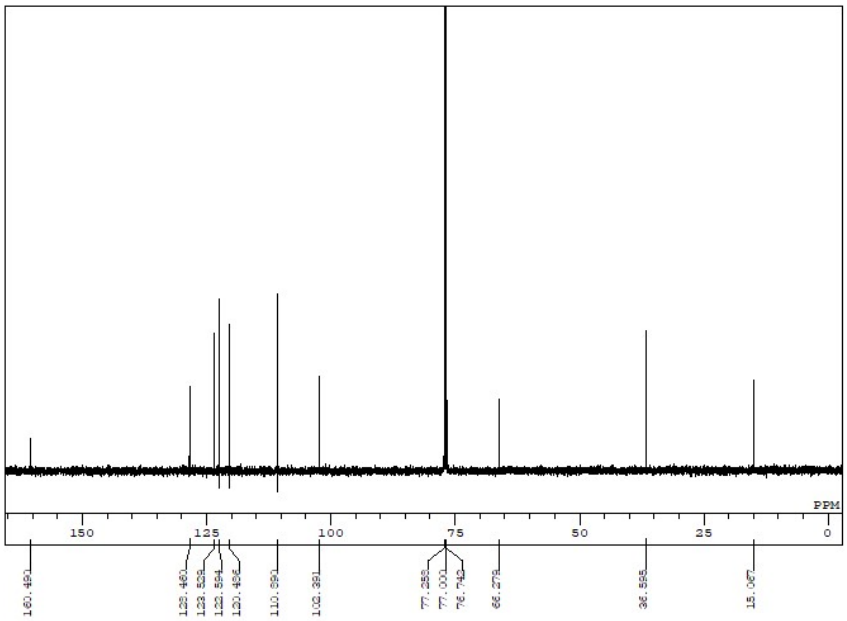


```
DFILE  2-O-B-rac alcohol_carbon-1-1.al
COMNT  single pulse decoupled gated NO
DATIM  2017-11-11 15:09:21
OBNUC  13C
EXMOD  carbon.jxp
OBFRQ        125.77 MHz
OBSET          7.87 KHz
OBFIN          4.21 Hz
POINT         26214
FREQU      31446.54 Hz
SCANS          1024
ACQTM         0.8336 sec
PD            2.0000 sec
PW1             3.12 usec
IRNUC  1H
CTEMP          16.6 c
SLVNT  CDCL3
EXREF         77.00 ppm
BF             0.10 Hz
RGAIN            60
```

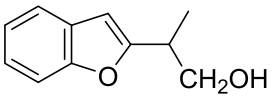

2*BB*

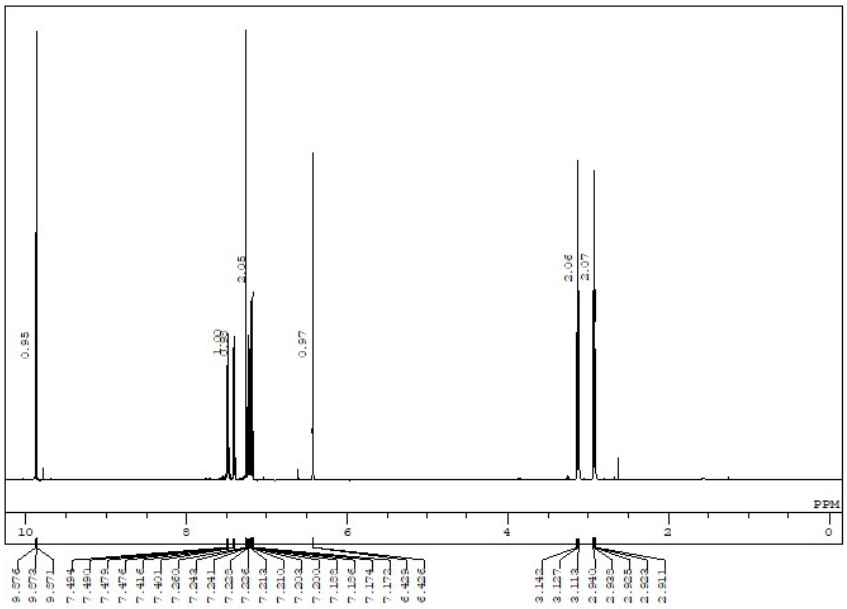


```
DFILE  2-O-L-aldehyde_proton-1-1.als
COMNT  single_pulse
DATIM  2017-11-10 14:48:06
OBNUC  1H
EXMOD  proton.jxp
OBFRQ        500.16 MHz
OBSET          2.41 KHz
OBFIN          6.01 Hz
POINT         13107
FREQU       7507.51 Hz
SCANS            8
ACQTM        1.7459 sec
PD           5.0000 sec
PW1            6.85 usec
IRNUC  1H
CTEMP         16.8 c
SLVNT  CDCL3
EXREF         7.26 ppm
BF            0.10 Hz
RGAIN           42
```

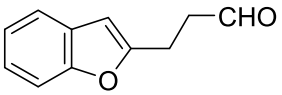

2*L*

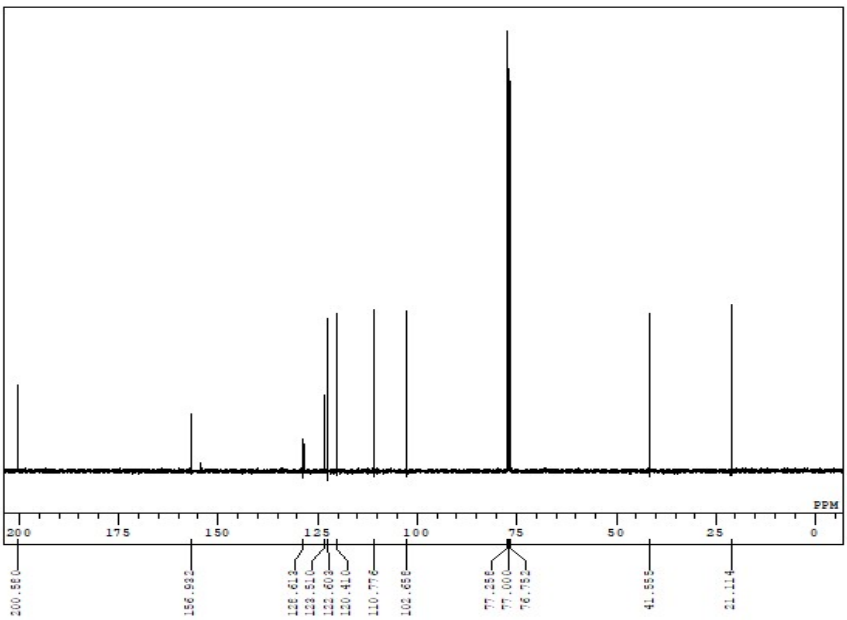


```
DFILE  2-O-L-aldehyde_carbon-1-1.als
COMNT  single pulse decoupled gated NC
DATIM  2017-11-10 14:56:10
OBNUC  13C
EXMOD  carbon.jxp
OBFRQ        125.77 MHz
OBSET          7.87 KHz
OBFIN          4.21 Hz
POINT         26214
FREQU      31446.54 Hz
SCANS          1024
ACQTM        0.8336 sec
PD           2.0000 sec
PW1            3.12 usec
IRNUC  1H
CTEMP         16.8 c
SLVNT  CDCL3
EXREF         77.00 ppm
BF            0.10 Hz
RGAIN           60
```

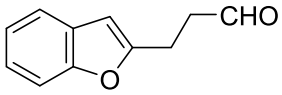

2*L*

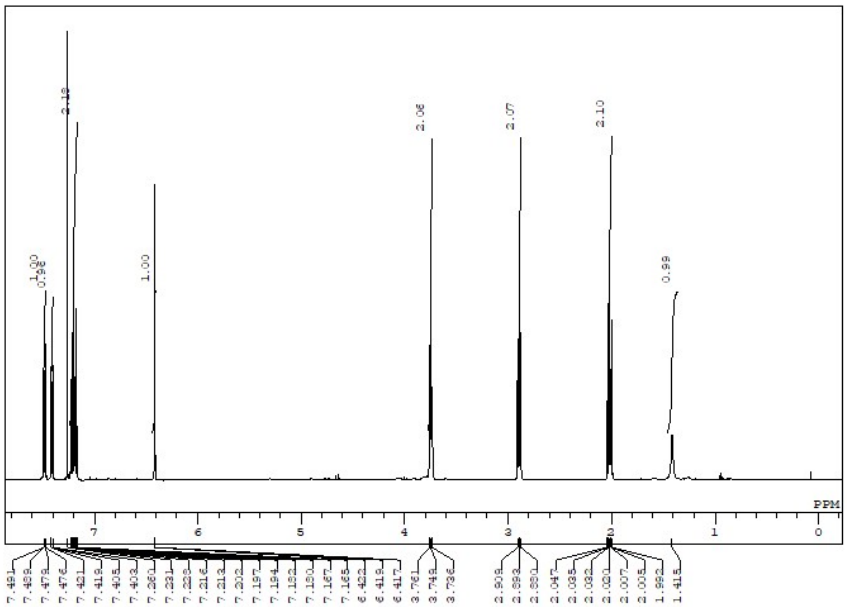


```
DFILE  2-O-L-alcohol_proton-1-1.als
COMNT  single_pulse
DATIM  2018-08-23 21:15:25
OBNUC  1H
EXMOD  proton.jxp
OBFRQ        500.16 MHz
OBSET          2.41 KHz
OBFIN          6.01 Hz
POINT         16384
FREQU       9384.38 Hz
SCANS             8
ACQTM         1.7459 sec
PD            5.0000 sec
PW1             6.85 usec
IRNUC  1H
CTEMP          18.2 c
SLVNT  CDCL3
EXREF          7.26 ppm
BF             0.10 Hz
RGAIN            44
```

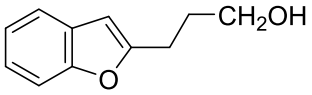

2*LL*

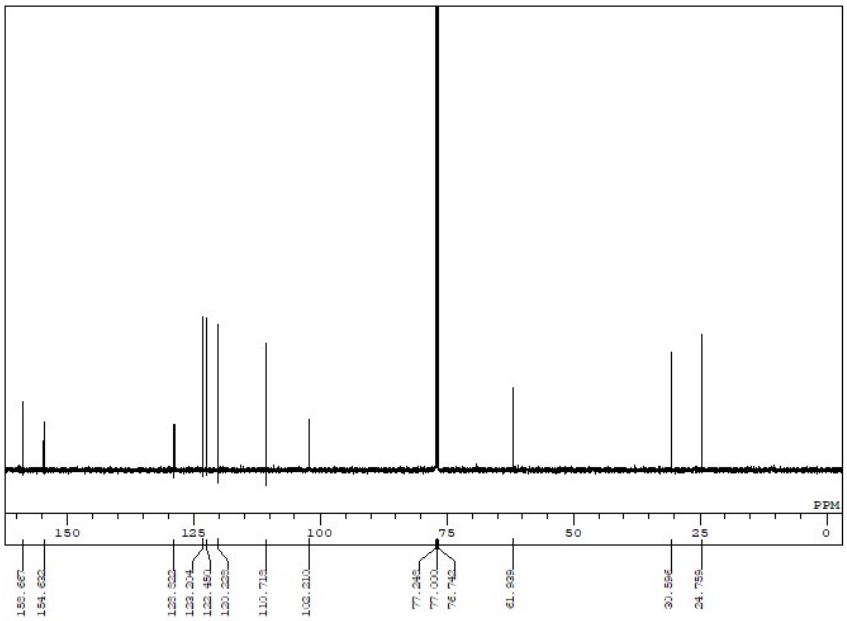


```
DFILE  2-O-L-alcohol_carbon-1-1.als
COMNT  single pulse decoupled gated NC
DATIM  2018-08-24 10:13:34
OBNUC  13C
EXMOD  carbon.jxp
OBFRQ        125.77 MHz
OBSET          7.87 KHz
OBFIN          4.21 Hz
POINT         32767
FREQU      39308.18 Hz
SCANS          1024
ACQTM         0.8336 sec
PD            2.0000 sec
PW1             3.12 usec
IRNUC  1H
CTEMP          18.5 c
SLVNT  CDCL3
EXREF         77.00 ppm
BF             0.10 Hz
RGAIN            58
```

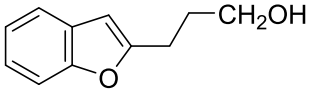

2*LL*

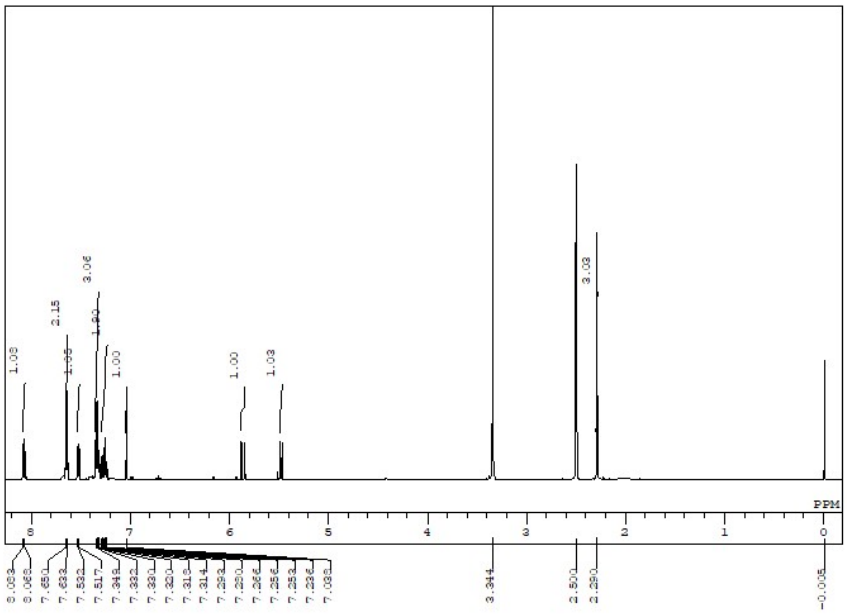

```
DFILE  2-NTs-olefin_proton-1-1.als
COMNT  single_pulse
DATIM  2018-11-10 16:35:19
OBNUC  1H
EXMOD  proton.jxp
OBFRQ        500.16 MHz
OBSET          2.41 KHz
OBFIN          6.01 Hz
POINT         16384
FREQU       9384.38 Hz
SCANS             8
ACQTM        1.7459 sec
PD           5.0000 sec
PW1            6.85 usec
IRNUC  1H
CTEMP         17.9 c
SLVNT  DMSO
EXREF         2.50 ppm
BF            0.10 Hz
RGAIN           44
```

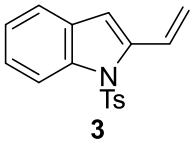

3

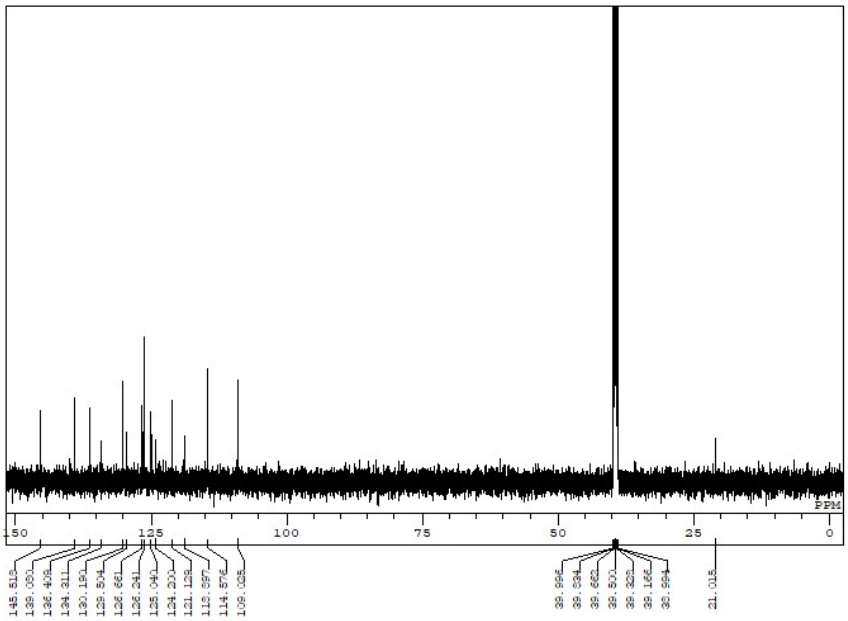

```
DFILE  2-NTs-olefin_carbon-1-1.als
COMNT  single pulse decoupled gated NC
DATIM  2018-11-10 16:38:14
OBNUC  13C
EXMOD  carbon.jxp
OBFRQ        125.77 MHz
OBSET          7.87 KHz
OBFIN          4.21 Hz
POINT         32767
FREQU      39308.18 Hz
SCANS          1024
ACQTM        0.8336 sec
PD           2.0000 sec
PW1            3.12 usec
IRNUC  1H
CTEMP         18.2 c
SLVNT  DMSO
EXREF        39.50 ppm
BF            0.10 Hz
RGAIN           56
```

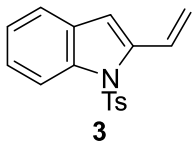

3

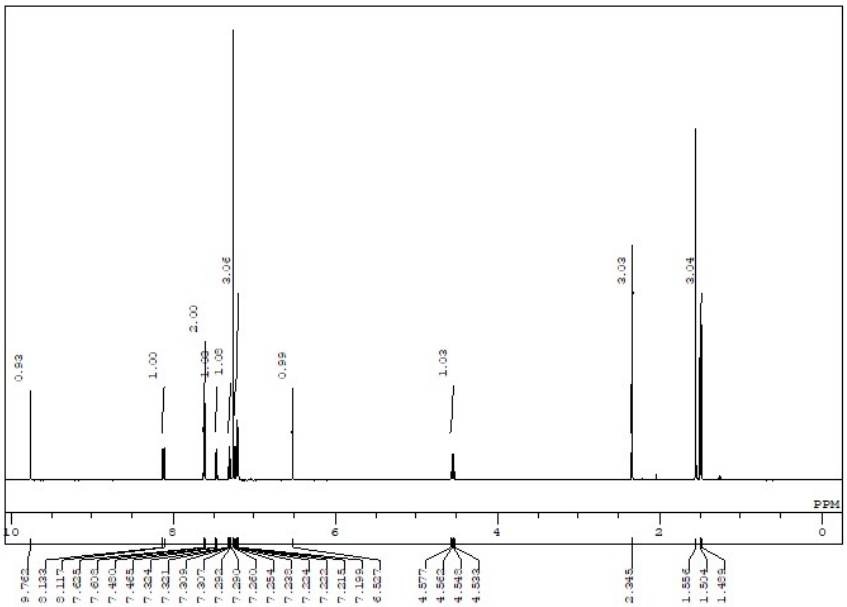

```
DFILE  2-NTs-B-aldehyde_proton-1-1.als
COMNT  single_pulse
DATIM  2016-12-17 20:29:40
OBNUC  1H
EXMOD  proton.jxp
OBFRQ        500.16 MHz
OBSET          2.41 KHz
OBFIN          6.01 Hz
POINT         13107
FREQU       7507.51 Hz
SCANS            8
ACQTM        1.7459 sec
PD           5.0000 sec
PW1            6.85 usec
IRNUC  1H
CTEMP         18.3 c
SLVNT  CDCL3
EXREF         7.26 ppm
BF            0.10 Hz
RGAIN           46
```

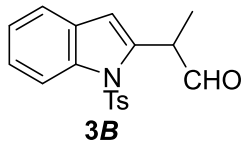

3*B*

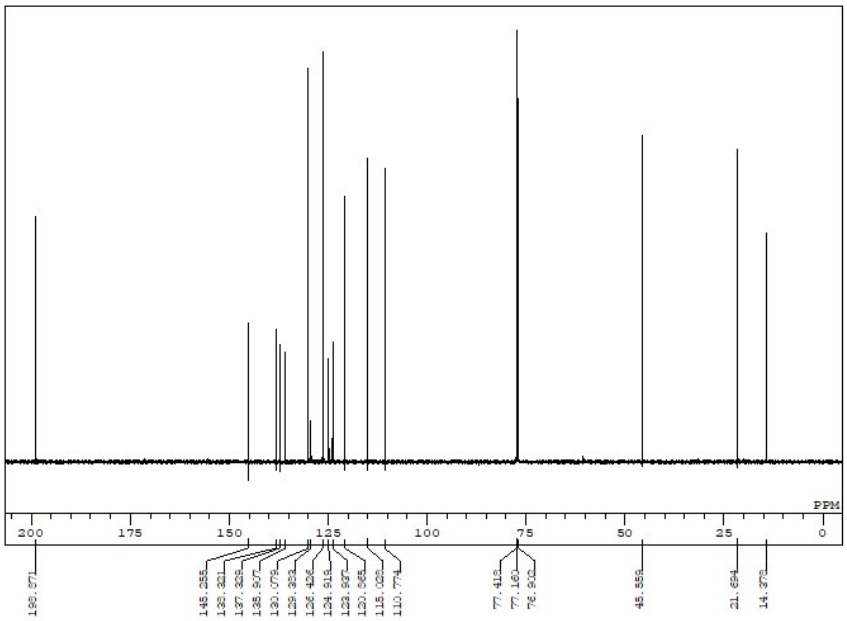

```
DFILE  2-NTs-aldehyde-13C.als
COMNT  single pulse decoupled gated NC
DATIM  2016-12-16 22:28:57
OBNUC  13C
EXMOD  carbon.jxp
OBFRQ        125.77 MHz
OBSET          7.87 KHz
OBFIN          4.21 Hz
POINT         26214
FREQU      31446.54 Hz
SCANS          1024
ACQTM        0.8336 sec
PD           2.0000 sec
PW1            3.12 usec
IRNUC  1H
CTEMP         17.1 c
SLVNT  CDCL3
EXREF        77.16 ppm
BF            0.10 Hz
RGAIN           60
```

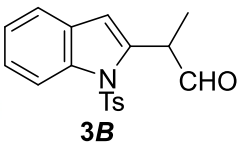

3*B*

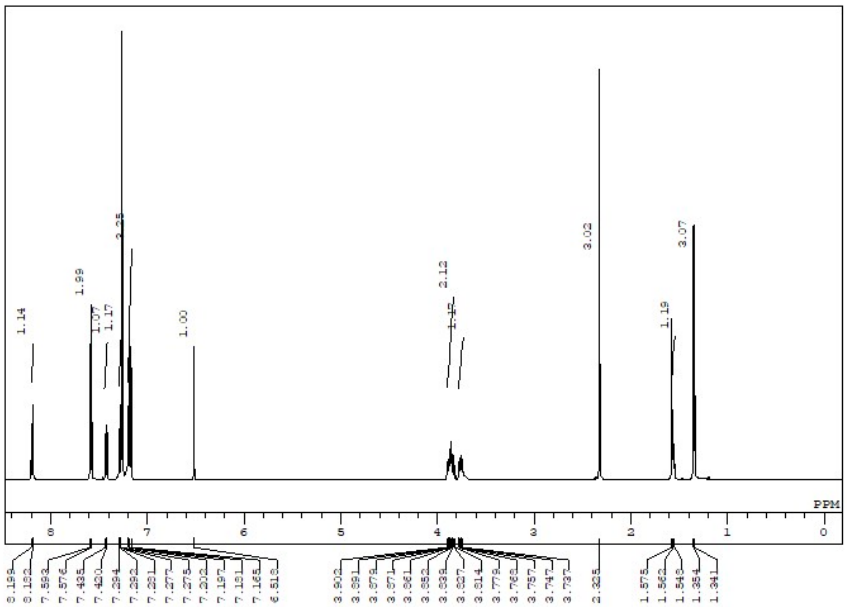

```
DFILE  2-NTs-B-alcohol_proton-1-1.als
COMNT  single_pulse
DATIM  2018-11-21 19:46:44
OBNUC  1H
EXMOD  proton.jxp
OBFRQ        500.16 MHz
OBSET          2.41 KHz
OBFIN          6.01 Hz
POINT         16384
FREQU       9384.38 Hz
SCANS             8
ACQTM        1.7459 sec
PD           5.0000 sec
PW1            6.85 usec
IRNUC  1H
CTEMP         17.8 c
SLVNT  CDCL3
EXREF         7.26 ppm
BF            0.10 Hz
RGAIN           44
```

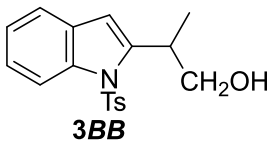

3*BB*

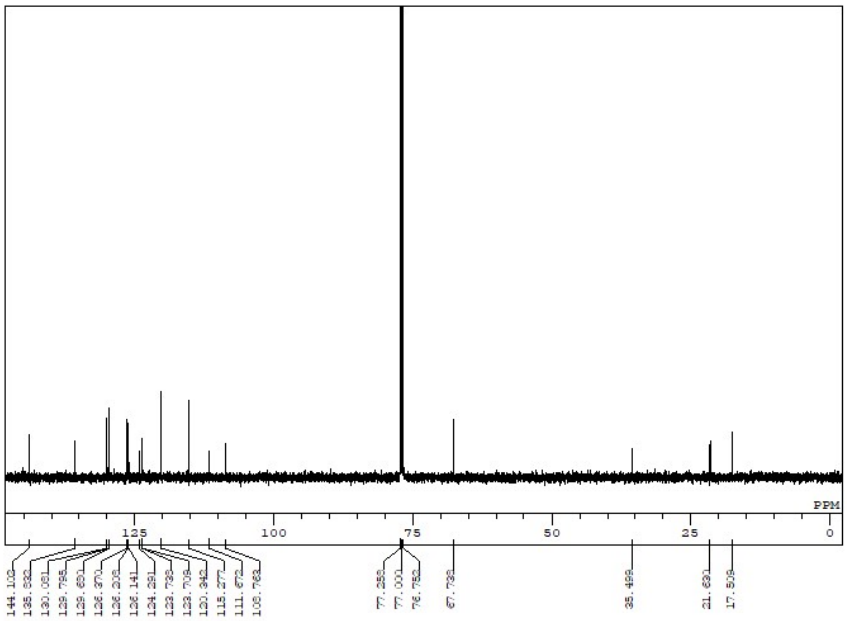

```
DFILE  2-NTs-B-alcohol_carbon-1-1.als
COMNT  single pulse decoupled gated NC
DATIM  2018-11-21 19:50:31
OBNUC  13C
EXMOD  carbon.jxp
OBFRQ        125.77 MHz
OBSET          7.87 KHz
OBFIN          4.21 Hz
POINT         32767
FREQU      39308.18 Hz
SCANS          1024
ACQTM        0.8336 sec
PD           2.0000 sec
PW1            3.12 usec
IRNUC  1H
CTEMP         18.2 c
SLVNT  CDCL3
EXREF        77.00 ppm
BF            0.10 Hz
RGAIN           60
```

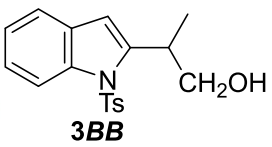

3*BB*

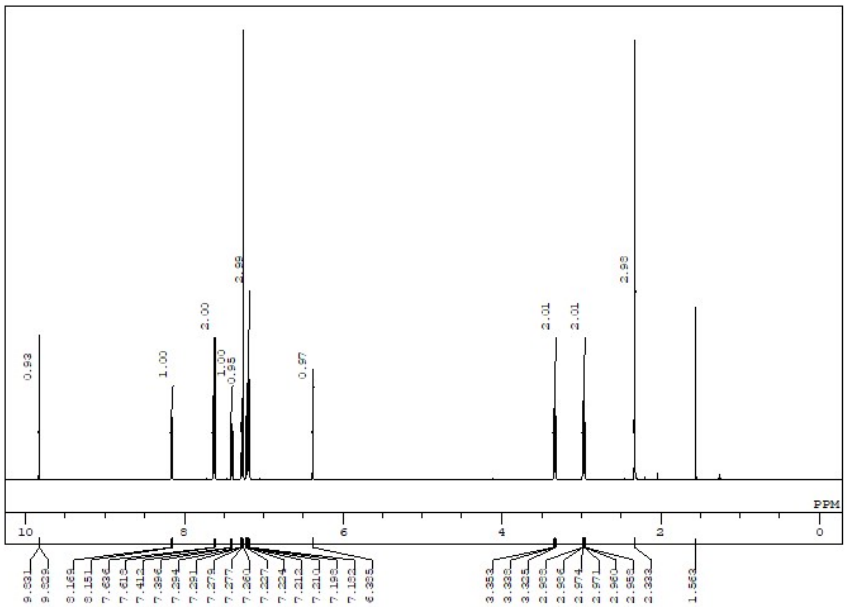

```
DFILE  2-NTs-L-aldehyde_proton-1-1.als
COMNT  single_pulse
DATIM  2018-09-07 20:42:25
OBNUC  1H
EXMOD  proton.jxp
OBFRQ        500.16 MHz
OBSET          2.41 KHz
OBFIN          6.01 Hz
POINT         16384
FREQU       9384.38 Hz
SCANS             8
ACQTM        1.7459 sec
PD           5.0000 sec
PW1            6.85 usec
IRNUC  1H
CTEMP         16.7 c
SLVNT  CDCL3
EXREF         7.26 ppm
BF            0.10 Hz
RGAIN           44
```

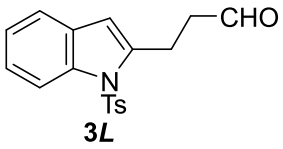

3*L*

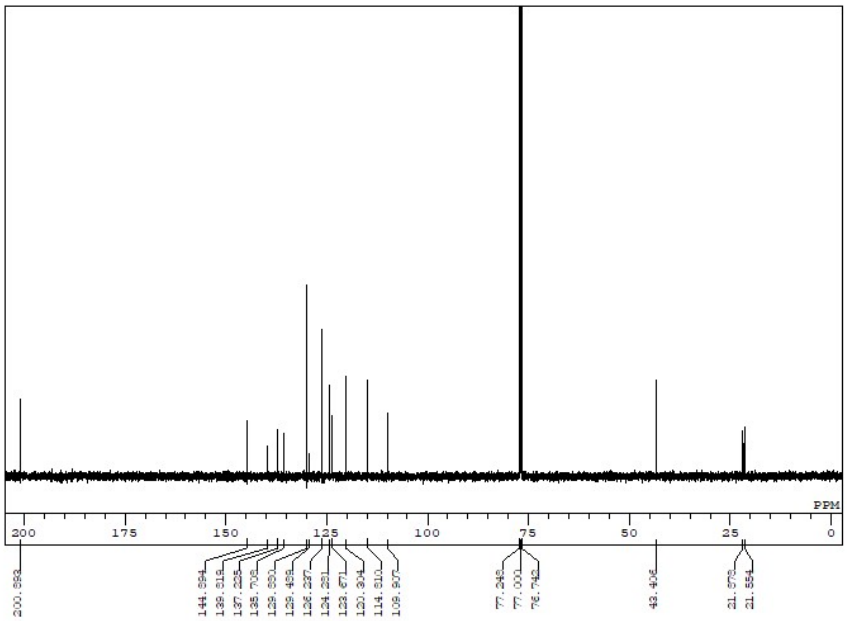

```
DFILE  2-NTs-L-aldehyde_carbon-1-1.als
COMNT  single pulse decoupled gated NO
DATIM  2018-09-07 20:44:42
OBNUC  13C
EXMOD  carbon.jxp
OBFRQ        125.77 MHz
OBSET          7.87 KHz
OBFIN          4.21 Hz
POINT         32767
FREQU      39308.18 Hz
SCANS          1024
ACQTM        0.8336 sec
PD           2.0000 sec
PW1            3.12 usec
IRNUC  1H
CTEMP         17.1 c
SLVNT  CDCL3
EXREF        77.00 ppm
BF            0.10 Hz
RGAIN           60
```

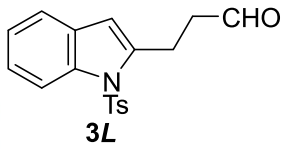

3*L*

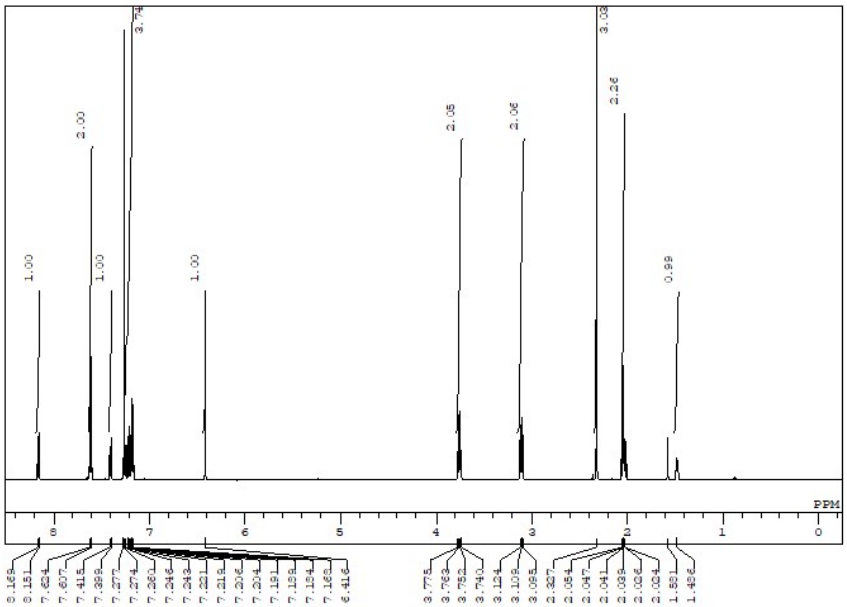

```
DFILE  2-NTs-L-alcohol_proton-1-1.als
COMNT  single_pulse
DATIM  2018-09-04 16:43:49
OBNUC  1H
EXMOD  proton.jxp
OBFRQ        500.16 MHz
OBSET          2.41 KHz
OBFIN          6.01 Hz
POINT         16384
FREQU       9384.38 Hz
SCANS             8
ACQTM         1.7459 sec
PD            5.0000 sec
PW1             6.85 usec
IRNUC  1H
CTEMP            16.8 c
SLVNT  CDCL3
EXREF          7.26 ppm
BF             0.10 Hz
RGAIN            46
```

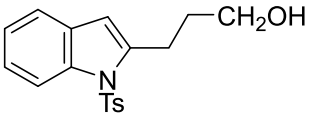

3*LL*

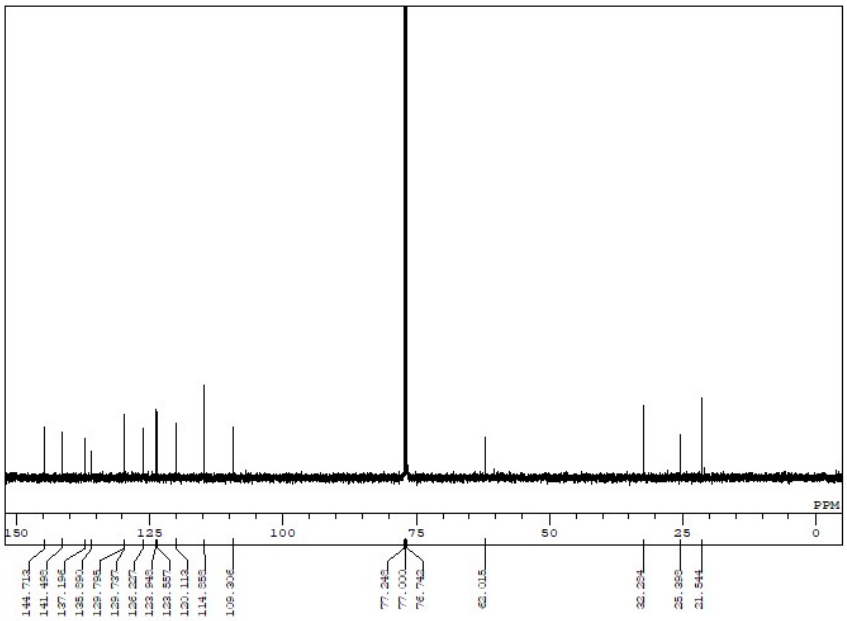

```
DFILE  2-NTs-L-alcohol_carbon-1-1.als
COMNT  single pulse decoupled gated NC
DATIM  2018-09-04 16:45:58
OBNUC  13C
EXMOD  carbon.jxp
OBFRQ        125.77 MHz
OBSET          7.87 KHz
OBFIN          4.21 Hz
POINT         32767
FREQU      39308.18 Hz
SCANS          1024
ACQTM         0.8336 sec
PD            2.0000 sec
PW1             3.12 usec
IRNUC  1H
CTEMP            17.3 c
SLVNT  CDCL3
EXREF         77.00 ppm
BF             0.10 Hz
RGAIN            60
```

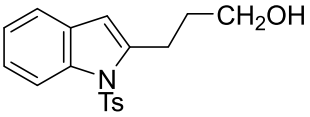

3*LL*

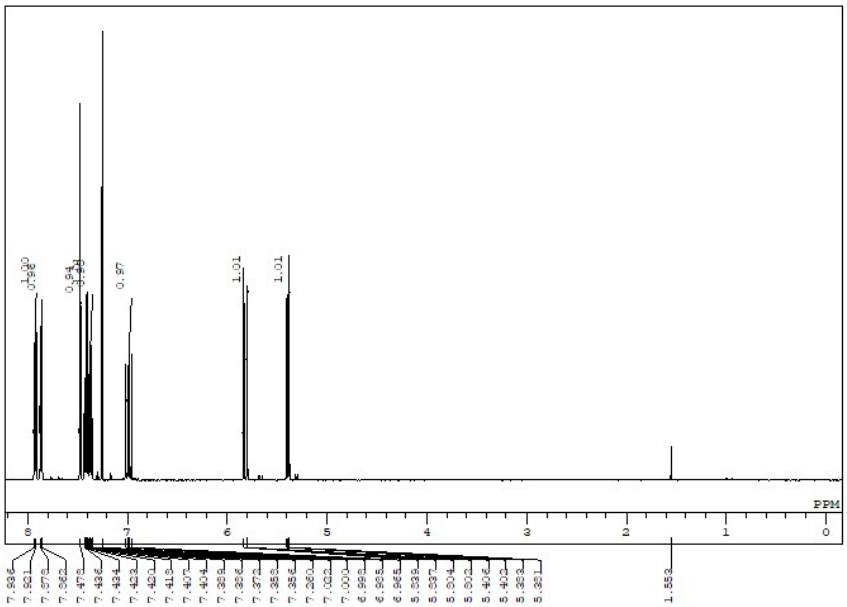

```
DFILE  3-S-olefin_proton-1-1.als
COMNT  single_pulse
DATIM  2018-02-24 16:02:21
OBNUC  1H
EXMOD  proton.jxp
OBFRQ        500.16 MHz
OBSET          2.41 KHz
OBFIN          6.01 Hz
POINT         13107
FREQU       7507.51 Hz
SCANS             8
ACQTM        1.7459 sec
PD           5.0000 sec
PW1            6.85 usec
IRNUC  1H
CTEMP         14.0 c
SLVNT  CDCL3
EXREF         7.26 ppm
BF            0.10 Hz
RGAIN           42
```

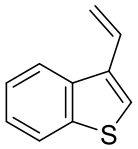

4

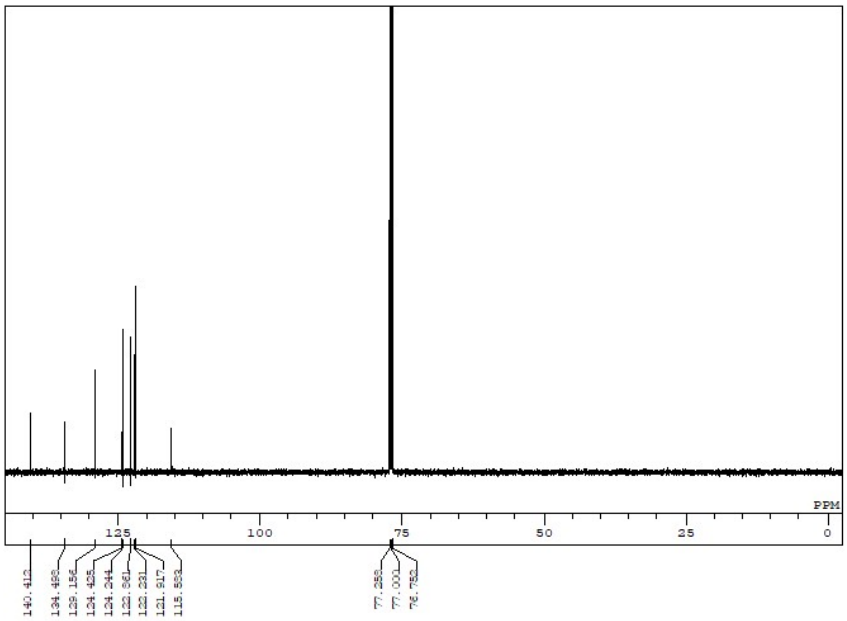

```
DFILE  3-S-olefin_carbon-1-1.als
COMNT  single pulse decoupled gated NC
DATIM  2018-02-24 16:10:01
OBNUC  13C
EXMOD  carbon.jxp
OBFRQ        125.77 MHz
OBSET          7.87 KHz
OBFIN          4.21 Hz
POINT         26214
FREQU      31446.54 Hz
SCANS          1024
ACQTM        0.8336 sec
PD           2.0000 sec
PW1            3.12 usec
IRNUC  1H
CTEMP         13.6 c
SLVNT  CDCL3
EXREF        77.00 ppm
BF            0.10 Hz
RGAIN           56
```

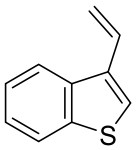

4

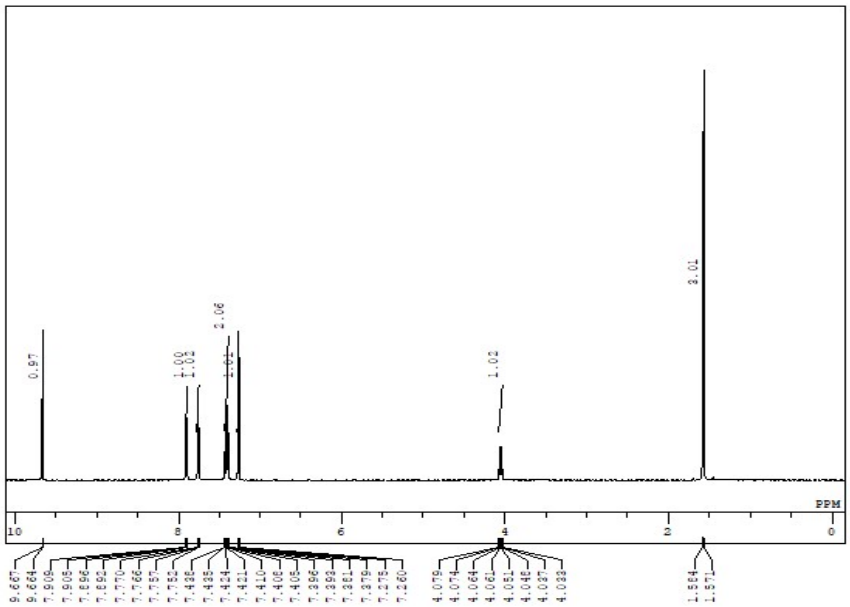


```
DFILE  3-S-B-aldehyde_proton-1-1.als
COMNT  single_pulse
DATIM  2018-02-27 15:25:26
OBNUC  1H
EXMOD  proton.jxp
OBFRQ        500.16 MHz
OBSET          2.41 KHz
OBFIN          6.01 Hz
POINT         16384
FREQU       9384.38 Hz
SCANS             8
ACQTM        1.7459 sec
PD           5.0000 sec
PW1            6.85 usec
IRNUC  1H
CTEMP         12.9 c
SLVNT  CDCL3
EXREF         7.26 ppm
BF            0.10 Hz
RGAIN           40
```

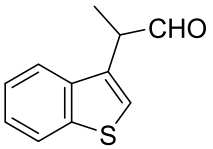

4*B*

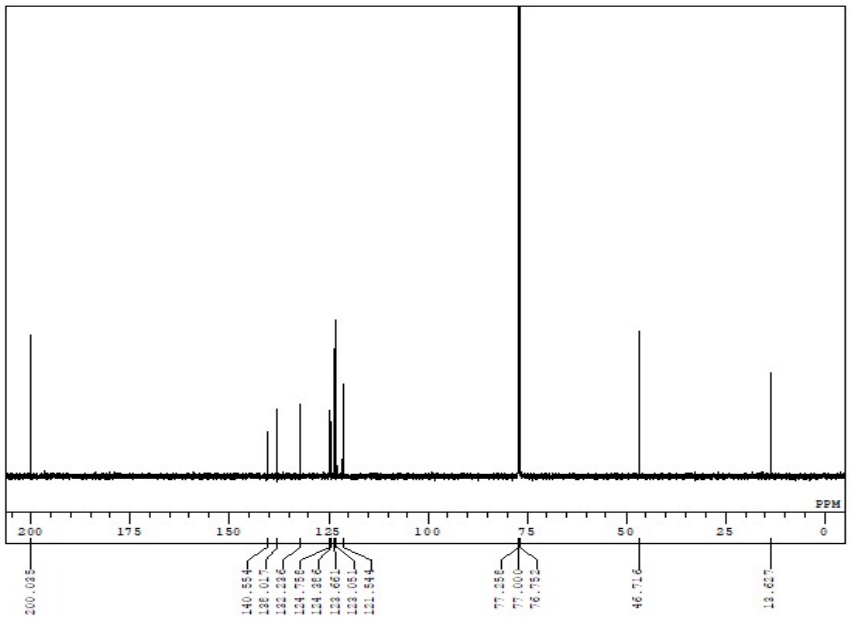


```
DFILE  3-S-B-aldehyde_carbon-1-1.als
COMNT  single pulse decoupled gated NC
DATIM  2018-02-27 16:48:34
OBNUC  13C
EXMOD  carbon.jxp
OBFRQ        125.77 MHz
OBSET          7.87 KHz
OBFIN          4.21 Hz
POINT         32767
FREQU      39308.18 Hz
SCANS          1024
ACQTM        0.8336 sec
PD           2.0000 sec
PW1            3.12 usec
IRNUC  1H
CTEMP         12.2 c
SLVNT  CDCL3
EXREF         77.00 ppm
BF            0.10 Hz
RGAIN           54
```

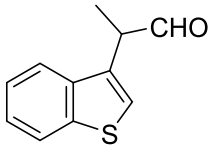

4*B*

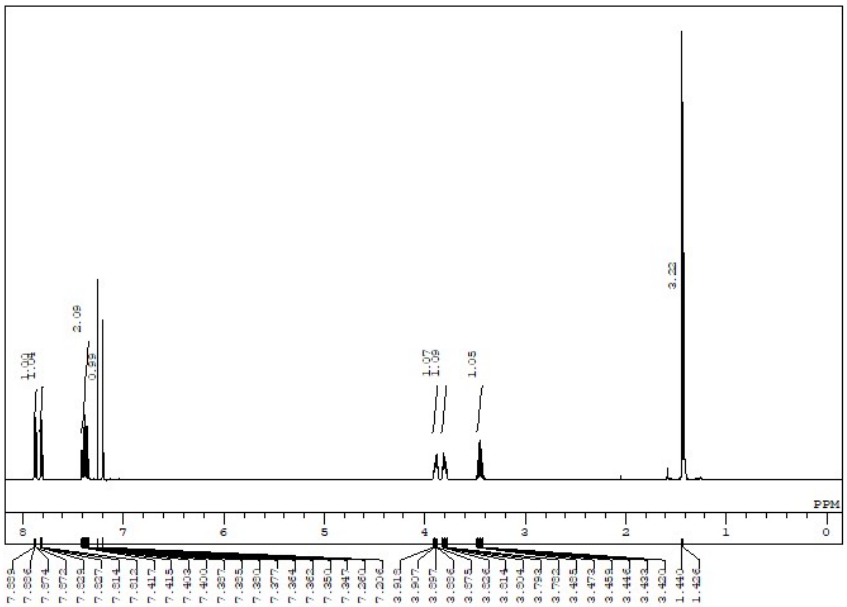


```
DFILE  3-S-B-alcohol_proton-1-1.als
COMNT  single_pulse
DATIM  2018-03-08 16:25:13
OBNUC  1H
EXMOD  proton.jxp
OBFRQ        500.16 MHz
OBSET          2.41 KHz
OBFIN          6.01 Hz
POINT         13107
FREQU       7507.51 Hz
SCANS            8
ACQTM        1.7459 sec
PD           5.0000 sec
PW1            6.85 usec
IRNUC  1H
CTEMP         14.5 c
SLVNT  CDCL3
EXREF         7.26 ppm
BF            0.10 Hz
RGAIN           42
```

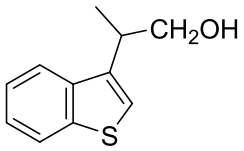

4*BB*

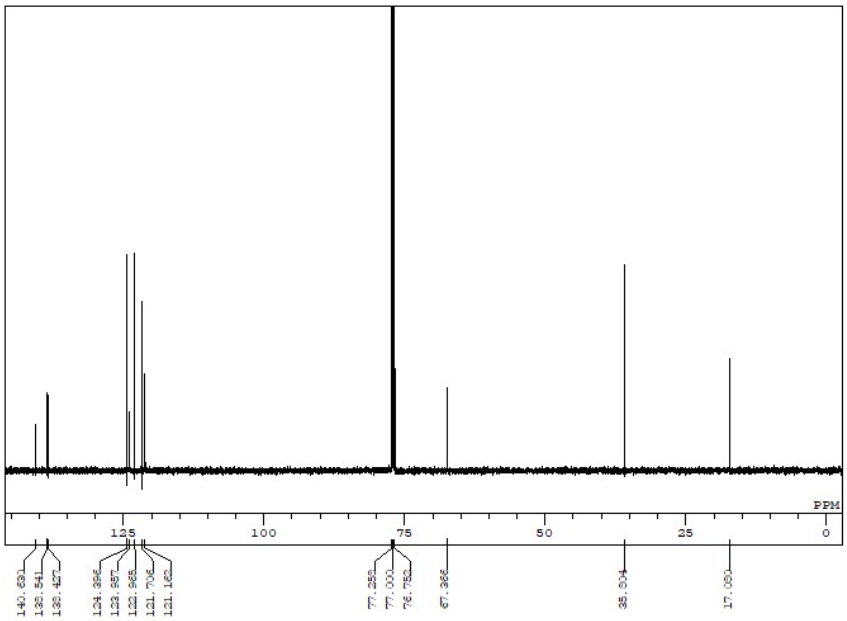


```
DFILE  3-S-B-alcohol_carbon-1-1.als
COMNT  single pulse decoupled gated NC
DATIM  2018-03-08 20:40:53
OBNUC  13C
EXMOD  carbon.jxp
OBFRQ        125.77 MHz
OBSET          7.87 KHz
OBFIN          4.21 Hz
POINT         32767
FREQU      39308.18 Hz
SCANS          1024
ACQTM        0.8336 sec
PD           2.0000 sec
PW1            3.12 usec
IRNUC  1H
CTEMP         14.5 c
SLVNT  CDCL3
EXREF        77.00 ppm
BF            0.10 Hz
RGAIN           58
```

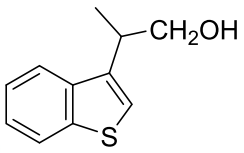

4*BB*

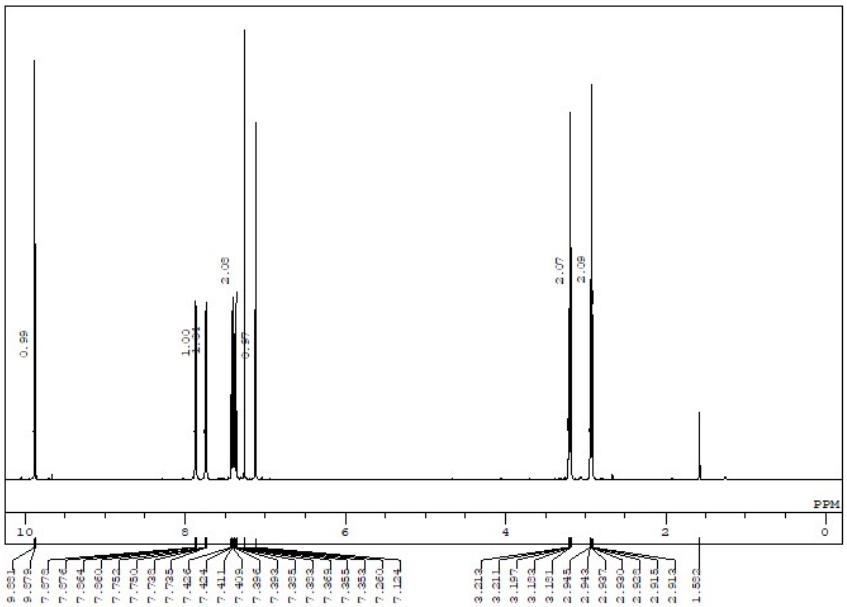

```
DFILE  3-S-L-aldehyde_proton-1-1.als
COMNT  single_pulse
DATIM  2018-02-28 19:53:09
OBNUC  1H
EXMOD  proton.jxp
OBFRQ        500.16 MHz
OBSET          2.41 KHz
OBFIN          6.01 Hz
POINT         13107
FREQU       7507.51 Hz
SCANS            8
ACQTM        1.7459 sec
PD           5.0000 sec
PW1            6.85 usec
IRNUC  1H
CTEMP         12.4 c
SLVNT  CDCL3
EXREF         7.26 ppm
BF            0.10 Hz
RGAIN           42
```

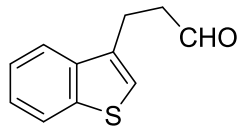

4L

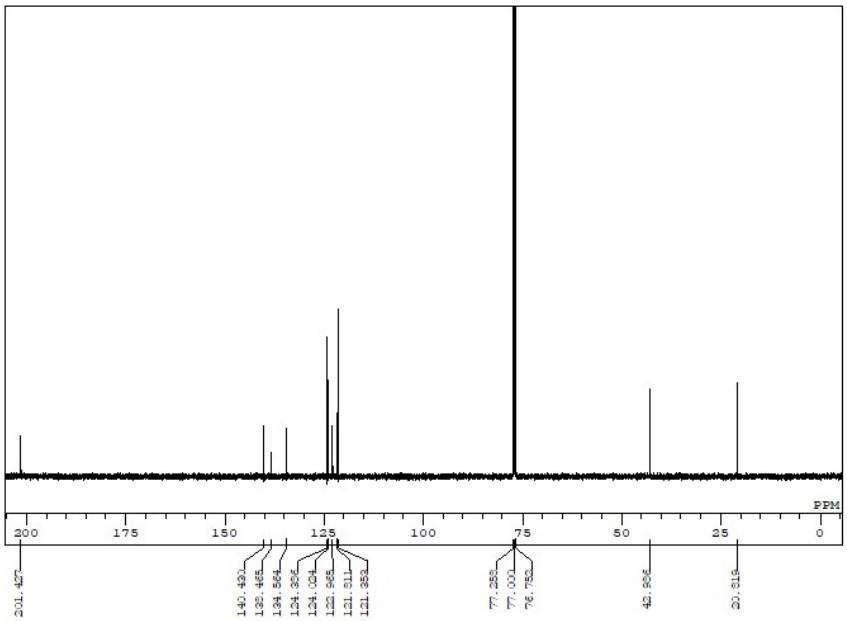

```
DFILE  3-S-L-aldehyde_carbon-1-1.als
COMNT  single pulse decoupled gated NC
DATIM  2018-02-28 21:16:54
OBNUC  13C
EXMOD  carbon.jxp
OBFRQ        125.77 MHz
OBSET          7.87 KHz
OBFIN          4.21 Hz
POINT         32767
FREQU      39308.18 Hz
SCANS          1024
ACQTM        0.8336 sec
PD           2.0000 sec
PW1            3.12 usec
IRNUC  1H
CTEMP         12.8 c
SLVNT  CDCL3
EXREF        77.00 ppm
BF            0.10 Hz
RGAIN           56
```

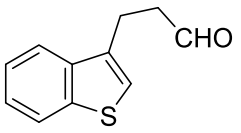

4L

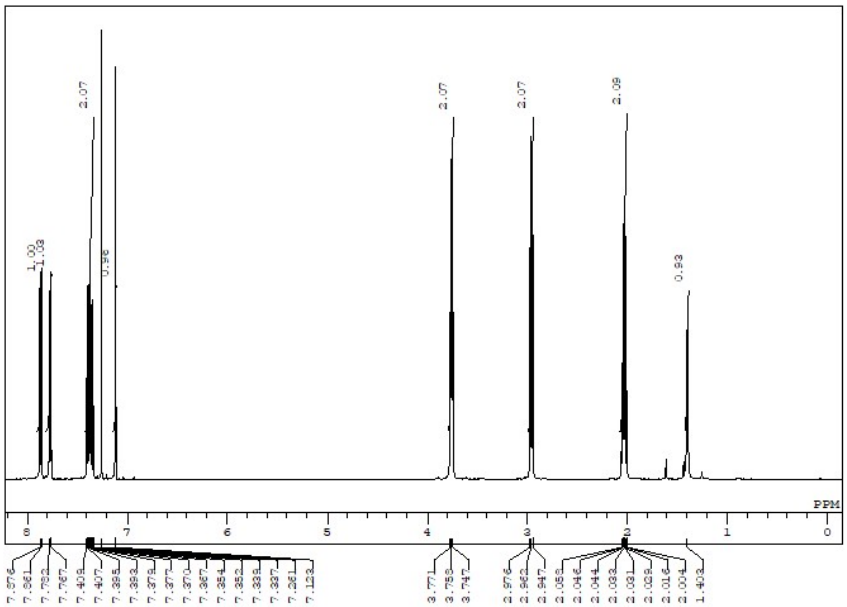


```
DFILE  3-S-L-alcohol_proton-1-1.als
COMNT  single_pulse
DATIM  2018-03-10 19:01:54
OBNUC  1H
EXMOD  proton.jxp
OBFRQ        500.16 MHz
OBSET          2.41 KHz
OBFIN          6.01 Hz
POINT         13107
FREQU       7507.51 Hz
SCANS             8
ACQTM         1.7459 sec
PD            5.0000 sec
PW1             6.85 usec
IRNUC  1H
CTEMP           13.2 c
SLVNT  CDCL3
EXREF           7.26 ppm
BF              0.10 Hz
RGAIN             40
```

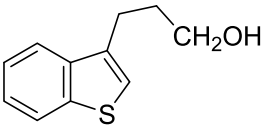

4LL

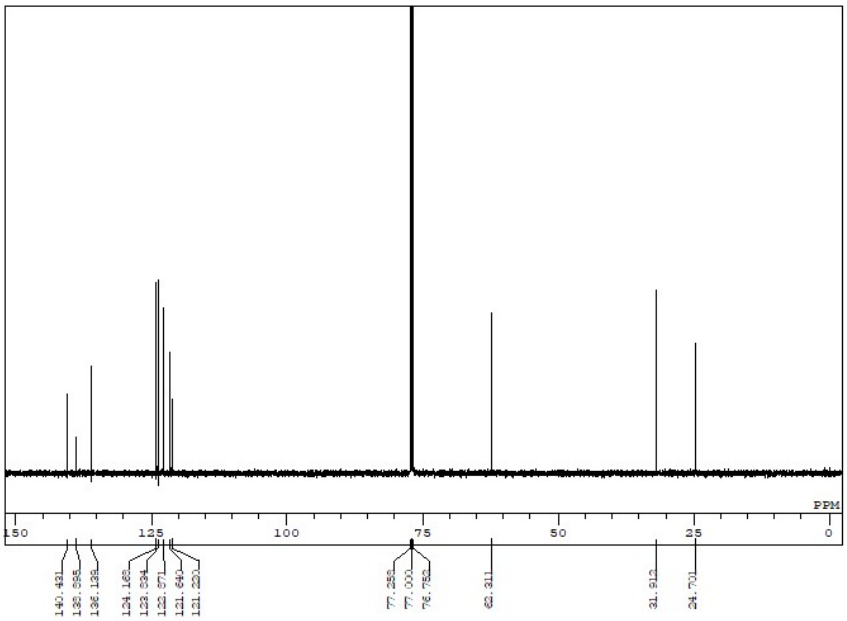


```
DFILE  3-S-L-alcohol_carbon-1-1.als
COMNT  single pulse decoupled gated NC
DATIM  2018-03-10 19:04:55
OBNUC  13C
EXMOD  carbon.jxp
OBFRQ        125.77 MHz
OBSET          7.87 KHz
OBFIN          4.21 Hz
POINT         26214
FREQU      31446.54 Hz
SCANS          1024
ACQTM         0.8336 sec
PD            2.0000 sec
PW1             3.12 usec
IRNUC  1H
CTEMP           13.5 c
SLVNT  CDCL3
EXREF          77.00 ppm
BF              0.10 Hz
RGAIN             60
```

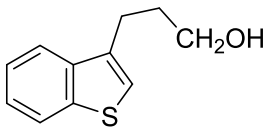

4LL

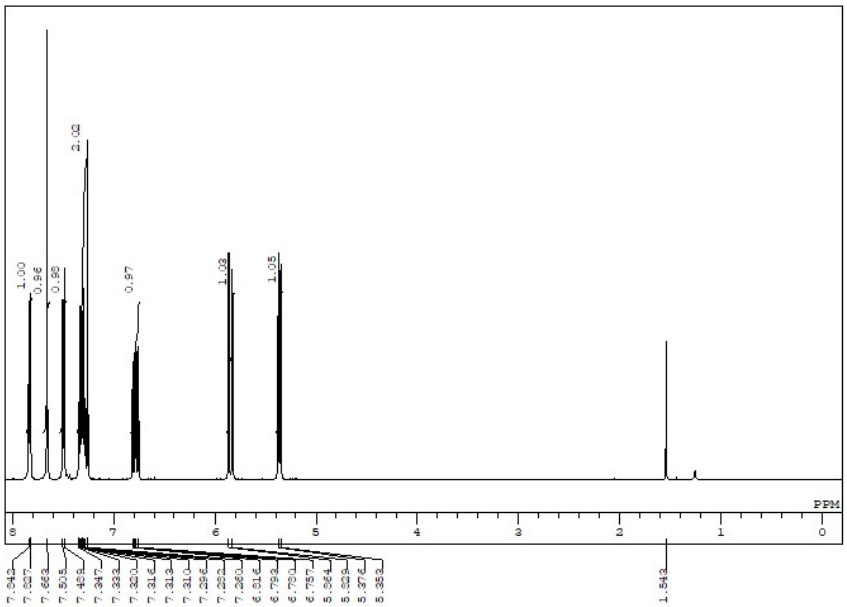


```
DFILE  3-O-olefin_proton-1-1.als
COMNT  single_pulse
DATIM  2018-07-26 16:44:10
OBNUC  1H
EXMOD  proton.jxp
OBFRQ        500.16 MHz
OBSET          2.41 KHz
OBFIN          6.01 Hz
POINT         16384
FREQU       9384.38 Hz
SCANS             8
ACQTM        1.7459 sec
PD           5.0000 sec
PW1            6.85 usec
IRNUC  1H
CTEMP         19.9 c
SLVNT  CDCL3
EXREF         7.26 ppm
BF            1.20 Hz
RGAIN           46
```

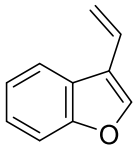

5

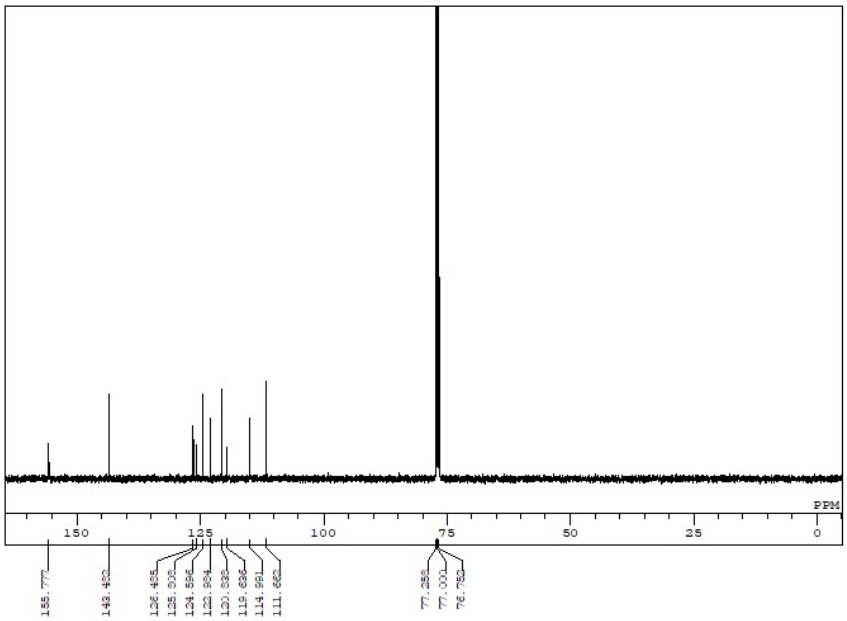


```
DFILE  3-O-olefin_carbon-1-1.als
COMNT  single pulse decoupled gated NC
DATIM  2018-07-26 16:46:15
OBNUC  13C
EXMOD  carbon.jxp
OBFRQ        125.77 MHz
OBSET          7.87 KHz
OBFIN          4.21 Hz
POINT         32767
FREQU      39308.18 Hz
SCANS          1024
ACQTM        0.8336 sec
PD           2.0000 sec
PW1            3.12 usec
IRNUC  1H
CTEMP         20.2 c
SLVNT  CDCL3
EXREF         77.00 ppm
BF            1.20 Hz
RGAIN           58
```

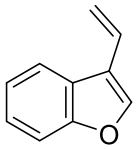

5

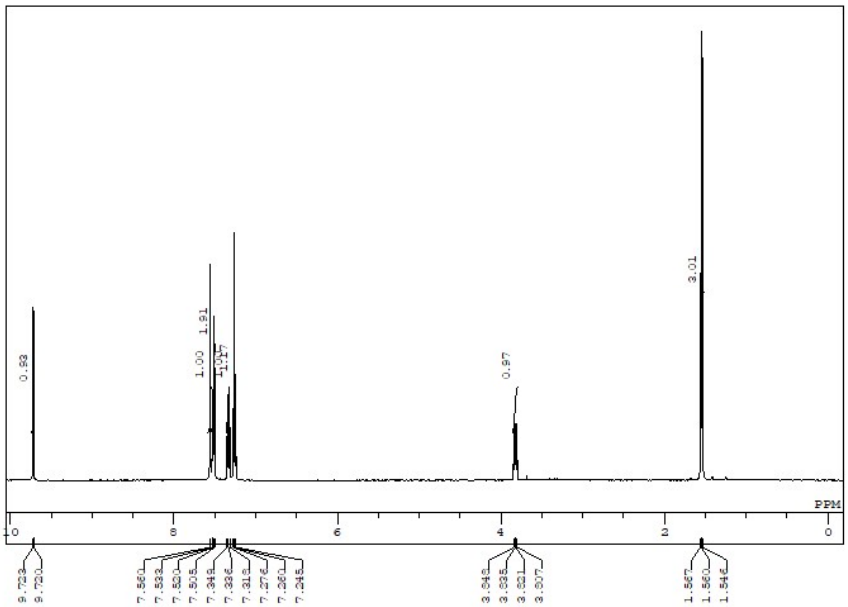


```
DFILE  3-O-B-aldehyde_proton-1-1.als
COMNT  single_pulse
DATIM  2018-07-31 20:34:20
OBNUC  1H
EXMOD  proton.jxp
OBFRQ        500.16 MHz
OBSET          2.41 KHz
OBFIN          6.01 Hz
POINT         16384
FREQU       9384.38 Hz
SCANS             8
ACQTM        1.7459 sec
PD           5.0000 sec
PW1            6.85 usec
IRNUC  1H
CTEMP         18.4 c
SLVNT  CDCL3
EXREF         7.26 ppm
BF            1.20 Hz
RGAIN           44
```

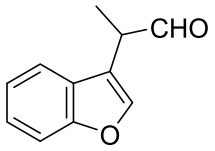

5B

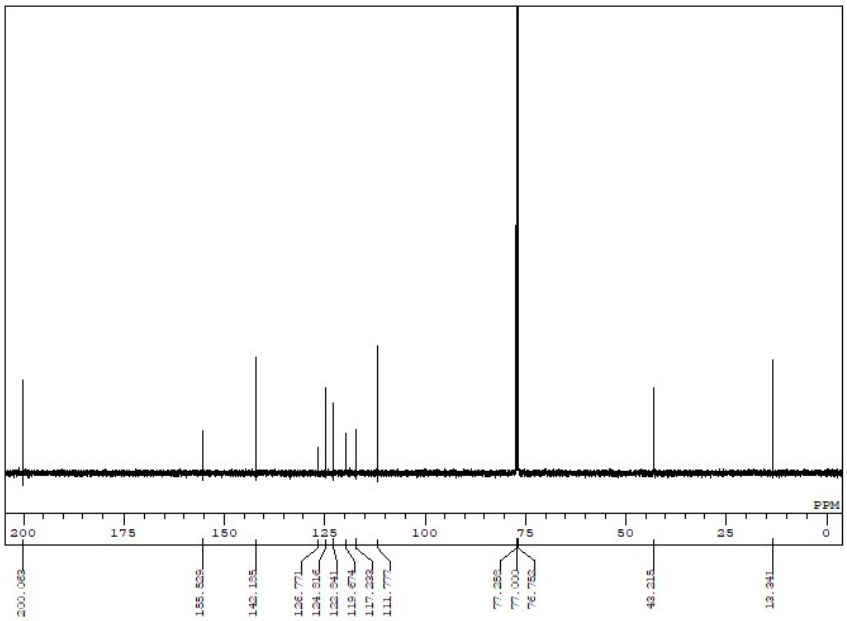


```
DFILE  3-O-B-aldehyde_carbon-1-1.als
COMNT  single pulse decoupled gated NC
DATIM  2018-07-31 22:28:46
OBNUC  13C
EXMOD  carbon.jxp
OBFRQ        125.77 MHz
OBSET          7.87 KHz
OBFIN          4.21 Hz
POINT         32767
FREQU      39308.18 Hz
SCANS          1024
ACQTM        0.8336 sec
PD           2.0000 sec
PW1            3.12 usec
IRNUC  1H
CTEMP         18.7 c
SLVNT  CDCL3
EXREF        77.00 ppm
BF            0.10 Hz
RGAIN           58
```

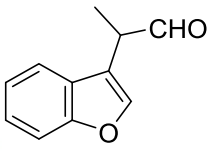

5B

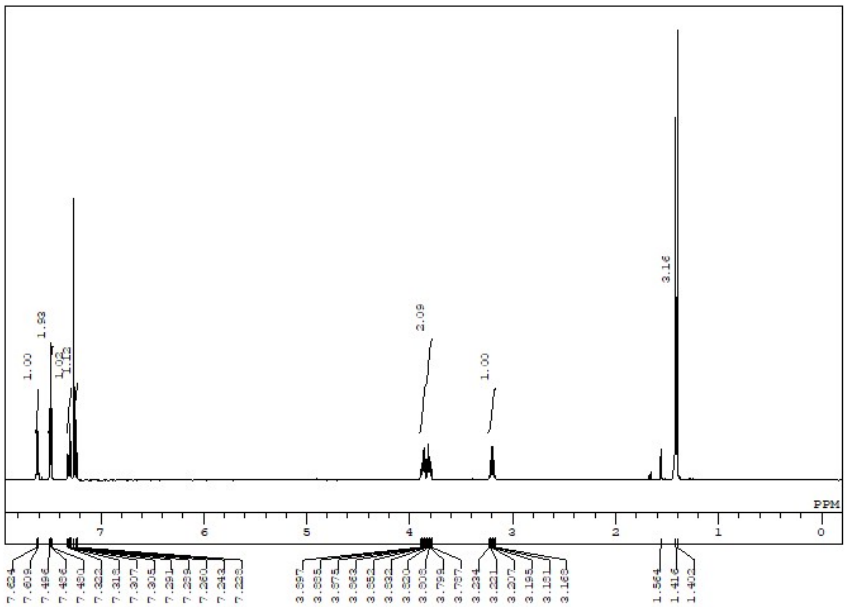


```
DFILE  3-O-B-alcohol_proton-1-1.als
COMNT  single_pulse
DATIM  2018-08-04 20:22:08
OBNUC  1H
EXMOD  proton.jxp
OBFRQ        500.16 MHz
OBSET          2.41 KHz
OBFIN          6.01 Hz
POINT         16384
FREQU       9384.38 Hz
SCANS             8
ACQTM        1.7459 sec
PD           5.0000 sec
PW1            6.85 usec
IRNUC  1H
CTEMP         18.5 c
SLVNT  CDCL3
EXREF         7.26 ppm
BF            0.10 Hz
RGAIN           46
```

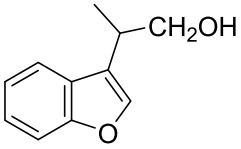

5*BB*

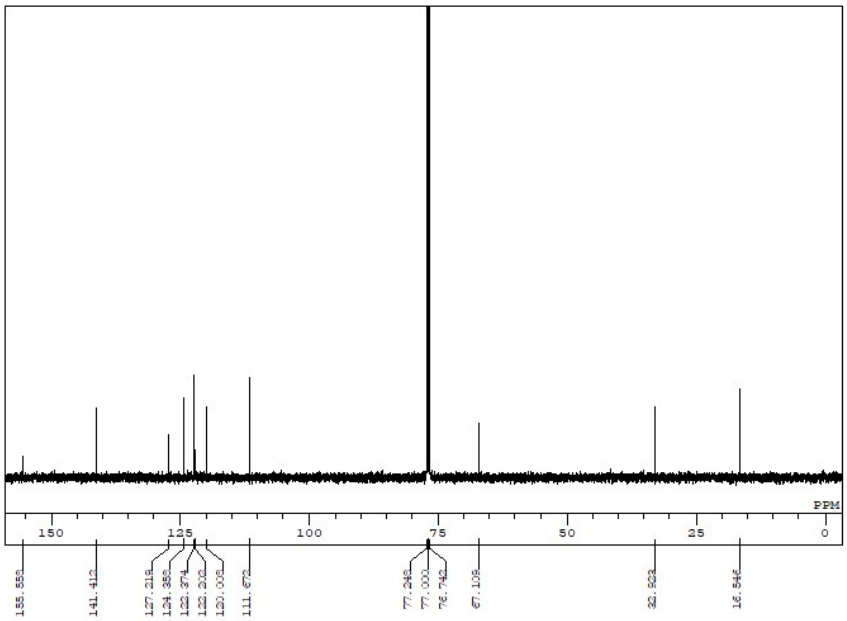


```
DFILE  3-O-B-alcohol_carbon-1-1.als
COMNT  single pulse decoupled gated NC
DATIM  2018-08-04 20:25:22
OBNUC  13C
EXMOD  carbon.jxp
OBFRQ        125.77 MHz
OBSET          7.87 KHz
OBFIN          4.21 Hz
POINT         32767
FREQU      39308.18 Hz
SCANS          1024
ACQTM        0.8336 sec
PD           2.0000 sec
PW1            3.12 usec
IRNUC  1H
CTEMP         18.8 c
SLVNT  CDCL3
EXREF        77.00 ppm
BF            0.10 Hz
RGAIN           58
```

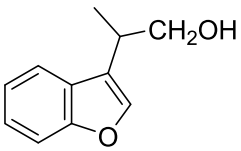

5*BB*

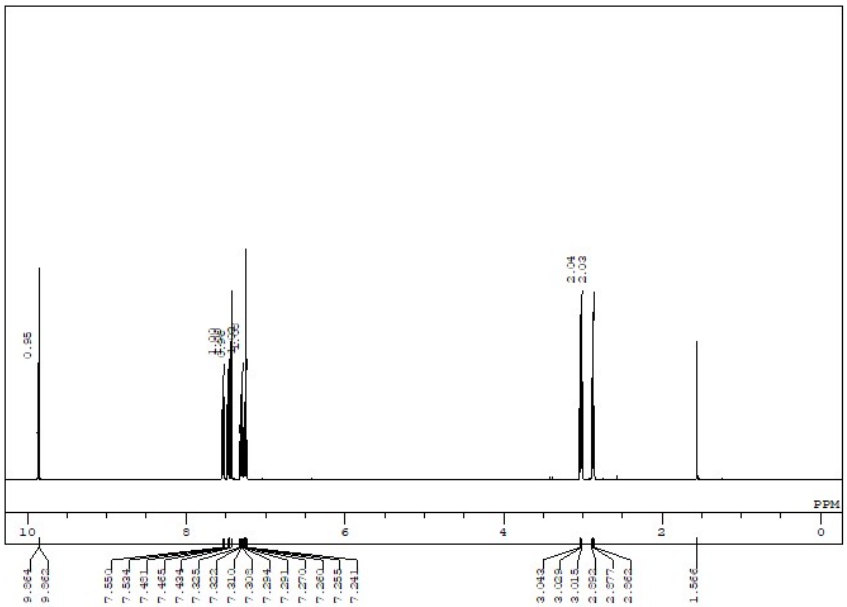

```
DFILE  3-O-L-aldehyde_proton-1-1.als
COMNT  single_pulse
DATIM  2018-08-01 16:16:12
OBNUC  1H
EXMOD  proton.jxp
OBFRQ        500.16 MHz
OBSET          2.41 KHz
OBFIN          6.01 Hz
POINT         16384
FREQU       9384.38 Hz
SCANS             8
ACQTM        1.7459 sec
PD           5.0000 sec
PW1            6.85 usec
IRNUC  1H
CTEMP          19.1 c
SLVNT  CDCL3
EXREF          7.26 ppm
BF             0.10 Hz
RGAIN            44
```

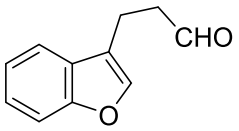

5*L*

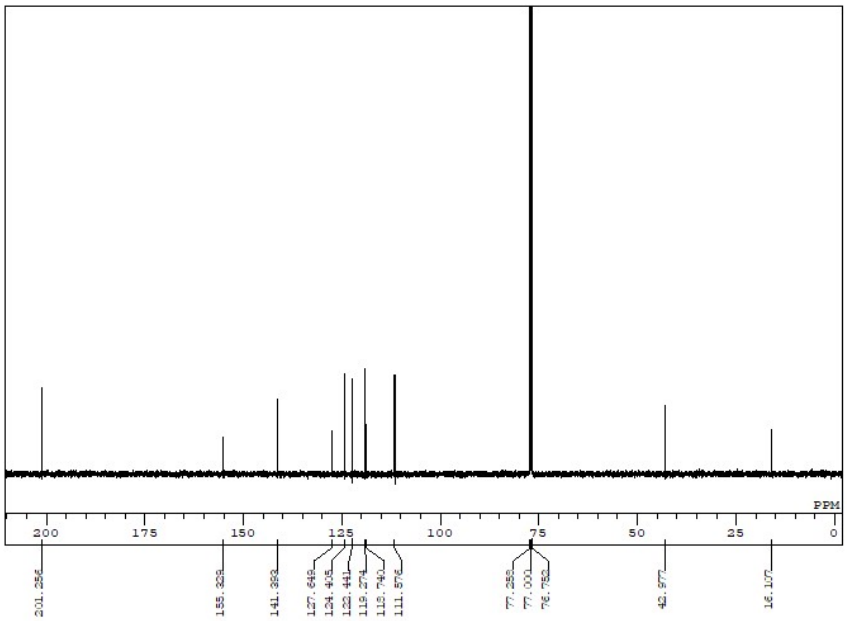

```
DFILE  3-O-L-aldehyde_carbon-1-1.als
COMNT  single pulse decoupled gated NC
DATIM  2018-08-01 16:20:52
OBNUC  13C
EXMOD  carbon.jxp
OBFRQ        125.77 MHz
OBSET          7.87 KHz
OBFIN          4.21 Hz
POINT         32767
FREQU      39308.18 Hz
SCANS          1024
ACQTM        0.8336 sec
PD           2.0000 sec
PW1            3.12 usec
IRNUC  1H
CTEMP          19.4 c
SLVNT  CDCL3
EXREF         77.00 ppm
BF             0.10 Hz
RGAIN            56
```

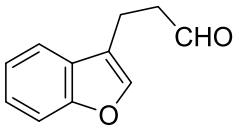

5*L*

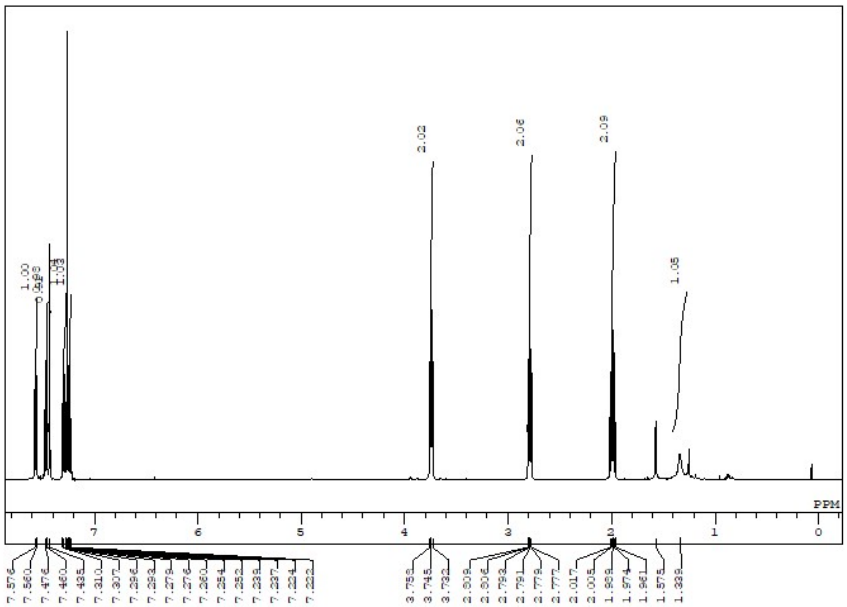

```
DFILE  3-O-L-alcohol_proton-1-1.als
COMNT  single_pulse
DATIM  2018-08-03 20:46:01
OBNUC  1H
EXMOD  proton.jxp
OBFRQ        500.16 MHz
OBSET          2.41 KHz
OBFIN          6.01 Hz
POINT         16384
FREQU       9384.38 Hz
SCANS             8
ACQTM         1.7459 sec
PD            5.0000 sec
PW1             6.85 usec
IRNUC  1H
CTEMP          18.2 c
SLVNT  CDCL3
EXREF          7.26 ppm
BF             0.10 Hz
RGAIN            46
```

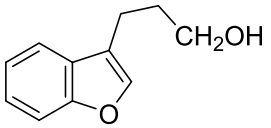

5*LL*

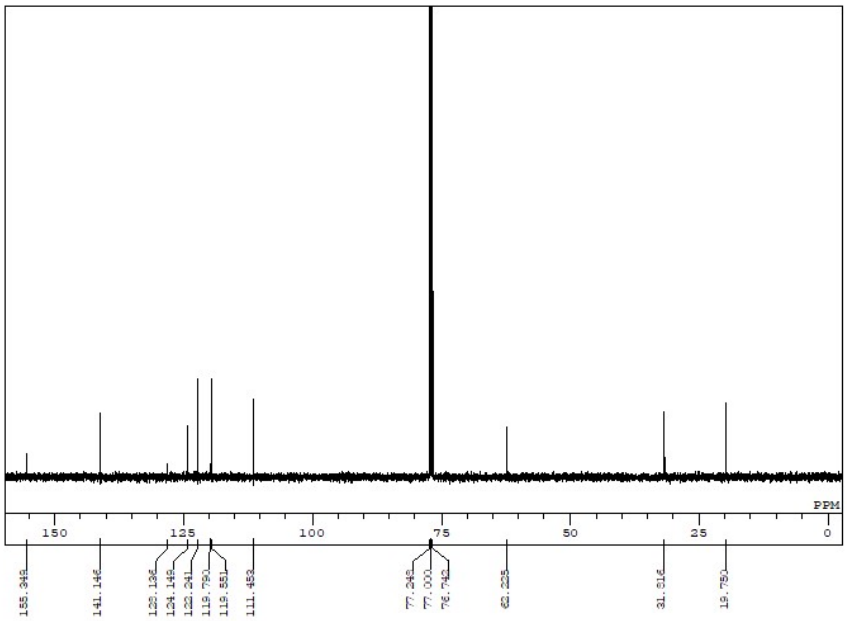

```
DFILE  3-O-L-alcohol_carbon-1-1.als
COMNT  single pulse decoupled gated NC
DATIM  2018-08-03 20:51:03
OBNUC  13C
EXMOD  carbon.jxp
OBFRQ        125.77 MHz
OBSET          7.87 KHz
OBFIN          4.21 Hz
POINT         26214
FREQU      31446.54 Hz
SCANS          1024
ACQTM         0.8336 sec
PD            2.0000 sec
PW1             3.12 usec
IRNUC  1H
CTEMP          18.4 c
SLVNT  CDCL3
EXREF         77.00 ppm
BF             0.10 Hz
RGAIN            56
```

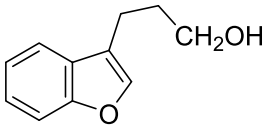

5*LL*

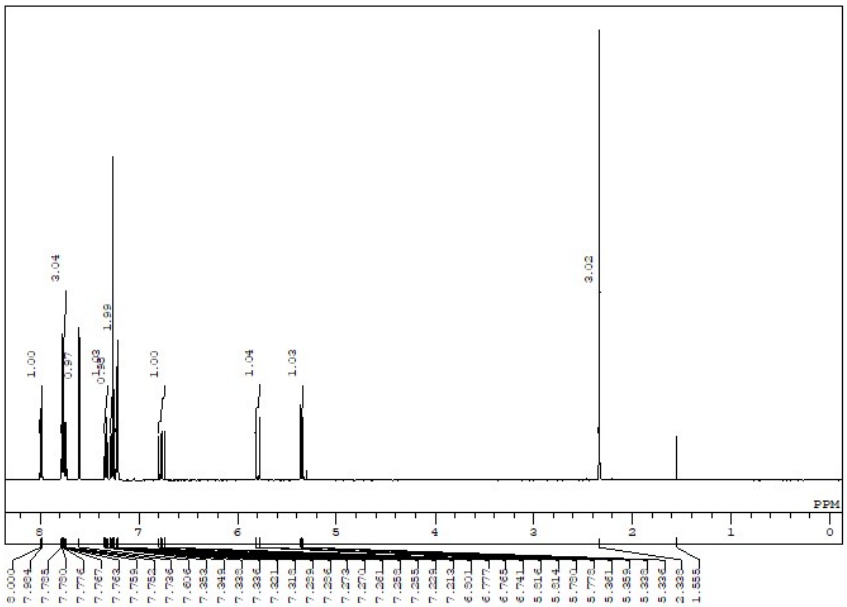

```
DFILE  3-NTs-olefin_proton-1-1.als
COMNT  single_pulse
DATIM  2017-11-15 20:27:31
OBNUC  1H
EXMOD  proton.jxp
OBFRQ        500.16 MHz
OBSET          2.41 KHz
OBFIN          6.01 Hz
POINT         13107
FREQU       7507.51 Hz
SCANS             8
ACQTM        1.7459 sec
PD           5.0000 sec
PW1            6.85 usec
IRNUC  1H
CTEMP         17.3 c
SLVNT  CDCL3
EXREF         7.26 ppm
BF            0.10 Hz
RGAIN           44
```

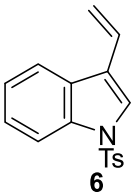

6

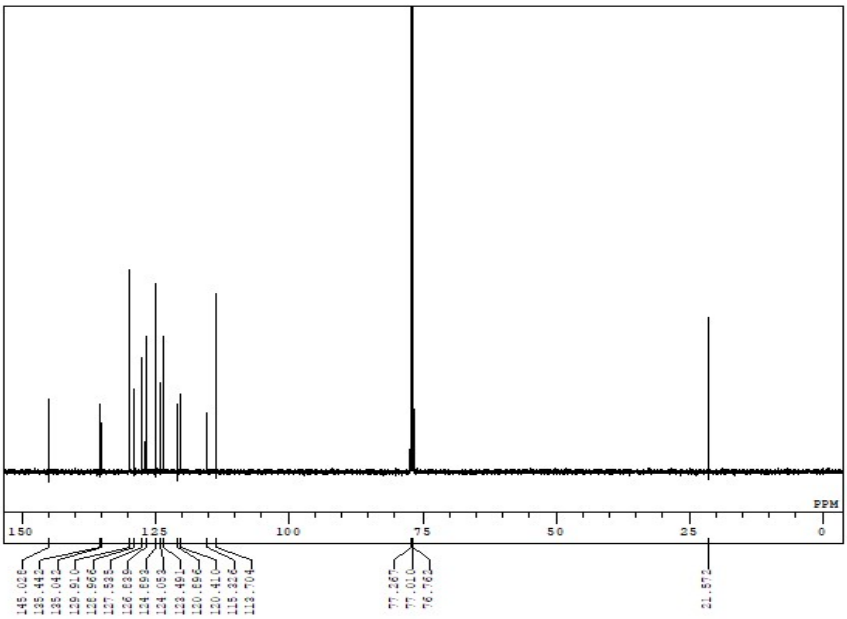

```
DFILE  3-NTs-olefin_carbon-1-1.als
COMNT  single pulse decoupled gated NC
DATIM  2017-11-15 20:37:46
OBNUC  13C
EXMOD  carbon.jxp
OBFRQ        125.77 MHz
OBSET          7.87 KHz
OBFIN          4.21 Hz
POINT         26214
FREQU      31446.54 Hz
SCANS          1024
ACQTM        0.8336 sec
PD           2.0000 sec
PW1            3.12 usec
IRNUC  1H
CTEMP         18.0 c
SLVNT  CDCL3
EXREF        77.00 ppm
BF            0.10 Hz
RGAIN           60
```

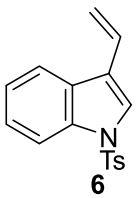

6

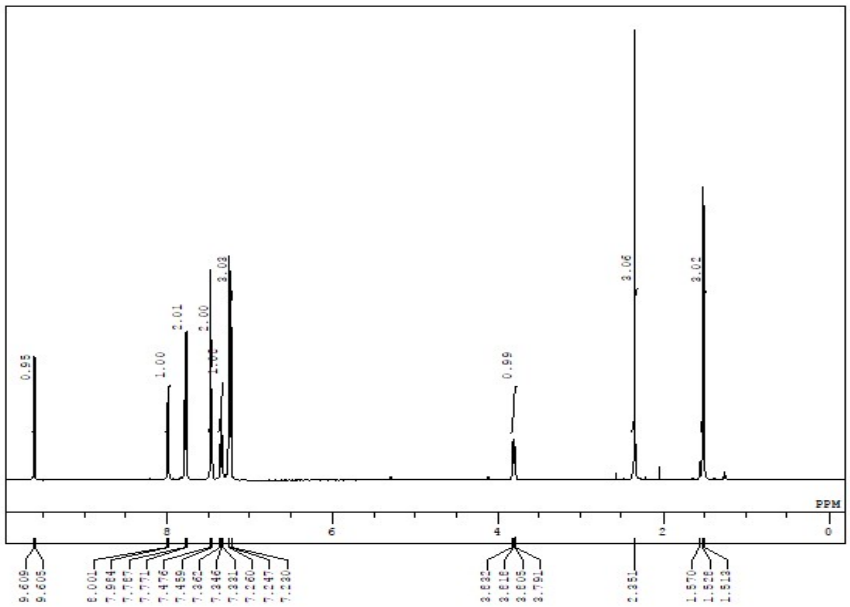


```
DFILE  3-NTs-B-aldehyde_proton-1-1.als
COMNT  single_pulse
DATIM  2017-11-27 11:57:53
OBNUC  1H
EXMOD  proton.jxp
OBFRQ        500.16 MHz
OBSET          2.41 KHz
OBFIN          6.01 Hz
POINT         16384
FREQU       9384.38 Hz
SCANS             8
ACQTM        1.7459 sec
PD           5.0000 sec
PW1            6.85 usec
IRNUC  1H
CTEMP         16.9 c
SLVNT  CDCL3
EXREF         7.26 ppm
BF            1.20 Hz
RGAIN           44
```

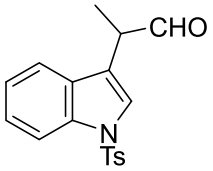

6*B*

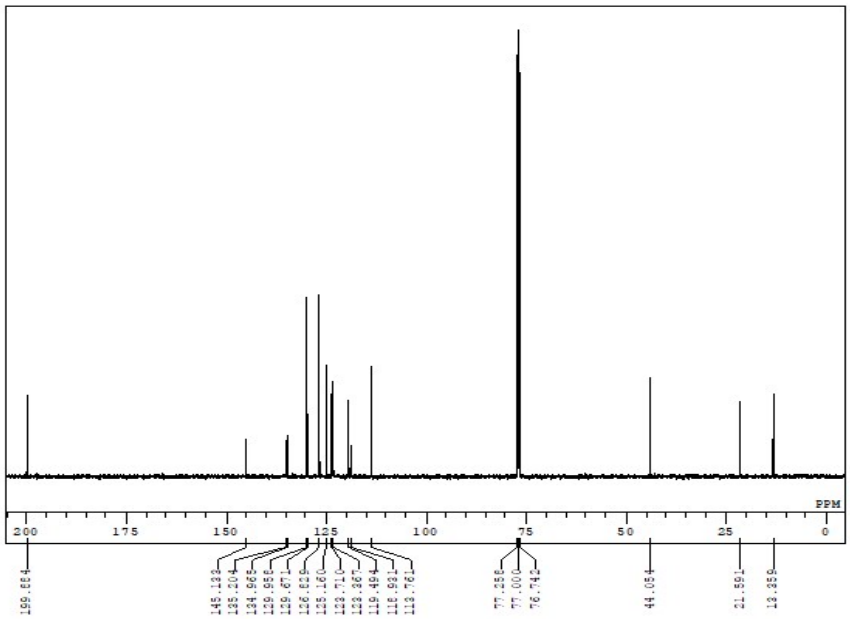


```
DFILE  3-NTS-B-aldehyde_carbon-1-1.als
COMNT  single pulse decoupled gated NC
DATIM  2017-11-27 16:47:43
OBNUC  13C
EXMOD  carbon.jxp
OBFRQ        125.77 MHz
OBSET          7.87 KHz
OBFIN          4.21 Hz
POINT         26214
FREQU      31446.54 Hz
SCANS          1024
ACQTM        0.8336 sec
PD           2.0000 sec
PW1            3.12 usec
IRNUC  1H
CTEMP         14.7 c
SLVNT  CDCL3
EXREF        77.00 ppm
BF            1.20 Hz
RGAIN           60
```

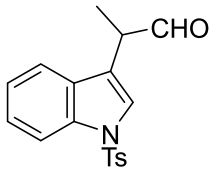

6*B*

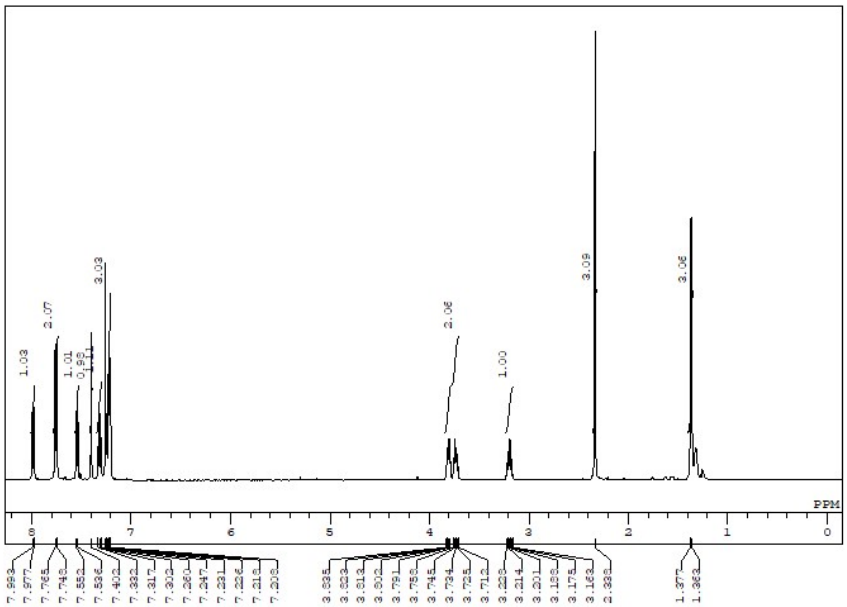

```
DFILE  3-NTs-B-alcohol_proton-1-1.als
COMNT  single_pulse
DATIM  2017-12-26 11:29:33
OBNUC  1H
EXMOD  proton.jxp
OBFRQ        500.16 MHz
OBSET          2.41 KHz
OBFIN          6.01 Hz
POINT         16384
FREQU       9384.38 Hz
SCANS             8
ACQTM        1.7459 sec
PD           5.0000 sec
PW1            6.85 usec
IRNUC  1H
CTEMP         18.2 c
SLVNT  CDCL3
EXREF         7.26 ppm
BF            1.20 Hz
RGAIN           44
```

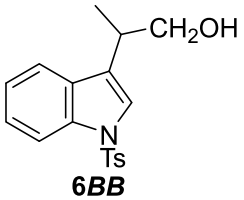

6*BB*

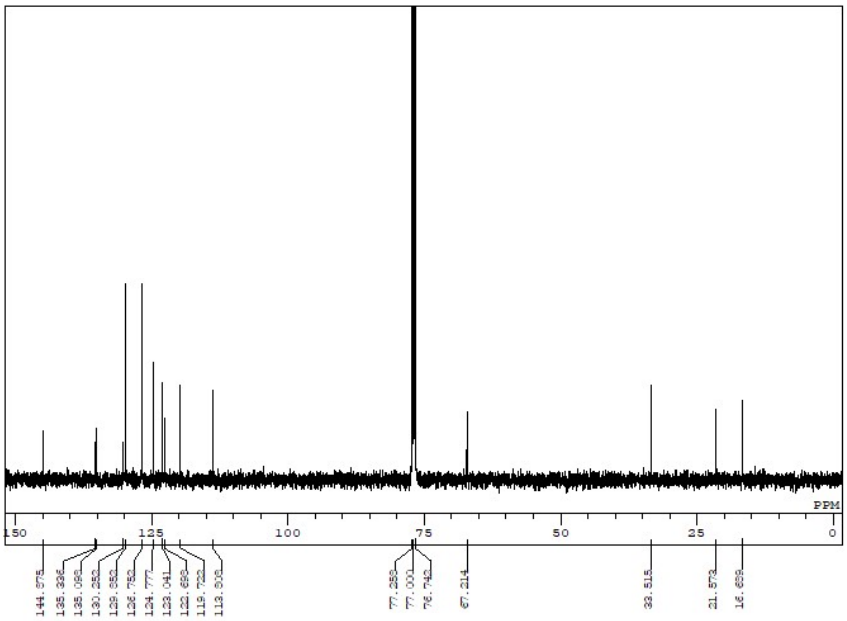

```
DFILE  3-NTS-B-alcohol_carbon-1-1.als
COMNT  single pulse decoupled gated NC
DATIM  2018-06-25 21:19:09
OBNUC  13C
EXMOD  carbon.jxp
OBFRQ        125.77 MHz
OBSET          7.87 KHz
OBFIN          4.21 Hz
POINT         32767
FREQU      39308.18 Hz
SCANS          1024
ACQTM        0.8336 sec
PD           2.0000 sec
PW1            3.12 usec
IRNUC  1H
CTEMP         15.5 c
SLVNT  CDCL3
EXREF        77.00 ppm
BF            1.20 Hz
RGAIN           56
```

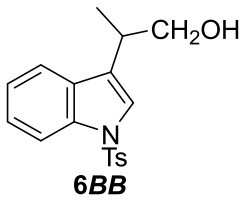

6*BB*

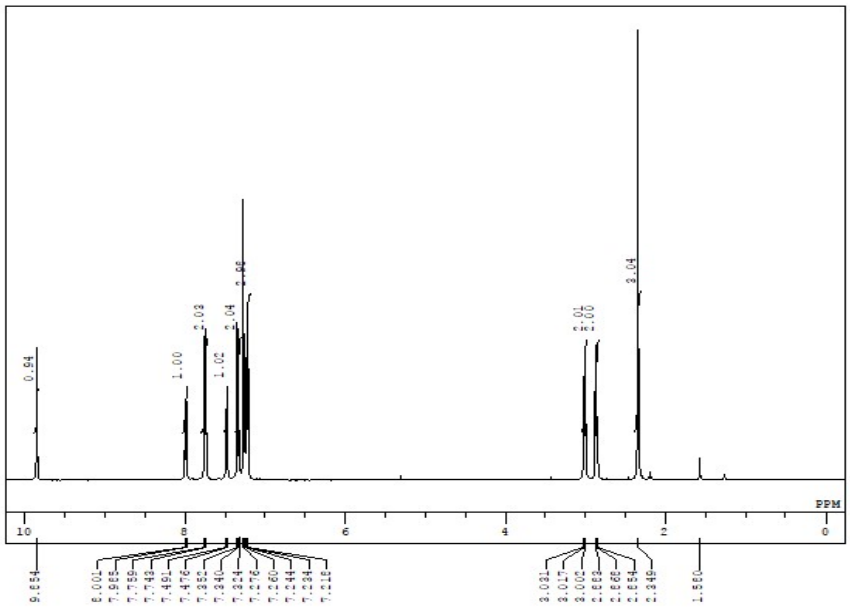


```
DFILE  3-NTs-L-aldehyde_proton-1-1.als
COMNT  single_pulse
DATIM  2017-11-21 20:35:50
OBNUC  1H
EXMOD  proton.jxp
OBFRQ        500.16 MHz
OBSET          2.41 KHz
OBFIN          6.01 Hz
POINT         16384
FREQU       9384.38 Hz
SCANS             8
ACQTM        1.7459 sec
PD           5.0000 sec
PW1            6.85 usec
IRNUC  1H
CTEMP         16.5 c
SLVNT  CDCL3
EXREF         7.26 ppm
BF            1.20 Hz
RGAIN           44
```

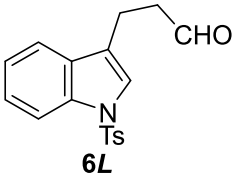

6*L*

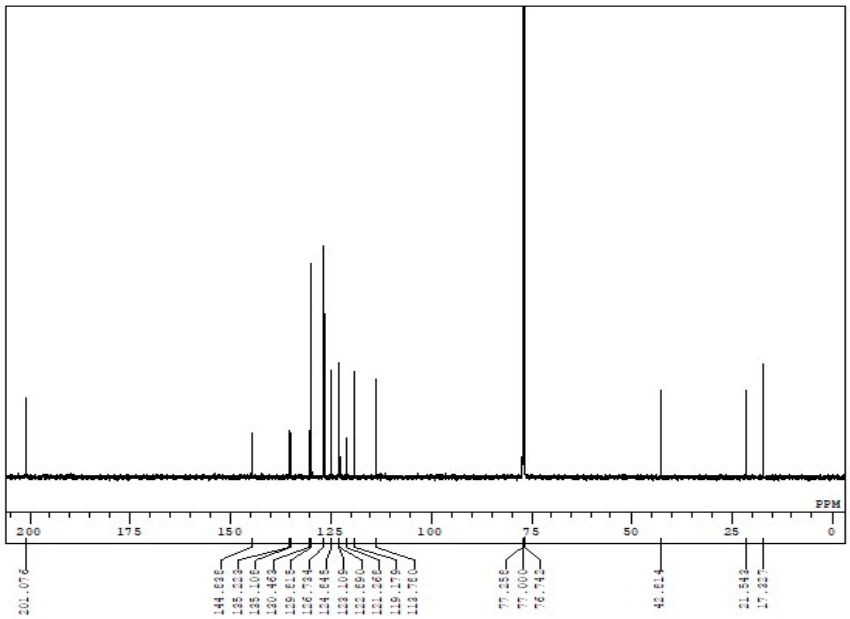


```
DFILE  3-NTs-L-aldehyde_carbon-1-1.als
COMNT  single pulse decoupled gated NC
DATIM  2017-11-21 20:45:28
OBNUC  13C
EXMOD  carbon.jxp
OBFRQ        125.77 MHz
OBSET          7.87 KHz
OBFIN          4.21 Hz
POINT         26214
FREQU      31446.54 Hz
SCANS          1024
ACQTM        0.8336 sec
PD           2.0000 sec
PW1            3.12 usec
IRNUC  1H
CTEMP         17.2 c
SLVNT  CDCL3
EXREF        77.00 ppm
BF            1.20 Hz
RGAIN           60
```

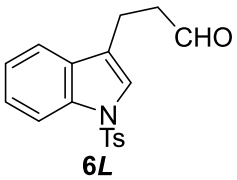

6*L*

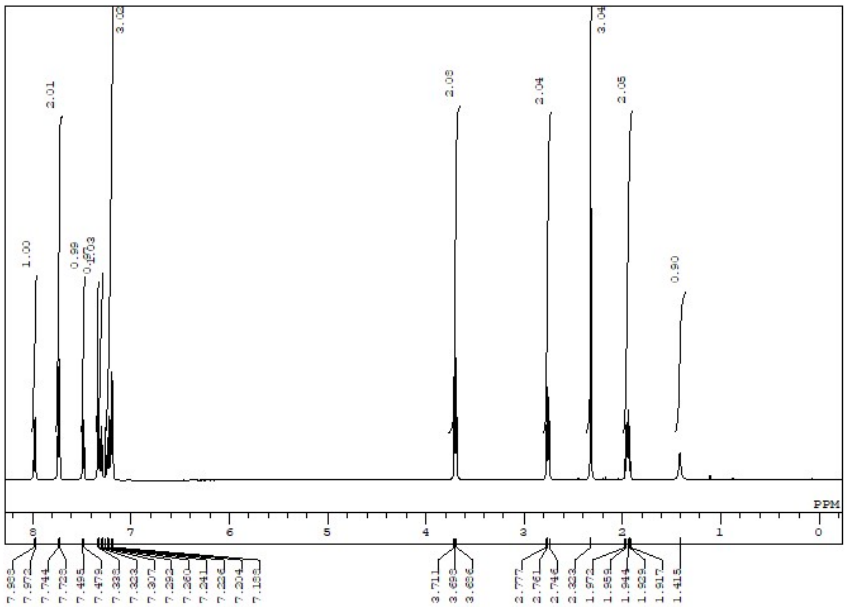


```
DFILE  3-NTs-L-alcohol_proton-1-1.als
COMNT  single_pulse
DATIM  2018-07-25 10:16:09
OBNUC  1H
EXMOD  proton.jxp
OBFRQ        500.16 MHz
OBSET          2.41 KHz
OBFIN          6.01 Hz
POINT         16384
FREQU       9384.38 Hz
SCANS             8
ACQTM         1.7459 sec
PD            5.0000 sec
PW1             6.85 usec
IRNUC  1H
CTEMP          18.3 c
SLVNT  CDCL3
EXREF          7.26 ppm
BF             1.20 Hz
RGAIN            38
```

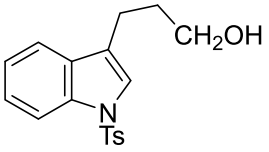

6*LL*

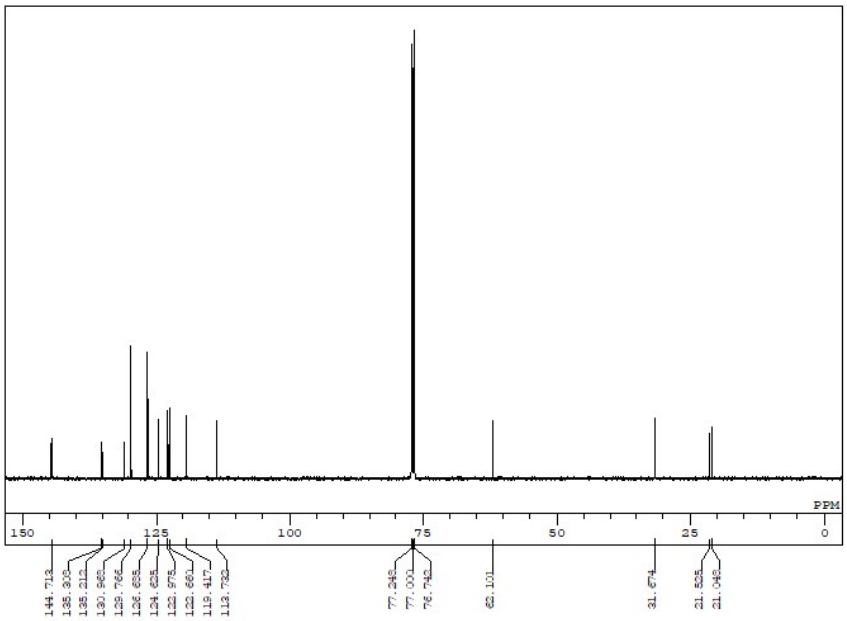


```
DFILE  3-NTs-L-alcohol_carbon-1-1.als
COMNT  single pulse decoupled gated NC
DATIM  2018-07-25 10:22:23
OBNUC  13C
EXMOD  carbon.jxp
OBFRQ        125.77 MHz
OBSET          7.87 KHz
OBFIN          4.21 Hz
POINT         32767
FREQU      39308.18 Hz
SCANS          1024
ACQTM         0.8336 sec
PD            2.0000 sec
PW1             3.12 usec
IRNUC  1H
CTEMP          18.9 c
SLVNT  CDCL3
EXREF         77.00 ppm
BF             1.20 Hz
RGAIN            58
```

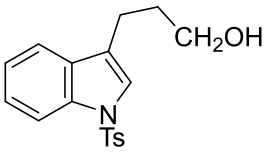

6*LL*

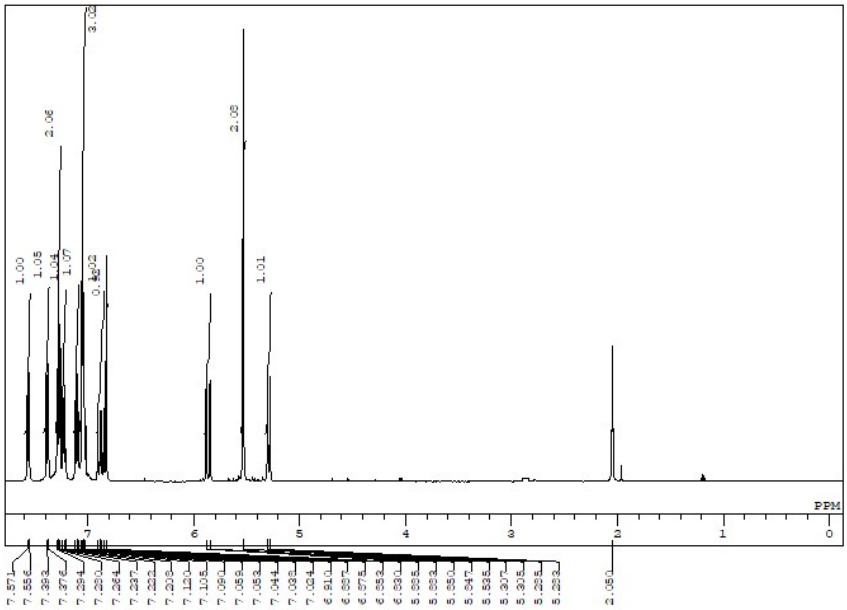

```
DFILE  2-NBn-olefin_proton-1-1.als
COMNT  single_pulse
DATIM  2018-04-26 20:45:34
OBNUC  1H
EXMOD  proton.jxp
OBFRQ        500.16 MHz
OBSET          2.41 KHz
OBFIN          6.01 Hz
POINT         16384
FREQU       9384.38 Hz
SCANS             8
ACQTM         1.7459 sec
PD            5.0000 sec
PW1             6.85 usec
IRNUC  1H
CTEMP          13.9 c
SLVNT  ACETN
EXREF          2.05 ppm
BF             1.20 Hz
RGAIN            38
```

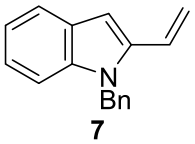

7

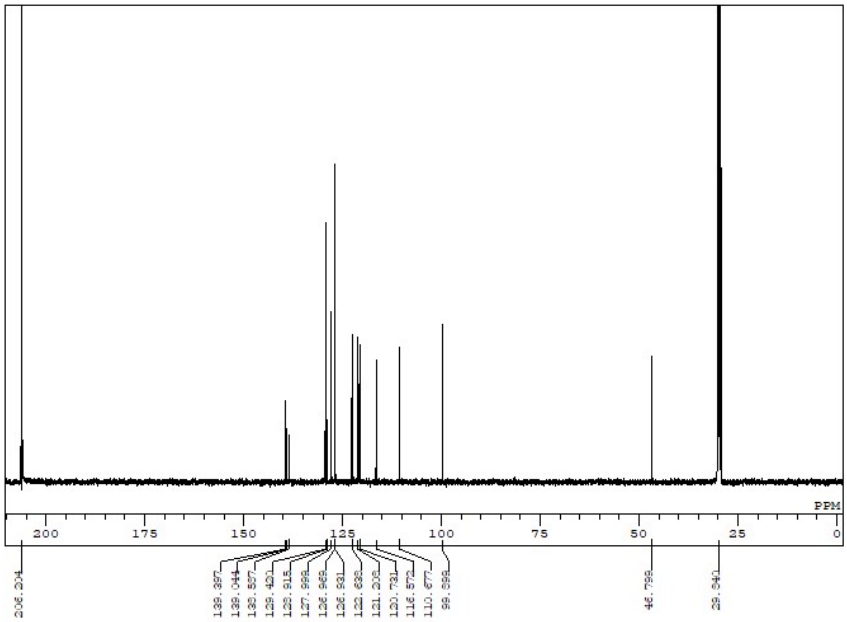

```
DFILE  2-NBn-olefin_carbon-1-1.als
COMNT  single pulse decoupled gated NO
DATIM  2018-04-26 20:47:44
OBNUC  13C
EXMOD  carbon.jxp
OBFRQ        125.77 MHz
OBSET          7.87 KHz
OBFIN          4.21 Hz
POINT         32767
FREQU      39308.18 Hz
SCANS          1024
ACQTM         0.8336 sec
PD            2.0000 sec
PW1             3.12 usec
IRNUC  1H
CTEMP          14.4 c
SLVNT  ACETN
EXREF         29.84 ppm
BF             1.20 Hz
RGAIN            58
```

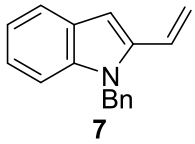

7

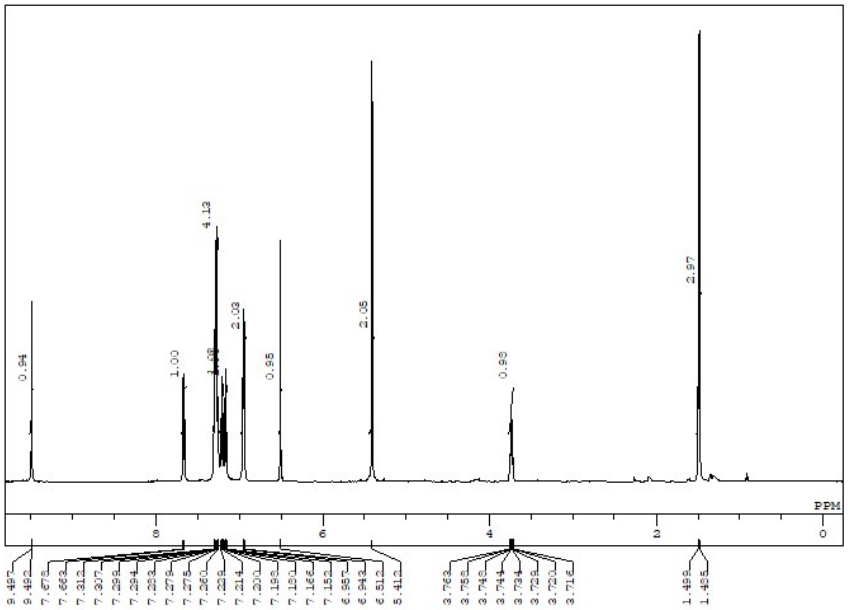


```
DFILE  2-NBn-B-aldehyde_proton-1-1.als
COMNT  single_pulse
DATIM  2018-05-12 17:48:22
OBNUC  1H
EXMOD  proton.jxp
OBFRQ        500.16 MHz
OBSET          2.41 KHz
OBFIN          6.01 Hz
POINT         16384
FREQU       9384.38 Hz
SCANS             8
ACQTM        1.7459 sec
PD           5.0000 sec
PW1            6.85 usec
IRNUC  1H
CTEMP         13.2 c
SLVNT  CDCL3
EXREF         7.26 ppm
BF            1.20 Hz
RGAIN           32
```

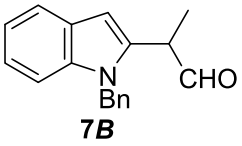

7B

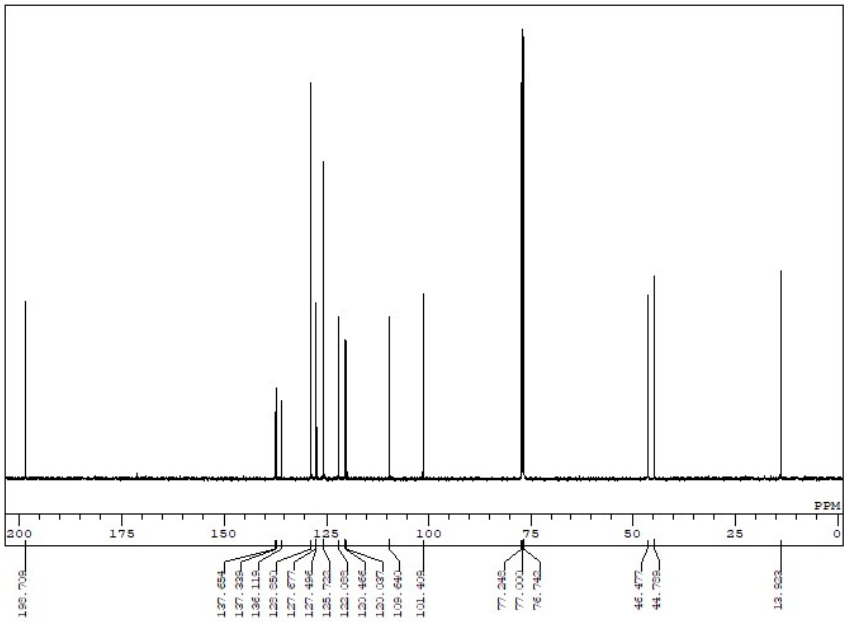


```
DFILE  2-NBn-B-aldehyde_carbon-1-1.als
COMNT  single pulse decoupled gated NO
DATIM  2018-05-12 17:52:06
OBNUC  13C
EXMOD  carbon.jxp
OBFRQ        125.77 MHz
OBSET          7.87 KHz
OBFIN          4.21 Hz
POINT         32767
FREQU      39308.18 Hz
SCANS          1024
ACQTM        0.8336 sec
PD           2.0000 sec
PW1            3.12 usec
IRNUC  1H
CTEMP         13.4 c
SLVNT  CDCL3
EXREF        77.00 ppm
BF            1.20 Hz
RGAIN           60
```

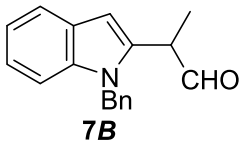

7B

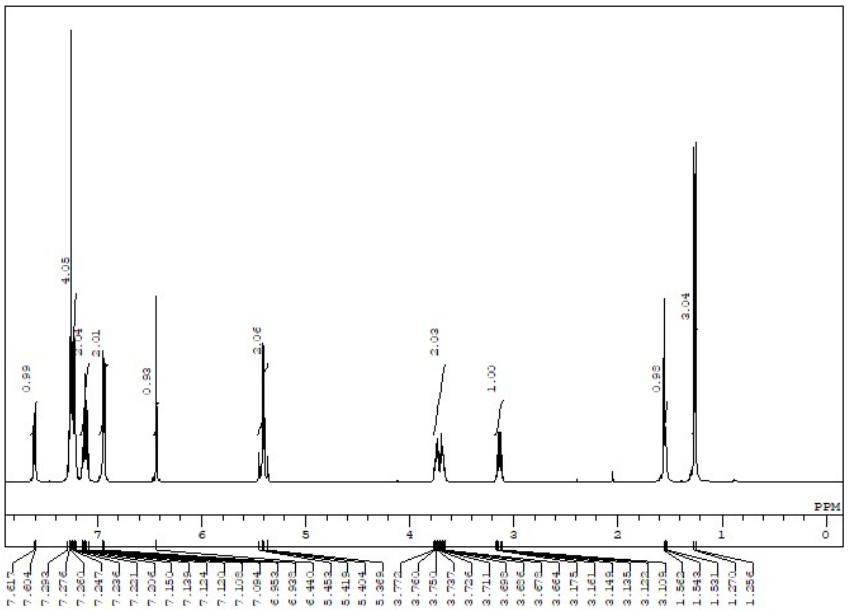


```
DFILE  2-NBn-B-alcohol_proton-1-1.als
COMNT  single_pulse
DATIM  2018-06-26 21:46:35
OBNUC  1H
EXMOD  proton.jxp
OBFRQ        500.16 MHz
OBSET          2.41 KHz
OBFIN          6.01 Hz
POINT         16384
FREQU       9384.38 Hz
SCANS             8
ACQTM         1.7459 sec
PD            5.0000 sec
PW1             6.85 usec
IRNUC  1H
CTEMP          17.1 c
SLVNT  CDCL3
EXREF          7.26 ppm
BF             1.20 Hz
RGAIN            44
```

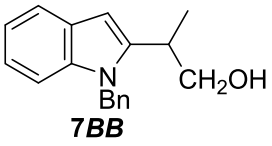

7*BB*

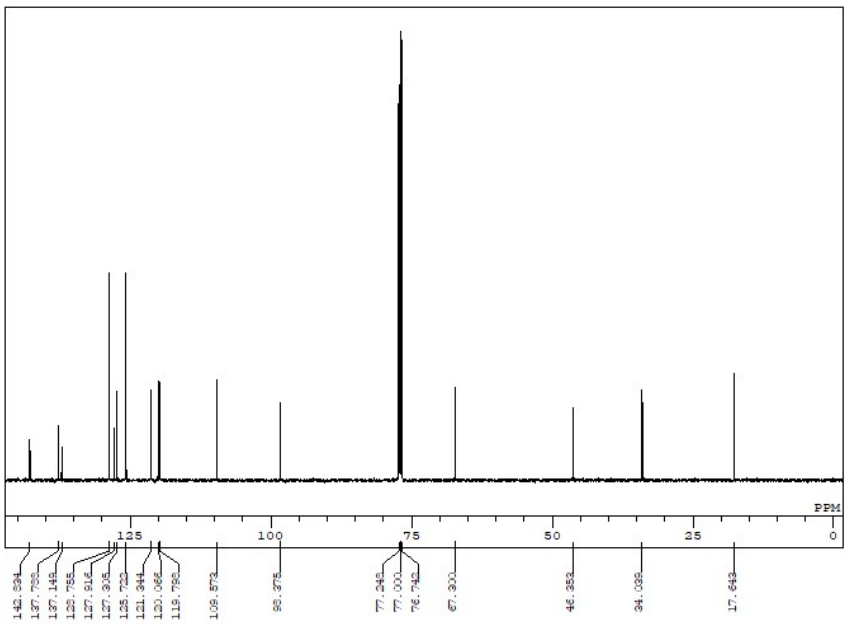


```
DFILE  2-NBn-B-alcohol_carbon-1-1.als
COMNT  single pulse decoupled gated NC
DATIM  2018-06-27 21:11:20
OBNUC  13C
EXMOD  carbon.jxp
OBFRQ        125.77 MHz
OBSET          7.87 KHz
OBFIN          4.21 Hz
POINT         32767
FREQU      39308.18 Hz
SCANS          1024
ACQTM         0.8336 sec
PD            2.0000 sec
PW1             3.12 usec
IRNUC  1H
CTEMP          17.8 c
SLVNT  CDCL3
EXREF         77.00 ppm
BF             1.20 Hz
RGAIN            58
```

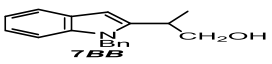

7BB

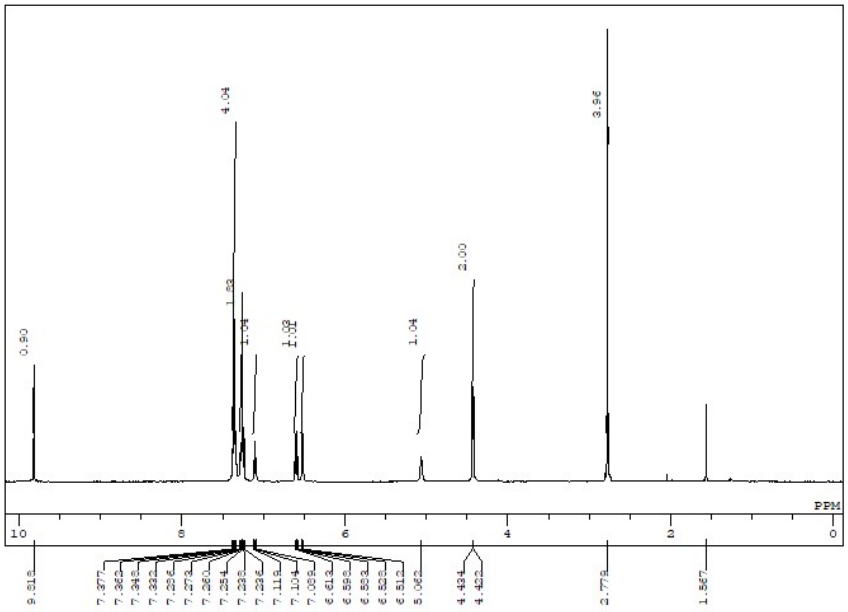


```
DFILE  2-NBn-L-aldehyde_proton-1-1.als
COMNT  single_pulse
DATIM  2018-06-18 11:49:05
OBNUC  1H
EXMOD  proton.jxp
OBFRQ        500.16 MHz
OBSET          2.41 KHz
OBFIN          6.01 Hz
POINT         16384
FREQU       9384.38 Hz
SCANS             8
ACQTM        1.7459 sec
PD           5.0000 sec
PW1            6.85 usec
IRNUC  1H
CTEMP         13.7 c
SLVNT  CDCL3
EXREF         7.26 ppm
BF            1.20 Hz
RGAIN           44
```

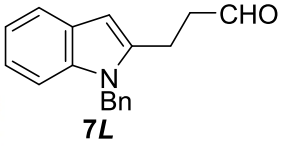

7L

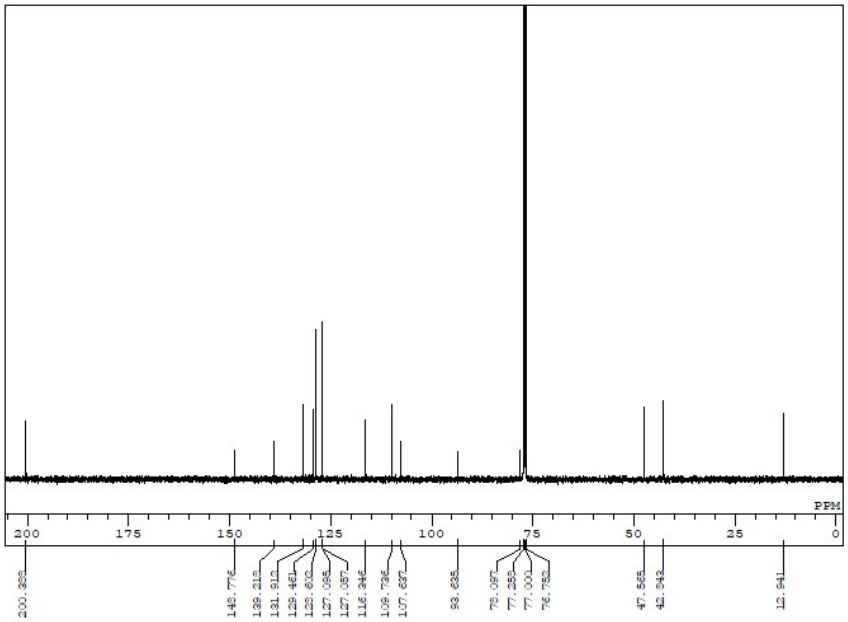


```
DFILE  2-NBn-L-aldehyde_carbon-1-1.als
COMNT  single pulse decoupled gated NO
DATIM  2018-06-18 15:12:24
OBNUC  13C
EXMOD  carbon.jxp
OBFRQ        125.77 MHz
OBSET          7.87 KHz
OBFIN          4.21 Hz
POINT         32767
FREQU      39308.18 Hz
SCANS          1024
ACQTM        0.8336 sec
PD           2.0000 sec
PW1            3.12 usec
IRNUC  1H
CTEMP         14.3 c
SLVNT  CDCL3
EXREF        77.00 ppm
BF            1.20 Hz
RGAIN           52
```

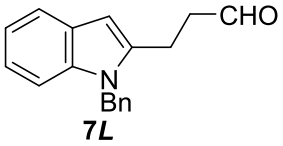

7L

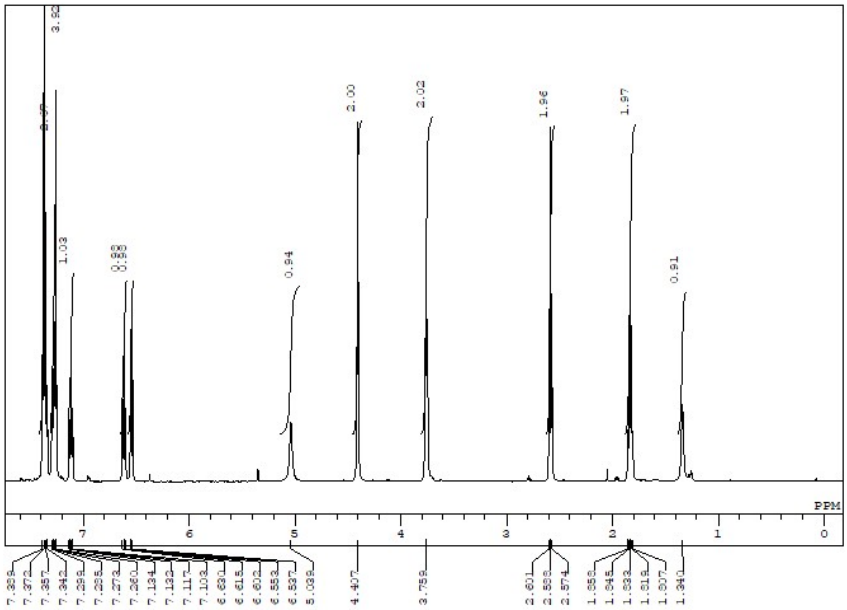

```
DFILE  2-NBn-L-alcohol_proton-1-1.als
COMNT  single_pulse
DATIM  2018-06-13 16:15:36
OBNUC  1H
EXMOD  proton.jxp
OBFRQ        500.16 MHz
OBSET          2.41 KHz
OBFIN          6.01 Hz
POINT         13107
FREQU       7507.51 Hz
SCANS             8
ACQTM        1.7459 sec
PD           5.0000 sec
PW1            6.85 usec
IRNUC  1H
CTEMP         13.4 c
SLVNT  CDCL3
EXREF         7.26 ppm
BF            1.20 Hz
RGAIN           40
```

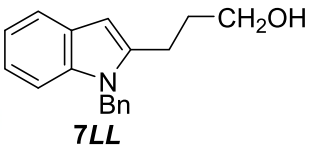

7LL

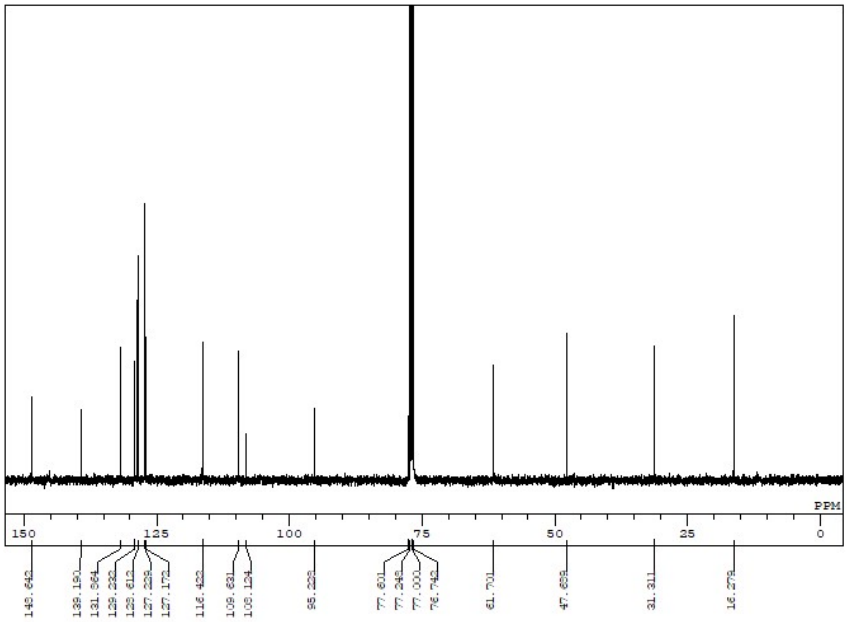

```
DFILE  2-NBn-L-alcohol_carbon-1-1.als
COMNT  single pulse decoupled gated NO
DATIM  2018-06-13 16:20:14
OBNUC  13C
EXMOD  carbon.jxp
OBFRQ        125.77 MHz
OBSET          7.87 KHz
OBFIN          4.21 Hz
POINT         32767
FREQU      39308.18 Hz
SCANS          1024
ACQTM        0.8336 sec
PD           2.0000 sec
PW1            3.12 usec
IRNUC  1H
CTEMP         13.7 c
SLVNT  CDCL3
EXREF        77.00 ppm
BF            1.20 Hz
RGAIN           58
```

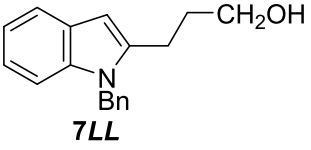

7LL

Acknowledgments

This dissertation is completed under the careful guidance of Professor Kiyomi Kakiuchi at Synthetic Organic Chemistry Laboratory of Division of Materials Science, Nara Institute of Science and Technology (NAIST).

My deepest gratitude goes first and foremost to Professor Kiyomi Kakiuchi, my supervisor, for his constant encouragement and guidance both in the study and daily life. Without his consistent and illuminating instruction, this dissertation could not reach its present level. With his help, I am lucky to have the opportunity to study in Kakiuchi sensei's group. In the three years of Ph.D., I have benefited enormously from his depth of knowledge. Specifically, I would like to express my heartfelt gratitude to Associate Professor Tsumoru Morimoto for his instructive advice and useful suggestions. When I meet a problem, he always gives valuable advice and comments patiently. Under his professional guidance, my research proceeds well. With his kind help, I have grown up to be a chemist and got more basic knowledge of organic and organometallic chemistries. I would also like to express sincere thanks to my dissertation committee, Professor Takahiro Honda and Associate Professor Takashi Matsuo for their comments and suggestions. And I thank Professor Leigh McDowell of NAIST for English language suggestions.

I am also deeply indebted to Assistant Professor Dr. Hiroki Tanimoto and the Assistant Professor Dr. Yasuhiro Nishiyama for help in laboratory life. I also express my gratitude to

Ms.Hisayo Fujiki for her help and support my research life in NAIST. And I appreciate all the members in the Synthetic Organic Chemistry Laboratory, particularly Mr. Hideyuki Kobayashi, Mr. Tatsuya Ueda, Mr. Naoto Akiyama, Mr. Hiroki Shima, Ms. Yoshiko Yamaguchi, Ms. Erin Hayashi, Ms. Mana Yamashita. They gave me a friendly research environment and wonderful research life. It will be a very meaningful and important part of my life.

I would like to thank the financial support from Division of Materials Science and the Japanese Government Scholarship from the Ministry of Education, Culture, Sports, Science and Technology. Many thanks to staff of Student Affairs Division and Division of Materials Science for supporting my research and daily life.

Finally, I would like to express my greatest love for my family. They always give me the motivation to do everything. Without their support, I can not finish my Ph.D. course smoothly.

Jian Pan

2019.03

List of Publications

1) The Use of Formaldehyde in the Rhodium-Catalyzed Linear-Selective Hydroformylation of Vinylheteroarenes

Jian Pan, Tsumoru Morimoto, Hideyuki Kobayashi, Hiroki Tanimoto, and Kiyomi Kakiuchi

Heterocycles **2019**, *98*, (DOI : 10.3987/COM-19-14064).

Reference(s)

1) Tsumoru Morimoto, Jian Pan, and Kiyomi Kakiuchi, "Rh(I)-Catalyzed Selective Hydroformylation of Vinyl Heteroarenes Using Formaldehyde," 22nd IUPAC International Conference on Organic Synthesis (ICOS-22), Florence (Italy), September 16-21, P-369 (2018). (Poster)